Thermo-Hydro-Mechanical Behavior of Compacted Bentonite-Sand Mixtures: An Experimental Study

Dissertation
as a requirement for the degree of

Doktor – Ingenieur

at the Faculty of Civil Engineering

Bauhaus-University Weimar

submitted by

Yulian Firmana Arifin
from Banjarmasin / Indonesia

Weimar

Reviewers:

1. Prof. Dr.-Ing. habil. Tom Schanz
2. Prof. Dr. Lyesse Laloui
3. Prof. Dr. Asuri Sridharan
4. Dr. Snehasis Tripathy

To my parents, my wife Dian, and my sons Rafi and Irfan

ABSTRACT

Heat, gas, and leachate are primary by-products of landfill processes in municipal solid waste landfills. In nuclear waste repository, temperature of the waste also raises due to radioactivity processes. Temperature increase in the repository induces hydro-mechanical processes of its sealing material. Moderate to high temperature is expected to be encountered in the field situation.

In this thesis, a study on the thermo-hydro-mechanical behavior of compacted bentonite-sand mixtures which are among the materials proposed to be used as sealing material for landfills and hazardous waste repository is presented. Mixtures of a calcium-type bentonite, Calcigel, and quartz sand were used in this study. Series of tests including suction and swelling pressure measurement, drying-wetting under unconfined and confined conditions were conducted at a moderately high temperature. Tests at room temperature including basic and physico-chemical characterization, microstructure and fabric studies, and osmotic suction were conducted in order to provide insight into understanding the hydro-mechanical processes taking place in the bentonite.

The experimental data obtained are presented and compared to the result of the previous tests for the same material performed by other researchers at room temperature. The changes in hydro-mechanical behavior due to elevated temperature were analyzed and discussed based on the suction components of soil which are influenced by temperature. At the end, conclusions concerning the temperature effects on the hydro-mechanical behavior of the materials are drawn and suggestions for future studies are made.

ZUSAMMENFASSUNG

In Folge der Prozesse in den Siedlungsabfalldeponien entstehen Wärme, Gas und Sickerwasser als Nebenprodukte. In Deponien für nukleare Abfälle nimmt die Wärme in Abhängigkeit deren Radioaktivität zu. Aufgrund der Wärmeentwicklung im Abfall kommt es in dem die Kanister umgebenden Dichtelement zu Temperaturänderungen, was verschiedene hydro-mechanische Prozesse verursacht, die sowohl bei niedrigen als auch bei mäßig hohen Temperaturen stattfinden.

In dieser Dissertation wird eine Studie über die Auswirkungen von Temperaturänderungen auf das hydro-mechanische Verhalten von Bentonit-Sand-Gemischen vorgestellt, welche ein mögliches Dichtungsmaterial für Verschlussbauwerke in Deponien für radioaktive Abfälle darstellen.

In dieser Studie wurden Mischungen von Kalzium-Bentonit, genannt “Calcigel“, und Quarzsand verwendet. Es wurden bei mäßig hohen Temperaturen Versuchsreihen durchgeführt, die die Messung der Saugspannungen und des Quelldrucks, als auch die Ermittlung der Saugspannungs-Wassergehalts-Beziehung auf dem Trocknungs- sowie Bewässerungspfad bei behinderter und nicht behinderter Volumenänderung beinhalten. Des weiteren wurden bei Raumtemperatur Versuche zur Bestimmung der physiko-chemischen Eigenschaften sowie Untersuchungen zur Struktur und der osmotischen Saugspannung durchgeführt. Das Ziel dieser Untersuchungen war es, einen besseres Verständnis der innerhalb des Bentonits stattfindenden hydro-mechanischen Prozesse zu erlangen.

Die experimentell gewonnenen Daten werden vorgestellt und mit Ergebnissen aus vorangegangenen Forschungsarbeiten am selben Material bei Raumtemperatur verglichen. Die beobachteten Änderungen im hydro-mechanischen Verhalten aufgrund der erhöhten Umgebungstemperatur werden analysiert und diskutiert, wobei besonderes Augenmerk auf die Materialkomponenten gelegt wird, deren Eigenschaften und Verhalten durch die Temperatur beeinflusst wird.

Aus den vorgestellten Untersuchungsergebnissen wurden Schlussfolgerungen über die Auswirkungen der Temperatur auf das hydro-mechanische Verhalten der Materialien gezogen, und es wurden Vorschläge für die zukünftige Untersuchungen unterbreitet.

ACKNOWLEDGEMENTS

Praise be to God, the most gracious and the most merciful, for His helps that enable me to finish this work. I would like to thank first and foremost my supervisor, Prof. Tom Schanz, for his meticulous guidance throughout my period of candidature. I am especially grateful with the opportunities given to me to carry out my research in Laboratory of Soil Mechanics, Bauhaus-Universität Weimar. I would like to acknowledge the financial support provided by the Ministry of National Education of Indonesia through Technological and Professional Skills Development Sector Project (TPSDP) for my study in Germany and Bundesministerium fur Bildung und Forschung (BMBF) through a project grant No. 02C0881 for my research

My thanks are for Rector and Dean of Faculty of Engineering, University of Lambung Mangkurat (Unlam) Banjarmasin, for their support during my study. Many thanks go to Mr. Rusliansyah, Director of Sub-Project Management Unit TPSDP Unlam, and his staffs for helping me to organize my scholarship.

My gratitude should also be extended to the members of the Laboratory of Soil Mechanics including the research and laboratory staffs. I thank Dr. Agus and Dr. Tripathy for their contribution to my PhD work. Thanks also to Ms. Tscheschlok and Mr. Hoppe for their assistance in the experiments. My gratitude goes also to Dr. Manju, Ms. Baille, Mr. Jamal, Mr. Al-Badran, and Mr. Khan for their shares of ideas. Thanks also to Mr. Prananda and Ms. Agnatasya for their support.

My thanks are also for Prof. Laloui and Prof. Sridharan for their agreement to be external reviewers of this dissertation together with Dr. Tripathy. I would like pass my gratefulness to all parties who indirectly assisted me during my period of stay in Weimar.

At last but not at least, I would like to gratitude my wife, Dian, who has been accompanying me patiently, and my sons, Rafi and Irfan, for their amusing and cheerful behavior at home.

This page intentionally left blank

LIST OF CONTENTS

This page intentionally left blank

LIST OF FIGURES

LIST OF TABLES

This page intentionally left blank

LIST OF SYMBOLS

ν	:	cation valence
ε	:	dielectric constant of the pore fluid
ξ	:	distance function
ϕ	:	osmotic coefficient
α_r	:	coefficient of thermal expansion of the ring
α_s	:	volumetric thermal dilatation of the clay particle
ρ_w	:	unit weight water in kg/m^3 as a function of temperature
a	:	fitting parameter for suction characteristic curve
b	:	fitting parameter for suction characteristic curve
c	:	fitting parameter for suction characteristic curve
d	:	fitting parameter for suction characteristic curve
d	:	half distance between two clay platelets in cm
d_p	:	soil pore diameter in mercury intrusion porosimetry
e	:	void ratio
e'	:	elementary electric charge in esu
e_L	:	void ratio at liquid limit
e_o	:	initial void ratio
G	:	specific gravity
$G_s^{bentonite}$	:	specific gravity of bentonite
G_s^{sand}	:	specific gravity of sand
k	:	Boltzmann's constant
K	:	double layer parameter
m	:	molal salt solution (mol/Kg)
$m_{fp\ dry}$	:	mass of dry filter paper
$m_{fp\ wet}$	:	mass of wet filter paper
M_w	:	molecular weight of water (i.e., 18.016 kg/kmol)
n	:	molar concentration of ions in the pore fluid
p	:	swelling pressure in kPa
p_{int}	:	intrusion pressure in mercury intrusion porosimetry
$P_{squeeze}$	:	pressure required to squeeze out first drop of soil pore-water
R	:	universal gas constant (i.e., 8.31432 J/mol K)

r_{bs} : bentonite-sand mass ratio (dry mass basis)

RH : relative humidity in percent

s_m : matric suction

S_r : degree of saturation

S_s : specific surface area of the soil in cm^2/gram

s_t : total suction in kPa

T : absolute temperature in Kelvin

T_2 : water proton relaxation time

T_b : relaxation time of the external water

T_s : relaxation time of internal water

u : nondimensional midplane potential

u_v : partial pressure of pore-water vapor in the specimen

u_{vo} : saturation pressure of water vapor over a flat surface of water at the same temperature

w_b : bentonite water content

w_e : estimated water content

w_{fp} : filter paper water content in percent

w_m : mixture water content

y : nondimensional potential at distance x from the clay surface

z : nondimensional potential at the clay surface

θ_{hw} : contact angle between mercury and pore water wall (i.e., 141.3°)

σ_{Hg} : tension of mercury (i.e., 0.484 N/m at 25 °C)

γ_w : unit weight of water in gram/cm^3

ρ_d : mixture dry density

u_a : air pressure

u_w : pore-water pressure

T_s : surface tension of water (i.e., 72.75 mN/m at 20 °C)

R_s : radius of curvature of meniscus (i.e., equal to pore radius of soils by assuming contact angle $\alpha = 0$)

CHAPTER 1

INTRODUCTION

1.1 Background

Bentonite is a very highly plastic clay generated frequently from the alteration of volcano ash, consisting predominantly of smectite mineral, usually montmorillonite. Several properties of bentonite such as low permeability and high swelling capability are favorable in relation to the use of the material as buffer and sealing element in nuclear waste disposal facilities and as liner and cover in landfill. Since the compacted bentonite has a low permeability, it is expected that hydro-geological transport of radionuclides from nuclear waste and leachate from landfill that flow with groundwater through the compacted bentonite is minimized. Moreover, the high ion exchange capacity of bentonite enables ions from radionuclide to be absorbed such that their transport is even more retarded.

Since excessive swelling pressure of bentonite may cause damage to the repository it self, a mixture of bentonite and sand is sometimes preferable. By adding sand to the bentonite, swelling, shrinkage, compressibility and deformability of the bentonite could be reduced. Furthermore, the addition of sand in the bentonite has been found to be advantageous with respect to ease of handling, manufacturing and cost.

Compacted bentonite-sand mixture has been proposed to be used as sealing material in nuclear waste disposal facilities in Germany and other countries in Europe. A bentonite, named Calcigel, is currently under investigation for this purpose. A mixture of 50% Calcigel and 50% sand has been proposed. Research studies have been performed to investigate the characteristics of this mixture and other compacted bentonite-sand mixtures including as soil-water characteristic curve, swelling pressure, consolidation, and shear strength. While many studies have been carried out on the hydro-mechanical characteristics of bentonite-sand mixtures, not many attempts have been made to investigate the characteristics of these mixtures as affected by temperature changes. It has hardly ever been known the effects of moderately high temperature on the hydro-mechanical behavior of bentonite-sand mixture as expected to occur as a result of radioactivity. This research focused on the thermo-hydro-

mechanical behavior of a bentonite-based material (i.e., bentonite-sand mixture) that can potentially be used as sealing element in the nuclear waste disposal facilities in Germany. This included studies on the material behavior in light of geotechnical engineering aspects encompassing the material behavior at saturated and unsaturated conditions. The elevated temperature up to 80 °C was used in this study since up to now most of the high-level nuclear and hazardous waste repository concepts are designed based on the design criteria that allows up to a maximum temperature of 80 °C for the bentonite buffer (SKB, 1999 and JNC, 2000). Pertaining of the use of bentonite-sand mixtures in the nuclear and hazardous waste repositories and landfill applications, the scope of investigation was extended to cover both at high and low densities. In order to develop understanding regarding the influence of bentonite content and compaction effort, bentonite-sand mixtures with different bentonite and sand ratios (i.e., 30%, 50%, 100% bentonite) were also used in this study.

1.2 Objectives and Scope

The general objective of this study was to investigate the thermo-hydro-mechanical behavior of compacted bentonite-sand mixtures pertaining to the use of these materials at low density (for landfill applications) and at high density (for sealing and buffer elements for highly toxic and nuclear waste repository applications). The study included hydraulic and coupled hydro-mechanical behavior of compacted bentonite-sand mixtures. The results obtained from this study are also compared with the data available in literature for isothermal cases at a temperature of 20-25 °C and are discussed further in this thesis. The scope of this investigation is as follow:

(a) **Characterization of physical, chemical, and mineralogical properties of the bentonite used**. Since sand is an inert material, the properties of the sand used in the mixtures were not considerably investigated in this study.

(b) **Microstructures and fabric studies of the bentonite and bentonite-sand mixtures**. The results of these particular studies provide information about microstructures and fabric of compacted mixtures that are expected to qualitatively describe the hydro-mechanical behavior of these materials.

(c) **Measurement of suction characteristics** including total suction and matric suction of the bentonite and the bentonite-sand mixtures at room and at elevated temperature (i.e., 80 °C).

(d) **Measurement of osmotic suction** of the bentonite used in this study. The measurement results provide information on pore-water chemistry of the bentonite

used and the qualitative influence of the pore-water chemistry on the hydro-mechanical behavior of the material, not only at room temperature but also at elevated temperature.

(e) **Characterization of the hydro-mechanical behavior of compacted bentonite and bentonite-sand mixtures.** This included water retention and swelling characteristics as also affected by elevated temperature.

1.3 Organization of the Thesis

This thesis is divided into ten chapters. The first chapter presents the background, objectives, and scopes of the study, and the organization of the thesis. The second chapter presents literature review on the hydro-mechanical behavior of expansive soils, including bentonites. The third chapter presents literature review on the temperature effects on aspects related to expansive soils and hydro-mechanical characteristics of compacted bentonites. The fourth chapter describes basic and the physical, chemical, and mineralogical properties of bentonite used in this study. The fifth chapter presents the microstructures and fabric of the compacted bentonite and bentonite-sand mixtures at low and high densities.

In Chapter 6 to 9, the experimental results of the total and matric suction measurements (Chapter 6), osmotic suction measurements (Chapter 7), drying-wetting experiments (Chapter 8), and swelling characterization (Chapter 9) of the compacted bentonite and bentonite-sand mixtures are presented. In these chapters, literature review on experimental techniques that are relevant to this study, and respective techniques and procedures adopted are described. The results are also presented and discussed in this chapter. The tenth chapter concludes the findings and provides suggestions for future research studies.

This page intentionally left blank

CHAPTER 2

HYDRO-MECHANICAL BEHAVIOR OF COMPACTED BENTONITE

2.1 General

This chapter discusses the hydro-mechanical behavior of compacted expansive soil. The discussion is commenced by the brief description about the structural units of expansive soil, water in expansive soil, hydration processes, concept of suction, swelling mechanisms, and bentonite as a semi-permeable membrane that are very important to understand pertaining to the study on the hydro-mechanical behavior of expansive soil not only at room temperature but also at elevated temperature. The hydraulic behavior (i.e., water retention behavior) and coupled hydro-mechanical behavior (i.e., swelling strain and swelling pressure) are described in order to present the previous investigations that have been done particularly for the same material as used in this study performed at a temperature of 20-25 °C.

2.2 Structural Units and Microstructure of Expansive Clays

Bentonite is a very highly plastic clay which contains large quantity of montmorillonite (or smectites) and expands when it is in contact with water in liquid form or in vapor form. This is related to the mineralogical composition of the elementary layer or structural unit of the montmorillonite. According to Mitchell (1993), the structure of montmorillonite is a unit made of an alumina octahedral sheet sandwiched between two silica tetrahedral sheets as shown in Figure 2.1. The alumina octahedral structure is composed of an aluminium atom and six hydroxyls in an octahedral coordination whereas the silica tetrahedral is composed of a silicon atom and four oxygen atoms in a tetrahedral coordination.

The elementary layers stacked together to form particle (platelet or crystal). In dry condition, bonding between the elementary layers is provided by van der Waals and by exchangeable cations. These types of bonding are weak and broken when water or polar liquid inserts between them (Mitchell, 1993).

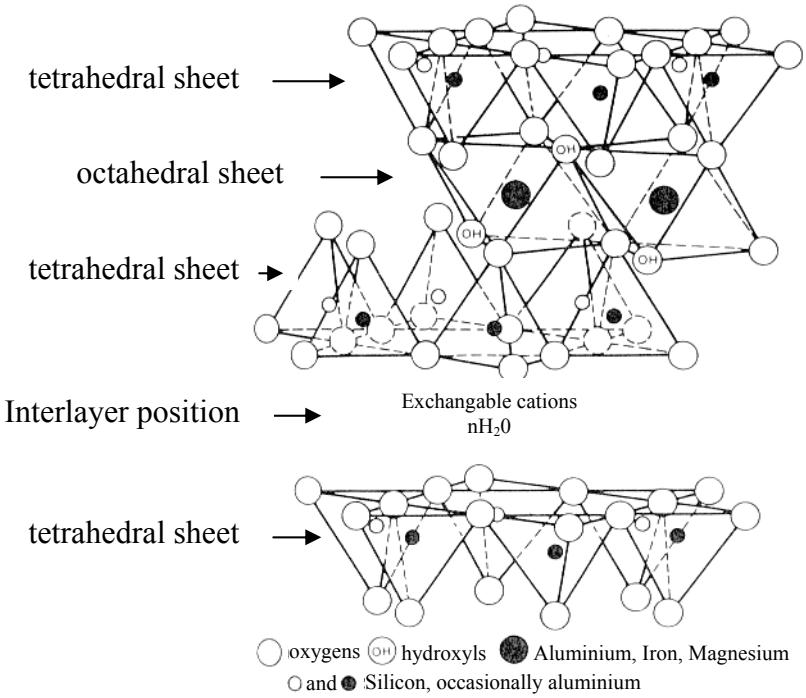

Figure 2.1 Sketch of the montmorillonite structure (Mitchell, 1993)

A particle is made of several to hundred elementary layers depending on the moisture conditions (Pusch et al., 1990). Using transmission electron microscope (TEM), Tessier et al. (1998) found that the microstructure of the Fourges clay (i.e., clay which contains calcium-type montmorillonite and kaolinite minerals) consists of aggregates of particle with 2-4 elementary layers on average. Inside each particle unit, it was found the interlayer distance is approximately 12Å. Moreover, the type of exchangeable cation also influences the number of elementary layer in a particle (Pusch et al., 1990; Mitchell, 1993; Saiyouri et al., 2004). In suspension, a particle is made of 3-5 elementary layers and 10-20 elementary layers for sodium-type bentonite and calcium-type bentonite, respectively (Pusch et al., 1990). Saiyouri et al. (2004) reported that the compaction also affected the number of elementary layers in a particle and the numbers were different for sodium and calcium type bentonites for suction higher than 3000 kPa. For suction less than 3000 kPa, they found that the number of elementary layers in a particle is almost the same for both bentonite types. The particles aggregated together to make an aggregate. These features are very important in order to investigate the behavior of expansive clays especially on the microstructure of the bentonite (Delage, 2007).

The presence of structural units (i.e., elementary layer), particles, and aggregates results in presence of different type of pores in the expansive soils. In general, compacted expansive soil has two types of pores (i.e., micro-pores and macro-pores) (Gens and Alonso, 1992; Yong, 1999). The micro-pores are defined as pores within the aggregates (i.e., pores

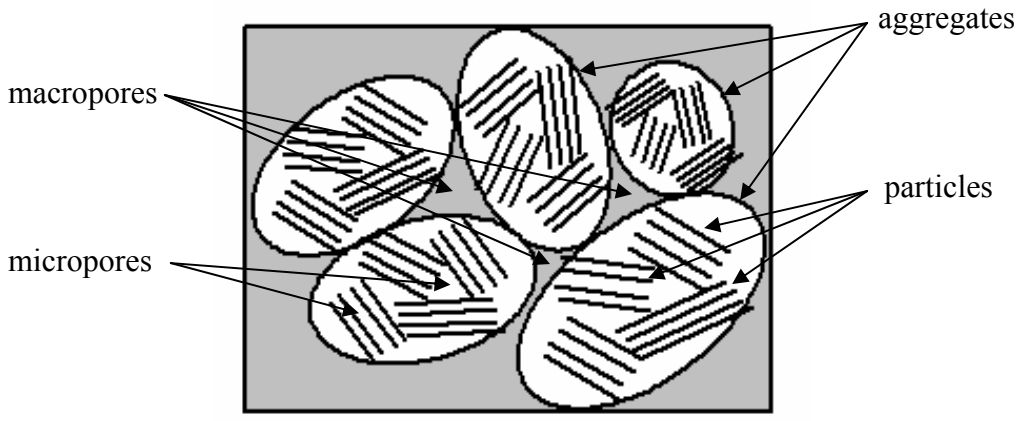

Figure 2.2 Sketch of the microstructure of expansive clays

between the elementary layers and between the particles) or called as intra-aggregate pores. The macro-pores are defined as pores existed between the aggregates or called as inter-aggregate pores. The sketch of the microstructure of expansive clays is shown in Figure 2.2.

2.3 Water in Expansive Clays

Mitchell (1993) summarized the possible mechanisms for clay-water interaction. The mechanisms are hydrogen bonding, hydration of exchangeable cations, attraction by osmosis, charged surface-dipole attraction, and attraction by London dispersion forces. For expansive clays, at dry or low water content the hydration of exchangeable cations is the main mechanism. In dry condition, the exchangeable cations are located on the surface of the layers or tetrahedral sheet to balance the negative charge of the clay surface. In the hydration process, the water molecules are absorbed in between the elementary clay layers to develop water layers. The thickness of dehydrated montmorillonite crystals and of complete hydrate layers depend on the exchangeable cation. Pusch et al. (1990) has reported the thickness and the complete hydrate layers of water molecules for different exchangeable cations as summarized in Table 2.1. From the table, it is shown that there are 3 layers of water molecules for Mg and Na bentonite and 2 layers of water molecules for Ca and Na bentonite developed on the clay surface in order to fulfill the hydration force. The total water thicknesses of the bentonites are 9.08, 5.64, 9.74, and 6.15 Å for Mg, Ca, Na, and K

Table 2.1. Thickness in Å and complete hydrate layers for different exchangeable cation (Pusch et al., 1990)

		0 hydrate	1st	2nd	3rd
Montmorillonite	Mg (001)	9.52	12.52	15.55	18.6
	Ca (001)	9.61	12.5	15.25	-
	Na (001)	9.62	12.65	15.88	19.36
	K (001)	10.08	12.5	16.23	-

bentonite, respectively.

Water content of bentonite at the end of the hydration process can be calculated roughly from data presented in Table 2.1 by calculating the weight of water per gram soil from multiplication of the total water thickness, specific surface area of the bentonite, and the volumetric weight of water. The water content is equal to the weight of water per gram soil multiplied by 100 percent devided by 2. For bentonite with 500 m^2/g and the volumetric weight of water of 1 g/cm^3, the water content of the bentonites are 22.7, 14.1, 23.9, and 15.4% for the Mg, Ca, Na, and K type bentonite, respectively. It seems that sodium type bentonite absorbs more water in hydration process compared to other bentonites. Since volumetric weight of water is more than 1 g/cm^3 for less than 3 layers of water molecules on the clay surfaces (Mitchell, 1993), the water content can be higher than those values. In addition, Saiyouri et al. (2004) reported that four water layers were developed on the clay surface of the bentonites used in their study (i.e., MX 80 and FoCa7). According to Mitchell (1993), for fully expanding, sodium type bentonite having specific surface area of 800 m^2/g would reach water content of 400% to fulfill the hydration of the exchangeable cation.

After about three to four monolayers of water molecules in between the elementary layers, surface hydration becomes less important. Water molecules tend to diffuse toward the surface in an attempt to equalize ion concentrations. This occurs in between the external surface of particle or crystal (Pusch et al., 1990; Bradbury and Baeyens, 2002; Pusch and Yong, 2003; Saiyouri et al., 2004). Since for Sodium bentonite, the particles break up to be elementary layers due to hydration (Pusch, 2001), the diffuse double layer can be developed in between elementary layers.

The remaining fraction of water can be regarded as “free water” which exists as inter connected thin film on the outside of the clay particle and also as films surrounding the other component mineral grains in bentonite. The amount of “free water” and concentration of dissolve salt in the “free water” in the compacted bentonite depend on the initial dry density of the specimen (Bradbury and Baeyens, 2002). A schematic picture of water in compacted bentonite is presented in Figure 2.3.

2.4 Hydration Processes in Compacted Expansive Clays

Pusch and Yong (2003) distinguished three boundary conditions that are believed to cause different hydration rates of unsaturated expansive clays. The three boundary conditions are the clay exposed to water vapor, the clay exposed to non-pressurized liquid water, and the

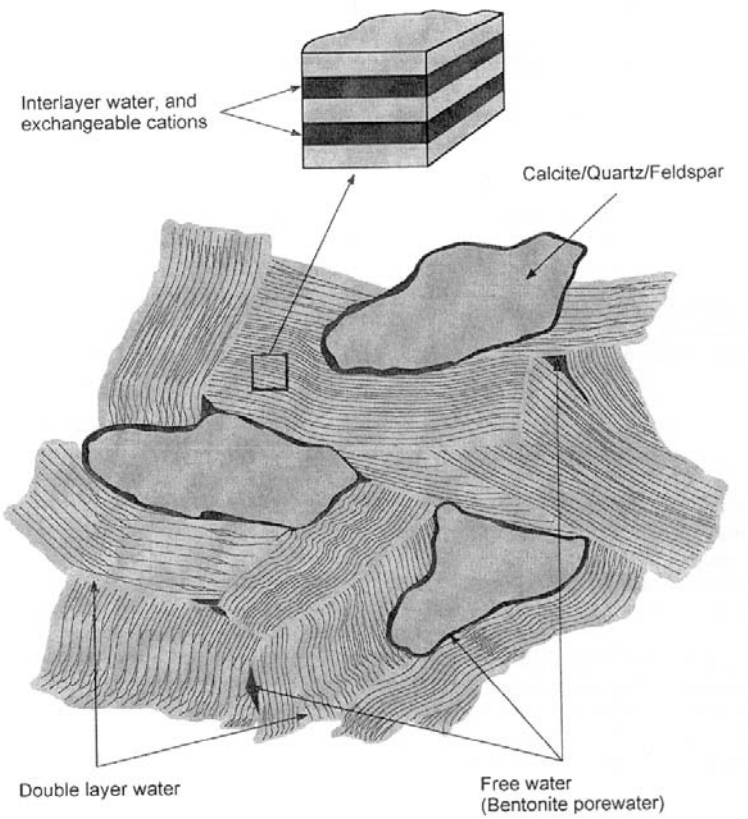

Figure 2.3 Schematic representation of interlayer water, double layer water and "free water" in compacted bentonite (Bradbury and Baeyens, 2002).

clay exposed to pressurized water. For the clay contacted with water vapor, the water molecules migrate into the open channels and adsorbed on exposed mineral surface. The water molecules then migrate into the elementary sheets that have higher hydration potential. The entire migration process of the water molecules is diffusion-like process. The saturation process is sufficiently slow to let entrapped air be dissolved and diffuse out from the clay without delaying saturation, which will, however, probably never be complete.

For the clay exposed to non-pressurized liquid water, water is absorbed by capillary forces in the open channels. Then the water migrates into finer void and further into the elementary sheets. Since water molecules entering the elementary sheets result in expanding clay particles and/or aggregates, the large channels become closed and hydration is then controlled by diffusion. In this case, the hydration rate is somewhat higher than the first condition (i.e., the clay exposed to water vapor) since the larger channels are filled quickly.

For the clay exposed to pressurized water, water is pressed into the large channels and move quickly. The penetrating water displaces air and compresses the unsaturated matrix. The hydration rate is faster than those of first and second conditions (i.e., water exposed to vapor and non pressurized water). However, when the large channels become closed by the

expansion of the clay aggregates, the hydration process follows the same procedure as the second procedure. This occurs in case of the heavily compacted bentonite.

Saiyouri et al. (2004) investigated the hydration mechanism by controlling suction to the compacted bentonites. Two types of bentonites (i.e., FoCa7 and MX80 which are calcium and sodium bentonites, respectively) were used in the study. Three methods were used in controlling suction (i.e., applying air pressure in Plexiglas tube equipped with pore filter for controlling suction from 1-100 kPa, a high-pressure membrane cell for applying suction at 1000 kPa, and vapor equilibrium technique for controlling suction from 3000-100000 kPa). Using XRD method, they found that the placement of water molecules is a function of suction, with 1 layer above 50000 kPa, 2 layers at suction from 50000 to 7000 kPa, 3 layers at suction from 7000 to 60 kPa, and 4 layers below 60 kPa. Both bentonite types showed similar phenomena. At the same time, the number of elementary layers in the particle decreases with suction.

2.5 Concept of Suction in Expansive Clays

According to Fredlund and Rahardjo (1993), generally, soil suction consists of two components (i.e., matric component and osmotic component). The matric suction component is related to the air-water interface (or surface tension) giving rise to the capillary phenomenon. The osmotic suction component is related to the dissolve solutes in bulk water which is defined as the "free water" as shown in Figure 2.3. The sum of these two components (i.e., matric and osmotic suction) is called total suction.

The general concept of soil suction mentioned above can not be applied to describe the suction in expansive soil such as montmorillonite due to presence of hydration of exchangeable cation on its surfaces and compressibility of this material due to external pressure. The complex suction development in the expansive soil leads to distinguish the terms of soil suction and soil-water potential. Since the soil suction does not exactly portrays the various mechanisms developed by the sets of thermodynamic forces in the expansive soil, Yong (1999) used the term of soil-water potential in order to describe the soil suction. According to Yong (1999), the components of soil-water potential consist of matric, osmotic, gravitational, pneumatic, and pressure potential. The matric potential pertaining to sorption forces between soil fraction and soil-water and pressure potential which is primarily due to externally applied pressure are not used for describing suction for the rigid porous or non expansive soil. In case of no external pressure imposed on the expansive clay (unconfined

condition), only the matric and osmotic potentials are responsible for the water holding capacity of the clay or the pressure potential is equal to zero. However, when constraints are placed on soil volume expansion (confined condition), the pressure potential is not equal to zero. Therefore, for example, in constant volume of swelling pressure measurement, at saturation condition (i.e., at the end of the test) the matric and osmotic potentials are balanced by pressure potential or swelling pressure. Thus, at this condition, the soil suction of the specimen is equal to swelling pressure. When the specimen is not full saturation condition or presence of air in the soil and the relative humidity of the air space on outer surface of the soil is less than 100%, capillary exists to balance the water potential of the air space (Agus, 2005). Considering the general concept of suction and the soil-water potential in expansive soil, it can be concluded that the matric component of soil suction comes from the hydration forces and capillary component effects. Therefore, the total suction is sum of the matric suction (i.e., hydration forces and capillary components) and osmotic suction from dissolve salt in the soil-pore water.

2.6 Swelling Mechanism of Expansive Clays

Swelling of expansive clay occurs when the clay is dispersed in a solvent, or when the clay is in contact with an atmosphere having a high vapor pressure of the solvent. Laird (2006) mentioned six separate processes controlling swelling of smectites in aqueous systems (i.e., crystalline swelling, double-layer swelling, the breakup of quasicrystals (or crystals), cation demixing, co-volume swelling, and Brownian swelling). He stated that crystalline swelling, double-layer swelling, and the breakup of clay particles (or crystals) control dominantly the swelling processes of expansive clays.

The crystalline swelling is a process whereby 0 to 4 discrete layers of water molecules are intercalated between elementary layers within a smectite particle. The crystalline swelling is controlled by the layer charge, interlayer cations, properties of adsorbed liquid and particle size (Yong, 1999). Considering the various potential energies presence in between the elementary layers, the crystalline swelling is balanced by the Columbic and van der Waals attraction and Born repulsion (Laird, 2006). In unconfined condition, the volume of smectite (or montmorillonite) might increase two times larger than its initial volume due to crystalline swelling, whereas, in constant volume condition, the swelling pressure as a result of crystalline swelling can reach more than 100000 kPa (Madsen and Müller-Vonmoos, 1989). In heavily compacted condition, the crystalline swelling is of major importance pertaining to

its use as a containment barrier for the nuclear waste repository (Bucher and Müller-Vonmoos, 1989).

Beyond the crystalline swelling, the double layer swelling becomes significant in the swelling mechanism. Double-layer swelling occurs due to overlapping diffuse double layer in between particles (or crystals) (Pusch et al., 1990; Bradbury and Baeyens, 2003; Laird, 2006) and also in between elementary layer (Mitchell, 1993; Delage et al., 2006). The diffuse double layer swelling depends on the mineralogical and chemical properties of soil (i.e., specific surface area and cation, cation concentration in the bulk water, dielectric constant, and valance of the cation), and the distance between the elementary layers (Sridharan and Jayadeva, 1982). Attempts have been done to calculate the swelling pressure of expansive clay or bentonite using diffuse double layer theory (e.g., Bolt 1956; van Olpen, 1963; Mitchell, 1993; Tripathy et al., 2004). Tripathy et al. (2004) reported that there is good aggrement between swelling pressure predicted using diffuse double layer theory and the experiment at low dry densities (i.e., below 1.6 Mg/m^3). The prediction data are less than that of experiment at dry density higher than 1.6 Mg/m^3. This is due to contribution of additional repulsive forces to the swelling pressure of heavily compacted bentonite (i.e., for spacing between two adjacent clay particles less than 1.5 nm) (Tripathy et al., 2006).

Using high resolution transmission electron microscope (TEM) image, Laird (2006) investigated the microstructure of bentonite from the particles orientation to the elementary layers. The TEM image showed that, first, the smectite microstructure was formed by individual particles (or crystals) which are curved and flexible. Second, the particles are joined together forming a smectite fabric. Third, the join between particles are both face-to-face and edge-to-face. These particles break up to be elementary layers due to hydration. This phenomenon was also reported by Pusch (2001) using TEM image for the sodium type bentonite (i.e., MX80). However, this is largely true for sodium type bentonite. Insertion of water molecules between elementary clay sheets occurs on a large scale for sodium bentonite. For calcium type bentonite, insertion of water molecules between elementary clay sheets is limited. Repulsion between the clay particles and aggregates surfaces plays important role in swelling mechanism after crystalline swelling for calcium type bentonite (Saiyouri et al., 2004).

2.7 Bentonite as a Semi-permeable Membrane

When a compacted clay is exposed to a concentrated salt solution, the fluid with or without dissolved salt will flow in response to osmotic gradients. In case where a soil behaves as a perfect semi-permeable membrane, only pure water will flow to medium with higher salt concentration. But, since there is no true semi-permeable membrane in soils, the water and dissolve salt will flow to medium with lower salt concentration. The degree to which the clay behaves as perfect semi-permeable membrane is entitled as osmotic efficiency. The osmotic efficiency of a soil is strongly dependent on pore fluid chemistry, pore fluid concentration, void ratio, and interparticle spacing (Barbour and Fredlund, 1989). From the osmotic efficiency versus interparticle spacing and salt concentration relationship as shown in Barbour and Fredlund (1989), at the same interparticle spacing and salt concentration, the osmotic efficiency of Na^+ soil is higher than that of Ca^{2+} soil. It means that the Ca^{2+} soil is more permeable than Na^+ soil.

Schanz and Tripathy (2005) investigated the soil-water characteristic curves of clays. According to Schanz and Tripathy (2005), the void ratio versus suction for Na^+ clays obtained from experiment were placed above those of the calculated from physico-chemical concept. For Ca^{2+} clays, the experimental data points were placed slightly below those of the calculated points. These differences were associated with the expulsion of pore fluid and ions from the clay system during the experiment.

In general, Dixon (2000) reviewed the role of salinity on the development of swelling pressure in bentonite buffer and backfill materials. It was found that the swelling pressures are unaffected by ground water salinity (i.e., concentration less than 75g/lt) for compacted bentonite having initial dry density of higher than 0.9 Mg/m^3. For compacted bentonite having dry density of higher than 1.5 Mg/m^3, even brines appear to have little or no influence on the swelling pressure value.

2.8 Hydro-Mechanical Behavior of Compacted Bentonite and Bentonite-Sand Mixtures

2.8.1 Soil-Water Characteristic Curve and Drying-Wetting behavior

Soil-water characteristic curve (SWCC) expresses the relationship between water content (i.e., in gravimetric or volumetric water content) and suction or degree of saturation and suction for specimen dried from saturated condition. In this condition, the water content of soil decreases as suction increases following a drying path. The reverse (i.e., wetting path)

is the process where the water content of soil increases as suction decreases. Normally, the wetting path is commenced from oven-dried condition. The suction corresponding to the oven-dried condition is 1000000 kPa. Croney and Coleman (1961) found that the total suction at zero water content for a variety of soils was slightly below 1000000 kPa. Fredlund and Rahardjo (1993) also found from the gravimetric water content versus suction relationship for various sand and clay soils that at zero water content the suction approaches a value of approximately 980000 kPa. This value is also supported by thermodynamic considerations (Richards, 1965).

The SWCC is influenced by type of soil, texture, and mineralogy. For clay soil type, the SWCC is influenced by the consistency limit of the clay. Fleureau et al. (2002) found a good correlation between the liquid limit and slope of void ratio versus suction and liquid limit and slope of water content versus suction for wetting path. Marinho (2005) used liquid limit of clay (i.e., higher than 25%) combined with suction capacity (i.e., reduction in water content over one logarithmic scale) and stress history to generate SWCC.

Specimen of a particular soil, in spite of having the same texture and mineralogy can have different SWCC due to different initial water content, void ratio, stress history, and compaction energy. Specimens compacted at different water contents result in different fabric of the soil (Lambe, 1960; Gens et al., 1995; Delage and Graham, 1996). Vanapalli et al., (1999) observed a significant different in the SWCC of clay till compacted at different water content (i.e., at wet of optimum, optimum, and dry of optimum) using the same compaction energy. They reported that the SWCC appears to be approximately the same over suction ranging from 20000-1000000 kPa for specimens tested with different initial water content. Soil fabric appears to have no influence on SWCC in this range of suctions.

Fleureau et al. (2002) found that drying path of specimen from slurry represent the highest capability to retain water or can be used as main drying curve of a soil. They also found that the wetting path of specimen compacted optimum water content was almost the same as wetting path of specimen from slurry.

Al-Mukhtar et al. (1999) investigated the effect of axial compaction stress on the drying curve of compacted smectite. It was found that the water content versus suction curve of specimen having lower axial stress (i.e., 1 MPa) was placed over that of specimen having higher axial stress (i.e., 10 MPa) for relative humidity (*RH*) range from 100% to 98% (or equal to total suction from 0 kPa to 2700 kPa). For *RH* less than 98% (or total suction higher than 2700 kPa), the drying curves of specimens were similar. Al-Mukhtar et al. (1999) stated that for *RH* ranging from 0 to 98%, suction is controlled by micro-pores; their size and

distribution are not influenced by the compaction process. At *RH*>98%, suction is controlled by macro-pores. The suction measurements at this *RH* range are more sensitive to the test boundary condition and variation in sample density.

Delage et al. (1998) studied the water retention and swelling properties of the FoCa7 clay under controlled suction and zero applied stress. They observed fairly reversible responses to suction cycles, in terms of water content and volume change. During these changes, it was observed that the air volume remained constant. They stated that the reversibility is related to the predominant role of a saturated microstructural level, strongly influenced by the physico-chemical bonds existing between water and the active clay minerals.

Agus (2005) investigated the drying-wetting behavior of a heavily compacted 50/50 bentonite-sand mixture. The specimens (i.e., as-prepared condition) have initial dry density of 2 Mg/m^3, water content of 9 %, and total suction of 22700 kPa. The specimens were saturated to degree of saturation of 100% in two conditions (i.e., under seating load of 7 kPa and constant volume condition) before drying process. It was found that the drying curves of the both specimens are different. The water content versus suction curve for the specimen initially saturated under seating load is placed under that for the specimen initially saturated under constant volume condition. From these two initial conditions, Agus (2005) concluded that no general main drying (i.e., the water content, void ratio and degree of saturation versus suction curves) can be defined from the experimental results since the main drying curve should be found from the specimen initially slurry condition. Agus (2005) also found that the as-prepared suction (i.e., 22700 kPa) is a limiting suction below which further reduction in suction does not induce any significant increase in the specimen degree of saturation. It was also found that the drying-wetting curves of the as-prepared specimen used was reversible as long as the drying and wetting paths do not ever touch the boundaries (i.e., the drying curve of specimen from saturated condition and the wetting curve of specimen from oven-dried condition).

2.8.2 Suction Characteristic Curve

Suction characteristic curve represents the relationship between water content and suction. Different from SWCC, suction characteristic curve is composed from the result of suction measurement of several specimens having different water content. Yahia-Aissa et al. (2000) studied the suction characteristic of an interstratified illite-smectite called Fourges clay. They found that no significant difference in the water content versus suction relationship

was obtained between the powder and compacted samples. Agus (2005) found that suction characteristic curves of bentonite and bentonite-sand mixtures were not influenced by the initial condition of the specimen (i.e., Proctor and modified compaction, or loose condition). Agus and Schanz (2005a) found that total suction of the bentonite-sand mixture is a function of mixture water content and mixture bentonite content or collectively a function of bentonite water content. These results show that the physico-chemical clay-water interactions play a dominant role in the suction characteristic curve (or water retention properties) of the soil, as compared to the standard hysteretic capillary effects that govern water retention in inactive porous media (Delage and Cui, 2008)

Suction characteristic curve is influenced by methods used in suction measurement (Agus and Schanz, 2005b), inaccuracy of the equipment used (Leong et al., 2007), temperature fluctuation (i.e., in total suction measurement) (Agus ans Schanz, 2006a) and combination of several factors (i.e., inaccuracy of the sensor used and temperature fluctuation) (Agus and Schanz, 2007).

For expansive clay, Agus and Schanz (2006b) emphasized the importance of specimen to reach the "true" equilibrium state before performing the suction measurement. This is related to the hydration mechanism in expansive clay (Pusch and Yong, 2003) and a fact that most of clay has a double porosity structure and consists of inter-aggregate pores (macro-pores) and intra-aggregate pores (micro-pores) (Gens and Alonso, 1992; Yong, 1999). When a specimen is mixed with distilled water, it is believed that the water is placed in the surface of aggregates (macro-pores). After some period of time, an internal redistribution of water is expected to occur because of an unbalanced total suction between the macro-pores and micro-pores.

2.8.3 Swelling Strain and Swelling Pressure of Compacted Bentonite and Bentonite-sand Mixture

The term of swelling for expansive soils includes both swelling strain and swelling pressure. Swelling potential had attracted more attention of many researchers who study expansive soil behavior related to the landfill applications for example. Swelling strain shows the ability of compacted expansive clays to swell after inundation under a seating load. The minimum seating load applied in the test is 1 kPa (ASTM D 4546; ASTM, 1997). The magnitude of swelling strain of clay is controlled by initial water content, dry density, surcharge pressure (or vertical pressure), fabric, and type and amount of clay (Mitchell, 1993). Aging also found to reduce the swelling potential of compacted expansive clay (Subba Rao

and Tripathy, 2003). In case of bentonite-sand mixture, the amount of bentonite content in the bentonite-sand mixtures influenced significantly the magnitude of swelling potential besides initial dry density and vertical pressure during the test (Komine and Ogata, 2003).

Swelling pressure is also an important issue in studying the behavior of compacted expansive clays. Swelling pressure is a manifestation of swelling potential or swelling (Mesri et al., 1994) and thus the development of swelling pressure is similar to the swelling mechanism and is only possible in the presence of water (or other polar solutions). The magnitude of pressure acting on an expansive soil at which the soil swells upon wetting represents the swelling pressure of the soil at the equilibrium void ratio.

Swelling pressure is defined as the pressure needed to maintain constant volume conditions when water is added to an expansive soil. This definition is broad and embraces specific definition for swelling pressure which has been defined for various test methods. Three different methods; namely, swell-load, swell-under-load, and constant volume test were suggested by Sridharan et al. (1986). Swelling pressure measurements using oedometer are also described in ASTM D 4546 (ASTM, 1997).

The magnitude of swelling pressure of compacted expansive soils is controlled by initial dry density of the specimen (Sridharan et al., 1986; Komine and Ogata, 2003, Villar and Lloret, 2004, and Agus and Schanz, 2005a). In case of bentonite-sand mixtures, the swelling pressure of bentonite-sand mixture is a function of mixture dry density and mixture bentonite content or is collectively a function of bentonite dry density (Agus and Schanz, 2005a).

Agus and Schanz (2005a) investigated the rate of swelling pressure of compacted bentonite-sand mixtures using plot of time versus pressure divided by maximum pressure (or swelling pressure). It was found that the rate of swelling pressure development is a function of initial total suction of the specimen. This is not true for low bentonite content (i.e., less than 50%) resulting low bentonite dry density and for heavily compacted 50/50 bentonite-sand mixture (i.e., dry density of 2 Mg/m^3 used in the study). The effect of density plays a role in the low bentonite dry density and heavily compacted bentonite-sand mixture.

Agus (2005) also investigated the swelling pressure and constant volume wetting behavior of heavily compacted 50/50 bentonite-sand mixture specimen. Two different methods were used (i.e., vapor equilibrium technique, VET for suction higher than 2000 kPa and axis translation technique, ATT for suction less than 2000 kPa). In the swelling pressure development at constant volume condition, it was found that very small development of swelling pressure occurs upon wetting from the as-prepared suction (i.e., 22700 kPa) to about

2000 kPa suction as shown in Figure 2.4. A rapid development of swelling pressure occurred afterward. Very small development in swelling pressure at suction higher than 2000 kPa is related to the method how to apply suction to the specimen (i.e., vapor equilibrium technique, VET. For the specimen exposed to water vapor, the water molecules migrate into the open channels (i.e., macro-pores) and absorbed on exposed mineral surface. An internal redistribution of water occurs in order to balance the water potential gradient exist between macro-pores and micro-pores. Agus (2005) stated that the insignificant swelling pressure development during wetting up to 2000 kPa suction might be due to a delayed 'true' equilibrium in the specimen and the 'true' equilibrium might be attained after long test duration.

Agus (2005) also investigated swelling pressure development for different initial conditions and bentonite content of the specimens as shown in Figure 2.4. It was found that different initial conditions of 50B/50S specimens (i.e., as-prepared and oven-dried conditions) do not influence the swelling pressure development of the specimens. Both specimens show insignificant swelling pressure development at suction higher than 2000 kPa. Agus (2005) stated that delayed 'true' equilibrium in the specimen with 50% bentonite content is mainly due to the low permeability of the specimen. The delayed 'true' equilibrium also occurs to the wet pure bentonite specimen. This is due to the low potential gradient of the wet specimen with initial total suction of 18000 kPa which much lower than initial total suction of oven-dried specimen (Agus, 2005).

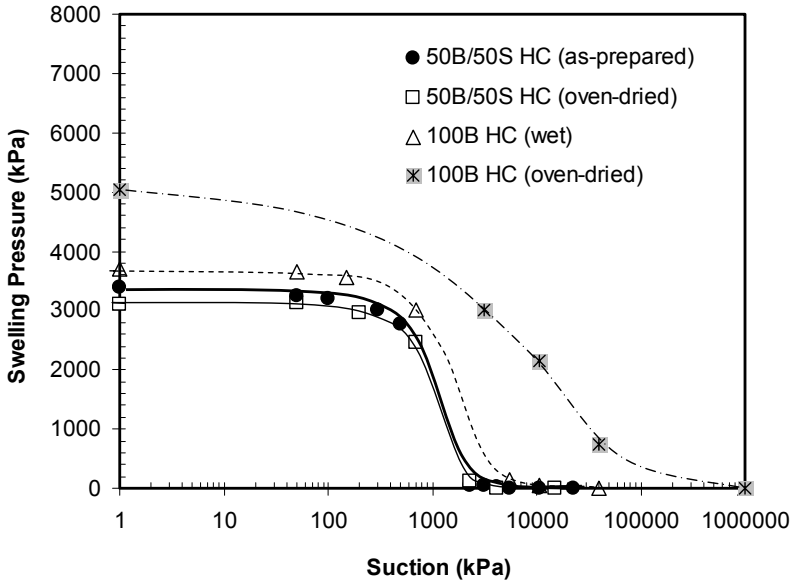

Figure 2.4 Swelling pressure development with decreasing suction for specimen with different initial conditions and bentonite content (Agus, 2005)

CHAPTER 3

TEMPERATURE EFFECTS ON THE HYDRO-MECHANICAL BEHAVIOR OF EXPANSIVE SOILS

3.1 General

This chapter discusses the temperature effects on the hydro-mechanical behavior of compacted expansive soils. The discussion is commenced by describing the aspects related to the expansive soils that are influenced by changing in temperature. The previous investigations regarding temperature effects on the water retention and swelling behavior of compacted bentonite are described.

3.2 Temperature Effects on Aspects related to Soil Behavior

3.2.1 Temperature effects on physical properties of water

Water is one of the components related to soil behavior that are influenced by temperature. Physical properties of water such as density, vapor pressure, viscosity, dielectric constant and surface tension are changed by changing temperature. Table 3.1 summarizes the temperature effects on physical properties of water. The data presented in Table 3.1 was taken from CRC handbook of chemistry and physics.

As shown in Table 3.1, water density decreases by increasing temperature. Since density presents how heavy a material compared to its size (or volume), it means that the weight of water at high temperature is less than the weight of water at low temperature at the same volume.

Table 3.1 also shows that water vapor pressure increases by increasing temperature. The vapor pressure is related to relative humidity (*RH*) which describes the amount of water vapor that exists in a gaseous mixture of air and water. At constant relative humidity, increase in temperature results in increasing the amount of water vapor in air.

Table 3.1 Temperature effects on physical properties of water[‡]

Temperature (°C)	Density (g/cm^3)	Vapor pressure (kPa)	Viscosity (μPa s)	Dielectric constant	Surface tension (mN/m)
0	0.99984	0.6113	1793	87.90	75.64
10	0.99970	1.2281	1307	83.96	74.23
20	0.99821	3.3388	1002	80.20	72.75
30	0.99565	4.2455	797.7	76.60	71.20
40	0.99222	7.3814	653.2	73.17	69.60
50	0.98803	12.344	547.0	69.88	67.94
60	0.98320	19.932	466.5	66.73	66.24
70	0.97778	31.176	404.0	63.73	64.47
80	0.97182	47.373	354.4	60.86	62.67
90	0.96535	70.117	314.5	58.12	60.82
100	0.95840	101.325	281.8	55.51	58.91

[‡]CRC handbook of chemistry and physics, 75th edition (Lide, 1995)

Based on Table 3.1, water viscosity decreases by increasing temperature. Viscosity is commonly perceived as 'thickness' or as resistance of a liquid to flow. Therefore, an increase in temperature results in the decrease in resistance of a liquid to flow. When hot water and cold water are placed in identical capillary tube and allowed to flow under the influence of gravity, cold water takes longer to flow through the tube than hot water. Increase in water viscosity due to increase in temperature is believed to be the reason why permeability of compacted soil increases with the increase in temperature (e.g., Pusch et al., 1990 for calcium and sodium bentonites; Cho et al., 1999 for calcium bentonite; Romero et al., 2003 for Boom clay; Lloret and Villar, 2004 for FEBEX bentonite).

Table 3.1 also shows that dielectric constant of water decreases with increase in temperature. In diffuse double layer theory, dielectric constant is used to calculate the diffuse double layer thickness and surface potential. According to Mitchell (1993), diffuse double layer thickness increases as dielectric constant increases, whereas for constant surface charge, the surface potential function increases as dielectric constant decreases. Therefore, an increase in temperature will result in the decrease in diffuse double layer thickness and the increase in surface potential of clay.

As shown in Table 3.1, temperature also influences surface tension of water. Table 3.1 shows that increase in temperature results in decreasing surface tension. Since surface tension is correlated to capillary pressure which acts in unsaturated soil as a component of matric suction, decrease in surface tension due to increase in temperature also results in decreasing the matric suction of soil.

3.2.2 Temperature effects on pore-water chemistry

Pore-water in expansive clay contains dissolved salt due to high concentration of cation on the surface of the clay to balance its negative charge when the clay is in dry condition. The dissolved salt in the soil pore-water produces one suction component of the expansive clay (i.e., osmotic suction). The osmotic suction is obtained from the total suction of the salt solution and is affected by the consentration of the solution. From relative humidity data, the total suction of salt solution can be calculated using Kelvin equation (Thomson, 1871) that is the thermodynamic relationship between total suction and relative humidity of the vapor space in the soil (Sposito, 1981) (Equation 3.1) and the total suction from osmotic coefficient data was calculated using Equation 3.2 suggested by Lang (1967).

$$s_t = -\frac{RT}{M_w(1/\rho_w)}\ln\left[\frac{RH}{100}\right] \tag{3.1}$$

where s_t is total suction in kPa, R the universal gas constant (i.e., 8.31432 J/mol K), T absolute temperature in Kelvin, M_w the molecular weight of water (i.e., 18.016 kg/kmol), ρ_w the unit weight water in kg/m^3 as a function of temperature, and RH relative humidity.

$$s_t = 2\,m\,R\,T\,\phi \tag{3.2}$$

where s_t is total suction in kPa, m molal salt solution (mol/Kg), R the universal gas constant (i.e., 8.31432 J/mol K), T absolute temperature in Kelvin, ϕ osmotic coefficient.

Since the main ions in the pore-water are Na^+, Ca^{2+}, Mg^{2+}, K^+ and Cl^-, the salt solution in the pore-water are NaCl, $CaCl_2$, $MgCl_2$, and KCl. Figure 3.1.a, 3.1.b, and 3.1d show the temperature effects (i.e., difference between 20 and 80 °C) on the total suction of NaCl, $CaCl_2$, and KCl calculated from osmotic coefficient or relative humidity data of molal salt solution reported by Pitzer et al. (1984), DOW (2003), and Archer (1999), respectively. Calculated from existing data reported by Wang et al. (1998), the change in total suction of $MgCl_2$ due to increase in temperature from 25 to 100 °C is presented in Figure 3.1.c. The change in water density due to temperature change was considered in the calculation.

Figure 3.1 shows that the total suction of molal salt solution increases by increasing temperature except for $CaCl_2$ salt solution. The total suction of molal $CaCl_2$ solution shows slightly decrease by increasing temperature. This is due to anomaly behavior of $CaCl_2$ at high consentration (Phutela and Pitcher, 1983). Phutela and Pitcher (1983) observed a weakness in

the hydrating nature of Ca^{2+} at high concentration of $CaCl_2$. In general, almost no change in the total suction of the salt solutions is found for suction less than 1000 kPa. Figure 3.1 also shows that increase in temperature results in increasing solubility of salt solution. Solubility of $CaCl_2$ increases significantly by increasing temperature. This condition may also affect the behavior of the solution by increasing temperature. Since temperature influences the suction of salt solution, it is important to investigate the pore-water chemistry and osmotic suction of the bentonite used in this study.

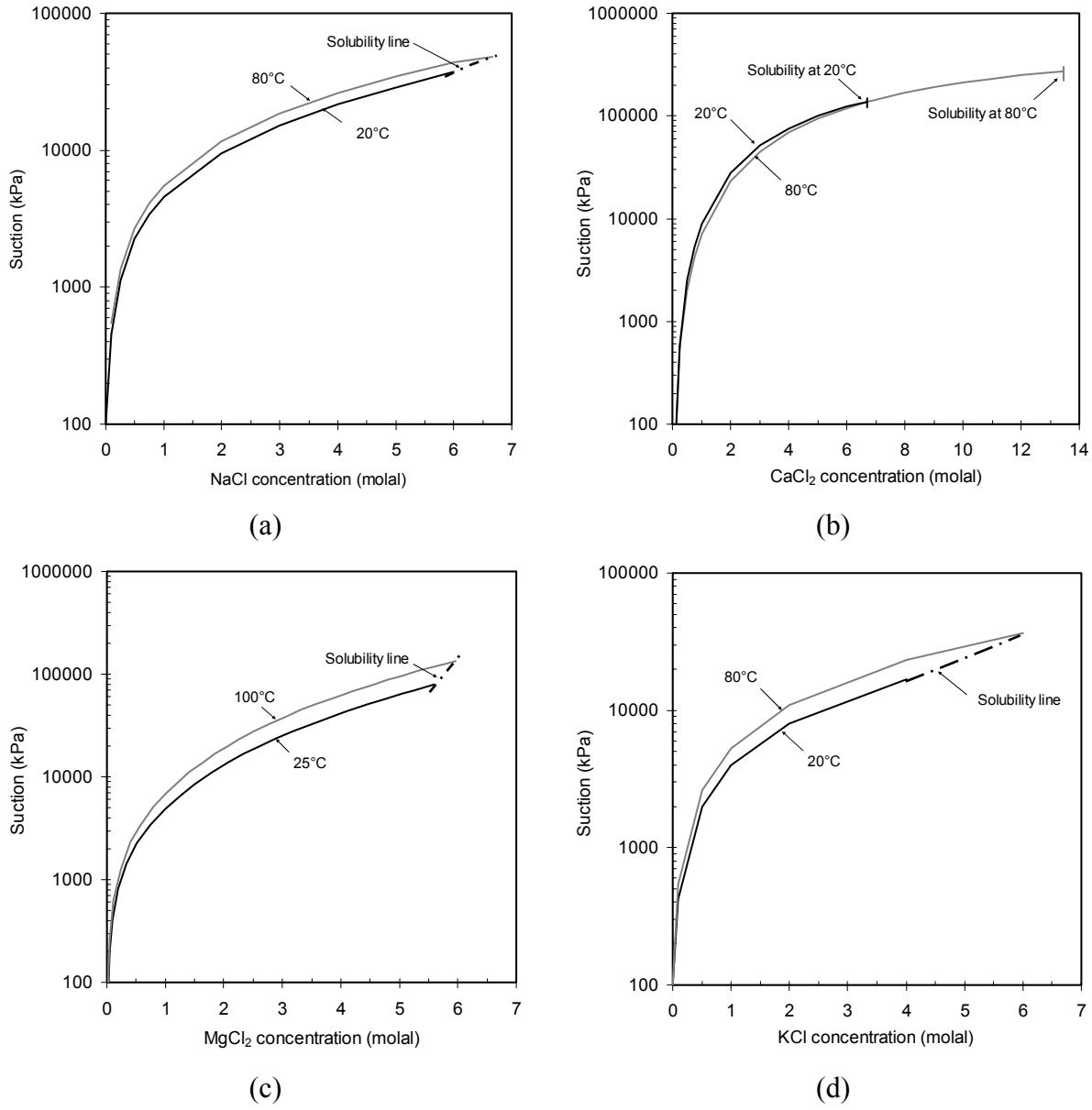

Figure 3.1 Temperature effect on total suction of molal salt solution (a) NaCl, (b) $CaCl_2$, (c) $MgCl_2$, and (d) KCl

3.2.3 Temperature effects on hydration force

The water content and the temperature effects on hydration forces were investigated and analyzed by Woessner (1980), Carlsson (1986) and Pusch et al. (1990) using proton nuclear magnetic resonance (NMR). The NMR technique can be used to determine and distinguish the different states of water (i.e., free and bound states). The different states of water in bentonite were specified by measuring the water proton relaxation time (T_2). Carlsson (1986) used parameter T_2 in order to investigate the internal water (i.e., water bound in between two elementary layers) and external water (i.e, water placed out of two elementary layers). The effects of water content and temperature on different types of bentonite were investigated in the study. It was found that increase in water content from 20-60% resulted in increasing the relaxation time (T_2) due to increase in external water in the bentonite. This is because the frequency of motion of water molecules is high in the external water. Thus, it takes longer time for protons to transfer their magnetic energy to lattice (clay surfaces).

Pusch et al. (1990) analyzed the data reported by Carlsson (1986) by separating the relaxation time (T_2) to relaxation time of the external water (T_b) and relaxation time of internal water (T_s) in order to calculate the number of absorbed water molecule layers in between two elementary layers. It was found that the T_s was extremely short and not significantly dependent on the total water content. It was observed that the internal water layers (i.e., 1-2 hydrates, 2-3 hydrates, and 3 hydrates) were developed for water content of 20, 40, and >50%, respectively.

At constant water content, Carlsson (1986) found that increase in temperature from 20-72 °C results in significantly increasing the proton relaxation time (T_2). The T_2 was almost 50% higher at 72 °C than T_2 at room temperature (i.e., 26 °C). This means that by increasing temperature, the amount of external water increases and the amount of internal water in between elementary layers reduces. Woessner (1980) found the same result on the effect of temperature on sodium saponite and beidelite (i.e., other smectite group minerals). It was found that increase in temperature from room temperature to a moderate temperature (i.e., 80 °C) results in increasing the relaxation time. The relaxation time at 80 °C was two times larger than that at 20 °C. This was because heat reduced in the number of hydrated layers. Carlsson (1986) also found that at the same water content, increase in relaxation time for calcium bentonite due to temperature increase was less than those of potassium and sodium bentonites. This means that the reduction water molecule layers in between elementary layers of calcium bentonite is less than those of potassium and sodium bentonites. In other words,

the internal water of calcium bentonite is more strongly bound in between elementary layers than those of potassium and sodium bentonites.

3.2.4 Temperature effects on diffuse double layer (DDL)

According to the diffuse double layer theory, an increase in temperature should cause an increase in the diffuse double layer thickness and a decrease in the surface potential for a constant surface charge. However, the increase in temperature also results in a decrease in the dielectric constant of the pore-fluid. As a result, the change in temperature does not influence significantly the thickness of diffuse double layer (Mitchell, 1993).

Sridharan and Jayadeva (1982) evaluated the temperature effect on the compressibility of sodium type bentonite using DDL theory. The bentonite had specific surface area of 800 m^2/g, cation exchange capacity of 100 meq/g, cation valance of 1, ion concentration of 10^{-4} and 10^{-1} M. Temperature change from 288-308 K resulted in change in dielectric constant from 82.22 to 75. The effect of temperature on the *d-log p* relationship is shown in Figure 3.2. As shown in the figure, for ion concentration of 10^{-4} M, increase in temperature of 20 K (i.e., from 288-308 K) results in slightly increasing the *d-log p* curve. But for ion concentration of 10^{-1} M, temperature effects on *d-log p* curve at 288 K and *d-log p* curve at 308 K are marginal.

Equations 3.2-3.6 are used by Sridharan and Choudhury (2002) and Tripathy et al. (2004) in order to calculate the swelling pressure of compacted bentonite from DDL theory.

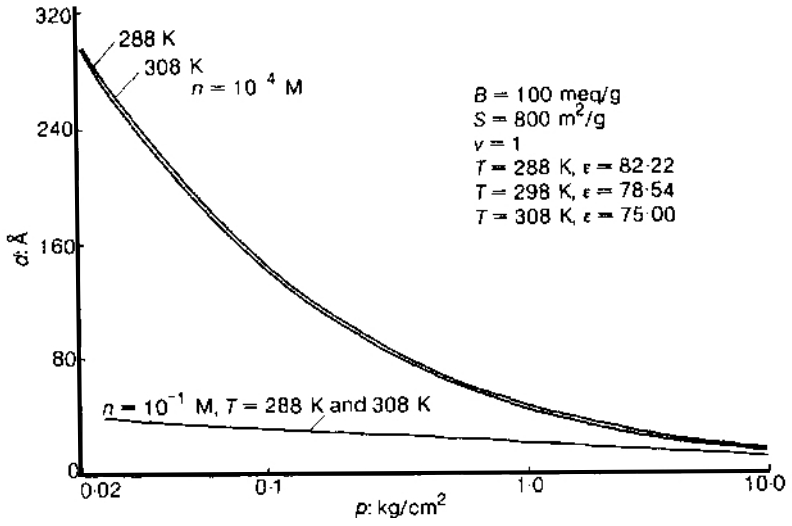

Figure 3.2 temperature effect on *d-log p* relationship calculated from DDL theory (Sridharan and Jayadeva, 1982)

$$e = G\gamma_w S_s\, d \tag{3.2}$$

$$\int_z^u \frac{1}{\sqrt{(2\cosh y - 2\cosh u)}}\, dy = \int_0^z d\xi = -Kd \tag{3.3}$$

$$-\left(\frac{dy}{d\xi}\right)_{x=0} = \sqrt{(2\cosh z - 2\cosh u} \tag{3.4}$$

$$= B / S_s \sqrt{(2\pi / \varepsilon nkT)} \quad at \quad y = z$$

$$p = 2nkT(\cosh u - 1) \tag{3.5}$$

$$K = \sqrt{\frac{8\pi (e')^2 \nu^2 n}{\varepsilon kT}} \tag{3.6}$$

where e is void ratio, G is the specific gravity, γ_w is the unit weight of water in g/cm^3, S_s is the specific surface area of the soil in cm^2/g. ξ is the distance function, y is the nondimensional potential at distance x from the clay surface, z is the nondimensional potential at the clay surface, and u is the nondimensional midplane potential. p is swelling pressure, n is the molar concentration of ions in the pore fluid, k is the Boltzmann's constant, T is the absolute temperature in Kelvin, K is the double layer parameter, and d is the half distance between two clay platelets in cm. e' is the elementary electric charge in esu, ν is the cation valence, and ε is the dielectric constant of the pore fluid.

For calculating swelling pressure from DDL theory, the nondimensional midplane potential function (u) is required. A relationship between u and the nondimensional distance function (Kd) must be established in order to determine u for any given value of Kd. By using n values of 10^{-3}, 10^{-4}, and 10^{-5}M and assuming pressure values of 50-40000 kPa, Tripathy et al. (2004) suggested 3 methods to establish u-Kd relationship from Equation 3.2-3.6. Method 1 considers all u and Kd values for pressure range from 50-20000 kPa, method 2 considers all u and Kd values for n=10^{-4}M, method 3 considers all u and Kd values for pressure range 50-400 kPa. Using the methods suggested by Tripathy et al. (2004), the u-Kd relationships of bentonite used in this study are obtained and summarized in Table 3.2. The calculation considered the change in dielectric constant due to temperature presented in Table 3.1 and physical and chemical properties of Calcigel summarized in Table 4.3 (Chapter 4).

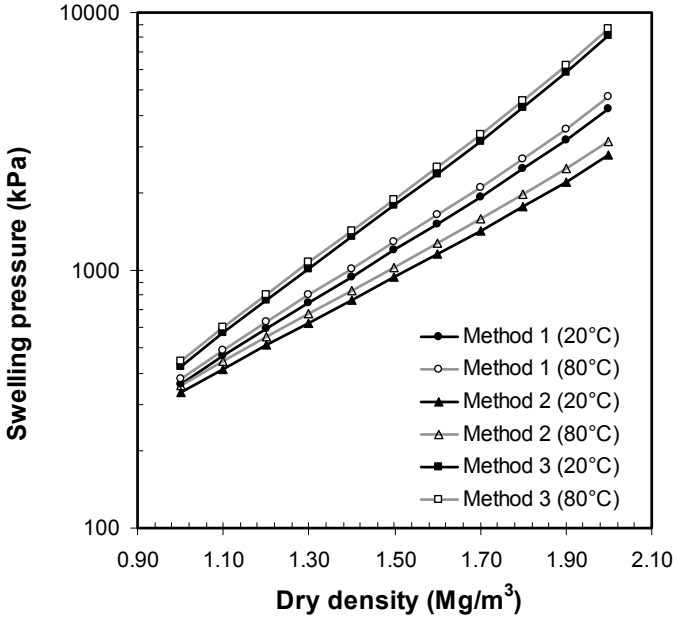

Figure 3.3 Swelling pressure versus dry density calculated from DDL theory

By taking the dry density values from 1.0-2.0 Mg/m^3, Figure 3.3 shows the swelling pressure versus dry density calculated using Equation 3.2, 3.5, and 3.6, and *u-Kd* relationship presented in Table 3.2. Based on Figure 3.3, for all *u-Kd* relationships it is shown that the swelling pressure at 80 °C is higher than swelling pressure at 20 °C. The result agrees with *d-log p* relationship obtained by Sridharan and Jayadeva (1982) presented in Figure 3.2. Based on Figure 3.2, at constant *d* value the pressure at 80 °C is higher than the pressure at 20 °C.

3.2.5 Temperature effects on micro structure of compacted clay

Romero and Li (2005) investigated the temperature effect on the pore size distribution of compacted OPHELIE mixture (i.e., 60%FoCa clay, 35% sand, and 5% graphite on dry mass basis). The specimen had initial dry density of 2.01-2.07 Mg/m^3, water content of 9%, and initial suction of 83-122 MPa. The specimens were hydrated at two different temperatures (i.e., 22 and 80 °C). The result is shown in Figure 3.4.

Table 3.2 Summary of *u-Kd* relationships calculated from Equations 3.2-3.6.

	Method 1	Method 2	Method 3
Temperature	*u*	*u*	*u*
20 °C (293 K)	2.569-3.758 log(*Kd*)	3.326-3.257 log(*Kd*)	2.029-4.521 log(*Kd*)
80 °C (253 K)	2.520-3.835 log(*Kd*)	3.221-3.352 log(*Kd*)	2.064-4.534 log(*Kd*)

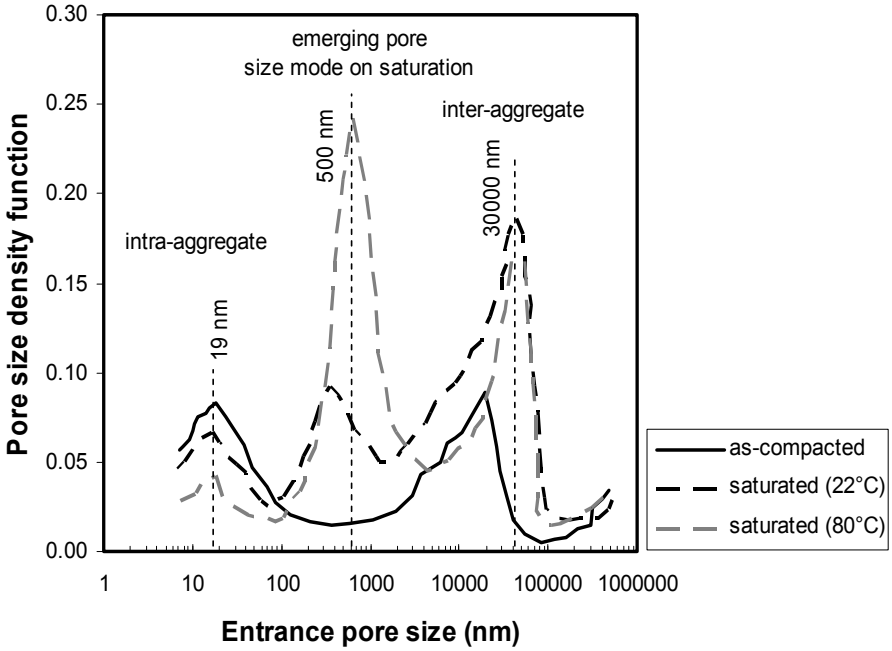

Figure 3.4 Pore size distribution of compacted OPHELIE at two different temperatures (Romero and Li, 2005)

As shown in Figure 3.4, the as-compacted specimen shows bimodal pore-size distribution (i.e., intra-aggregate pores and inter-aggregate pores). For specimen saturated at 22 °C, a new mode of pore emerges in between the inter-aggregate pore and intra-aggregate pore. This is thought as a result of separation of elementary layers due to hydration. For specimen saturated at 80 °C, it is shown that decrease in intra-aggregate pores is significantly larger than that of specimen saturated at 22 °C. A new mode of pore size also emerges in between the inter-aggregate pore and intra-aggregate pore. The peak of new mode of pore size for specimen saturated at 80 °C is significantly larger than that of specimen saturated at 22 °C. Figure 3.4 also shows that the inter-aggregate pores of both specimens are almost the same. These results reviel that increase in temperature influences the intra-aggregate pores (i.e., in between the elementary layers and in between particles or crystals) due to change in hydration force and diffuse double layer.

3.2.6 Temperature effects on clay mineralogy

The increase in temperature may cause the smectite mineral to become unstable and transform to more stable silicate phases or known as illitation. This also results in decreasing the ability of the bentonite to retain water. The kinetics of the smectite to illite reaction strongly depends on temperature, time, and K^+ pore-water concentration (Wersin et al., 2006). de la Fuente et al. (2000) found that the transformation to illite occurred to the bentonite undergo heating for 180-360 days at temperatures of 120-160 °C which is higher than

maximum temperature considered for bentonite buffer (i.e., 80 °C). Drief et al. (2002) found that the transformation from smectite to illite also occurs to the smectite heated up to 50 °C for 30 days in K-enriched sea water solution. But for K-rich bentonite, a smectite-illite transformation is possible without external supply of K^+ (Drief and Nieto, 2000). Based on these results, it is very important to understand the pore-water chemistry of the bentonite related to temperature effect since the pore-water chemistry affects not only on the osmotic component of total suction as discussed in section 3.2.2 but also on the mineralogy of the bentonite.

Besides illitation, the cementation also occurs to the bentonite exposed to elevated temperature. Pusch (2000) reported precipitated Si on the surfaces of the MX80 aggregates heated up to 110 °C resulting coherent particle aggregates. Mokrejš et al. (2005) stated the reduction in the water absorption of calcium type bentonite due to formation of a covalent bonding between Ca^{2+} with clay surface after heating at temperature higher than 100 °C.

3.3 Temperature Effects of Hydro-Mechanical Behavior of Compacted Clay

3.3.1 Water retention behavior

Tang and Cui (2005) investigated the temperature effects on water retention behavior of compacted sodium type bentonite (i.e., MX80) from as prepared condition using vapor equilibrium technique (VET) in desiccator. It was found that the water retention curve of compacted bentonite at 20 °C was placed above the water retention curve of compacted bentonite at 80 °C. It means that increase in temperature results in decreasing the ability of bentonite to retain water. They found that for a given water content, the suction change rate by increasing temperature was -2.9×10^{-3} (log Mpa/°C). Tang and Cui (2005) compared the value with a calculation using Jurin's law (Jurin, 1718). The calculation is based on assumsion that the suction is due to capillary pressure and a function of pore radius. From calculation, they found that the suction change rate by increasing temperature is -1.1×10^{-3} (log Mpa/°C). They concluded that the reduction of water retention was due to reduction in surface tension or capillary component, eventhough their experimental result showed two times larger than the calculation using Jurin's law.

Using VET, Romero et al. (2000) performed a study on the effects of temperature on the water retention behavior of Boom clay. The results indicated that for a given water content, total suction at 20 °C was higher than that at 80 °C. The change in total suction obtained from the experiment was higher than the change in total suction due to the change in

the surface tension of water. Romero et al. (2000) stated that the differences are not only due to the change in the surface tension but also due to the change in the clay fabric and the pore-water chemistry of the clay. The change in the clay fabric and pore-water chemistry due to temperature is expected to be irreversible (Romero et al., 2000).

Villar and Lloret (2004) investigated the water retention behavior of compacted calcium-type bentonite (FEBEX) also using VET in desiccator. In the study, the effects of confined and unconfined condition were observed. They found that the water retention curve of compacted bentonite at 20 °C was placed over the water retention curve of compacted betonite at 80 °C for both conditions (i.e., unconfined and confined conditions). Villar and Lloret (2004) had the same opinion as Romero et al. (2000) that the reduction in water retention behavior of compacted bentonite by increasing temperature was not only due to reduction in surface tension of water but also due to alteration of clay fabric and intra-aggregate fluid chemistry. Villar and Lloret (2004) also found that retention capacity of swelling material was highly affected by boundary conditions (i.e., confined or unconfined conditions) of the specimen. The retention capacity of specimen in unconfined condition was higher than that of specimen in confined condition.

3.3.2 Swelling behavior of compacted bentonite

Temperature effects on swelling strain of compacted bentonite

Temperature effects on the swelling strain or swelling under load have been investigated by some researchers (e.g., Komine and Ogata, 1998; Romero et al. (2005); Villar and Lloret, 2004). For the same vertical load (i.e., 500 kPa), Romero et al. (2005) reported that increase in temperature (i.e., from 30-80 °C) resulted in decreasing swelling strain of compacted FEBEX bentonite. For different vertical loads (i.e., 500, 1500, and 3000 kPa), Lloret and Villar (2004) found that the reduction in swelling strain due to increase in temperature decreases by increasing vertical load. This reduction is due to decrease in hydration in between the elementary layers which is the prevailing mechanism in the swelling of calcium-type bentonite (Pusch et al., 1990). Moreover, Lloret and Villar (2004) stated that increase in temperature forced movement of high density intra-aggregate water to free inter-aggregate water which occupies a higher volume.

Temperature effects on swelling pressure of compacted bentonite

Earlier investigations on the swelling pressure show that the increase in temperature induced increase in the swelling pressure of bentonite (e.g., Pusch et al., 1990 for Na-bentonite). Pusch et al. (1990) stated that the increase in temperature of a bentonite decreased the hydration force due to a reduction in the number of hydrates in the smectite surface within bentonite and increased the osmotic pressure in the molecular system. These led to reduction or increase in the swelling pressure of compacted bentonite depending on the dominant factor happen in the type of bentonite used. In case of Na-bentonite that diffuse double layer is dominant, the increase in temperature results in increasing double layer repulsion of adjacent particles. This is analogous to the heat-induced increase in osmotic pressure in ionic or molecular system (see section 3.2.2) which leads to increase in the swelling pressure. Interestingly, Cho et al. (2000) reported that increase in temperature results in increasing swelling pressure of Ca-bentonite used in their study. Cho et al. (2000) stated that besides the balance between the two components (i.e., hydration force and osmotic pressure), increase in temperature also results in increasing pore-water pressure due to the differences of thermal expansion of the pore water and the skeleton. However, there is no information about pore-water chemistry and osmotic suction of the bentonite used in the study performed by Cho et al. (2000).

Pusch et al. (1990) and Villar and Lloret (2004) found that increase in temperature results in decreasing swelling pressure of Ca-bentonite and FEBEX bentonite (i.e., Ca-Mg-bentonite), respectively. Pusch et al. (1990) stated that the reduction in swelling pressure of calcium-type bentonite by increasing temperature was due to reduction in hydration force in between the elementary layers which is dominant in the swelling pressure development of Ca-bentonite. ENRESA (2000) reported the electric conductivity of soil pore-water of FEBEX from 7.5-13.2 mS/cm at water content from 23-30%. Using correlation between electric conductivity versus osmotic pressure reported by Fredlund and Rahardjo (1993), the specimens have osmotic pressure of 319-579 kPa which is very small compared to the total suction of FEBEX at the same water content range (i.e., 3500-35000 kPa). The data shows that matric components (i.e., hydration force and capillary component) are dominant in this type bentonite. However, at saturated condition the capillary component is neglectable. Therefore, temperature increase results in decreasing swelling pressure due to decrease in hydration force.

Romero et al. (2003) reported the temperature effects on controlled-suction swelling pressure test or multi-step swelling pressure test for compacted Boom clay. They found that the swelling pressure values at each equilibrium suctions (i.e., 4500, 2000, 600 kPa, and saturated condition) at 22 °C are higher than those at 80 °C. In the study, drying-wetting tests at both temperatures were also performed. They found the reversible response of the specimen to the drying-wetting paths showing no significant changes in the micro structure and mineralogy in the specimen at temperature range from 20-80 °C in constant volume condition.

This page intentionally left blank

CHAPTER 4

MATERIAL PROPERTIES

4.1 General

The materials used in this study are Calcigel and quartz sand. The Calcigel was mined from Bavaria, Southern part of Germany. This chapter discusses mainly basic and physical, chemical, and mineralogical properties of the Calcigel. Several properties of the material used were obtained from the experiments in this study. The others were collected from previous studies.

4.2 Basic Properties

The basic properties investigated in this study included the determination of specific gravity, grain-size distribution, and Atterberg limits. The tests were performed based on ASTM standards (ASTM, 1997) and DIN standards (DIN, 1987).

For specific gravity determination, method proposed in DIN 18124 KP (DIN, 1987) was adopted in this study. The method proposed in ASTM D 854 (ASTM, 1987) for high plastic clay was performed for comparison. In order to release entrapped air in the specimen, the picnometer with the saturated specimen was placed on sand bath and stirred carefully. The test was performed in 5-7 days to ensure that there is no entrapped air in the specimen. This is longer than time proposed by DIN and ASTM standard (i.e., only 2 hours). The specific gravity of 2.794 and 2.808 were obtained from the tests based on DIN and ASTM standard, respectively. The average specific gravity of 2.8 was used in this study.

The Atterberg limits were performed according to DIN 18 122 (DIN, 1987). The tests included the liquid limit using Casagrande, the plastic limit, and the shrinkage limit determination. Additional test for the liquid limit was performed according to British standard BS 1377 (British Standards Institution, 1990) using fall cone penetration test. The samples were mixed with distilled water to reach different values of water content and remixed everyday for minimum one week before investigation. The liquid limit using Casagrande, the plastic limit, and the shrinkage limit obtained were 178%, 56%, and 18%, respectively. The

result of the liquid limit determination using fall cone penetration test is shown in Figure 4.1.a. From the figure, the liquid limit obtained using this method is 180%.

The grain size distribution of Calcigel was investigated using sedimentation method (i.e., DIN 18123-7) (DIN, 1987) and laser particle sizer. In the sedimentation method, the sample was dispersed using a dispersing solution (i.e., sodium pyrophosphate) during experiment. The result is shown in Figure 4.1.b. As shown in Figure 4.1.b, the amount of clay particle size fraction is 40%. Using laser particle sizer, the amount of clay size fraction in the Calcigel is 15%. The result shows that the amount of clay fraction obtained using sedimentation method is higher than that obtained using laser particle sizer. This is because for sedimentation method, the specimen was dispersed using dispersing agent. This results in more dissociated structure than that of using particle sizer. In addition, for the sedimentation method the particle size is calculated using Stokes equation (DIN 18123-7) that is dependent on the surface area of the particle. For laser particle sizer, the particle size is related to the particle volume and assumed to have sperical shape (Campbell, 2003). Since soil contains a mixture of particles with non-sperical shape, the particle size obtained using laser particle sizer always shows higher value due to the volume over estimation effects (Campbell, 2003).

4.3 Physical, Chemical, Mineralogical Characterisations

In this study, the physical, chemical, and mineralogical of the bentonite are of concern since it has been known that the bentonite behavior such as compressibility, swelling

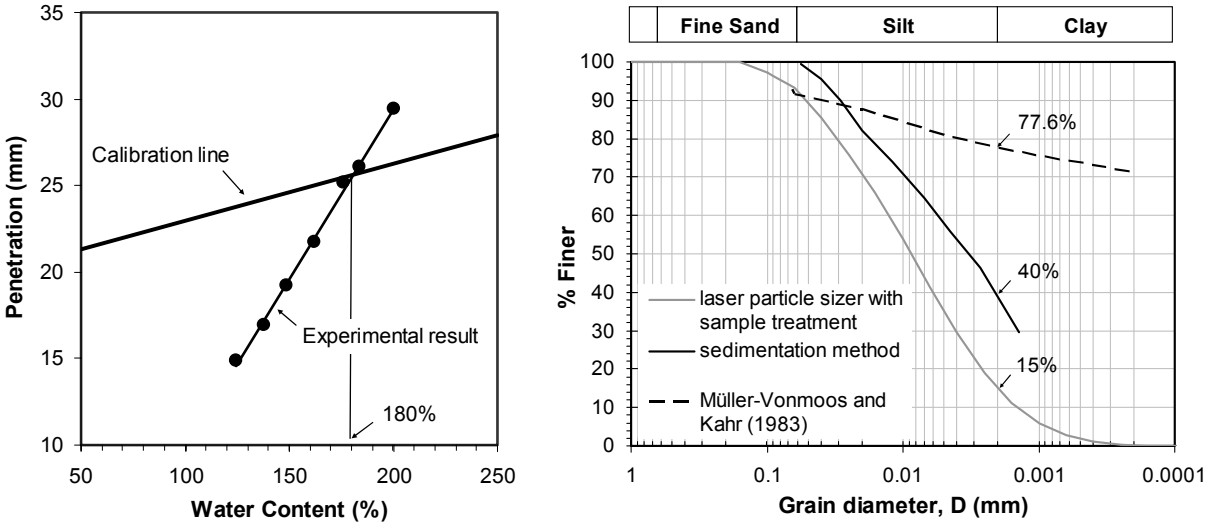

(a) (b)

Figure 4.1 (a) Fall cone penetration result, and (b) grain size distribution of Calcigel

behavior, permeability, etc are controlled by its physical, chemical, and mineralogical properties. The physical, chemical, and mineralogical determinations of bentonite used in this study included determination of specific surface area (S_s), cation exchange capacity (CEC), and mineralogical and chemical compositions.

4.3.1 Specific surface area

In clay soils (i.e., including bentonite-based material), the water is located in between clay particles and also within clay particles. Therefore, both external specific surface which represents the area of external particles and total specific surface area which represent the area of internal- and external-particles are considered in this study.

The external specific surface area was investigated using Brunette-Emmet-Teller (BET) method (Chiou et al., 1993, ASTM 1997 (D3663-03)). The method uses a rule of physical adsorption of gas molecules on a solid surface. The external specific surface area of the material used in this study is 67 m^2/g. The result obtained is in the range of external specific surface area of montmorillonite clay (i.e, 50-120 m^2/g) (Mitchell, 1993).

The total specific surface area was determined using Ethylene Glycol Monoethyl Ether (EGME) method (Cerato and Lutenegger, 2002). The amount of EGME, age of desiccant, amount of soil tested, and size of desiccator used were considered carefully. The total specific area of material used in this study was 525 m^2/g.

The specific surface area can also be determined using the pore size distribution (PSD) calculated from mercury intrusion porosimetry (MIP) result (Romero, 1999). The specific surface area values were calculated by assumption of the cylindrical shape pores using Equation 5.1 discussed in Section 5.3.1. Figure 4.2 shows the specific surface area of compacted Calcigel and Calcigel-sand mixture calculated from MIP data based on method used by Romero (1999). The specimens were pure bentonite, namely 100B and bentonite-sand mixture with proportion by weight of 50% bentonite and 50% sand, namely 50B/50S. The specimens were compacted in two different conditions from the Proctor curve (i.e., dry of optimum (DOP) and wet of optimum (WOP)). The preparation and initial condition of the specimen are presented in Chapter 5. The mercury intrusion porosimetry (MIP) result is also presented and discussed in Chapter 5. As shown in Figure 4.2, the specific surface area of 100B DOP and 100B WOP specimens are 193 m^2/g and 143 m^2/g, respectively. The values are smaller than those obtained using EGME method because the non-intruded pores by mercury which is observed and discussed in Chapter 5 were not taken into account. The

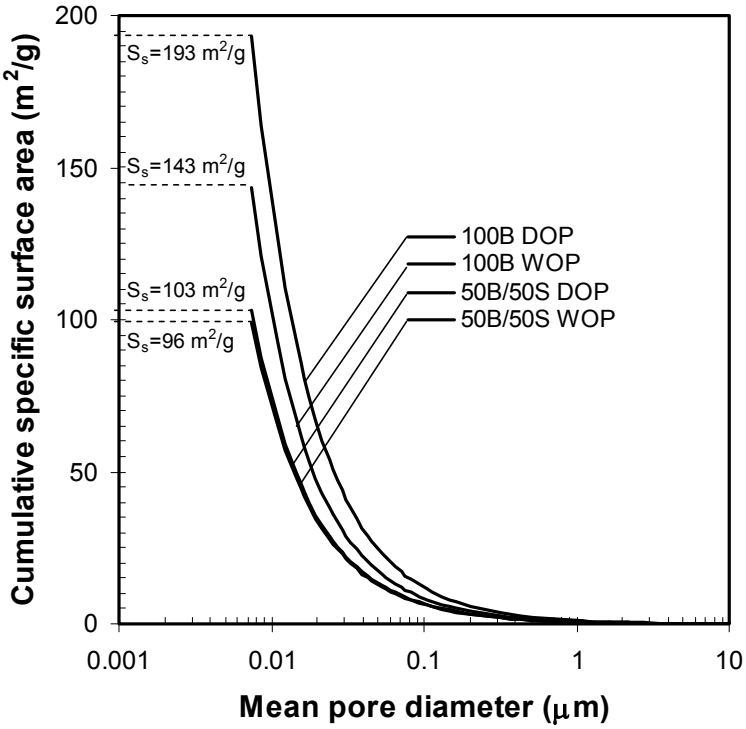

Figure 4.2 Specific surface area of compacted bentonite (Calcigel) and bentonite-sand mixture from MIP data

different values between 100B DOP and WOP specimens are due to different amount of non-intruded pores for different water content of the specimens. The specific surface area of 50B/50S DOP and WOP specimens are approximately a half of those of 100B specimen i.e., 103 m^2/g and 96 m^2/g, respectively.

4.3.2 Cation Exchange Capacity (CEC)

In this study, the CEC was measured using silver thiourea (AgTU) method according to Dohrmann (1997). The specimen was saturated with calcium carbonate prior to investigation since it was found the amount of calcium carbonate in the specimen. The result obtained from this method is called potential CEC. The potential CEC of specimen used in this study is 74 meq/100g. The amount of basic exchangeable cations (i.e., Na^+, K^+, Ca^{2+}, and Mg^{2+}) was determined using inductively couples plasma atomic emission (ICP) according to the European Standard EN ISO 11885 (1985). The amount of cations (i.e., Na^+, Ca^{2+}, and Mg^{2+}) are 2, 29, and 17 meq/100g, respectively. The K^+ is not found in this bentonite. Therefore, the total of basic exchangeable cations is 48 meq/100g. The differences between the potential CEC with the total of basic exchangeable cations are possibly due to the presence of carbonate (i.e., Dolomite), which is calcium magnesium-rich in the crystals.

Herbert and Moog (2002) have reported the CEC of Calcigel of 49 meq/100g using Ammonium Acetat method. The value is smaller than that of reported by Müller-Vonmoos and Kahr (1983) using the same method. Müller-Vonmoos and Kahr (1983) reported the CEC of 62 meq/100g with the amount of Na^{+}, Ca^{2+}, Mg^{2+}, and K^{+} exchangeable cations of 1.8, 37.6, 22.4, and 0.2 meq/100g, respectively.

4.3.3 Mineralogy and Chemical Compositions

In this study, the mineralogy of Calcigel was investigated using X-ray diffraction (XRD) method. The result is shown in Figure 4.3. The result shows that the predominant clay mineral of Calcigel used in this study are montmorillonite, muscovite which is known as common mica, quartz, chlorite, Anorthite which is one of the plagioclase feldspars, and Dolomite which is the sedimentary carbonate rock and composed of calcium-magnesium carbonate in crystals. The predominant clay mineral of Calcigel used in this study is similar to the mineral composition of Calcigel reported by Müller-Vonmoos and Kahr (1983) and Agus (2005) as shown in Table 4.1.

The chemical composition of Calcigel was determined using emission spectroscopy method. The result is summarized in Table 4.2. The chemical compositions of Calcigel used in this study are similar to the chemical compositions of Calcigel reported by Müller-Vonmoos and Kahr (1983) and Agus (2005) particularly for the predominant chemical compounds such as SiO, Al_2O_3, FeO_3, MgO, and CaO.

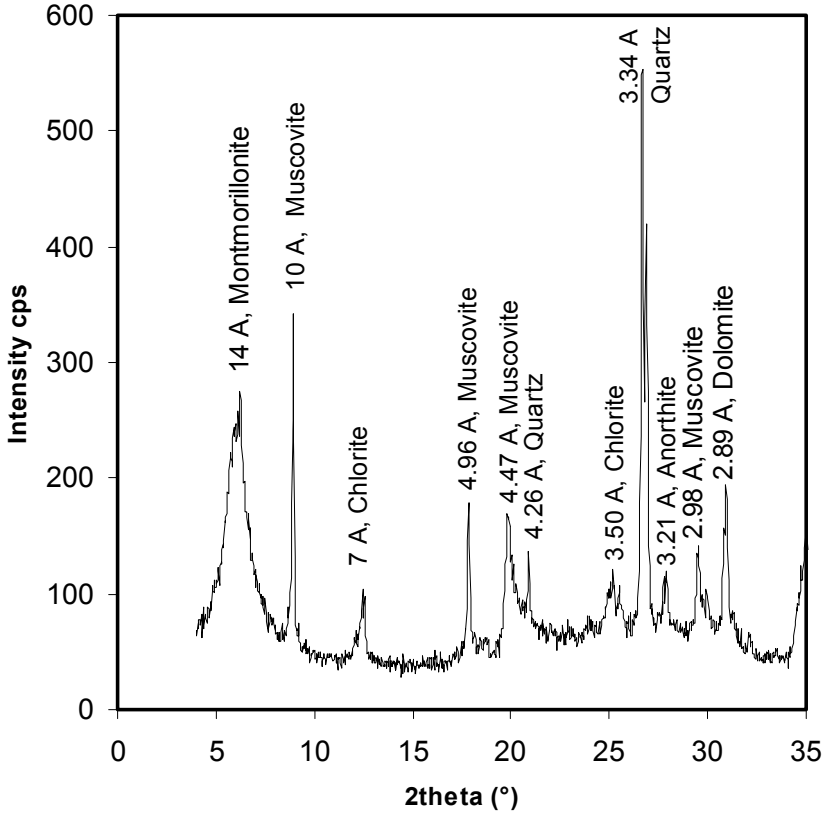

Figure 4.3 X-ray diffraction result of Calcigel

Table 4.1. Mineral compositions of Calcigel

Mineral	Montmorillonite	Quartz	Feldspar	Mica	Carbonate	Calcite	Dolomite	Others
Müller-Vonmoos and Kahr (1983) %	66	8.3	2-4	12-15	3.8	-	-	8
Agus (2005) %	50-60	5-10	5-8	-	-	1-5	10-15	2-29

Table 4.2 Chemical compositions of Calcigel

Chemical	SiO	Al_2O_3	Fe_2O_3	FeO	MgO	CaO	Na_2O	K_2O	MnO	CO_2	TiO_2
In this study	50	17	5	-	4	4	-	1	-	-	-
Müller-Vonmoos and Kahr (1983) %	58.35	18.52	5.51	0.17	3.12	1.87	0.07	0.73	0.02	-	traces
Agus (2005) %	53.2	18.4	5.4	-	3.8	3.6	0.74	1.7	0.05	2.78	0.32

4.4 Summary of Material Characteristics

Table 4.3 summarizes characteristics of bentonite used in this study. The properties of sand used in this study reported by Agus (2005) are summarized in Table 4.4.

Table 4.3 Summary of properties of bentonite used in this study

Properties	**Calcigel**
Specific gravity	2.80
Liquid limit (%)	180
Plastic limit (%)	56
Plasticity index (%)	124
Shrinkage limit (%)	18
Clay content (%)	40
Fine content (%)	100
External specific surface area (m^2/g)	67
Total specific surface area (m^2/g)	525
Cation exchange capacity (meq/100g)	74
Basic exchangeable cation Na^+, Ca^{2+}, Mg^{2+}, K^+ (meq/100g)	2, 29, 17, 0
Total basic exchangeable cation (meq/100g)	48
Monmorillonite content (%)	50-60[§]

[§]Agus (2005) determined using XRD

Table 4.4 Summary of sand characteristics (Agus, 2005)

Properties	
Specific gravity	2.65
D_{10}	0.25
D_{60}	0.40
D_{30}	0.70
Specific surface area (m^2/g)	0.25

This page intentionally left blank

CHAPTER 5

MICROSTRUCTURE STUDY

5.1 Introduction

The pore size distribution (PSD) obtained from mercury intrusion porosimetry (MIP) test has been used to study the microstructure of clays. Generally, it was found from the MIP results that compacted clays show bimodal PSD (i.e., micro-pores and macro-pores) (e.g., Delage et al., 1996 for illite, Thom et al., 2007 for kaolinite, and Agus and Schanz, 2005c for heavily compacted bentonite-sand mixture).

In the MIP test, specimen preparation and drying process are very important. Diamond (1970) found that dry specimen was much less affected by oven drying. However, a large shrinkage (i.e., 20%) was found for wet specimen in air-drying method (Diamond, 1970). Delage et al. (1996) reported the effect of compaction conditions (i.e., dry of optimum (DOP), optimum (OP), and wet of optimum (WOP)) on the PSD curves of Jossigny silt. To avoid change in PSD of the specimens in the drying process, freeze drying method was used before MIP test. Delage et al. (1996) found that the PSD of DOP specimen shows a clear bimodal PSD whereas the PSD of OP and WOP specimens tend to have unimodal PSD. Different from low plastic clay (e.g., kaolinite and illite) where the mercury fills entire pores, the non-intruded pores have been found in the highly plastic clay such as bentonite (Lloret et al., 2003 for Almeria clay, Agus and Schanz, 2005c for heavily compacted bentonite-sand mixture, and Delage et al., 2006 for MX-80). The total non-intruded pores increase by increasing the water content of the specimen as shown in the PSD data reported by Agus and Schanz (2005c) and Delage et al. (2006).

For the specimen which is hydrated in confined condition, the sample preparations including freeze drying must be considered carefully. By considering the permeability and microstructure of compacted bentonite, Delage et al. (2006) stated that the immediate stress release modifies mainly the macro-pores (i.e., inter-aggregate pores) due to decrease in inter-aggregate stresses and hence allowing global volume expansion. They stated that no change in

the micro-pores occurs due to the very small pore size, slow water transfer phenomena, and strong attraction between water and minerals.

Delage et al. (2006) also investigated the density effects on the PSD of compacted MX-80. It was found that, at the same water content, the change in porosity of specimen compacted with higher dry density was due to the change in the large pores. These large pores correspond to the pore located between clay aggregates or inter-aggregate pores.

The MIP study has been used to investigate the PSD of compacted different type of bentonite and sand mixtures after wetting process (Agus and Schanz, 2005c; Cui et al., 2002a). Agus and Schanz (2005c) used Calcigel which is Ca-Mg bentonite whereas Cui et al. (2002a) used Kunigel which is Na bentonite. Wetting in unconfined condition of heavily compacted Calcigel bentonite-sand mixture resulted in enlarging and separating of the aggregates (Agus and Schanz, 2005c). Besides enlarging and separating the aggregates, wetting by decreasing suction at constant volume condition resulted in separating of clay sheets in the aggregate of Kunigel (Cui et al., 2002a).

For different purposes, the PSD data obtained from MIP test has been used to predict specific surface area, saturated coefficient of permeability, and soil water characteristic curve of compacted clay (Romero, 1999). However, the predictions using the PSD data are not valid for compacted bentonite-sand mixture due to presence of the non-intruded pores, changing in PSD during wetting, osmotic effects, and hydration force. Agus and Schanz (2005c) found the hysteresis between the experimental result and prediction of SWCC of heavily compacted bentonite-sand mixture.

Besides the PSD data, photografs of clay fabric obtained from scanning electron microscopy (SEM) and environmental scanning electron microscopy (ESEM) have been used to study microstructure of compacted clay (e.g., Delage et al., 1996; Cui et al., 2002a; Agus and Schanz, 2005c). Delage et al. (1996) found that a granular aggregate structure with inter-aggregate pore was developed in the illite compacted at DOP condition whereas a structure of clay matrix that envelops silt grain and fills the inter-aggregate pores was found in the specimen compacted at WOP condition. For compacted bentonite-sand mixture, a wavy flake-like structure was observed for the bentonite with high water content (Cui et al., 2002a and Agus, 2005). This results in very thin intra-aggregate pores and mercury can not intrude to these pores (Delage, 2007).

In this study, the MIP data was used to study the distribution of pores (i.e., micro-pores and macro-pores) of bentonite and bentonite-sand mixture compacted at different conditions (i.e., dry of optimum and wet of optimum). The change in the PSD of heavily compacted bentonite-sand mixture specimen that was hydrated under constant volume condition was also investigated in this study. For heavily compacted bentonite-sand mixture, the result is compared to the PSD of the specimen from as-prepared condition reported by Agus and Schanz (2005c). The ESEM photografs were used to support the result obtained from MIP test.

5.2 Experimental techniques

Two types of specimens were prepared with different bentonite contents (on a dry mass basis); namely, 50B/50S for specimen with bentonite content of 50% and 100B for pure bentonite specimen. The sand was sieved through 2-mm sieve openings before mixing. The sufficient amount of water was added to the specimens to reach the target water content based on standard Proctor curves presented in Chapter 6. The mixtures were stored in the two layers plastic bag for 2 weeks for equalisation. The specimens were statically compacted to reach desired dry densities. The initial conditions of specimens tested are summarised in Table 5.1.

The heavily compacted bentonite-sand mixture was used in this study. The specimen was mixtures of 50% bentonite and 50% sand, namely 50B/50S HC. The specimen was hydrated under constant volume condition in the UPC isochoric cell (Villar et al., 2001; Agus and Schanz, 2005a) in order to obtain the saturated specimen under constant volume condition. The method used in swelling pressure test is described in Chapter 9. The initial condition of the heavily compacted specimen tested in this study is presented in Table 5.1.

Table 5.1 Summary of initial conditions of specimens tested in this study.

Specimen		Water content (%)	Dry density (Mg/m^3)	Initial total suction* (kPa)
100B	DOP	24	1.17	6524
	WOP	45	1.17	406
50B/50S	DOP	14	1.61	2186
	WOP	24	1.61	271
50B/50S	HC	9	2.00	22700

*measured using chilled-mirror hygrometer

The specimens were cut into a small cubic with approximately 1 cm length. The specimen was freeze-dried prior to the MIP test. The MIP equipment used was Autopore II 9220 from micromeritics, Berlin.

In order to investigate the fabric of bentonite used, environmental scanning electron microscope (ESEM) type-XL30 from Philips was used. In this study, the fabrics of low compacted bentonite and bentonite-sand mixture at DOP and WOP conditions were investigated.

5.3 Results and Discussion

5.3.1 Pore-size distribution of compacted bentonite and bentonite-sand mixtures

The MIP test results have been interpreted using Washburn method (Washburn, 1921; Sridharan et al., 1971; and Al-Mukhtar, 1995). The pores in the specimens are assumed to be cylindrical shape. The relationship between the intrusion pressure (p_{int}) and the pore diameter (d_p) is calculated using Equation 5.1.

$$p_{\text{int}} = -\frac{4\sigma_{Hg}\cos\theta_{hw}}{d_p} \tag{5.1}$$

where σ_{Hg} is the surface tension of mercury (i.e., 0.484 N/m at 25 °C) and θ_{hw} is the contact angle between mercury and pore-water wall (i.e., 141.3°).

Figure 5.1.a and 5.1.b show the method to determine the limit between micro-pore and macro-pore for the 100B and 50B/50S specimens, respectively. This method follows the method suggested by Agus (2005). As shown in Figure 5.1.a, the limits of micro- and macro-pores of 100B DOP and WOP specimens are approximately 0.03 and 0.04 μm, respectively. Figure 5.1.b shows that the limits of micro- and macro-pores of 50B/50S DOP and WOP specimens are the same (i.e., 0.035 μm).

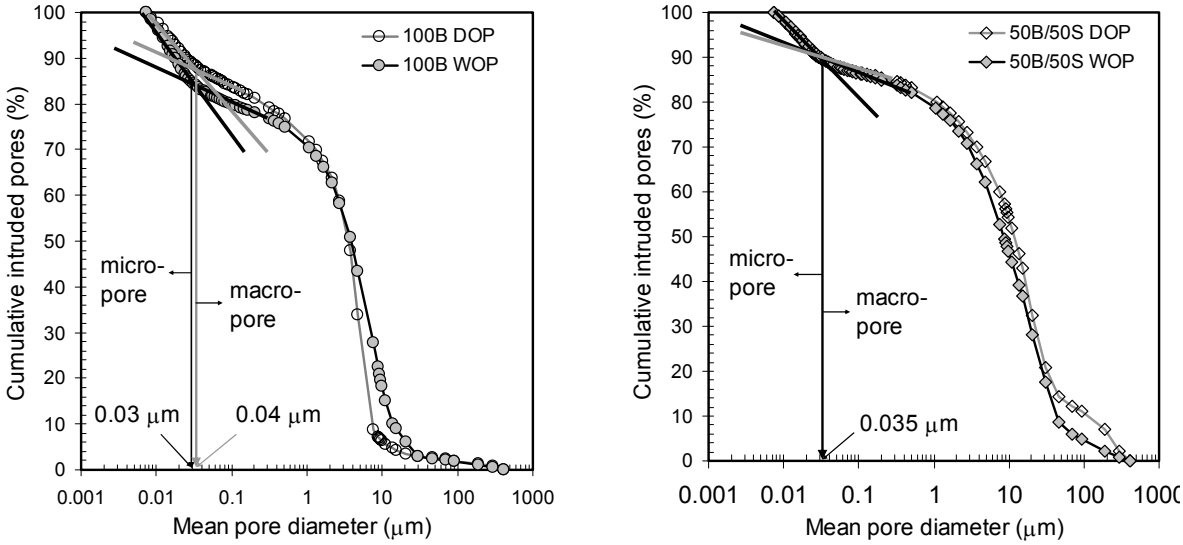

(a) (b)

Figure 5.1 Determination of limits between micro-and macro-pores from the PSD data (a) 100B specimens and (b) 50B/50S specimens

Figure 5.2 shows the pore-size distribution (PSD) curves of the compacted bentonite (i.e., 100B DOP and 100B WOP specimens) tested in this study. The figure shows that the two PSD curves show the same shape. However, the PSD of 100B WOP is placed below the PSD of 100B DOP. It is found also that the total non-intruded pores volume of 100B WOP specimen is larger than that of 100B DOP specimen. The result agrees well with the result reported by Delage et al, 2006 for a sodium type of bentonite (i.e., MX 80) that higher specimen water content results in larger the total non-intruded pores volume.

Figure 5.2.b. shows curves of the mean pore diameter of pores versus percentage of intruded pores. As shown in Figure 5.2.b, the curves show like a uni-modal PSD since the peak of pore size distribution in the micro-pores level is not clearly shown. However, considering the non-intruded pores are the intra-laminar pores which are existed in the intra-aggregate pores, actually the two specimens have bimodal pore size distribution. The figure also shows that the pore population of both specimens are the same with very small different in the pores with diameter higher than 10 μm. As shown in the figure, the diameter of macro-pores (i.e., inter-aggregate pores) are concentrated at 5 μm. The percentage of pores of 100B WOP specimen at corresponding diameter is lower than that of 100B DOP specimen. This is because, at higher water content, the aggregates enlarge and soft enough to deform and fill the inter-aggregates pores during the compaction.

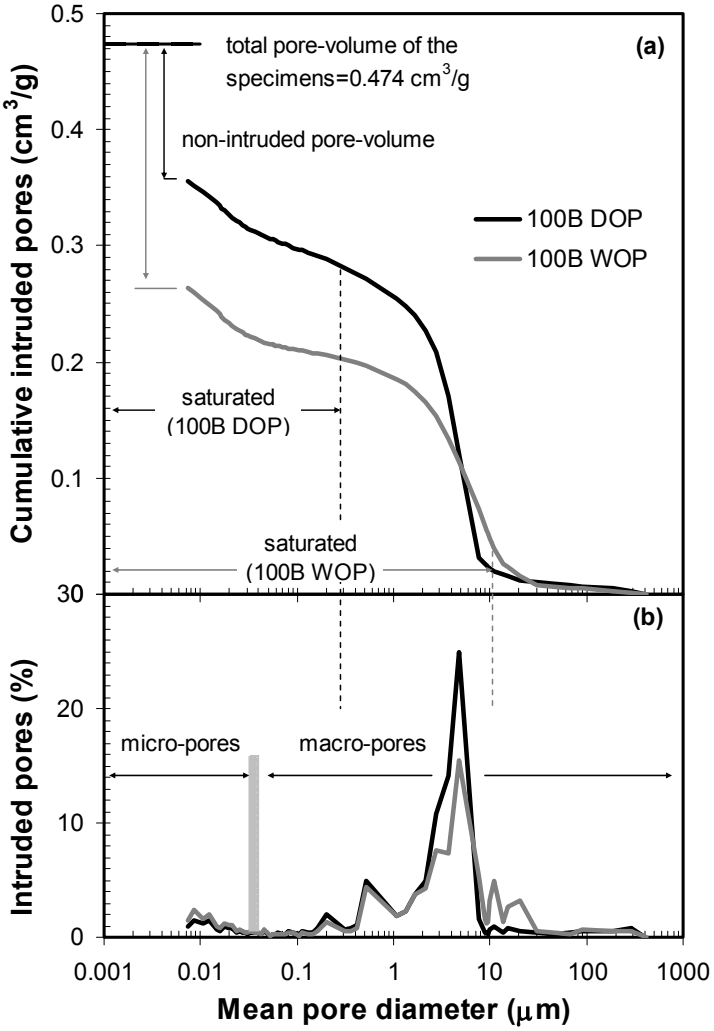

Figure 5.2 Pore size distribution curves of low compacted 100B specimens

Figure 5.2 also shows the distribution of air and water within the specimens. The pore volume full of water (saturated) is obtained by multiplying the degree of saturation (*Sr*) and total pore volume of the specimen intruded by mercury. By considering only the smaller pores of the specimen would be full of water (Delage et al., 1996), the pore volume full of air is obtained by subtracting the total pore volume intruded by mercury with the pore volume full of water. From the *Sr* data (i.e., 100B DOP with *Sr* of 40% and 100B WOP with *Sr* of 91%), it is found that the total of pores full with water are 0.19 cm^3/g and 0.43 cm^3/g and the total of pores full with air are 0.28 cm^3/g and 0.05 cm^3/g for 100B DOP and 100B WOP specimens, respectively. The data is then plotted to the figure by assuming that the water is placed in the smaller pores due to the hydration force and capillary effects. For 100B DOP specimen, it is shown that the water is mainly placed in the intra-aggregate pores, leaving the air in the inter-aggregate pores. For 100B WOP specimen, the water fills the intra-and inter-aggregate pores, leaving the air in the pores with diameter higher than 10 μm.

Figure 5.3 shows the pore-size distribution (PSD) curves of the compacted bentonite-sand mixtures (i.e., 50B/50S DOP and 50B/50S WOP specimens) tested in this study. From Figure 5.3.a, it is shown that both PSD curves are almost the same not only the shape but also the total of non-intruded pores. This is also shown in the curves of mean pore diameter versus percentage of intruded pores (Figure 5.3.b). As shown in Figure 5.3.b, there are two main populations in the macro-pores of PSD of bentonite-sand mixture (i.e., at diameter of 5 μm and diameter of 20 μm). The first pore population (i.e., at diameter of 5 μm) is the same as the pore population of PSD of compacted bentonite as shown in Figure 5.2 (i.e., the inter-aggregate pores). The second pore population (i.e., at diameter of 10 μm) is probably the pore developed between clay aggregates and sand in the mixture. The small pore population with pore diameter between 80-200 μm as shown in Figure 5.3.b may be developed in the contact between sand surfaces and the clay aggregates.

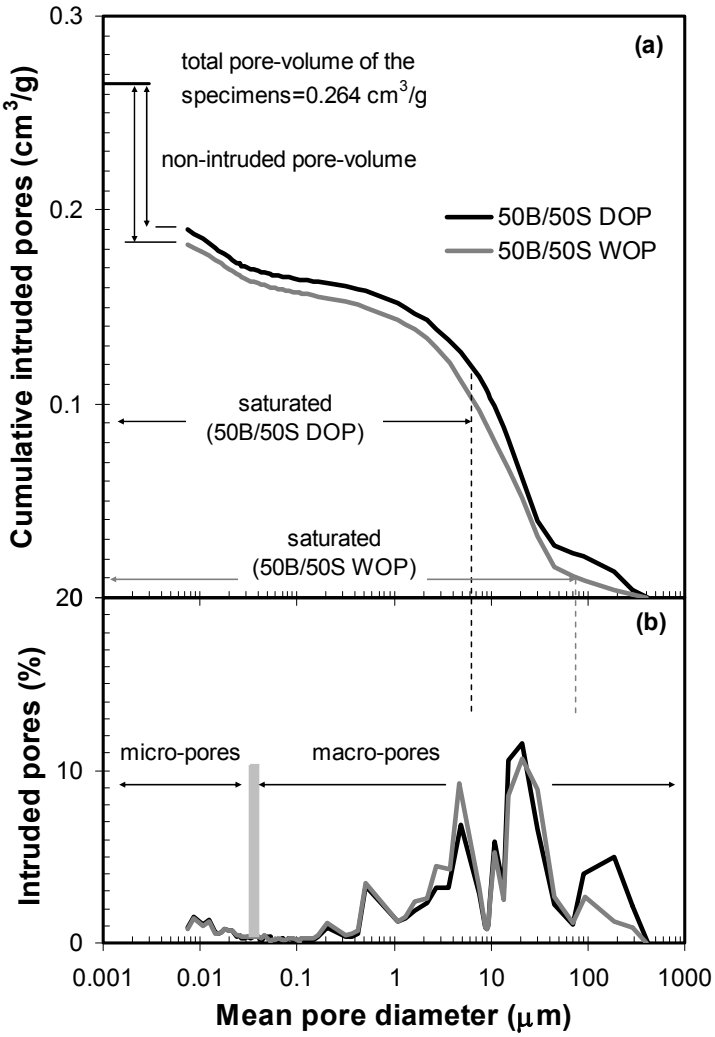

Figure 5.3 Pore size distribution curves of low compacted 50B/50S specimens

Using the same method as compacted bentonite, the water-air distribution of the compacted bentonite-sand mixture was also plotted in Figure 5.3. For 50B/50S DOP specimen, the water fills not only the micro-pores (or intra-aggregate pores) but also the macro-pores (i.e., almost the entire inter-aggregate pores). For 50B/50S WOP specimen, water fills almost the whole pores leaving air in the pores with diameter larger than 80 μm. Since sand is not swelling material, the water placed in the second pore population (i.e., at diameter of 20 μm) do not make significant difference in PSD of the specimen. This results in almost the same PSD of both specimens even they are compacted at different conditions (i.e., DOP and WOP conditions).

Figure 5.4 shows the pore-size distribution (PSD) of low compacted material (i.e., 50B/50S DOP) performed in this study. The result is compared to the PSD of heavily compacted bentonite-sand mixture reported by Agus and Schanz (2005c) and.

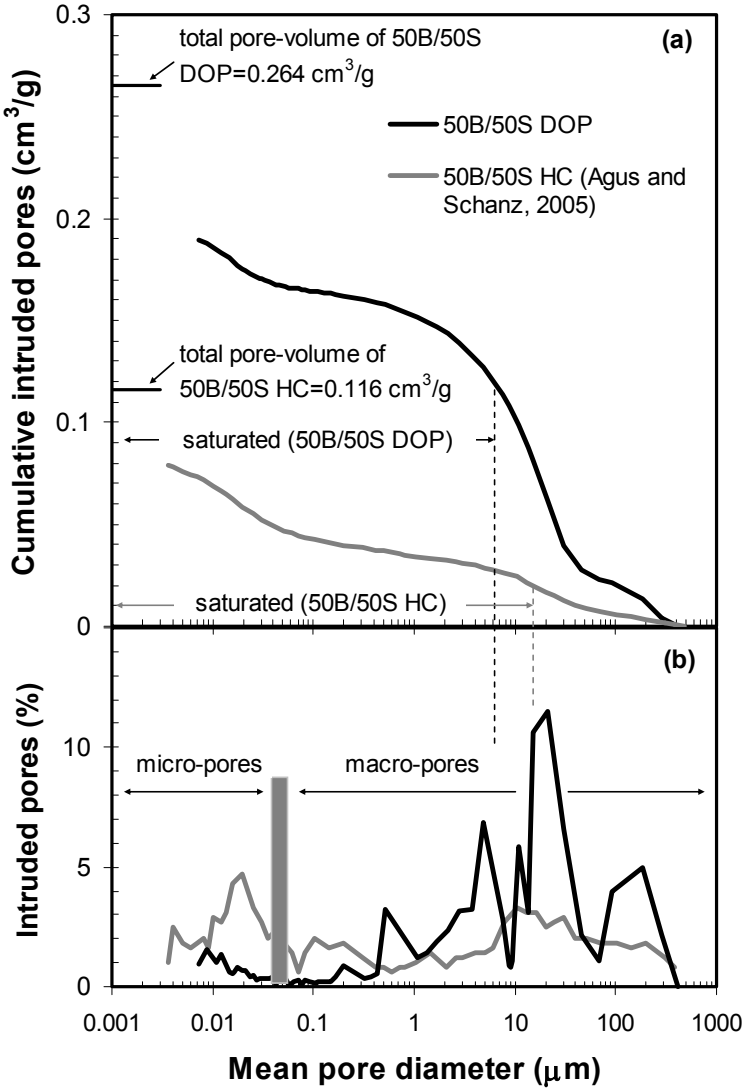

Figure 5.4 Density effects on the PSD curves of compacted bentonite-sand mixture

As shown the Figure 5.4, because the 50B/50S HC has higher dry density, the total pore-volume of 50B/50S HC reflecting the void ratio of the specimen is smaller than that of 50B/50S DOP. The non-intruded pore of 50B/50S DOP which has higher water content is larger than that of 50B/50S HC. It seems that the non-intruded pore is more affected by water content of specimen rather than the dry density of specimen. Figure 5.4.b shows the mean pores diameter versus intruded pores of the specimens. From Figure 5.4.b, it is revealed that the limits of micro- and macro-pores of 50B/50S DOP and 50B/50S HC specimens which are determined by using the same method as shown in Figure 5.1 are placed in very narrow range (i.e., at pore diameter of 0.04-0.05 μm). This is close to the limit of micro- and macro-pores of 100B specimens (i.e., 0.03-0.04 μm). It seems that the limits of micro- and micro-pores are not influenced by water content, dry density, and presence of sand in the mixtures.

Figure 5.4.b shows that the inter-aggregate pores and pores between sand surface and aggregates are reduced by increasing the density of specimen resulting increasing the intra-aggregate pores. The small peak developed in the micro-pore zone at pore diameter of 0.02 μm may be due to the 50B/50S HC has low water content. The lower water content of heavily compacted specimen may result in more flocculate clay structure compare to the lower density with higher water content. Moreover, the wavy flake shapes are not completely developed in the specimen with low water content. Until now, it is not known clearly when the bentonite particles start to have a wavy flake like shapes.

Figure 5.5 shows the PSDs of heavily compacted bentonite-sand mixture at as-prepared condition and at after swelling pressure test under constant volume condition. Small increase in the total pore-volume shown is due to deformation of the cell during swelling pressure test. Based on the Figure 5.5.a, the PSD curve of the specimen after swelling pressure test is placed over the PSD curve of the as compacted specimen leaving a small amount of non-intruded pore. It seems that during wetting the water was absorbed by bentonite particle surface in the inter-particle pores resulting higher diameter of pores. This may not make enlarging the aggregate size but separating the aggregates to be smaller sizes followed by development of inter-aggregate pores in the specimen (Figure 5.5.b). Release in swelling pressure about 3000 kPa after the specimen removed from the cell might also contribute to the creating of the inter-aggregate pores.

Table 5.2 summarizes the information of PSD of specimens that can be derived from MIP test result. As mentioned above, the non-intruded pore volume of WOP specimens is higher than that of DOP specimen. This results in decreasing the total intruded pore volume of the WOP specimen. As shown in Table 5.2, the limits between micro-pore and macro-pore of

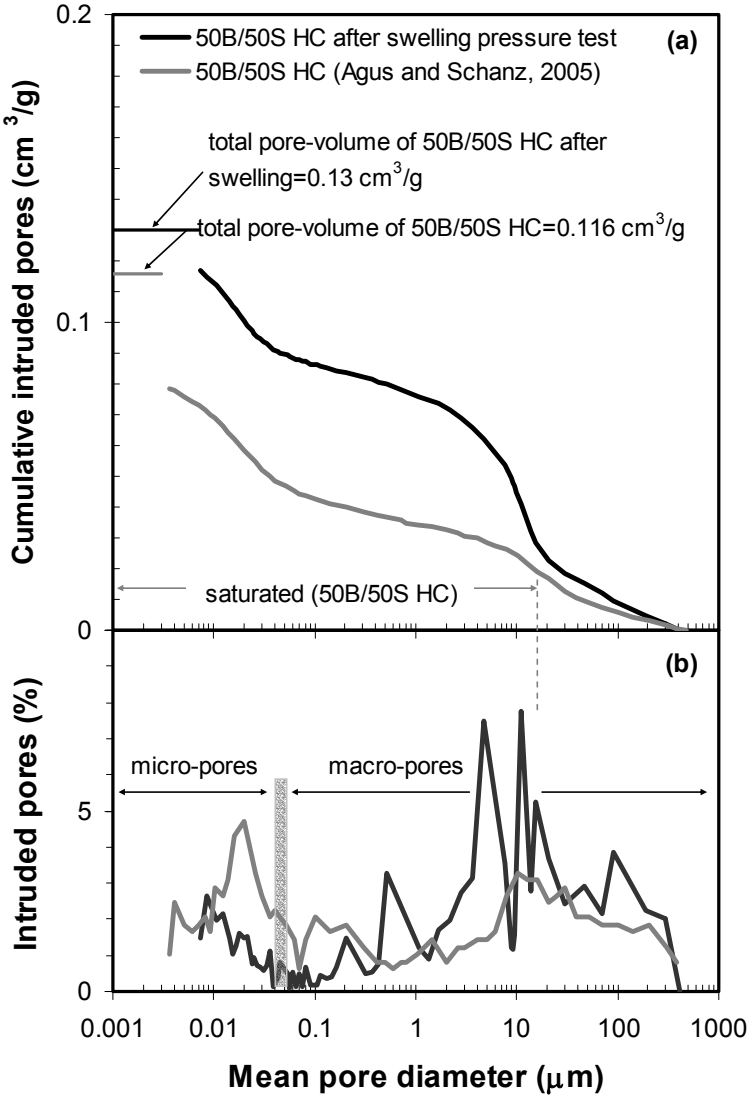

Figure 5.5 Wetting effects on PSD curves of heavily compacted bentonite-sand mixture

specimens investigated in this study vary in very small range (i.e., 0.03-0.05 μm). The values are not affected by water content and dry density of specimens. Different conditions and types of bentonite also do not show various values (e.g., Agus and Schanz (2005c) reported 0.02-0.05 μm for highly compacted bentonite-sand mixture for 3 different conditions, and Wan et al. (1995) reported the value of 0.02 μm for sodium-type bentonite-sand mixture). Other limit values can be observed from the MIP result reported in literatures for different types of bentonite e.g., 0.07-0.1 μm for Kunigel-sand mixture (Cui et al., 2002a), 0.03-0.04 μm for bentonite from Almeria (Lloret et al., 2003), and 0.02-0.03 μm for MX-80 (Dellage et al., 2006). These are due to the thickness of bentonite particles varies from 0.001-0.01 μm (Yong and Warkentin, 1975).

Table 5.2 Mercury intrusion porosimetry data of the specimens tested

	100B		50B/50S		50B/50S HC	
	DOP	WOP	DOP	WOP	As-prepared[§]	Swollen
Total pore volume, $V_{p\,tot}$ (cm^3/g)	0.474	0.474	0.264	0.264	0.113	0.13
Total non-intr. pore volume, $V_{p\,non\text{-}intr.}$ (cm^3/g)	0.139	0.211	0.075	0.081	0.034	0.015
Total intr. pore volume, $V_{p\,intr.}$ (cm^3/g)	0.335	0.263	0.189	0.183	0.079	0.117
Percent of total intr. pore volume, $V_{p\,tot}$	71	56	71	70	70	88
Micro-pore: Diameter, $D_{p\,micro}$ (μm)	<0.04	<0.03	<0.035	<0.035	<0.05	<0.04
Volume, $V_{p\,micro}$ (cm^3/g)	0.165	0.254	0.095	0.100	0.067	0.066
Percent of total pore volume, $V_{p\,tot}$	35	54	36	38	59	30
Macro-pore: Diameter, $D_{p\,macro}$ (μm)	0.04-407		0.035-408		0.05-500	0.035-408
Volume, $V_{p\,macro}$ (cm^3/g)	0.309	0.219	0.169	0.164	0.046	0.092
Percent of total pore volume, $V_{p\,tot}$	65	46	64	62	41	70

[§]Data from Agus and Schanz (2005)

5.3.2 Study of Fabric of Compacted Bentonite and Bentonite-Sand Mixture

Figures 5.6.a and 5.6.b show the ESEM photos of 100B DOP and 100B WOP tested in this study, respectively. The figures have magnification of 500x. As shown in Figure 5.6.a, the aggregation is clearly shown in the fabric of specimen compacted at DOP condition. At this condition, the aggregates are strong enough to resist the deformation during compaction. This results in high percentage of inter-aggregate pores.

The 100B WOP specimen shows quite different overall image (Figure 5.6.b) from that of 100B DOP specimen, despite the dry densities of the specimens are the same. The higher water content of 100B WOP specimen results in the bigger size of aggregates and become deformable. As a result, the macro-pores which represent the pores between clay aggregates are filled during compaction and no apparent aggregation shows in WOP condition. This makes the 100B WOP has less percentage of inter-aggregate pores.

Figures 5.7.a and 5.7.b show the ESEM photos of 100B DOP and 100B WOP with magnification of 2000x, respectively. Figure 5.7.a shows association of small aggregates with diameter varies from 2-5 μm. Wavy flake-like structure of the aggregates consisting of clay

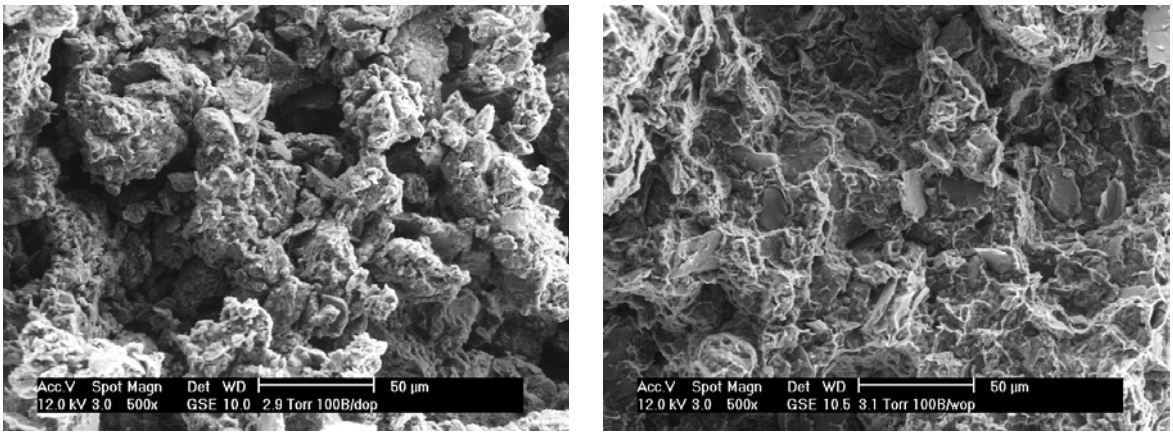

(a) **(b)**

Figure 5.6 ESEM photo of compacted bentonite: (a) 100B DOP and (b) 100B WOP (magnification: 500X)

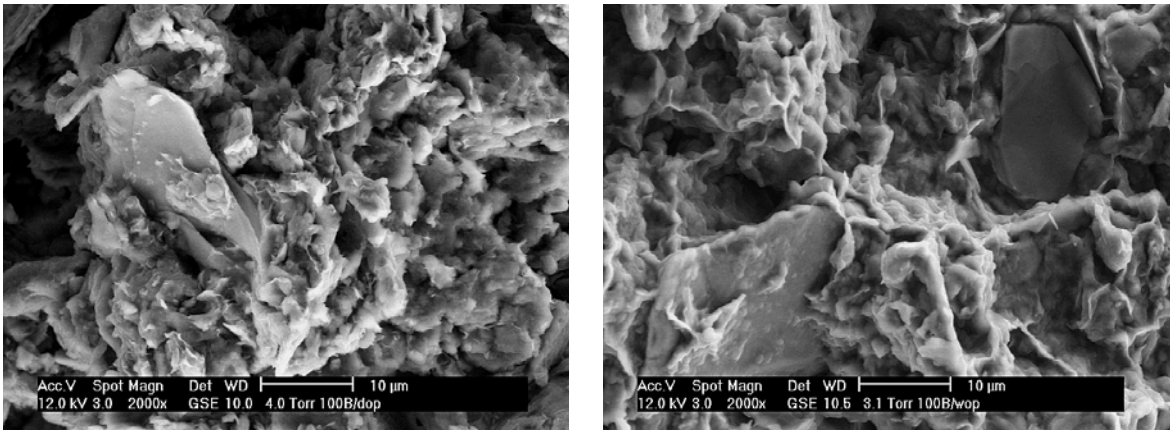

(a) **(b)**

Figure 5.7 ESEM photo of compacted bentonite: (a) 100B DOP and (b) 100B WOP (magnification: 2000X)

platelets are shown in the figure even the specimen compacted at DOP condition. The shapes result in the non-intruded pores within the aggregates. Figure 5.7.b shows the ESEM photo of the 100B WOP specimen with magnification of 2000x. It is depicted in the figure that aggregation is not appeared resulting unclear inter-aggregate pores. Wavy flake-like structure is shown in the edge of the association of aggregates.

Figure 5.8.a and Figure 5.8.b show the ESEM photos of 50B/50S bentonite-sand mixture compacted at Proctor densities on dry and wet condition (i.e., 50B/50S DOP and 50B/50S WOP), respectively. As shown in Figure 5.8.a, the bentonite aggregates do not stick on the surface of sand leaving pores between them. The same as 100B specimen, wavy flake-

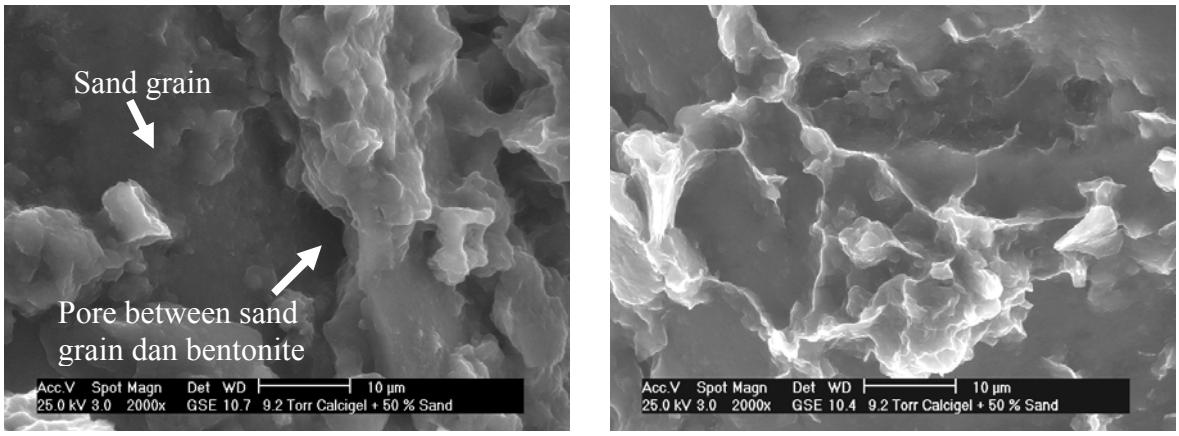

(a) (b)

Figure 5.8 ESEM photo of compacted bentonite-sand mixture: (a) 50B/50S DOP and (b) 50B/50S WOP (magnification: 2000X)

like structure of clay is seen in the figure even the specimen compacted on DOP condition. This also results in the non-intruded pores within the aggregates as shown in Figure 5.3. The wavy flake-like structure of clay is shown clearly in Figure 5.6.b since the specimen has higher water content.

5.3.3 Summary of Microstructure of Compacted Bentonite and Bentonite-Sand Mixtures

The following conclusions can be drawn based on the results of microstructure investigations on the bentonite and bentonite-sand mixture.

1. The PSD of specimens tested in this study show bimodal characteristics in spite of their different compaction conditions.
2. For 100B mixture, at the same void ratio, the specimen compacted DOP has a greater volume of macro-pores compared to the specimen compacted WOP.
3. The 50B/50S mixture specimens do not show the same phenomenon. The volumes of macro-pores are the almost same for both the DOP and WOP specimens.
4. New pore population (i.e., pores between clay aggregate and sand surface) is developed in the PSD of compacted bentonite-sand mixture.
5. The non-intruded pores exist in all specimen tested in this study and mainly affected by water content.

6. The limits of macro- and micro-pores are almost the same for specimens tested in this study and those of compacted bentonite and bentonite-sand mixtures obtained from literature. The values are not influenced by water content, dry density, and presence of sand in the mixture.
7. Increase in density of specimen results in decreasing the percentage of inter-aggregate pores of the specimen with higher density.
8. Hydration under constant volume condition for heavily compacted specimen results in separating the aggregates to be smaller sizes followed by development of inter-aggregate pores in the specimen. Release in swelling pressure about 3000 kPa after the specimen removed from the cell might also contribute to the creating of the inter-aggregate pores.
9. As shown in the ESEM results, the aggregation is clearly shown in the fabric of low compacted 100B DOP specimen.
10. Wavy flake-like structure is shown not only for the low compacted WOP specimen but also for the low compacted DOP specimen.

CHAPTER 6

SUCTION MEASUREMENTS

6.1 Introduction

The effects of temperature on water sorption characteristics can be qualitatively described from different points of view. According to the diffuse double layer theory, an increase in temperature should cause an increase in the diffuse double layer thickness and a decrease in the surface potential for a constant surface charge. However, the increase in temperature also results in a decrease in the dielectric constant of the pore-fluid. As a result, the change in temperature does not influence significantly the thickness of diffuse double layer and therefore the amount of absorbed water (Mitchell, 1993).

Since the unit weight of water and the saturated pressure of water vapor change with temperature, based on Equation 3.1, total suction is also affected by temperature. However, the change in total suction due to the variation in temperature as inferred from Equation 3.1 is not significant.

Romero et al. (2000) performed a study on the effects of temperature on the magnitude of total suction of Boom clay. The results indicated that for a given water content, total suction at 20 °C was higher than that at 80 °C. They found that the change in total suction resulted from the experiment was higher than that of calculated from the change in total suction due to change in the surface tension of water. Besides that, Romero et al. (2000) cited that the differences are due to the change in the clay fabric, and the change in the pore-water chemistry of the clay. The change in the clay fabric and pore-water chemistry due to temperature is expected to be irreversible. Nevertheless, it is thought that the alteration of a clay fabric and pore-water chemistry does not significantly affect the total suction magnitude for clays with low organic contents for the range of temperature under consideration (i.e., from 20 to 80 °C). Therefore, the measured change in the total suction due to the change in temperature may not only be caused by the change on the capillary component of suction but also caused by other reasons. For instance, Pusch et al. (1990) stated that the increase in temperature of a bentonite decreased the hydration force due to a reduction in the number of

hydrates in the smectite surface within bentonite. This may lead to reduce the ability of the bentonite to retain water. Or else, it may only be an apparent change in the total suction as caused by the inaccuracy of the device used for measuring total suction.

On the other hand, the increase in temperature may cause the smectite mineral to become unstable and transform to more stable silicate phases or known as illitation as discussed in Section 3.2.6.

This chapter presents the effects temperature on the total suction. The sensors used were verified by comparing the result at room temperature with different techniques. Experimental techniques and procedures adopted in this study including the calibrations that were performed prior investigation are discribed. The results including the comparison between the different techniques and the error in the measurements are presented and discussed. Addional tests were performed to the pretreated specimen in order to study the change in the mineralogy of the bentonite after heating.

6.2 Literature Review Related to Suction Measurements

Soil suction is an essential property of unsaturated soils describing the ability of soils to absorb and retain pore water at a certain water content. The soil suction consists of two main components (i.e., matric suction and osmotic suction). The matric component of soil suction occurs from the capillary and hydration force mechanisms, and the osmotic component is related to the dissolve salt in the soil pore-water. The sum of these two components is entitled as total soil suction.

In geotechnical engineering, suction constitutes a special interest because many of the geotechnical processes are suction dependent (Fredlund and Rahardjo, 1993). Vanapalli et al. (1996), for instance, used the soil water characteristic curve (SWCC) which shows the suction-water content relationship to predict the shear strength of soils. Morris et al. (1992) found that the tensile strength of soil is a function of suction. Water permeability of soils in unsaturated condition can also be predicted using statistical model derived from SWCC of soil (Mualem, 1976; Leong and Rahardjo, 1997). The value coefficient permeability of soil has been found to decrease several orders as suction increases together with decrease in the degree of saturation (Huang et al., 1998; Agus et al., 2003). The slope of total suction characteristic curve may also be used to quantitatively classify the relative swelling potential of expansive soils, e.g., as low, moderate, high, or very high (McKeen, 1992). Based on the

above studies, the measurement of suction is crucial for understanding the engineering behavior of unsaturated soil.

There are two main categories of suction measurements (i.e., direct methods of suction measurements and indirect methods of suction measurements). In direct suction measurement, the suction measured is matric suction. Null-type axis-translation apparatus and tensiometer are commonly used in direct measurement of the matric suction. The working principle of the null-type axis-translation apparatus is described in Fredlund and Rahardjo (1993). The limitation of this method is that the matric suction that can be measured is limited to 1500 kPa or the highest air entry values of ceramic disk which is available. For the tensiometer, the matric suction that can be measured is limited to 90 kPa. Higher than this value, the error will be caused by the movement of water. Flow of water from the measurement system into the specimen will cause an under estimate of the suction and flow in other direction will cause an over estimate. Ridley and Burland (1993) successes to increase the matric suction measured using tensiometer (i.e., up to 1200 kPa) by a reduction in the volume of water and increasing water pressure in reservoir of the tensiometer to avoid formation of air bubbles in the measuring system. The increase in water pressure in the reservoir may result in unstable for long period reading. The sensitivity of the transducer can make it susceptible to the thermal/contraction of the water in the system and this can result in errors when continues monitoring is necessary.

For indirect methods of suction measurement, the measurement is performed by first to calibrate the sensor against some other physical properties, such as dielectric constant of the bulk soil water, relative humidity, water content, etc. Time domain reflectometry (TDR) is an example of indirect method to measure matric suction. The sensor has an ability to accurately measure the dielectric constant of soil which has close relationship with the volumetric water content (Topp et al., 1980). TDR requires SWCC of soil tested to relate the measured volumetric water content with the matric suction. The limitation is that the SWCC of clay depends on initial water content, void ratio, stress history, and compaction energy as discussed in Section 2.8.1. Therefore, the initial condition of specimen in SWCC data should be the same as that tested using TDR. Other limitation of this sensor is that the sensor is used for estimating water content to mostly non saline soils and non dispersive medium such as fine sand. The use of TDR for measuring water content of strongly disperse medium such as bentonite must be considered carefully due to presence of dissolve salt in the soil pore-water

and complex clay-water-ion interaction (Kelleners et al., 2005). The cable length and temperature also influence the TDR reading (Robinson et al., 2003).

Contact filter paper method is another example of matric suction for indirect methods of suction measurement. The method is simple and not labor-intensive. The matric suction is obtained from calibration curve of the filter paper water content with suction. The calibration techniques and experimental procedures for contact filter paper method were described in Leong at al. (2002) and Bulut and Wray (2005). According to Ridley and Wray (1996), the contact filter paper method can be used for matric suction measurement in the range 30-30000 kPa.

The osmotic component of soil suction is measured indirectly. The osmotic suction is calculated from the relationship of electric conductivity of soil pore-water with osmotic pressure of salt solution. The detail procedures of measurement and factors influencing the osmotic suction are discussed in Chapter 7.

All total suction measurements are indirect methods of suction measurement. Non-contact filter paper is indirect method for measuring total suction. The filter paper method has been used by some researchers to determine the total suction of soils (e.g., Houston et al., 1994; Deka et al., 1995; Leong at al., 2002; Likos and Lu, 2003a; Bulut and Wray, 2005; Agus and Schanz, 2005b). The uses of filter paper for measuring matric and total suction are also discribed in ASTM standards (i.e., ASTM D 5298-94). The same as matric suction, the total suction is also obtained from calibration curve of the filter paper water content with suction. Leong et al. (2002) used different calibration curves for the total and matric suction measurement for suction less than 1000 kPa. Bulut and Wray (2005) stated that the use of two different calibration curves is inconsistent with the fundamental relationships of suction components; the differences are due to alteration of the fiber structure of filter paper when the filter paper calibrated using pressure plate. However, the non contact filter paper for measuring total suction should be limited to a lowest suction of approximately 1000 kPa if an error limit of 30% is allowed with temperature fluctuation of 0.5 °C (Agus and Schanz, 2006).

Other methods used for total suction measurements are capacitance relative humidity sensors and chilled-mirror hygrometer technique. In these methods, the sensors measure the relative humidity of the air space over the soil specimen at a given temperature. The total suction is calculated from the thermodynamic relationship between total suction and relative humidity of the vapor space in the soil (Equation 3.1).

The capacitance relative humidity (*RH*) sensors have been used by some researchers for measuring total suction of soils. The working principle of these sensors is to measure the capacitance of two electrodes separated by polymer film that absorb or release water as the relative humidity of the surrounding changes. The relative humidity is obtained from calibration curve as a relationship between the capacitance and the relative humidity. Using a balance and capacitance *RH* sensor, Likos and Lu (2003b) developed a system for measuring suction characteristic curves (i.e., drying and wetting processes) from a single specimen. The capacitance sensor has also been used for measuring total suction of compacted bentonite at elevated temperature (Villar et al., 2005). This type of sensor can be used for suction measurement in range 7000-700000 kPa (Likos and Lu, 2003b).

The chilled-mirror hygrometer technique is used for measuring the relative humidity of the air space over the soil specimen (Leong et al., 2003; Agus and Schanz, 2005b). The technique has been used as a reference for verifying performance of other sensors and relative humidity of salt solution (Agus and Schanz, 2005b; Albrecht et al., 2003; Tang and Cui, 2005). The technique can be used for suction measurement in almost the whole range of total suction measurement with accuracy of 0.3% (Decagon Devices Inc, 2002). However, according to Leong et al. (2007), the sensor has high resolution but low accuracy. Agus and Schanz (2007) stated that the sensor can be used for suction measurement as low as 1500 kPa if the maximum measurement error is limited to 30%.

6.3 Experimental Techniques and Procedures

The suction measurements performed in this study were contact and non contact filter paper methods for measuring matric suction and total suction, respectively, chilled mirror hygrometer technique for measuring total suction, and two types of capacitance relative humidity (*RH*) sensors for measuring total suction at room temperature and elevated temperature (i.e., 80 °C). The specimens used in this study were 100% bentonite (100B) and 50% bentonite and 50% sand mixture (50B/50S). The specimens had initial dry density and water content along the Proctor curve as shown in Figure 6.1. Two compaction energies (i.e., standard Proctor compaction (SP) and enhanced Proctor (EH) with compaction energies of 600 kN-m/m^3 and 1000 kN-m/m^3, respectively) were used in this study. Since only small specimen is required, static compaction and loose specimens were used for filter paper method and chilled mirror hygrometer, respectively.

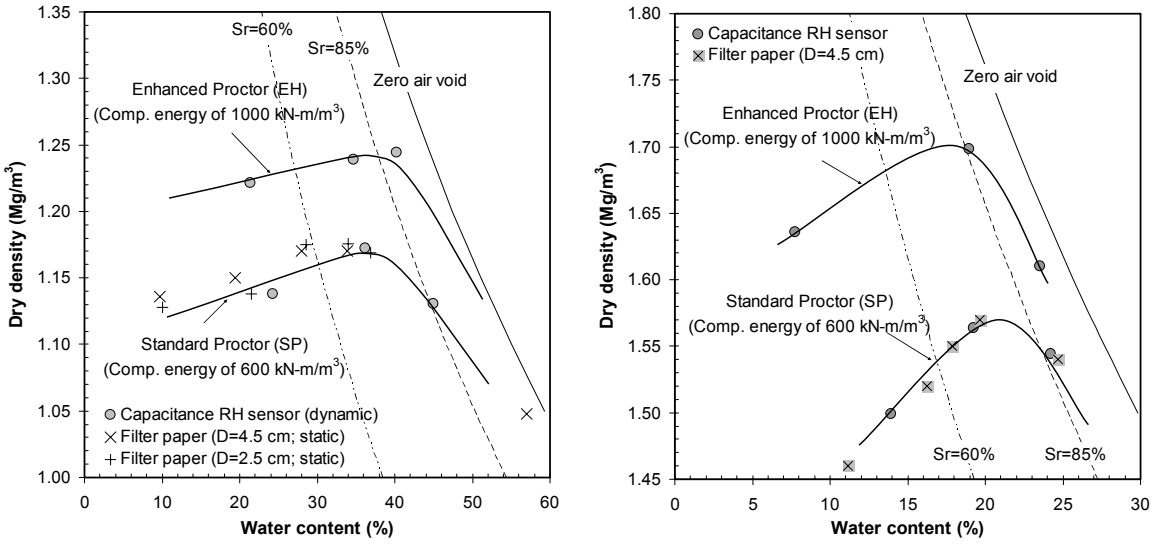

(a) (b)

Figure 6.1 Data points corresponding to the specimens used in suction measurements: (a) pure bentonite (100B) ; (b) 50B/50S bentonite-sand mixture

6.3.1 Filter Paper Method

6.3.1.1 Calibration

There are two types of filter papers which are commonly used in suction measurements (i.e., Whatman No.42 and S&S 589). Filter paper used in this study was Whatman No. 42 filter paper disk which was also used by many researchers such as Deka et al. (1995), Leong at al. (2002), Likos and Lu (2003), and Agus and Schanz (2005b). Leong et al. (2002) found that the calibration curves of the Whatman No. 42 obtained by different researchers, at different times, with different batches of filter paper show more consistent than that of the S&S 589.

In this study, the matric suction and total suction were calculated using the empirical equation provided by Agus (2005). The calibration curves of the filter paper were established using a pressure plate apparatus or using axis translation technique (ATT) for suction less than 1500 kPa and using a desiccator or vapor equilibrium technique (VET) for suction higher than 2000 kPa. The matric suction and the total suction were calculated using Equation 6.1 and 6.2 (Agus, 2005).

$$s_m = 93.82\left[\exp\left(\frac{299.93}{w_{fp}}\right)^{0.148} - \exp(1)\right]^{5.235} \quad \text{for suction less than 1000 kPa} \qquad (6.1)$$

$$s_t = 2223\left[\exp\left(\frac{235.57}{w_{fp}}\right)^{0.129} - \exp(1)\right]^{3.822} \quad \text{for suction higher than 1000 kPa} \qquad (6.2)$$

where s_m and s_t is matric and total suction, respectively, in kPa and w_{fp} is filter paper water content in percent.

6.3.1.2 Experimental Procedures

In this study, the diameters of filter papers used were considered. The diameters of 2.5 cm and 4.5 cm were utilized. A new device for measuring suction using filter paper was used. The advantage of using this device is that the measurement is directly performed in the place where the specimen is compacted. This assures a good contact between filter paper and specimen for contact filter paper method. Since the specimen is in contact with the wall of the device, the air space in the device can be minimized. The device consists of a cylinder made of stainless steel with diameter of 5 cm and height of 3.5 cm, the top cap, and the bottom cap. The top and the bottom cup were fixed using 4 rods. The bases of the bottom and top caps were equipped by 1 mm thick of rubber plate. Figure 6.2.a and 6.2.c shows the drawing and photograph of the device used, respectively.

The specimens used in this method were compacted pure Calcigel (100B) and 50%/50 bentonite-sand mixture. Deaired-distilled water was added to the specimen to reach desired water content. The specimens were cured in the doubled-layers plastic bag for 2 weeks. Then the specimens were statically compacted in the stainless steel cylinder in two layers. After the first layer was compacted, a sandwich filter paper was placed on the specimen for matric suction measurement. The sandwich filter paper consists of a filter paper with diameter of 2.5 cm and two protective filter papers with diameter of 3 cm. For larger filter paper, the sandwich filter paper consists of a filter paper with diameter of 4.5 cm and two protective filter papers with diameter of 5 cm. The second layer was subsequently compacted such that specimen with a height of 2 cm was produced.

The targeted dry densities were based on the predetermined compaction curves as shown in Figure 6.1. For total suction measurements, a filter paper with diameter of 2.5 cm for small filter paper and 4.5 cm for large filter paper was placed on a stainless steel wire mesh directly upper surface of the specimen. Without dismantling the specimen, the cylinder was closed with the top and bottom caps and fixed with four rods. This procedure avoids the specimen to deform and to keep a good contact between the filter paper and the soil for matric

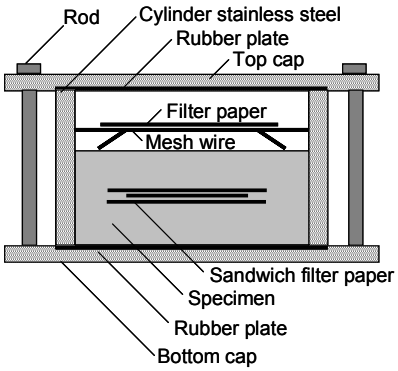

(a)

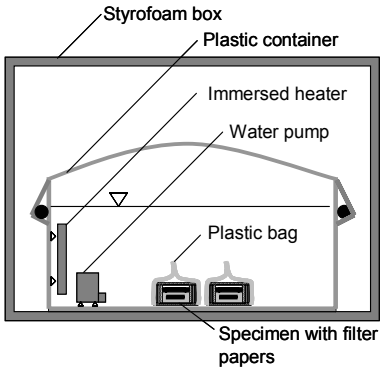

(b)

(c)

Figure 6.2 Device for suction measurement using filter paper method

suction measurement. The entire device was placed in the doubled-layers plastic bags and then immersed in the water bath. It was found that the temperature in the water bath was fluctuated between 18-19 °C. A heater was used to maintain constant temperature during measurement (i.e., 22 ± 0.2 °C) and a small pump was placed close to the heater to spread the head in the water bath (Figure 6.2.b). A five-week equilibration time was adopted in this study. The water contents of the two filter papers were determined and suctions were calculated using Equations 6.1 and 6.2. The water content of each specimen after the test was determined and used as the compaction water content.

6.3.2 Warmed-Head Capacitance Relative Humidity (RH) Sensor

6.3.2.1 Equipment and Verification

The Relative humidity and temperature sensor used in this study was a capacitance sensor Humicap® HMP 243 and a temperature sensor, respectively, both from Vaisala Oyj (Figure 6.3). Dueck and Börgesson (2001) used a similar sensor to monitor total suction of a swelling clay specimen wetted under constant volume conditions. In this study, the sensor is called warmed-head capacitance sensor because beside the thin polymer film, the sensor is

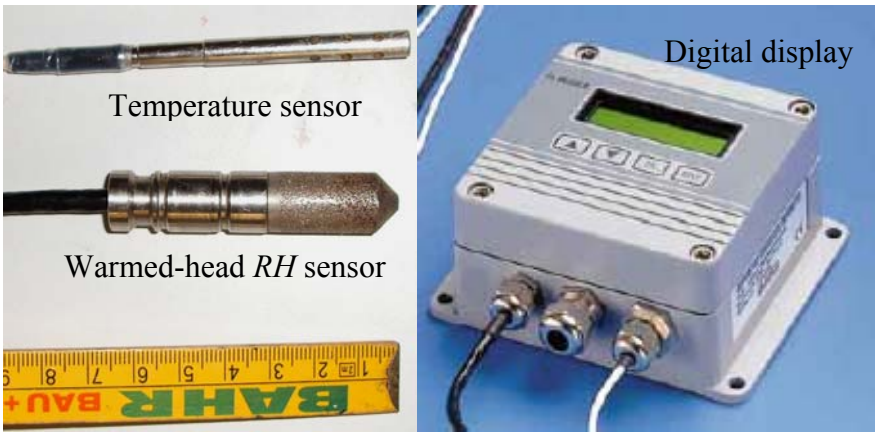

Figure 6.3 Warmed-head relative humidity sensor and the temperature sensor

also equipped with a warming function to keep the polymer film always in dry conditions. This gives advantage to avoid excessive condensation which is the biggest problem and commonly happens in the total suction measurement. The sensor (together with a temperature sensor) was connected to a digital data display that is connectable to a personal computer. The sensor measures relative humidity (*RH*) of vapor space in the specimen, which is then converted to suction using Equation 3.1. No calibration curve is required for this sensor since the sensor was calibrated by the factory and the relative humidity is shown directly from the digital data display and recorded by computer. However, the verification has been performed to investigate the effect of warming function on the result obtained.

The warmed-head *RH* sensor was verified using saturated and molal salt solution. The *RH* of the salt solutions used for verification was measured using the chilled-mirror hygrometer prior to use. Therefore, the relative humidity obtained from the chilled-mirror hygrometer was used as reference. It was found the relative humidity of salt solution measured by the warmed-head capacitance sensor was less than relative humidity obtained from the chilled-mirror hygrometer as shown in Figure 6.4. This is due to the warming function of the sensor. The warming function sends a signal to the heater equipped close to the thin polymer film in the head of the sensor when excessive condensation happens. Figure 6.4 shows that the warming function affects the relative humidity at the value higher than 50% and reaches approximately 95% at relative humidity of distilled water (i.e., 100%). Using similar sensor, Likos and Lu (2001) also found that the apparent relative humidity of pure water was 89%.

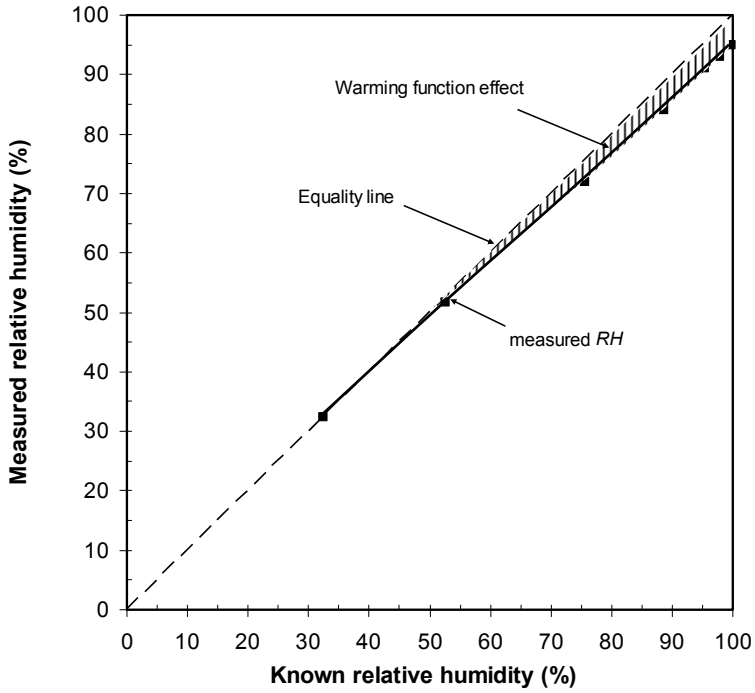

Figure 6.4 The measured relative humidity measured using warm-head *RH* sensor versus known relative humidity measured with the chilled-mirror hygrometer

6.3.2.2 Experimental Procedures

The measurements of total suction using the warmed-head RH sensor were performed on compacted specimens. The specimens used in this test were dynamically compacted. After compaction, the as-compacted specimen was transferred carefully to a special container which is designed to be air-tight even at high temperature (i.e., up to 100 °C) (Figure 6.5.a). The dimensions of the container used were the same as those of the mold used in the Proctor compaction. The cap of the container had four holes latch with a bushing (cable-gland) attached. Four holes were drilled in the specimen to insert the warmed-head *RH* sensor, the temperature sensor, and two non warmed-head RH sensors into the specimen. In order to avoid direct contact of the sensors with the soil, perforated PVC pipes were used as housings. The container was placed in a climate chamber that could control temperature to ±0.1 °C (Figure 6.5.b). The specimen was allowed to reach *RH* equilibrium at 20 °C in the chamber. In order to investigate the temperature effects, subsequently, the temperature of the chamber was increased to 80 °C after the relative humidity, as measured by the sensor, achieve equilibrium. The data (i.e., the relative humidity and temperature) were recorded using a personal computer. The water content of the specimen was checked at the end of the test. No significant changes in water content, before and after the test, were found. Figure 6.6 shows typical result of relative humidity measurement using warmed-head RH sensor.

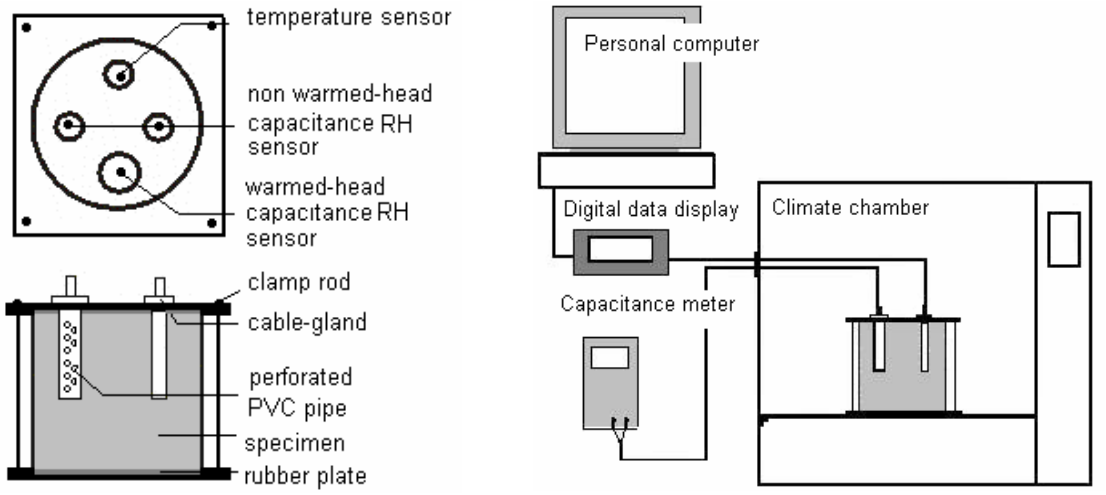

(a) (b)

Figure 6.5 The schematic drawing of the test setup adopted in the study

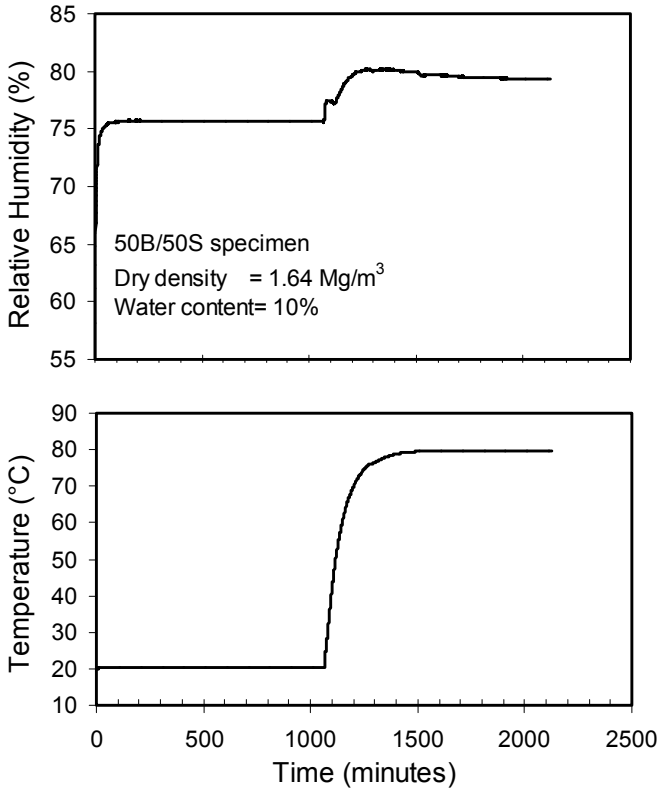

Figure 6.6 Typical result of RH reading using non warmed-head RH sensor at 20 and 80 °C

6.3.3 Non Warmed-Head Capacitance RH Sensor

6.3.3.1 Equipment and Calibration

The non warmed-head *RH* sensor was used by Albrecht et al. (2003) for measuring low relative humidity (or high total suction) at room temperature (i.e., about 20°C). The operation of the sensor is based on changes in the capacitance of the sensor as its thin polymer film absorbs water molecules. The sensor was connected to a portable capacitance meter. The sensor was calibrated using molal and saturated solutions of sodium chloride (NaCl) and magnesium chloride hexa-hydrate ($MgCl_2.6H_2O$). The suction of the molal sodium chloride solution used in the calibration was calculated according to the equations given by Lang (1967) and Pitzer and Pelper (1984). The relative humidity above each solution at room temperature was verified using the chilled-mirror hygrometer as also done by Albrecht et al. (2003). The small differences between the theoretical and the measured values of relative humidity above solution have been found to exist because the NaCl used consisted of constituents other than sodium chloride (Tang and Cui, 2005). Since two non-warmed head *RH* sensors used in this study, both sensors were calibrated. It was observed that the two non warmed-head *RH* sensors showed small differences in the calibration curves. However, the curves obtained show almost the same trend. This occurs not only at 20 °C but also at 80 °C. The non warmed-head *RH* sensor and the typical calibration curve of the sensor at 20 and 80 °C are shown in Figure 6.7.a and Figure 6.7.b, respectively.

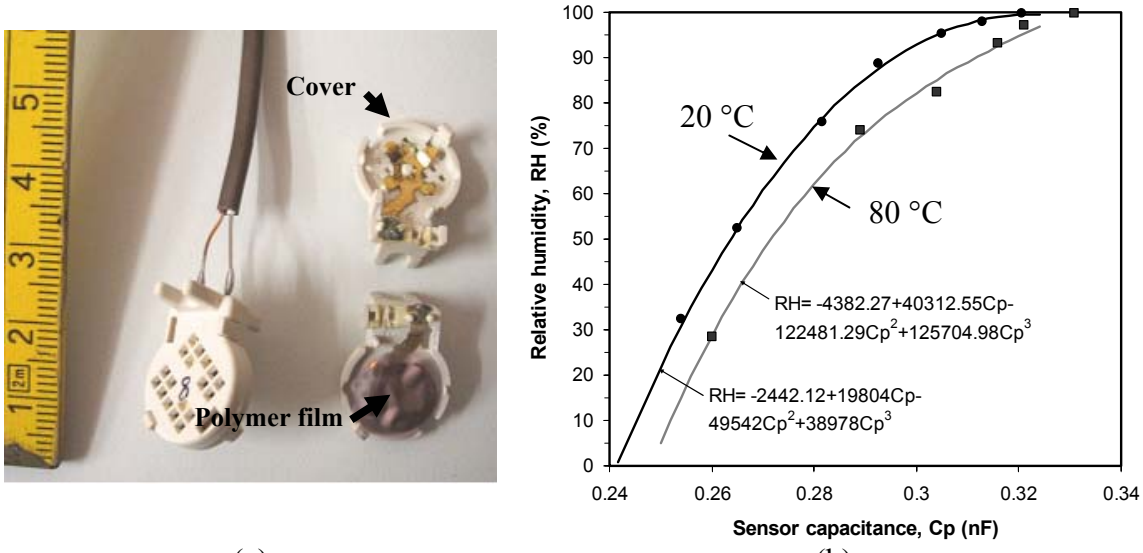

(a) (b)

Figure 6.7 Non warmed-head capacitance sensor for measuring relative humidity and the typical calibration curves of the non warmed-head capacitance sensor

6.3.3.2 Experimental Procedures

The measurements of total suction using the non warm-head capacitance sensor were performed on the dynamically compacted specimens. Two non-warmed head were used in this study. The sensors were inserted in two holes in the container together with the warmed-head capacitance sensor (Figure 6.5). The data was recorded manually from display shown in the capacitance meter. The recorded data was capacitance in nano Farad (nF) and transformed to relative humidity using the calibration equation of the sensor (Figure 6.7.b). The total suction was calculated using Equation 3.1. The temperature data used in the calculation was the temperature recorded by the temperature sensor of warmed-head capacitance sensor.

6.3.4 Chilled-Mirror Hygrometer Technique

In this study, the chilled-mirror hygrometer was used for measuring suction at room temperature and verifying the salt solution used in calibration and verification of the two capacitance sensors mentioned above. The chilled-mirror used in this study was a water activity meter type 3TE produced by Decagon Devices Inc. as shown in Figure 6.8. The equipment has a special specimen closed chamber of about 12 cc in volume, where the soil specimen is placed. The components and principal working of the equipment were described in Leong et al. (2003), Albrecht et al. (2003), and Agus and Schanz (2005b).

Figure 6.8 The chilled-mirror hygrometer used in this study

6.3.4.1 Verification

The chilled-mirror hygrometer was verified for its performance in measuring total suction prior to use. The verification was performed using standard salt solutions provided by the manufacturer. The salt solutions used for verification were 6.0 molal NaCl, 8.57 molal LiCl, and 13.41 molal LiCl giving water activity (a_w) or *RH* of 0.760, 0.500, and 0.250, respectively (Decagon Devices Inc, 2002). The salt solution used is close to the range of the suction measured. The readings obtained for the standard salt solutions were found to vary less than 0.3% *RH* with a response time of no longer than 3 minutes.

6.3.4.2 Experimental Procedures

The measurement of total suction using this technique was commenced by placing the soil specimen in the special chamber not more than half its capacity. Immediately, the chamber with the specimen inside was placed in the device. The soil in the specimen chamber in the device was allowed to reach isothermal equilibrium which was defined as the difference between temperature of the vapor space and the specimen. The device showed the difference in temperature between the headspace and the mirror. The chamber was closed and after reaching equilibrium in about 3 minutes, the relative humidity and the temperature of the vapor space were shown in the display. The measurement was performed two times each specimen. The same procedure was applied for verifying salt solutions used in sensor calibration.

6.4 Error in Total Suction Measurements

The error in total suction measurement may be due to the inaccuracy of the sensors used. The error of total suction measurement due to the inaccuracy of the measuring devices is calculated using Equation 6.4 which is ratio of the derivative of Equation 3.1 with respect to relative humidity (Equation 6.3) to the measured total suction (Equation 3.1).

$$\frac{\Delta s_t}{\Delta RH} = \frac{RT}{M_w(1/\rho_w)\,RH} \tag{6.3}$$

By assuming $\frac{RT}{M_w(1/\rho_w)} = a$, Equation 3.1 can be written as $s_t = a\ln(RH)$ and Equation 6.3 can be written as $\Delta s_t = \frac{a}{RH}\Delta RH$. The error of total suction measurement is defined as:

$$Error(\%) = \frac{\Delta s_t}{s_t} x100\% = \frac{a\ \Delta RH}{a\ RH\ln(RH)} x100\% = \frac{\Delta RH}{RH\ln(RH)} x100\% \tag{6.4}$$

ΔRH is essentially the accuracy of the sensors (i.e., 0.3%RH for the chilled-mirror hygrometer (Decagon Devices Inc, 2002), 0.4pF/%RH for the non warmed-head capacitance sensor (BC Component, 1999), and 0.5+2.5%RH for warmed-head capacitance RH sensor (Vaisala, 2002).

For the filter paper, the error that can be computed is due to the error of balance used in the water content of filter paper measurement. Using the ASTM calibration curve for the standard-sized-55-mm of Whatman 42 filter paper, Agus and Schanz (2007) found the error of 10.5% of measured total suction at water content ranging from 0 to 45.3% and error of 2% at water content ranging from 45.3 to 90%. However, the error of the total suction measurement using filter paper depends on the size of the filter paper. The size of filter paper used depends on the specimen size which is commonly less than that of the standard filter paper. Houston et al. (1994) and Agus and Schanz (2005b), for instance, used diameter of 2 cm and 2.5 cm of filter paper, respectively. The smaller diameter of filter paper, the lighter dry weight of the filter paper is. This results in high sensitivity changing the water content of filter paper and thus the total suction. The maximum error of filter paper method can be defined from the difference of suction calculated from the measured water content and suction from the estimated water content due to inaccuracy of balance (i.e., 0.0002 g). The estimated water content is calculated using Equation 6.5.

$$w_e = \frac{m_{fp\ wet} + 0.0002}{m_{fp\ dry} - 0.0002} - 1 \tag{6.5}$$

where w_e is the estimated water content, $m_{fp\ wet}$ and $m_{fp\ dry}$ are the mass of wet and dry filter paper, respectively.

Figure 6.9 shows the errors in total suction measurements due to inaccuracy of the sensors used (i.e., inaccuracy of sensor for chilled-mirror hygrometer and two types of capacitance RH sensors, and inaccuracy of balance used for filter paper). As shown in Figure 6.9, if the error is limited to 30% of measured suction, the suction that can be measured using chilled-mirror hygrometer is 1500 kPa, warmed-head capacitance sensor is 15000 kPa, and non warmed-head capacitance sensor is 200000 kPa. The figure also shows that the error of total suction measurement using filter paper with diameter of 2.5 cm is higher than that with diameter of 4.5 cm. As shown in Figure 6.9, the suction that can be measured using filter paper with diameter of 4.5 cm is between 600-150000 kPa for maximum error of 30%. For the same range of suction measurement (i.e., 600-150000 kPa), the filter paper with diameter of 2.5 cm gives approximately 100% maximum error.

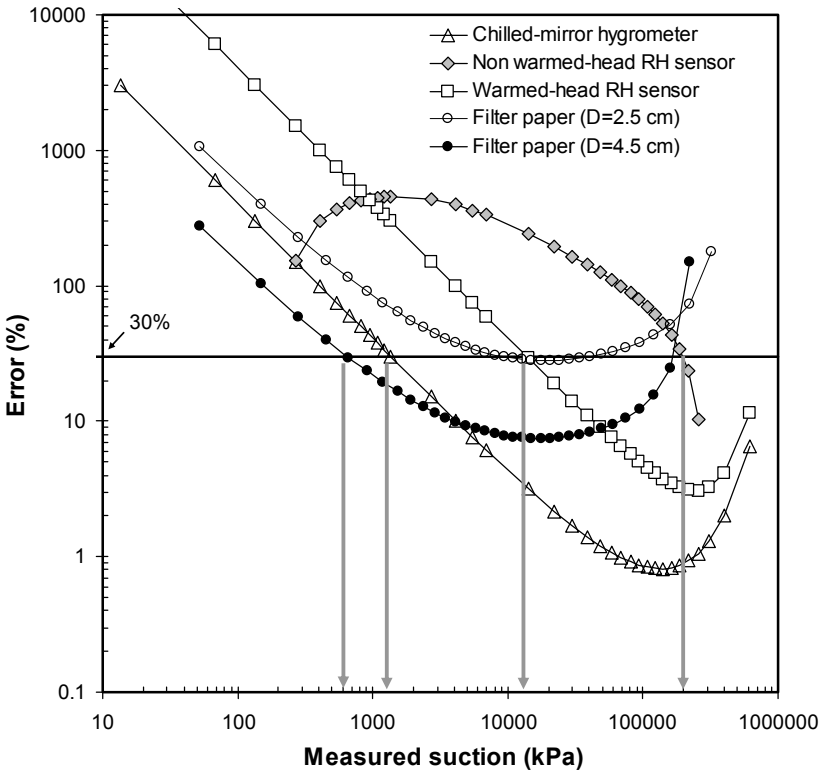

Figure 6.9 Error in the total suction measurement due to the inaccuracy of the sensors

Figure 6.9 also shows if the error is limited to 30% of measured suction, the suction that can be measured using chilled-mirror hygrometer is 1500 kPa, warmed-head capacitance sensor is 15000 kPa, and non warmed-head capacitance sensor is 200000 kPa. The figure also shows that the error of total suction measurement using filter paper with diameter of 2.5 cm is higher than that with diameter of 4.5 cm. As shown in Figure 6.9, the suction that can be measured using filter paper with diameter of 4.5 cm is between 600-150000 kPa for maximum error of 30%. For the same range of suction measurement (i.e., 600-150000 kPa), the filter paper with diameter of 2.5 cm gives approximately 100% maximum error.

The change in total suction (or the error in suction measurement) due to a temperature gradient can be estimated by taking the first derivative of Equation 3.1 with respect to temperature (Equation 6.6) (Agus and Schanz, 2006a).

$$\frac{d(\ln s_t)}{dT} = \frac{1}{T} - \frac{1}{u_{vo} \ln(RH)} \frac{d(u_{vo})}{dT} \tag{6.6}$$

Figure 6.10 shows the suction measurement errors due to temperature gradient calculated using Equation 6.6. The figure shows if the error of total suction measurement is limited to 30% of measured value and temperature gradient is maintained 0.1 and 1 °C, the minimum suctions that can be measured are 200 kPa and 1500 kPa, respectively.

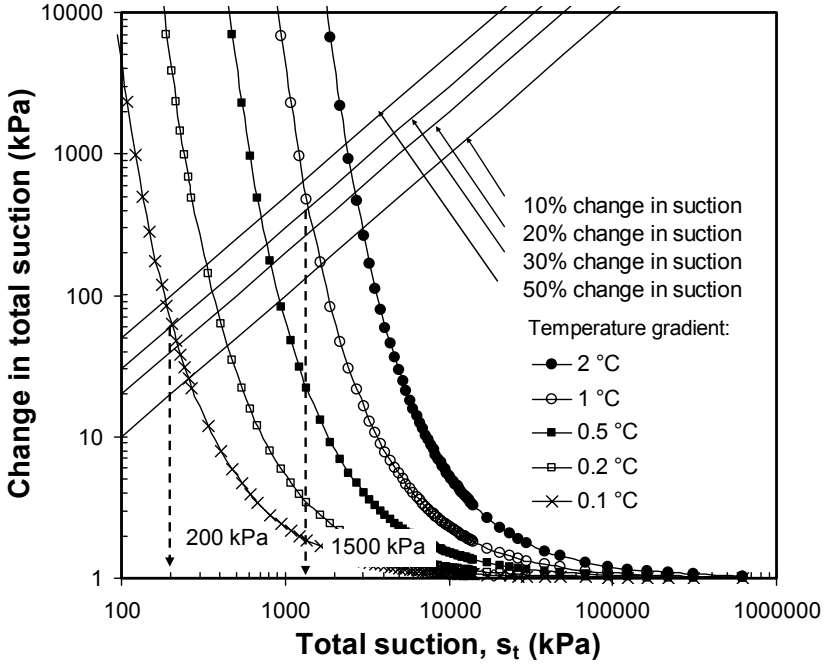

Figure 6.10 Suction measurement error due to temperature gradient (Agus and Schanz, 2006a)

6.5 Result and Discussion

6.5.1 Comparison different sensors in total suction measurement at 20 °C

The results of total suction measurement for compacted bentonite (100B) specimen using four different methods are shown in Figure 6.11. The specimens compacted using standard Proctor compaction are denoted as SP and specimens compacted using enhanced Proctor compaction as EH. As shown in the figure, the total suction of the SP and EH specimens measured using warmed-head and non-warmed head RH sensor is converged to be one line. Therefore, no apparent effects of dry density are detected and the total suction is only affected by water content. The result agrees well with finding by Agus and Schanz (2005b) for total suction measured using relative humidity sensor and psychrometer method. This is denoted that the total suction values measured using chilled-mirror hygrometer for loose specimen and filter paper method for static compaction are not distinguishable from those obtained using RH sensors. Therefore, the chilled-mirror hygrometer result can be used as a reference. In order to observe the tendency of the experimental result, the data were fitted using Equation 6.7 which is similar to SWCC equation suggested Fredlund and Xing (1994).

$$s_t = a\left[\exp\left(\frac{b}{w_m}\right)^c - \exp(1)\right]^d \tag{6.7}$$

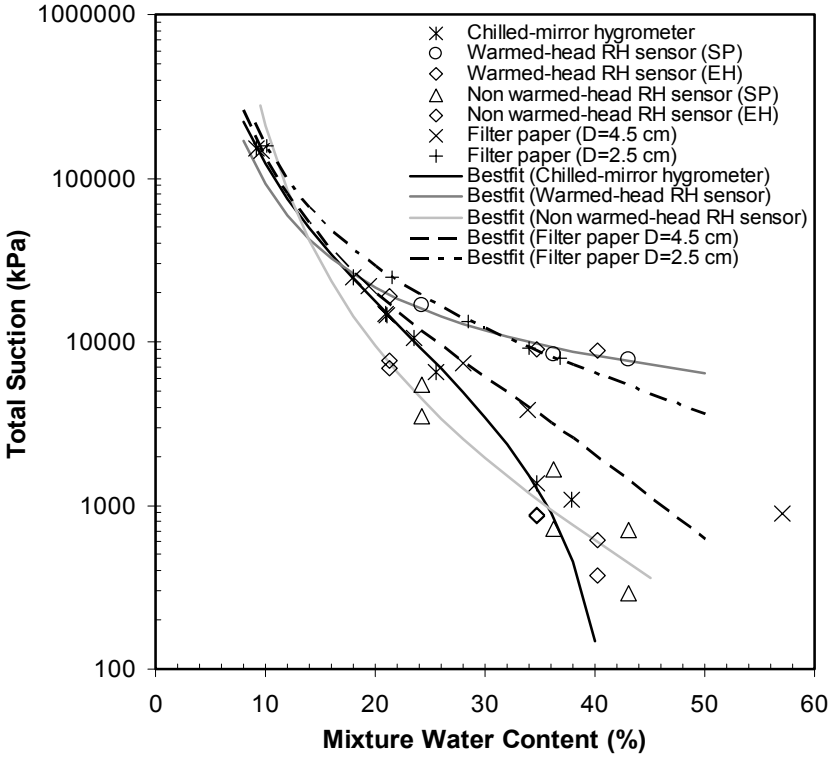

Figure 6.11 Mixture water content versus total suction obtained from different methods used for pure bentonite (100B) specimens

where s_t is total suction, w is the compaction water content, and a (kPa), b (%), c, and d are the fitting parameters.

The fitting parameters and the goodness of fit of Equation 6.7 for different total suction measurements used in this study are summarized in Table 6.1. The goodness of fit of Equation 6.7 is shown by R^2 (coefficient of determination). The standard error of estimate (*SEE*) shows the dispersion of prediction error if Equation 6.7 is used to predict the total suction from the water content. The *SEE* values are calculated using Equation 6.8.

$$SEE = \sqrt{\frac{\sum_{i=1}^{n} \hat{\varepsilon}_i^{\,2}}{n-1}} \tag{6.8}$$

where $\hat{\varepsilon}$ is errors (i.e., the actual suction minus predicted suction using fitting equation) and n is number of data.

As shown in Table 1, the R^2 values are close to 1.0. This shows that the Equation 6.7 fits to the data obtained in this study. The non warmed-head *RH* sensor shows the lowest R^2 values (i.e., 0.962 for 100B specimen). For 100B specimen, The *SEE* of warmed-head *RH* sensor using Equation 6.7 shows the highest value (i.e., 1095) whereas the filter paper (D = 4.5 cm) shows the smallest value (i.e., 62).

Table 6.1. Fitting parameters and goodness of fit of Equation 6.7 for different total suction measurements used in this study.

Mixture	Method used	Fitting parameter				Statistic	
		a **(kPa)**	***b*** **(%)**	***c***	***d***	R^2	***SEE***
100B	Chilled-mirror hygrometer	7054.29	42.062	0.557	1.514	0.999	646
	Warmed-head RH sensor	1161.92	1114.9	0.582	0.282	0.980	1095
	Non warmed-head RH sensor	133.03	81.720	0.669	1.829	0.962	623
	Filter paper (D=4.5 cm)	2304.99	68.536	0.476	1.809	0.999	62
	Filter paper (D=2.5 cm)	2394.93	88.643	0.629	1.077	0.999	250
50B/50S	Chilled-mirror hygrometer	4909.12	22.112	0.562	1.713	0.999	509
	Warmed-head RH sensor	2523.84	189.943	0.685	0.303	0.993	690
	Non warmed-head RH sensor	483.30	36.514	0.720	1.294	0.940	1780
	Filter paper (D=4.5 cm)	72.237	112.796	0.706	1.004	0.998	403

As shown in Figure 6.11, the bestfit lines of total suction measured using warmed-head RH sensor and filter paper (D=4.5 cm) merge to the chilled-mirror hygrometer bestfit line at total suction higher than 20000 kPa (20 MPa). The result is almost the same as result reported by Likos and Lu (2003). Likos and Lu (2003) found a good agreement between total suction measured using almost similar capacitance *RH* sensor used in this study and filter paper method with standard size (i.e., 5.5 cm) at total suction higher than 4 in log scale (kPa) or the same as 10000 kPa. The bestfit lines of total suction measured using non-warmed head *RH* sensor and filter paper method with diameter filter paper of 2.5 cm merge to others at suction higher than 40000 kPa (40 MPa) and 100000 kPa (100 MPa) for non-warmed head *RH* sensor and filter paper with diameter of 2.5 cm, respectively. These differences are possible due to temperature gradient and/or inaccuracy of the sensor used or other reasons which are discussed thoroughly in suction measurements error section.

Based on Figure 6.11, the total suction measured using warmed-head *RH* sensor and filter paper method is higher than that measured using chilled-mirror hygrometer. Different from others, the total suction measured using the non warmed-head *RH* sensor is less than that measured using chilled-mirror for total suction range of 1000-20000 kPa. This is possible due to excessive condensation happen to the non warmed-head RH sensor resulting under estimate of total suction measured. For total suction less than 1000 kPa, the total suction measured using non warmed-head *RH* sensor is higher than measured using chilled-mirror hygrometer. Figure 6.11 also shows that the total suction measured using chilled-mirror hygrometer drops at suction less than 1500 kPa. This is due to inaccuracy of the equipment resulting higher error when it is used to measure small total suction (i.e., less than 1500 kPa). Leong et al.

(2007) concluded that chilled-mirror hygrometer has high resolution but low accuracy. This might be true since they used the device to measure total suction less than 2000 kPa.

Figure 6.12 shows the total suction versus compaction water content of bentonite-sand mixture (i.e., 50B/50S) specimen. The same as the total suction result of 100B, the total suction of specimens compacted with enhance Proctor (EH) and standard Proctor (SP) is placed in one bestfit line. The figure shows consistent result as 100B specimen. Compared to the total suction measured using chilled-mirror hygrometer, the warmed-head *RH* sensor results in higher value at total suction less than 20000 kPa and the non-warmed head *RH* sensor results in lower total suction for suction higher than 1500 kPa.

As shown in Table 1, the non warmed-head RH sensor shows the lowest R^2 values (i.e., 0.94 for 50B/50S specimen). The *SEE* of non-warmed head RH sensor shows the highest value (i.e., 1780). However, the R^2 and *SEE* values show only the goodness of the data with respect to Equation 6.7. These do not reveal directly the accuracy and precision of the sensor to measure the total suction. In order to observe the performance of the sensor used in this study, the total suction obtained from the respective sensor is compared to the total suction obtained using chilled-mirror hygrometer which has the best in accuracy (i.e., 0.3%*RH*).

Due to the much larger specific surface area of the bentonite compared to that of the sand in the mixture, water is mostly retained by the bentonite. Therefore, it can be assumed that water is only bounded within the bentonite particles and based on this assumption, the bentonite water content (w_b) can be calculated according to the following equation:

$$w_b = w_m(1+\frac{1}{r_{bs}}) \tag{6.9}$$

where w_m (%) is the mixture water content and r_{bs} is the bentonite-sand mass ratio (dry mass basis).

Figure 6.13 shows the total suction of bentonite and bentonite-sand mixture as a function of bentonite water content for three different methods (i.e., chilled-mirror hygrometer, non warmed- and warmed-head RH sensor. As shown in the figure, the total suction of bentonite and bentonite-sand mixture merges into a single curve for respective methods used. This result agrees with result reported by Agus and Schanz (2005a) and supports the statement that total suction is strongly affected by mixture water content and mixture bentonite content, or collectively is a function of bentonite water content.

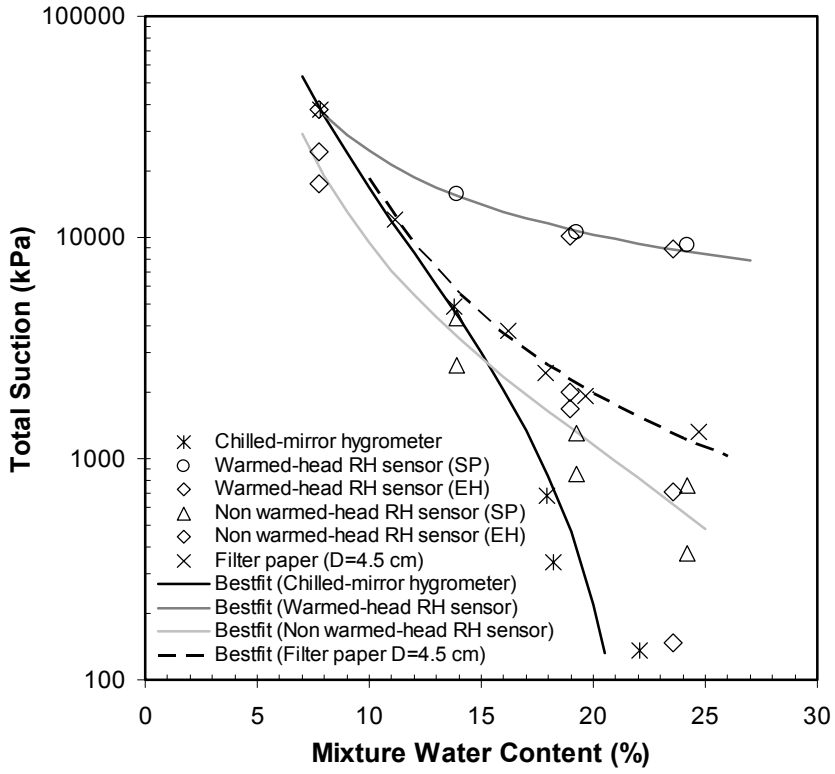

Figure 6.12 Mixture water content versus total suction obtained from different methods used for bentonite-sand mixture (50B/50S) specimens

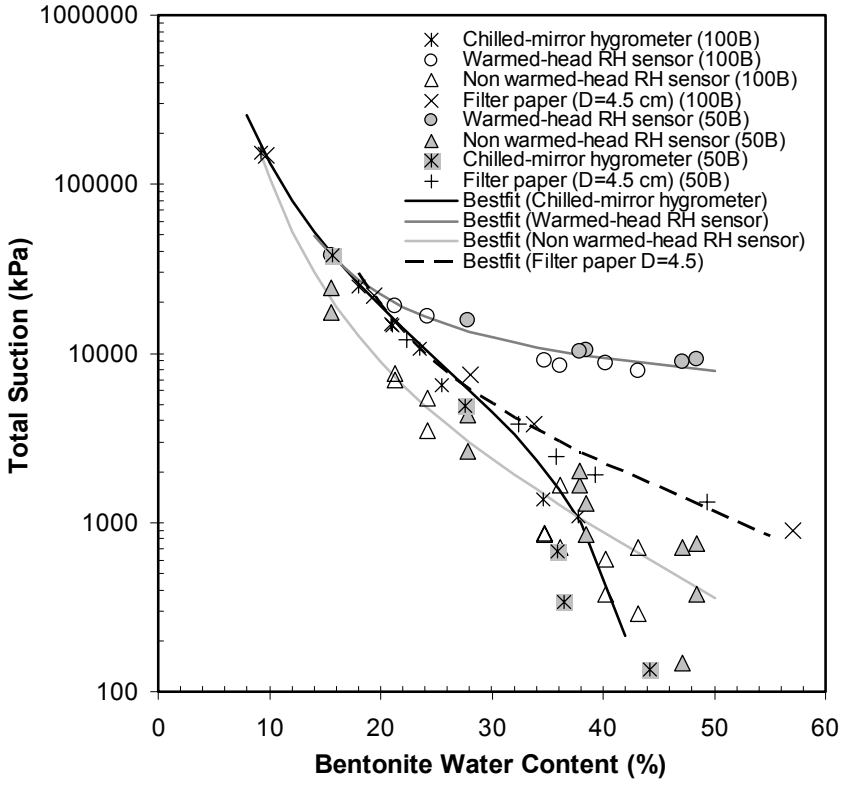

Figure 6.13 Total suction results measured from different methods used as a function of bentonite water content

Figure 6.14 shows the total suction obtained from different methods compared to the known total suction. The known total suction is the result of total suction measured using chilled-mirror hygrometer. As mentioned above, chilled-mirror hygrometer was taken as a reference since the technique has the highest accuracy compared to other techniques. Figure 6.14 shows clearly that the total suction measured by warmed-head *RH* sensor, filter paper (D = 4.5 cm) and filter paper (D = 2.5) diverges from the equality line at suction lower than 20000 kPa, 10000 kPa, and 100000 kPa, respectively. The total suction measured by these three methods tends higher than that of chilled-mirror hygrometer. For filter paper method, the result shows the effect of filter paper size used on the measured total suction. As expected, the use of small filter paper results in higher possible error in total suction measurement. As mentioned above, the total suction measured using non warmed-head *RH* sensor are lower than that of measured using chilled-mirror hygrometer at suction higher than 2000 kPa. At total suction lower than 2000 kPa, the total suction measured using the sensor is higher than that of chilled-mirror hygrometer. The lower suction measured using non-warmed head sensor is because the sensor can not remove the condensate water in the sensor. After the test has been finished, small amount of condensed water was found in the cover part and/or in the polymer film of the non-warmed head sensor. In case of suction less than 2000 kPa where the total suction measured using chilled-mirror is lower than the total suction measured using the non-warmed head *RH* sensor, this is due to the inaccuracy of the chilled-mirror hygrometer

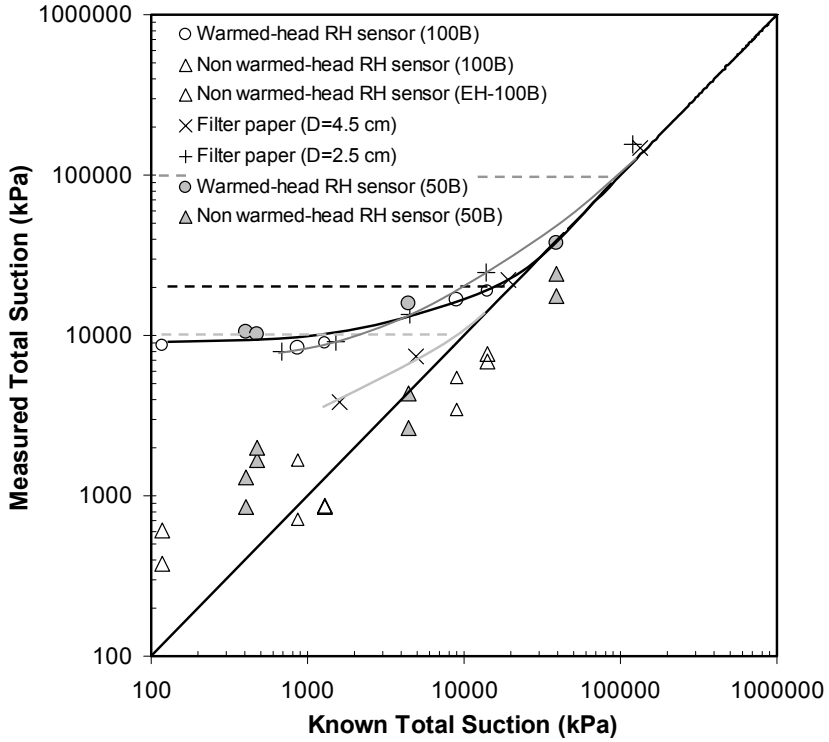

Figure 6.14 Measured total suction versus known total suction

used in this study for measuring low suction (i.e., less than 1500 kPa) as shown in Figure 6.9.

6.5.2 Error of total suction measurements

Figure 6.15 shows the inferred total suction error for the sensors used in this study. As shown in the figure, the filter paper method with diameter of 4.5 cm (D = 4.5 cm) shows maximum error of 30% at suction of 10000 kPa, whereas the filter paper (D = 2.5 cm) shows maximum error of 30% at suction of 100000 kPa. The warmed-head RH sensor shows maximum error of 30% at suction of 15000 kPa. The non warmed-head RH sensor's error is placed close to 50% error. According to the error value, the filter paper (D = 4.5 cm) shows the best method in measuring total suction after the chilled-mirror hygrometer technique. The possible errors are caused by temperature gradient, inaccuracy of the equipment, and also combination from the two reasons.

Figure 6.16 shows the temperature gradients that existed in the total suction measurements using the sensors used in this study. The temperature gradient was calculated using Equation 6.6 and taking the chilled-mirror hygrometer reading as reference. As depicted in Figure 6.16, the estimate temperature gradients in the non-warmed head *RH* sensor are negative indicating possible excessive water vapor condensation. However, the estimated temperature gradients are higher than that of maximum temperature gradient happened in the chamber where the sensor was placed. This also occurs to the other sensors (i.e., warmed-

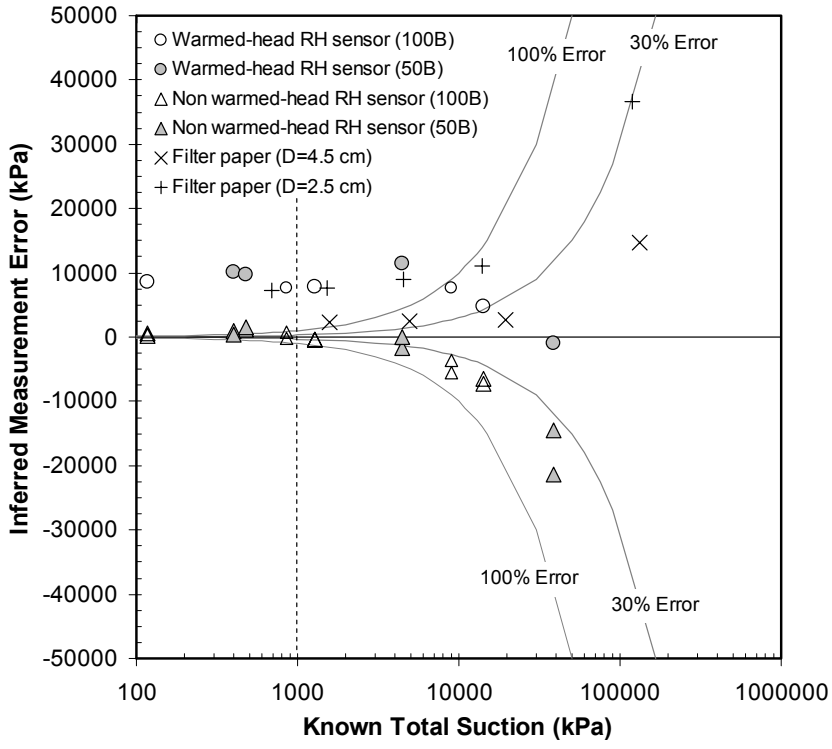

Figure 6.15 Inferred total suction measurements error

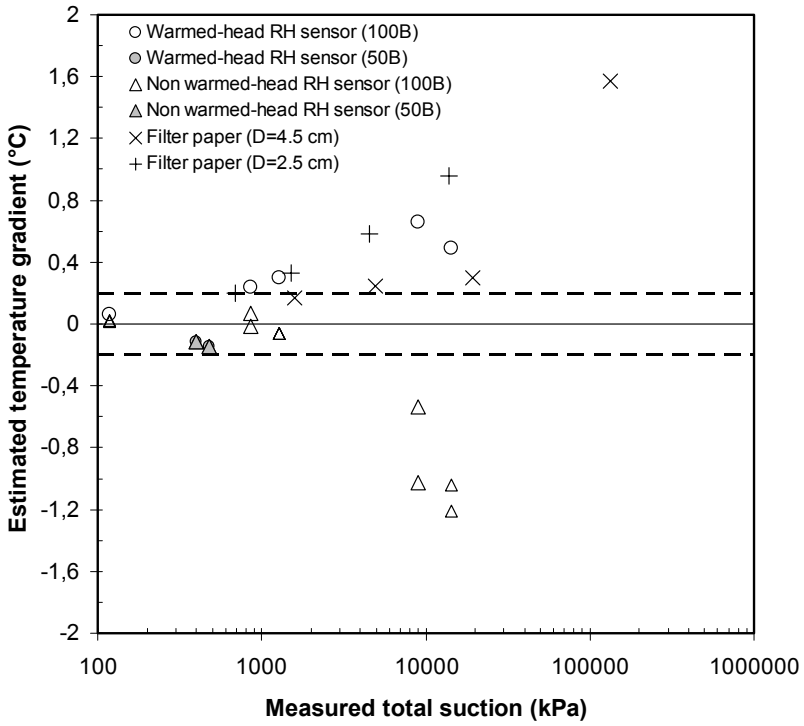

Figure 6.16 Estimated temperature gradient in total suction measurements

head *RH* sensor and filter paper). Even the estimate temperature gradients in the warmed-head *RH* sensor and filter paper method are positive, the values are higher than the temperature gradient occurs in the chamber (i.e., ± 0.2 °C). Therefore, temperature gradient is not the only thing that causes the error in the total suction measurement using the sensor.

Figure 6.17 shows the error lines due to inaccuracy of the sensors used in the total suction measurements and combination of error due to inaccuracy of the sensors and temperature gradient (i.e., ΔT of 0.2 °C). Figure 6.17.a shows the total suction result of chilled-mirror hygrometer and error line due to inaccuracy of the equipment. Since the total suction measurement is commenced at no temperature differences between the specimen and air in the chamber, the error due to temperature gradient does not exist in the chilled-mirror hygrometer (Agus and Schanz, 2007).

As shown in Figure 6.17.a, the error appears at total suction lower than 1000 kPa (or *RH*>99.2%). This agrees with the result in Figure 6.9 that the error higher than 30% occurs at total suction less than 1500 kPa. Interestingly, the total suction measured using warmed-head *RH* sensor is placed out of the error envelopes neither the error due to inaccuracy of the sensor nor the error due to combination of inaccuracy of the sensor and temperature gradient (Figure 6.17.b). This is plausible due to the warming function of the sensor. A correction has been done to the measured total suction using the verification curve as shown in Figure 6.4. As

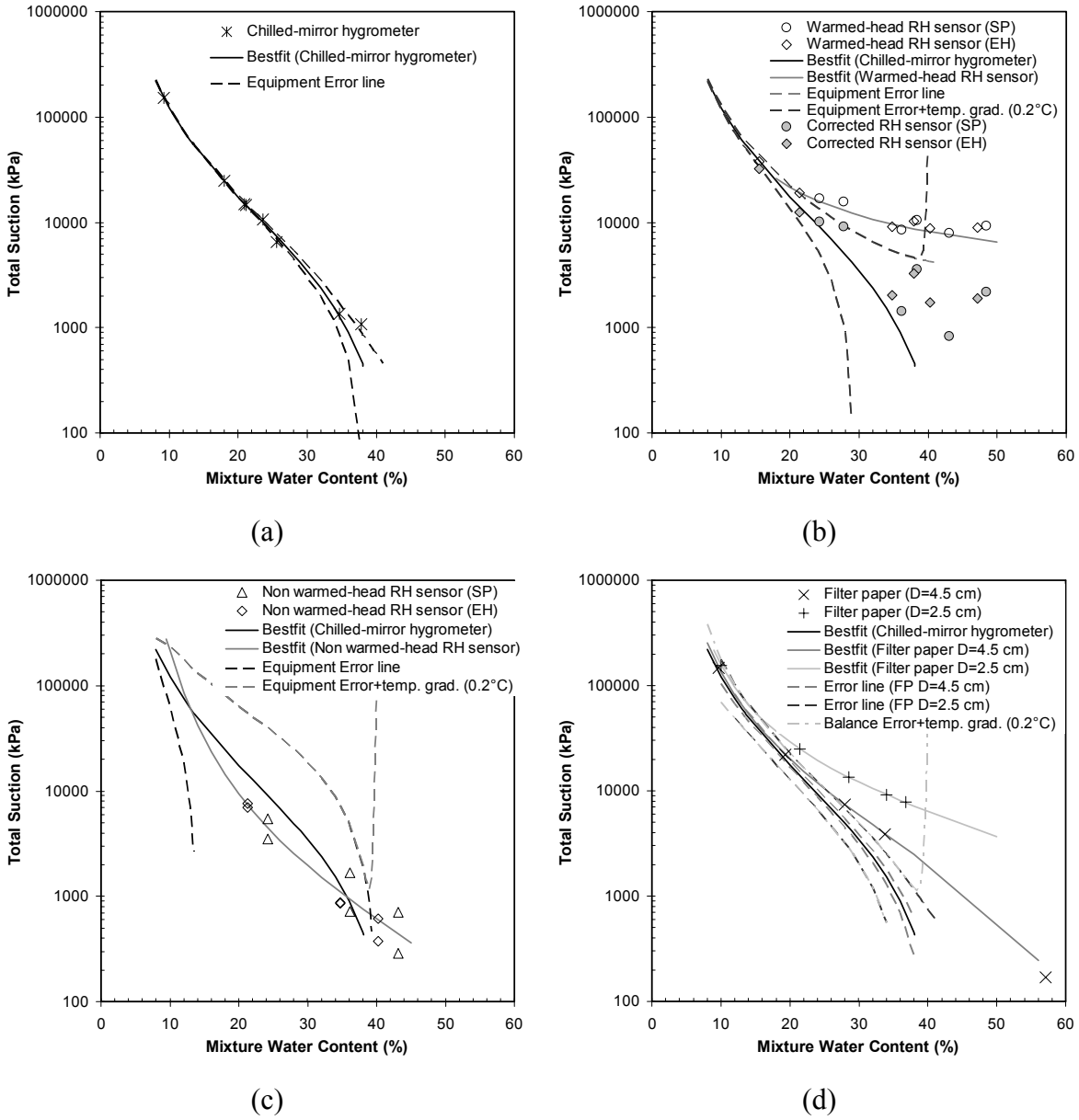

Figure 6.17 Error due to inaccuracy of the equipment used in total suction measurement and temperature gradient (a) chilled-mirror hygrometer, (b) warmed-head *RH* sensor, (c) non warmed-head *RH* sensor, and (d) filter paper method.

shown in Figure 6.17.b, the corrected total suction is placed close to the total suction measured using chilled-mirror hygrometer and placed inside the error envelope of the sensor.

Figure 6.17.c shows the error envelope for non-warmed *RH* sensor. Compared to other sensors used in this study, the non-warmed *RH* sensor shows very large error envelope. However, the measured total suction is placed in the envelope and close to the chilled-mirror hygrometer result (i.e., ± 50% error based on Figure 6.15). The result confirms that good in calibration technique and controlled temperature gradient can minimize the error in the total suction measurement.

Figure 6.17.d shows the error envelope for filter paper methods. The same as warmed-head *RH* sensor, the total suction result measured using filter paper is placed out of the error envelopes. This is possible because of weight lost due to evaporation when the filter paper was removed from the container to the sealed plastic bag before weighing. The weight lost of 0.0004g of filter paper with diameter of 4.5 cm results in error of 5%-33% for total suction range of 1000-100000 kPa. The error of 24%-76% for total suction range from 6000-75000 kPa occurs if the filter paper with diameter of 2.5 cm is used.

6.5.3 Matric suction of Calcigel

As mentioned above in Section 2.5, matric suction consists of capillary pressure and hydration force. However, the matric suction measured using contact filter paper method provides only the value of the capillary component of soil suction since the filter paper is not a true semi-permeable membrane and therefore the effect of cation in the soil pore-water is not taken into account. Figure 6.18 shows the matric due to capillary pressure and total suction of compacted bentonite measured using filter paper method (D = 4.5 cm) plotted as a function of bentonite water content. The suction data measured using filter paper (D = 2.5 cm) were not used due to high possible error obtained from the small diameter of filter paper. The matric suction due to capillary pressure and total suction data were calculated using Equation 6.1 and Equation 6.2, respectively. The Equation 6.1 was extrapolated for calculating the matric suction value higher than 1500 kPa and the Equation 6.2 was extrapolated for total suction less 1500 kPa. The total suction minus matric suction due to capillary pressure was calculated using the best-fit curves of respective suction. Since the matric suction presents only the capillary component, the total suction minus matric suction due to capillary pressure curve as shown in Figure 6.18 provides not only osmotic suction but also hydration force.

The data of matric suction due to capillary component of 50B/50S specimen merge with those of 100B when the data plotted in bentonite water content as shown in Figure 6.18. It seems that presence of sand in the compacted bentonite does not affect the magnitude of capillary component of total suction since the capillary phenomena were developed inside the aggregate. Presence of new pore population (i.e., at pore diameter of 20 μm) due to addition of sand in the mixture as shown in Figure 5.3 does not give significant difference. This can be proved by calculating the capillary pressure due to presence of new pore population at 20 μm using Jurin's law (Jurin, 1718) with Equation 6.10 (Fredlund and Rahardjo, 1993).

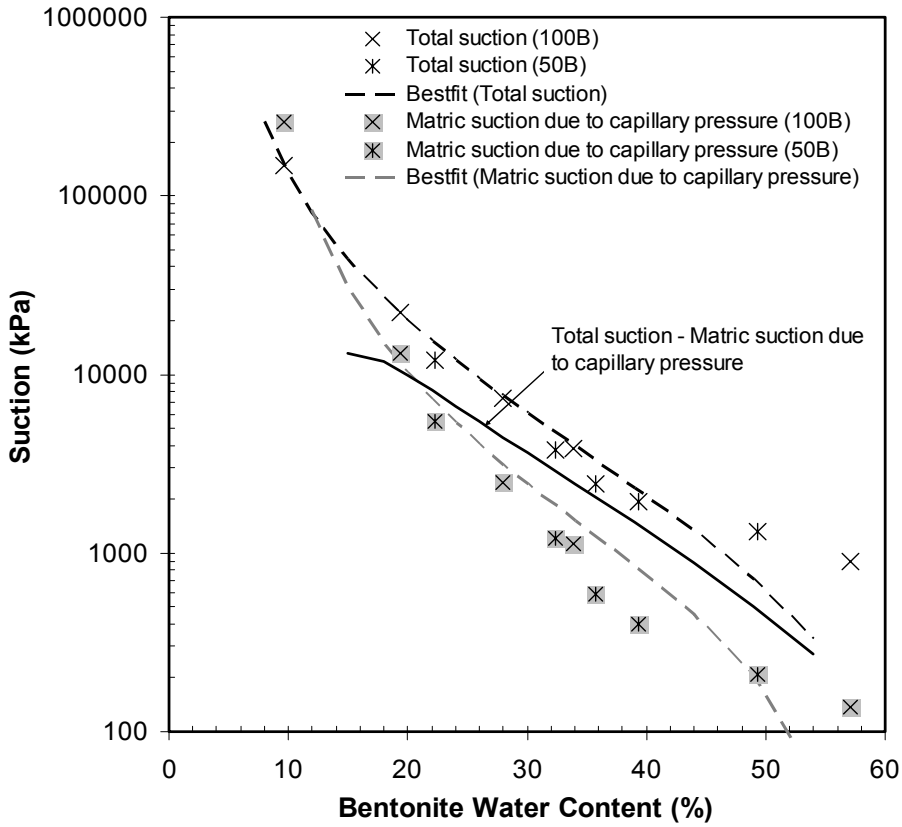

Figure 6.18 Total and matric suction of Calcigel

$$(u_a - u_w) = \frac{T_s}{R_s} \tag{6.10}$$

where (u_a-u_w) is capillary pressure, T_s is surface tension of water (i.e., 72.75 mN/m at 20 °C), and R_s is radius of curvature of meniscus (i.e., equal to pore radius of soils by assuming contact angle α = 0). It is found that the new pore population at diameter of 20 μm results in capillary pressure of 14.6 kPa.

Figure 6.18 also shows that the total suction and matric suction curves merge at water content less than 12% corresponding to suction higher than 50000 kPa. This is close to the water content required to fulfill the hydration force (i.e., w = 15 %) calculated using data presented in Table 2.1 by considering S_s = 525 m^2/g. It means that the capillary component is not developed at suction higher than 50000 kPa. In this condition, at high suction value, water in the specimens flows mainly in vapor form. The contact filter paper method does not measure the capillary component but the total suction. The figure also shows that at water content of 9% the matric suction due to capillary component obtained from contact filter paper method is higher than total suction obtained from non contact filter paper method. This is because in the contact filter paper method, three layers of filter paper (i.e., one smaller filter

paper and two protective papers) are used. The filter paper placed in the middle (i.e., the smaller one) may absorb less water due to the presence of the protective filter papers and result in over estimate the suction obtained. Therefore, contact filter paper method is not recommended to measure capillary component of bentonite for high suction value (i.e., less than 50000 kPa). This value is close to the matric suction range that can be measured using the contact filter paper method suggested by Ridley and Wray (1996) (i.e., 30-30000 kPa).

6.5.4 Temperature effects on Suction Characteristic Curve

In this study, the two capacitance relative humidity sensors (i.e., non warmed-head *RH* sensor and warmed-head *RH* sensor) were used. The non warmed-head *RH* sensor was used because the sensor shows a good performance in measuring suction at 20 °C and the technical specification shows that the sensor can be used for measuring *RH* at temperature up to 85 °C (BC Components, 1999). The warmed-head *RH* sensor was used since the sensor equipped with warming function that can prevent the excessive condensation during the test and the technical specification shows that the sensor can be used for measuring *RH* at temperature up to 100 °C (Vaisala, 2002). The chilled-mirror hygrometer was not used due to technical limitation that the equipment can be used for maximum temperature of 40 °C. Filter paper method was not used because its color change to be brown after prolonged to expose at elevated temperature of 80 °C. This should change the fiber structures and adsorption behavior of the filter paper.

Figure 6.19 shows a typical reading of the relative humidity and temperature versus time for both sensors (i.e., warmed-head and non warmed-head *RH* sensors). The figure indicates that the non warmed-head *RH* sensor (dash line) attains equilibrium more quickly at both temperatures (i.e., at 20 and at 80 °C) compared to the warmed-head *RH* sensor. The non warmed-head *RH* sensor was not sensitive to the change in temperature higher than 60 °C indicating that excessive condensation possibly occurred in the sensor.

Figure 6.19 also shows that the relative humidity decreased at the initial reading as the temperature of the air space, where the sensors were placed, increased above the temperature of the specimen resulting in an increase in the saturated water vapor of the air space. The increase in the saturated water vapor caused the relative humidity of the air space to decrease. The relative humidity increased as a temperature equilibrium was reached slowly between the vapor space in the specimen and that in the hole. At equilibrium, the temperatures of the air space and the specimen were the same and the relative humidity equilibrated.

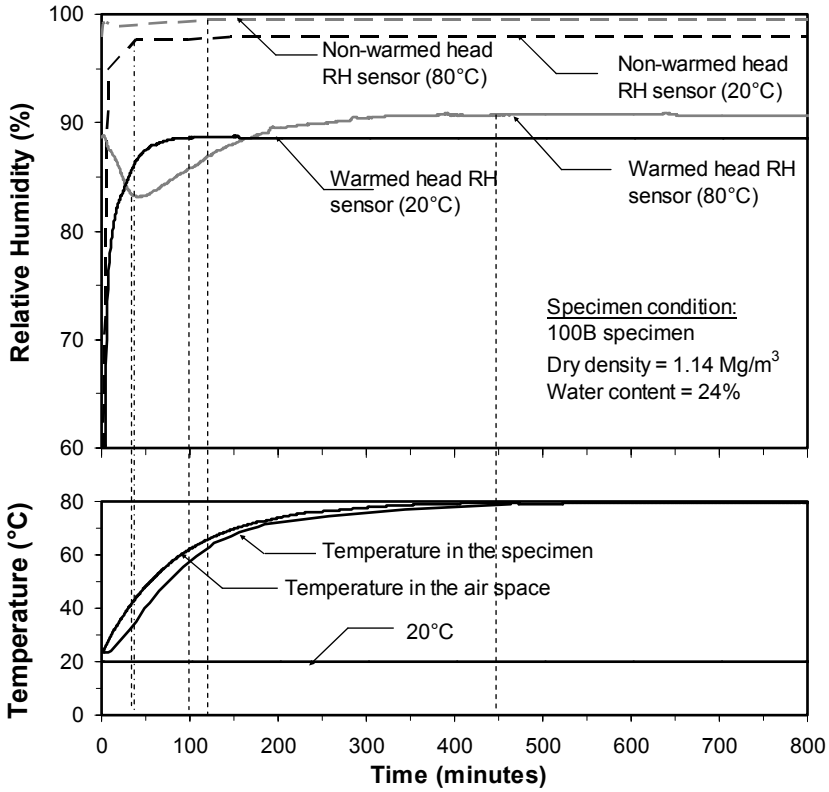

Figure 6.19 Typical reading of the relative humidity and temperature versus time of the non warmed-head RH sensor and the warmed-head RH sensors.

The change in the capillary suction component due to a change in temperature can be approximated using the following equation (Grant and Salehzadeh, 1996).

$$\frac{s(w,T)}{s(w,T_r)} = \left(\frac{a_1 + b_1 T}{a_1 + b_1 T_r} \right)^{b_1} \tag{6.11}$$

where b_1 is equal to 1 and a_1 is equal to -766.45 K, T is temperature and T_r is a reference temperature. Equation 6.11 was derived based on an assumption that temperature only affects the surface tension while the contact angle between pore-water and the soil matrix remains unaffected. The result of the computation of the change in total suction as affected by the change in temperature is plotted (as dotted lines) and compared with the measured values (as solid lines) in Figure 6.20 and Figure 6.21.

Figure 6.20.a and 6.20.b show the effects of temperature on the total suction measured by the non warmed-head *RH* sensor for the compacted bentonite-sand mixtures with bentonite content of 50% and 100%, respectively. The specimens used were named based on the compaction energies (i.e., standard Proctor as SP and enhanced Proctor as EH), mixture water content (e.g., 14 means the specimens has 14% mixture water content), and bentonite content in the mixtures (i.e., 50B for 50% bentonite in the mixture and 100B for pure bentonite). The figures show that the total suction measured at 80 °C is less than that of measured at 20 °C

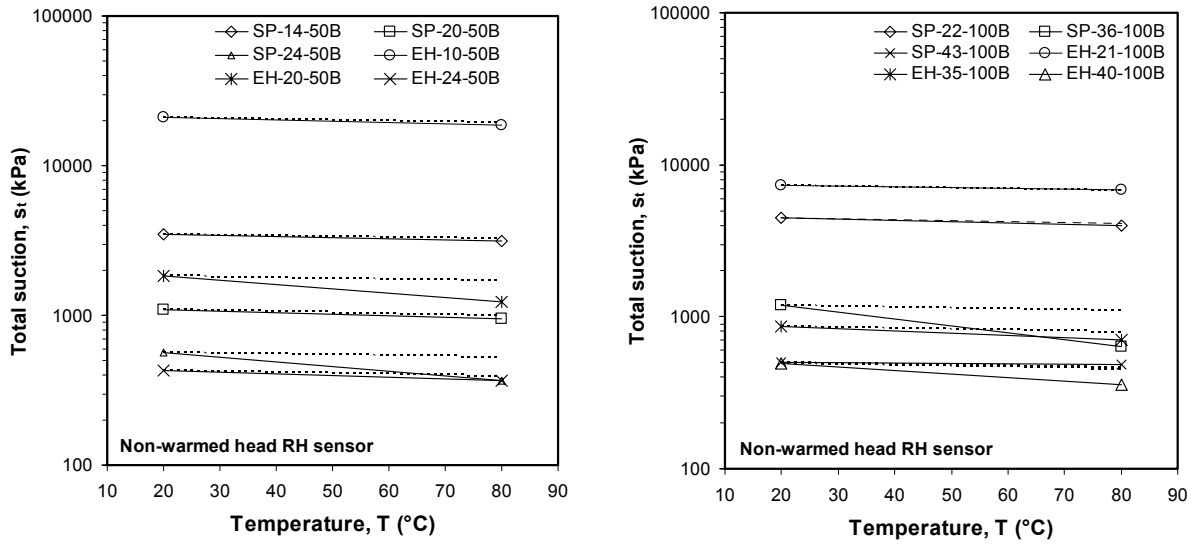

(a) (b)

Figure 6.20 Temperature effects on the total suction of the compacted bentonite-sand mixtures at constant water contents for (a) 50% bentonite content and (b) pure bentonite measured using the non warmed-head *RH* sensor

and, generally, the computed total suctions using Equation 6.11 as shown in dash line are slightly greater than the measured values as shown in solid line. At total suction less than 2000 kPa, some results show different trend due to possible occurrence of condensation when using the sensor (e.g., EH-20-50B, SP-24-50B, SP-36-100B, and EH-40-100B).

Figure 6.21.a and 6.21.b show the effects of temperature on the total suction measured by the warmed-head RH sensor for the compacted bentonite-sand mixtures with bentonite content of 50% and 100%, respectively. As shown in the figures, the total suction measured at 80 °C is less than that at 20 °C and the measured total suctions (solid line) are slightly greater than the total suctions predicted using Equation 6.11 (dash line) for suction higher than 10000 kPa. For suction less than 10000 kPa, the total suction measured at 80 °C is still less than that of at 20 °C but the change in total suction due to temperature effect is the same as that of the prediction.

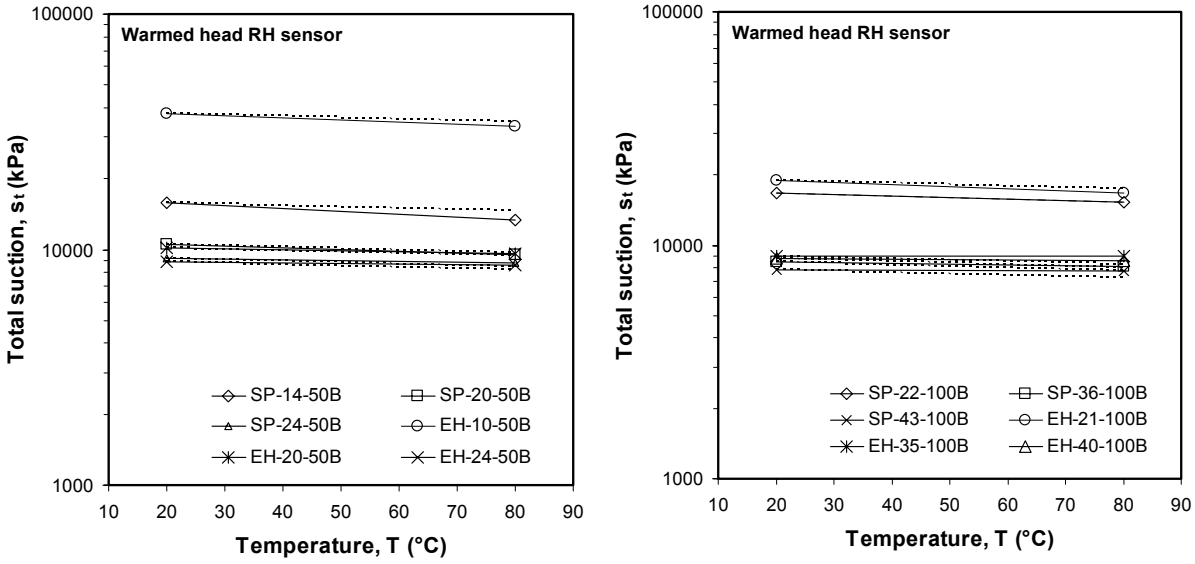

(a) (b)

Figure 6.21 Temperature effects on the total suction of the compacted mixtures at constant water contents for (a) 50% bentonite content and (b) pure bentonite measured using the warmed-head *RH* sensor

Figure 6.22 and 6.23 show the effect of temperature on the measured total suction, presented as a plot of total suction versus bentonite water content measured using the warmed-head and non warmed-head *RH* sensors, respectively. As shown in Figure 6.22, the total suction obtained using warmed-head *RH* sensor shows almost constant valued at suction lower than 10000 kPa due to warming function of the sensor. This occurs not only at 20 °C as shown by empty symbols but also at 80 °C as shown by filled symbols. As depicted in Figure 6.23, the total suction obtained using non warmed-head *RH* sensor appears scatter at total suction less than 2000 kPa. This is due to condensation happen on the surface of the sensor at low suction. It seems that the total suction data obtained from both sensors (i.e., warm-head and non warmed-head *RH* sensors) are affected by the physical behavior of the sensor used. However, in general the results show that the total suction data obtained at 80 °C as shown by gray curve are lower than those at 20 °C as shown by black curve.

Figure 6.22 shows that for total suction higher than 20000 kPa the computed curve based on the change in the capillary component of total suction (Equation 6.11) as shown by dash line is located between the total suction curves measured using both sensor at 20 °C and at 80 °C. For total suctions less than 20000 kPa, the prediction lies close to the total suction curves measured at 80 °C. This also happens to the result obtained using non warmed-head *RH* sensor as shown in Figure 6.23. The total suction measured using non-warmed head *RH* sensor at 80 °C shows to diverge from that of at 20 °C for total suction less than 2000 kPa. As mentioned above, this is due to possible condensation happen during the experiment at 80 °C

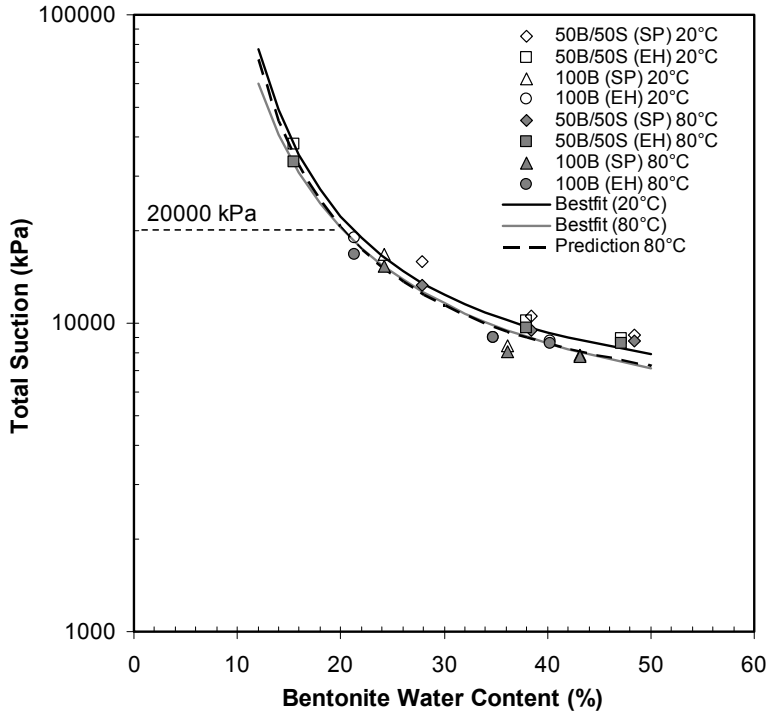

Figure 6.22 The effect of temperature on the total suction measured using the warmed-head *RH* sensor

resulting drop in total suction measured. Based on the results, it can be stated that the effect of temperature on the total suction at constant water content for the materials investigated herein for total suction higher than 20000 kPa is mainly due to decrease in the hydration force. For suction less than 20000 kPa, the prediction of temperature effect on the total suction is close to experimental result. The result indicates that, for suction less than 20000 kPa, the change in total suction due to temperature effect is due to the change in capillary component of total suction. The results also suggest a significant contribution of capillary component in the magnitude of total suction in this range. The change in the osmotic component of total suction is insignificant for the bentonite used in this study. The result which supports this statement is discussed in the Chapter 7.

Additional tests have been done in order to verify whether these phenomena were caused by the change in the clay fabric and pore-fluid chemistry of the soils. A pure bentonite specimen with water content of 22% was prepared and alternately heated at 25-80 °C following heating cycles. If the change in the clay fabric and pore-water chemistry is irreversible, there will be a permanent and irreversible change in the total suction due to cyclic heating. The results show that the alteration of total suction due to heating cycles was not obvious and reversible (Figure 6.24).

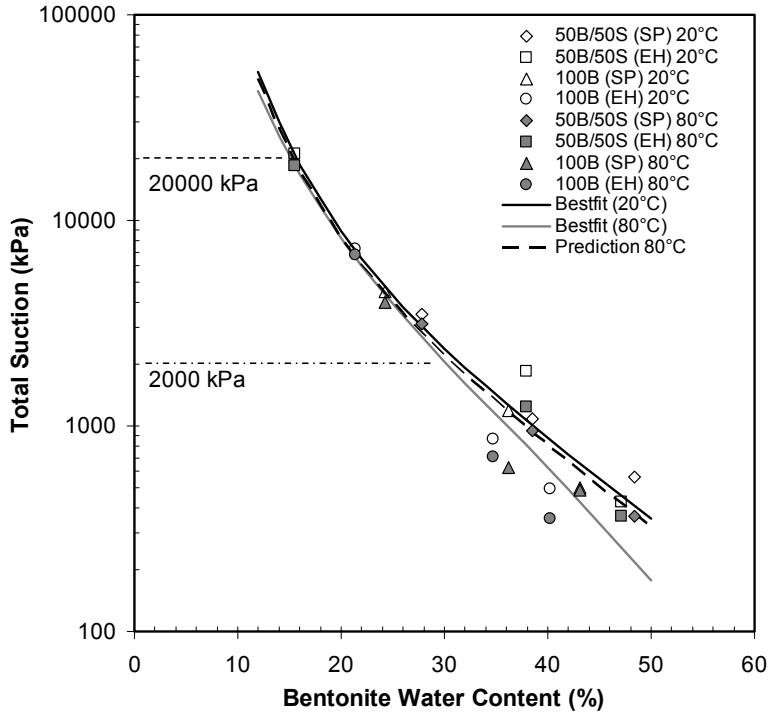

Figure 6.23 The effect of temperature on the total suction measured using the non warmed-head *RH* sensor.

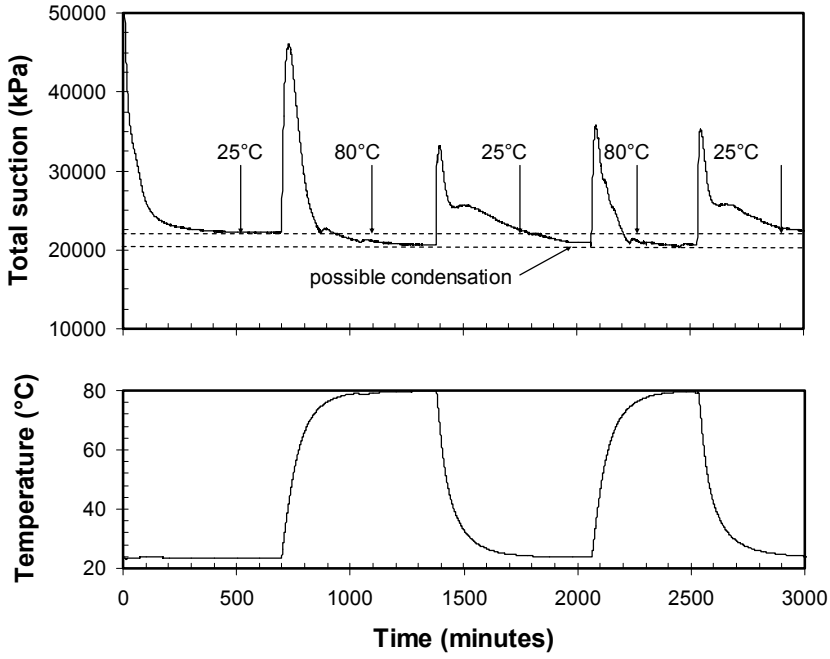

Figure 6.24 Effect of cyclic heating on the total suction at constant water contents measured using warmed-head *RH* sensor.

6.5.5 Total Suction of Pretreated specimen

In order to investigate the temperature effects on the specimen (i.e., Calcigel) experienced heating for long time, the specimen that has experienced heating for 423 days at 80 °C was used. The specimen was cooled in a desiccator contained silica gel. After that, the specimen was soaked in the deaired-distilled water for two weeks. Since the specimen was mixture of bentonite-sand mixture, the specimen was sieved using sieve 200# to take only the clay portion from the mixture. Small amount of the bentonite was placed in the specimen chamber of chilled-mirror hygrometer. The chamber together with the specimen was placed in a desiccator with salt solution having a particular suction for drying. The total suction of specimen was measured using chilled-mirror hygrometer at room temperature. The weight of the specimen was measured using the balance with readibility of 0.0001 g directly after the total suction measurement. Afterward, the specimen was placed in a desiccator with salt solution having higher total suction. The procedures were repeated until the highest total suction in drying processes was applied (i.e., saturated $MgCl_2$ solution). The specimens were placed in the oven with temperature of 100 °C in order to determine the dry weight of the specimen. The result is compared to the bentonite-sand mixture specimen called as non treated specimen. The same procedures (i.e., soaking, sieving, drying, and measuring total suction) were applied to the non treated specimen. The result is presented in Figure 6.25.

Figure 6.25 shows that the ability of specimen after heated at 80 °C for 423 days to retain water as shown in suction characteristic curve does not change. Very small change is observed for total suction less than 10000 kPa. This is possible due to cementation of the clay particles resulting larger particle size that affects only the capillary component of total suction at suction less than 10000 kPa.

In order to investigate at which temperature that permanent and irreversible changes happen to the bentonite used in this study, the total suction measurements were performed to the specimen heated at temperature of 100, 200, 300, 400, and 500 °C. In this test, the pure bentonite was placed in oven at 100 °C for 24 hours which is the same as water content determination. After cooled in desiccator, the specimen were placed in a special container and put in electric furnace that can be used for temperature up to 1000 °C. In this study, temperatures of 200, 300, 400, and 500 °C were applied. After specimens were heated for 3 hours at these temperatures and cooled in desiccator, the specimens were placed in the chamber of chilled-mirror hygrometer. The specimens were soaked in the chamber with deaired-distilled water for 2 weeks. The specimens were dried in the dessicator with salt

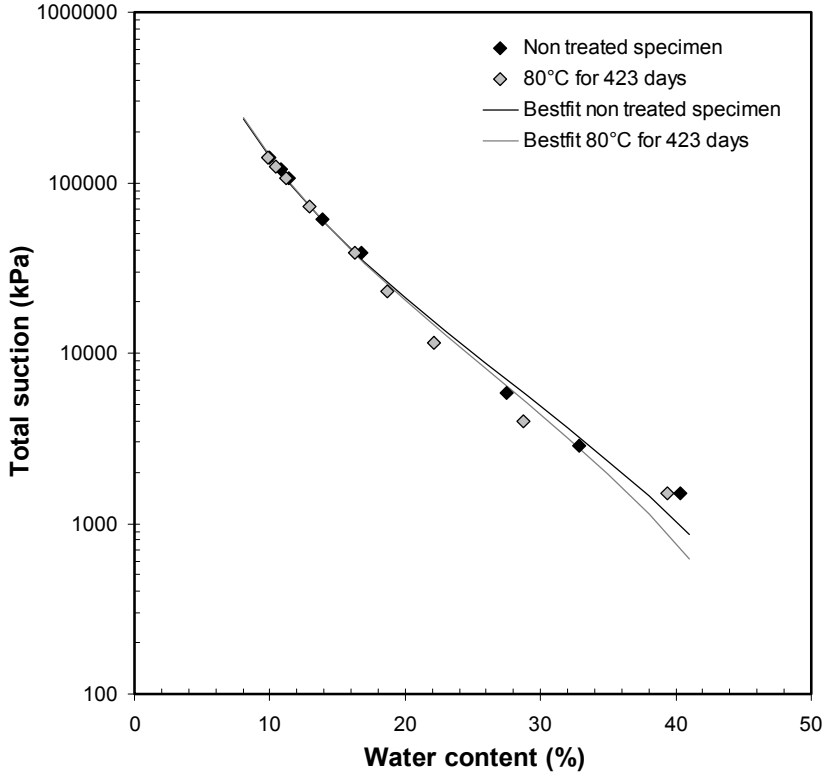

Figure 6.25 Effect of heat pretreatment on the Calcigel heated at 80 °C for 423 days

solution. The relative humidity of the specimens was measured using the chilled-mirror hygrometer. The weights of the specimens were measured using the balance with readibility of 0.0001 g directly after the total suction measurement. Afterward, the specimen was placed in a desiccator with salt solution having higher total suction. The specimens were placed in the oven with temperature of 100 °C in order to determine the dry weights of the specimens. The result is presented in Figure 6.26. The experimental data were fitted with solid line and the alteration of retention capacity of the specimen (calculation) compared to that of untreated specimen was shown in dash line.

Figure 6.26 shows that no difference in the total suction versus water content of non treated and treated specimen at 100 °C was observed in the result providing evidence that the changes in the suction characteristic of compacted bentonite due to elevated temperature less than 100 °C are reversible. The ability of specimen to retain water reduces approximately 15% after the specimen was pretreated at temperature higher than 200 °C. The reductions increase up to 25%, 35%, and 40-50% after the specimens were pretreated at temperature of 300, 400, and 500 °C, respectively.

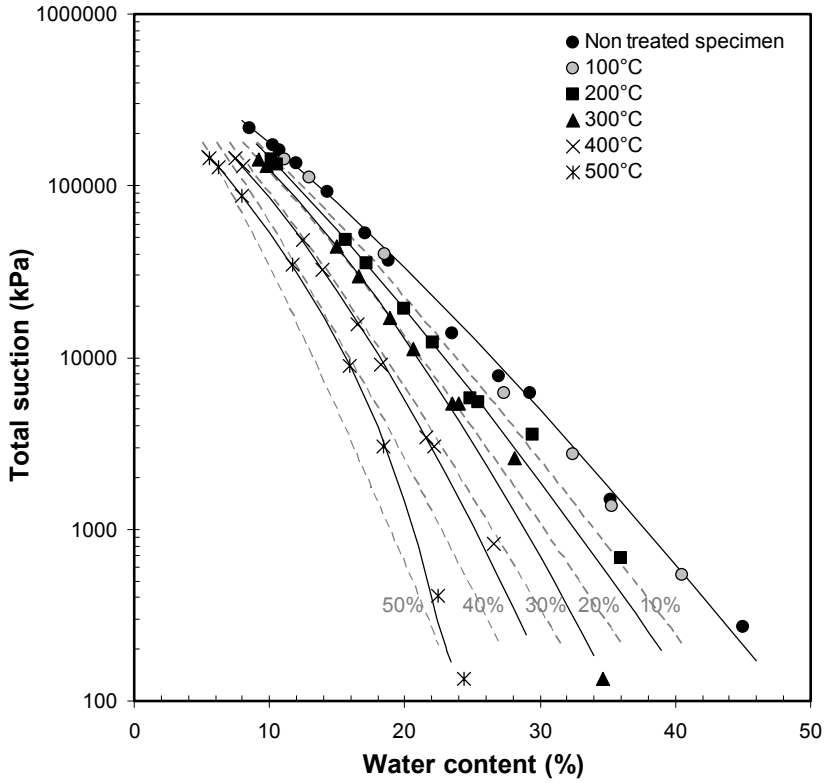

Figure 6.26 Effect of heat pretreatment on the Calcigel heated from 100-500 °C

Figure 6.27 shows the X-ray diffraction result of Calcigel before and after heating at 100 to 500 °C. As shown in the figure, the peaks of montmorillonite mineral reduce after heating at temperature of 200 °C and disappear after heating at temperature of 400 °C. Considering almost no K^+ cation found in the exchangeable cation as shown in the CEC examination (Chapter 4) and very low concentration K^+ cation in the free pore water as shown in osmotic suction investigation (Chapter 7), the reduction in the ability of the pretreated bentonite used in this study to retain water may be caused by cementation due to precipitated Si on the surface of bentonite aggregates (Pusch, 2000) and/or by formation of a covalent bonding between Ca^{2+} cation with clay surface (Mokrejš et al., 2005).

6.6 Summary

The following conclusion can be drawn based on the results of suction measurements on bentonite and bentonite-sand mixture.

1. No influence of compaction condition (or dry density) on the total suction is observed. Total suction of the bentonite-sand mixtures is a function of mixture water content and mixture bentonite content or collectively a function of bentonite water content. These are valid not only at room temperature but also at elevated temperature.

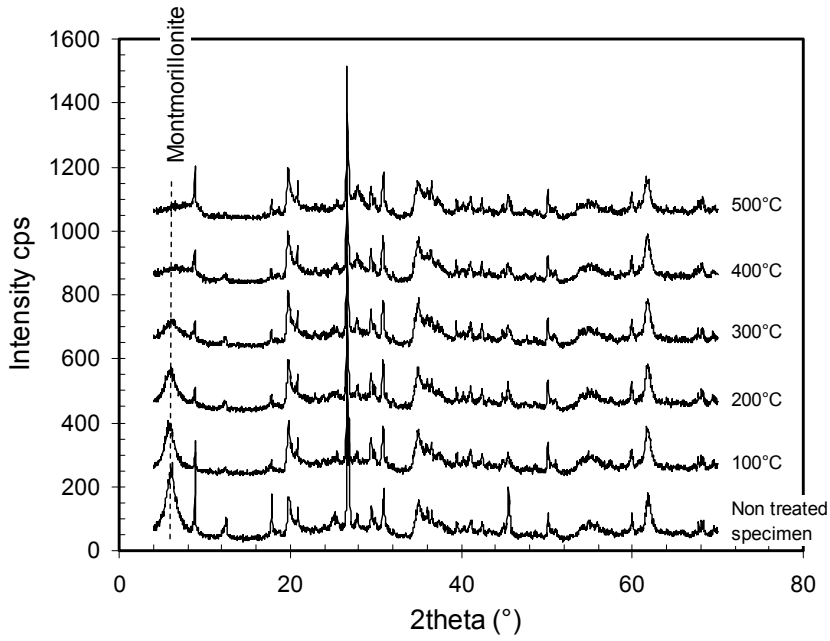

Figure 6.27 X-ray diffraction result of Calcigel before and after heating

2. The chilled-mirror hygrometer shows the best accuracy among the other sensors used in this study but it is limited to temperature less than 40 °C.
3. The filter paper technique is influenced by the size of the filter paper used. The bigger diameter of the filter paper results in lower error of the total suction measurement obtained.
4. The total suction obtained using warmed-head *RH* sensor is influenced by the warming function of the sensor.
5. Good calibration technique and temperature control can improve the performance of non warmed-head *RH* sensor for measuring suction.
6. At a given water content, increase in temperature results in decreasing total suction. The reduction of the total suction is due to reduction in the capillary component of total suction for total suction less than 20000 kPa. For total suction higher than 20000 kPa, the reduction in total suction is due to reduction of capillary component and/or hydration force.
7. Effect of heating to the specimen at 80 °C for 423 days on the total suction versus water content is very small.
8. The change in total suction due to temperature increase is reversible and no evidence of mineralogical change is found to the bentonite exposed to temperature less than 100 °C.

9. The montmorillonite mineral in the bentonite used in this study alters after the specimen was heated at the temperature higher than 100 °C and fades after the specimen was heated at the temperature of 500 °C.

CHAPTER 7

PORE-WATER CHEMISTRY AND OSMOTIC SUCTION OF HIGHLY PLASTIC CLAYS

7.1 Introduction

In unsaturated soil mechanics, when significant changes in salt consentration in soil pore-water, osmotic suction is one of important components influencing the behavior of soils (Miller and Nelson, 1992). Osmotic suction is related to the dissolved salt content in the soil pore-water (Barbour and Fredlund, 1989). The wide use of compacted unsaturated soils as a sealing material, e.g., as a clay liner in landfill and as a bentonite barrier in high level waste repository, leads to consider osmotic suction as an important issue. This is due to the fact that the material will be in contact with salt solution from leachate in the landfill or salt water of surrounding rocks in the high level waste repository.

Dissolve salt solution (or pore-water chemistry) in the soil is one of the soil aspects that is influenced by temperature (Section 3.2.2). Since the osmotic suction is related to dissolved-salt content in the soil pore-water, it is thought that the osmotic suction changes by changing in temperature. According to Section 3.2.2, the suction of salt solution decreases or increases due to increase in temperature depending on the type of the cation. Therefore, it is important to investigate the magnitude of osmotic suction and the cation in the pore-water of bentonite used in this study. Some researchers have investigated the osmotic suction of low plastic clay. However, until now the method to investigate osmotic suction of highly plastic clay such as bentonite has not been clearly described.

This chapter presents the pore-water chemistry and osmotic suction determination of bentonite. Since bentonite behavior is highly influenced by cations type of its exchangeable cation, two different types of bentonite (i.e., sodium bentonite and Calcigel) were used. In this chapter, the effects of osmotic suction on the hydro-mechanical behavior (i.e., swelling pressure) of the two types of bentonites used are also presented and discussed. The temperature effect on the osmotic suction of Calcigel is also discussed. The relationships

between physico-chemical properties of soils and osmotic suction obtained in this study and in literatures are also presented and discussed.

7.2 Literature Review Related to Osmotic Suction

When a compacted clay is exposed to a concentrated salt solution, the fluid with or without dissolved salt will flow in response to osmotic gradient. In case where a soil behaves as a perfect semi-permeable membrane, only pure water will flow to medium with higher salt concentration. But, since there is no true semi-permeable membrane in soils, the water and dissolved salt will flow to medium with lower salt concentration. The degree to which the clay behaves as perfect semi-permeable membrane is entitled as osmotic efficiency. The osmotic efficiency of a soil is strongly dependent on pore fluid chemistry, pore fluid concentration, void ratio, and interparticle spacing (Barbour and Fredlund, 1989). According to osmotic efficiency versus interparticle spacing and salt concentration relationship as shown in Barbour and Fredlund (1989), at the same interparticle spacing and salt concentration, the osmotic efficiency of Na^+ soil is higher than that of Ca^{2+} soil. It means that the Ca^{2+} soil is more permeable than Na^+ soil. Therefore, in Ca^{2+} soils the water flows with carrying some dissolved salts from the micro-pores or double layer in order to response the change in bulk water or free water concentration.

In nature, evaporation causes decrease in the amount of pore-water in soil. This results in increasing the concentration of dissolved ion or the osmotic suction of the soil. At low water content in which there is no dissolve salt in the soil pore-water, the osmotic suction being zero and negligible (Sreedep and Singh, 2006). Mata et al. (2002) proposed a cut-off law that the osmotic suction is being constant at water content lower than micro-structural water content. The micro-structural water content is defined as water in the intra-aggregate pores. This is not easy to determine in practice and may need a complex micro-structure investigation.

Miller and Nelson (1992) studied the effect of salt concentration in the soil pore-water on the shringkage curve (i.e., water content versus volume of specimens). They found that the volumes of specimens prepared with sodium chloride solution are smaller than those of specimens prepared with distilled water indicating an additional stress acting on the sodium chloride specimens. In swelling strain investigation, Rao and Shivananda (2005) found that the difference in salt concentration did not influence the magnitude of swelling strain of salt-amended clay. But the specimen with high salt concentration showed delay to reach

maximum swelling strain due to migration of cation from the specimen to the reservoir. This delay was also observed by Di Maio (1996) in the osmotic consolidation and swelling of sodium montmorillonite. Di Maio (1996) stated that the small rates of ion diffusion through clay pores causes delay in the osmotic consolidation relative to mechanical consolidation.

Miller and Nelson (1992) and Sreedeep and Singh (2006) determined the osmotic suction of clayey soils from the difference between total suction and matric suction that are measured independently. Miller and Nelson (1992) used filter paper technique and pressure plate apparatus to measure total suction and matric suction, respectively. Sreedeep and Singh (2006) used chilled-mirror hygrometer and pressure membrane extractor to measuring total and matric suction, respectively. Moreover, the pressure plate apparatus and pressure membrane extractor measure only the capillary component of total suction. Therefore, the determination of osmotic suction from the difference between total suction and matric suction might be true for soils with low montmorillonite content or specimen at high water content where the hydration force component is insignificant in matric suction component. For soil with high montmorillonite content, the difference between the total suction and capillary component results in osmotic suction plus hydration force component. Therefore, an independent measurement of osmotic suction should be performed in order to determine osmotic suction due to dissolved salt concentration in the free soil pore-water.

Osmotic suction of a soil can be determined by measuring the electrical conductivity of an extract of the soil pore-water. Squeezing technique has been widely used to squeeze out the soil pore-water (Krahn and Fredlund, 1972; Morgenstern and Balasubramonian, 1980; Romero, 1999; ENRESA, 2000; Leong et al., 2003; Peroni and Tarantino, 2005; Rao and Shivananda, 2005). For different purposes, the squeezing technique was also used for measuring the soil water chemistry and soluble salt content in soils (e.g., von Engelhardt and Gaida, 1963; Manheim, 1966; Manheim and Giekes, 1983; Iyer, 1990; ASTM D 4542-95 (ASTM, 1997); Sacchi et al., 2001). The squeezing technique shows reasonable result compared to other method (e.g., saturation extract method) for measuring osmotic suction (Krahn and Fredlund, 1972) and soil pore-water chemistry (Iyer, 1990). The problem in using squeezing technique is that the magnitude of the squeezing pressure applied influencing the result obtained (Iyer, 1990; Fredlund and Rahardjo, 1993; Sacchi et al., 2001). Interestingly, all researchers mentioned above have been used a single squeezing pressure to extract pore-water from the soils at different water content. In case of porous material or material with small montmorillonite content, until a certain value of pressure (i.e., approximately 50 MPa) the concentration of salt in the extracted soil pore-water does not change by increasing

squeezing pressure (Manheim, 1966). However, the salt concentration of the pore-water squeezed out from the soil with high montmorillonite content decreases by increasing squeezing pressure (von Engelhardt and Gaida, 1963). Therefore, it is important to investigate the magnitude of squeezing pressure applied without affecting the salt consentration in the soil pore-water.

7.3 Material Used and Specimen Conditions

In this study, a sodium type bentonite from Indian, namely Indian bentonite from here on, and Calcigel were used in order to study the osmotic suction from the different types of highly plastic clay. Tabel 7.1 summarizes the physico-chemical properties of Indian bentonite determined using the same methods as used for Calcigel (Chapter 4). As shown in Table 7.1, Indian bentonite has Na^+ exchangeable cation of 64 meq/100g or almost 80% from the total basic exchangeable cation.

The bentonites were mixed with distilled water with an electric conductivity of 10 μS. Since the electric conductivity of distilled water is very small, it is expected that no effect of the electric conductivity of distilled water on the osmotic suction of the compacted bentonite in this study. After curing for 2 weeks, the specimens were statically compacted to reach the required dry density based on the Proctor compaction curves. Since the amount of Indian bentonite for this study is limited, it is assumed that the dry density and water content of the specimens follow the trend of Calcigel Proctor curves. Figure 7.1 shows the water content and dry density of specimens used.

Table 7.1 Summary of Indian bentonite characteristics

Properties	**Indian Bentonite**
Specific gravity	2.85
Liquid limit (%)	400
Plastic limit (%)	33
Plasticity index (%)	417
Shrinkage limit (%)	14
Clay content (%)	82
Fine content (%)	100
External specific surface area (m^2/g)	81
Total specific surface area (m^2/g)	400
Cation exchange capacity (meq/100g)	62
Basic exchangeable cation Na^+, Ca^{2+}, Mg^{2+}, K^+ (meq/100g)	64, 10, 7, 1
Total basic exchangeable cation (meq/100g)	82

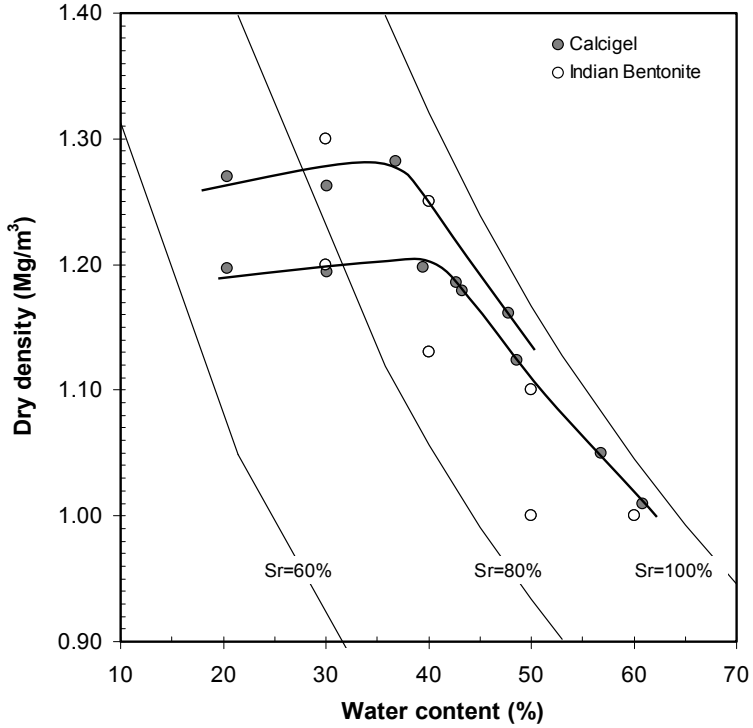

Figure 7.1 Data points corresponding to the specimens used

7.4 Experimental Techniques and Procedures

The squeezing process to extract the specimen's pore-water was performed using a squeezer that has similar shapes and dimensions to the squeezer used by Krahn and Fredlund (1972). Figure 7.2.a shows the squeezer used in this study. As shown in the figure, the squeezer is divided into three main parts (i.e., ram, cylinder, and base). The squeezer was equipped by accessories such as Teflon disk, rubber disk, filter holder, and rubber washer. The Teflon disk was used to separate the ram and rubber disk and to avoid damage in the rubber disk. The rubber disk and rubber washer were used to avoid leakage in the cylinder and between filter holder and base, respectively. The filter holder was used for placing the wire mesh and filter paper.

The osmotic pressure of the pore-water obtained from the squeezing technique was inferred using an empirical relationship between osmotic pressure and electrical conductivity (or a calibration curve) which was measured using a conductivity meter. The calibration of the conductivity meter was performed using molal NaCl solutions. The water potentials (or osmotic suctions) of the solutions used were calculated using equation suggested by Lang (1967) (Equation 3.2).

(a) (b)

Figure 7.2 Device used in the squeezing technique (a) squeezer (b) squeezer in the triaxial load frame.

Figure 7.3 shows the relationship between electrical conductivity and osmotic pressure or the calibration curve determined in this study. The calibration curve obtained is in a good agreement with the calibration curve presented by USDA (1950) which was established for salt mixtures in saline soils. Rao and Shivananda (2005) found a single calibration line for sodium chloride and calcium chloride. The osmotic suction can be computed from the measured electrical conductivity using the following equation.

$$\pi = 38.54 EC^{1.0489} \tag{7.1}$$

where π is osmotic suction (kPa) and EC is electrical conductivity (mS/cm).

The osmotic suction measurement using the squeezing technique was performed on several statically compacted specimens. After compaction, the specimen with diameter of 5 cm was trimmed to reach the same diameter as the squeezer. Pressure was applied one dimensionally using triaxial-load frame (Figure 7.2.b) until the first drop of pore-water expelled. The pressure of 500, 1000, 2000, 4000, 8000, 15000, 20000, 25000, 30000, 35000, 40000, 45000, 50000, 55000, 60000, 65000, 70000, 75000, 80000 kPa were applied with duration for each pressures of 5 minutes. The use of low pressure is unfavorable since lowering squeezing pressure causes longer time to obtain the first drop of soil pore-water.

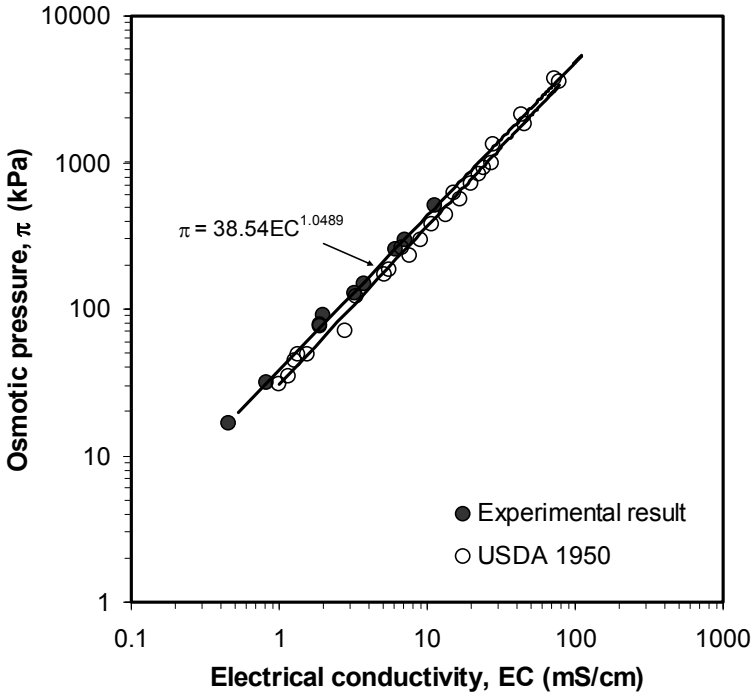

Figure 7.3 Calibration curve for determining osmotic pressure by means of electrical conductivity measurement of soil pore-water

This will change the salt consentration due to evaporation or cation exchange in between elementary layers and in the free pore-water in order to balance the external pressure applied (Sacchi et al., 2001). The soil pore-water was collected using a syringe and was subsequently transferred to the conductivity meter to measure its electrical conductivity. About 2 ml of soil pore-water was required for the measurement and was carefully placed on the sensor surface of the conductivity meter. In about less than 5 seconds after the pore-water placement, the value of the electrical conductivity in μS/cm or mS/cm was shown on the digital display of the equipment. In order to investigate the squeezing pressure effect, the pressure was subsequently increased until the next drop of water was obtained. The osmotic pressure of the extracted soil pore-water was determined from the electric conductivity reading and calculated using Equation 7.1.

A series of constant volume swelling pressure tests was performed in this study using an isochoric cell. The initial conditions of the specimens were the same as those of osmotic suction determination as shown in Figure 7.1. The specimen preparation, experimental techniques and procedures follow the one step swelling pressure test procedures as described in Chapter 9.

7.5 Result and Discussion

7.5.1 Squeezing Pressure Effects on the Osmotic Pressure of Soil Pore-Water

Figure 7.4 shows the influence of squeezing pressure applied on the osmotic pressure of soil pore-water for some compacted Calcigel specimens. As depicted in the figure, all specimens show the same trend that the osmotic pressure of soil pore-water decreases by increasing squeezing pressure. As shown in Figure 7.4, the squeezing pressures required to obtain the first drop of soil pore-water are 45 MPa, 60 MPa, and 70 MPa for the specimens with water content of 60%, 48%, and 43%, respectively. It seems that the squeezing pressure required obtaining the first drop of soil pore-water increases by decreasing the water content of specimen.

Figure 7.4 also shows that, if only a squeezing pressure of 45 MPa is utilized, no water is obtained for the specimens with water content of 48% and 43%. The use of a squeezing pressure of 70 MPa results in under estimation of the osmotic pressure of specimens with water content of 48% and 60%. Consequently, it is not possible to use a single squeezing pressure for the material used in this study and the pressure applied should be determined experimentally. On the other hand, the osmotic suction of the specimens is the osmotic pressure of soil pore-water obtained from the first drop of soil pore-water. Therefore, the term

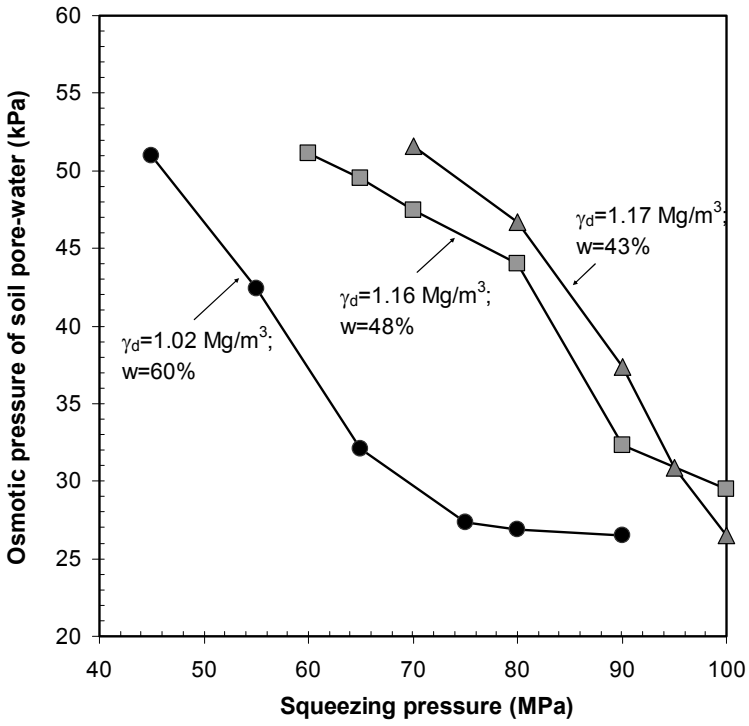

Figure 7.4 Squeezing pressure effect on the osmotic pressure of soil pore-water of compacted Calcigel specimens

of osmotic suction is used only for the osmotic pressure of soil pore-water obtained from the first drop of soil pore-water.

Figure 7.5 shows the squeezing pressure effects on the osmotic pressure of soil pore-water and cation concentration of the squeezed soil pore-water of specimens with water content at liquid limit (i.e., 180% for Calcigel and 400% for Indian bentonite). As shown in Figure 7.5, the osmotic pressure of soil pore-water decreased by an increasing squeezing pressure for both specimens. The result reveals that it happens not only to the unsaturated specimens (Figure 7.4) but also to the initially saturated specimens (Figure 7.5). This occurs due to decrease in the concentration of cation in the squeezed soil pore-water by increasing squeezing pressure as shown in the cation concentration versus squeezing pressure relationship.

As shown in Figure 7.5, from the highest to lowest concentration, cations in the pore-water of Calcigel are Ca^{2+}, Na^{+}, K^{+}, and Mg^{2+}, whereas the cations in the pore-water of Indian bentonite are Na^{+}, Ca^{2+}, K^{+}, and Mg^{2+}. Interestingly, in the CEC determination of Calcigel, the K^{+} cation was not found in the basic exchangeable cation. Figure 7.5.a also shows that the Na^{+} concentration is higher than Mg^{2+} concentration in the extracted soil pore-water of Calcigel. The opposite result was obtained in the CEC determination that the Mg^{2+}

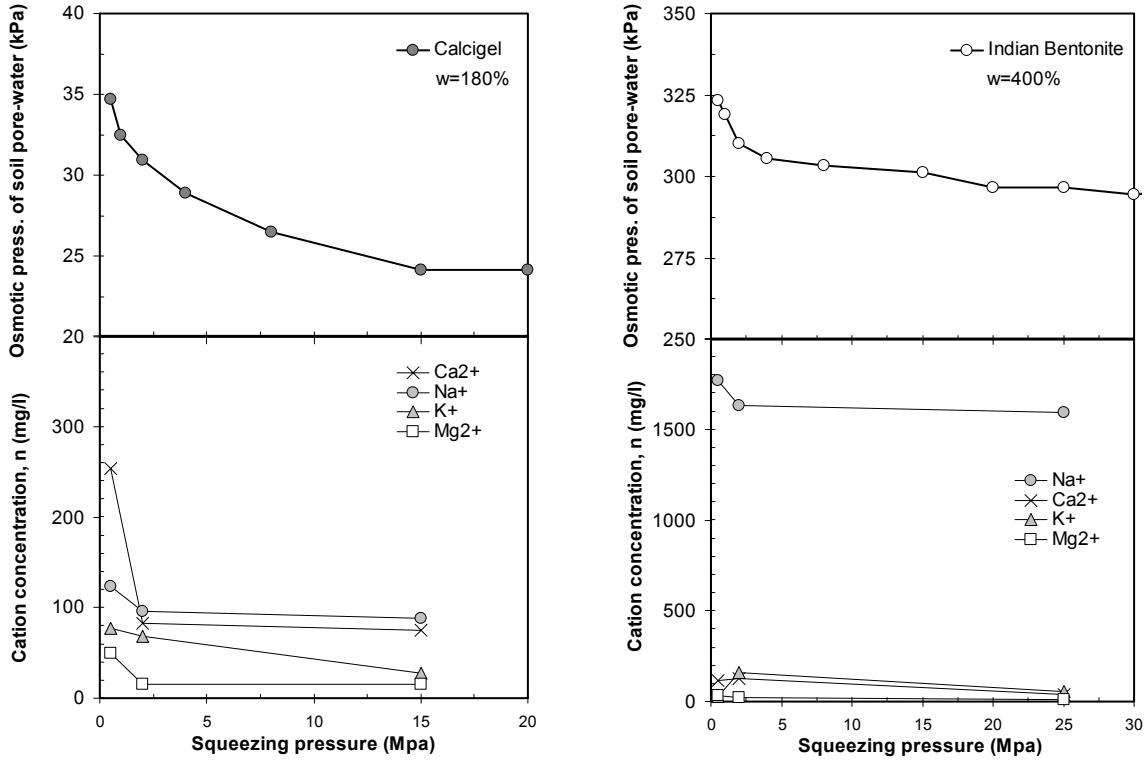

(a) (b)

Figure 7.5 Squeezing pressure effects on the osmotic pressure of soil pore-water and cation concentration for (a) Calcigel and (b) Indian Bentonite with water content at liquid limit

concentration is higher than Na^+ concentration. For the Indian bentonite, based on the result of CEC investigation, the Mg^{2+} concentration is higher than K^+ concentration. Reverse result was obtained in the soil pore-water as shown in cation concentration versus squeezing pressure of Indian bentonite (Figure 7.5.b). The result obtained in this study shows that the cations observed in the CEC determination are different from cations in the osmotic suction determination. The cations obtained in the CEC are immobile cations which are possibly obtained by chemical reaction whereas the cations obtained in osmotic suction determination using the squeezing technique are mobile cations which are free from the electrical charge of clay surface when the water is added to the soils. It is plausible that the cations obtained from CEC determination are responsible for the hydration force of soil suction (matric suction component) whereas the cations in the free pore-water are responsible for the osmotic component of soil suction.

7.5.2 Effects of Initial Conditions of the Specimens on Squeezing Pressure

Figure 7.6 shows the influence of initial conditions of the specimens on the squeezing pressure required to obtain the first drop of soil pore-water and, thus, osmotic suction. As shown in Figure 7.6.a, the pressure required to squeeze out the soil pore-water for the specimens with low water content is higher than pressure needed to be applied to the specimens with high water content. The magnitude of the squeezing pressure used depends on the initial water content of the specimen. Therefore, the use of single pressure that is applied to squeeze soil pore-water is not possible adopted in this study. Figure 7.6.a also shows that at a given water content the squeezing pressure required to obtain the first drop of soil pore-water for Calcigel specimen is higher than that for Indian bentonite. The result shows the ability of Calcigel (Ca-Mg bentonite) to hold water molecules is stronger than that of Indian bentonite (Na bentonite).

Figure 7.6.b and Figure 7.6.c show the relationship between squeezing pressures versus initial dry density and squeezing pressure versus initial degree of saturation of the specimens, respectively. As shown in Figure 7.6.b, the squeezing pressure used to squeeze out soil pore-water for the specimens with high dry density is higher than pressure needed to be applied to the specimens with low dry density. Based on Figure 7.6.c, the squeezing pressure applied for osmotic suction determination decreases by increasing the degree of saturation of specimens. Even the dependency of squeezing pressure on the initial water content of specimen is higher than the dependency on the initial dry density and degree of saturation as shown from the their coefficient of correlation, it can be concluded that the squeezing

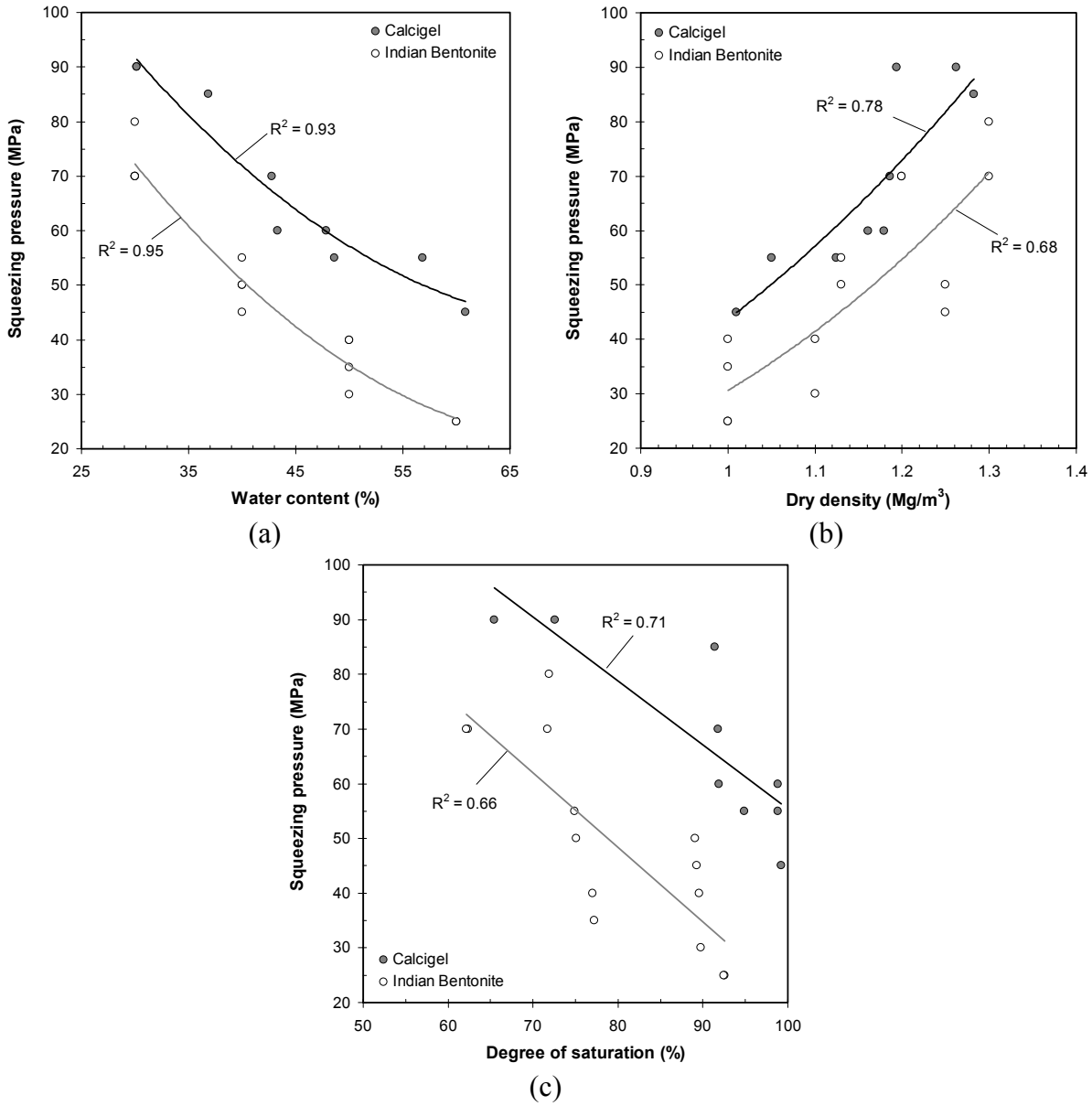

Figure 7.6 The magnitude of squeezing pressure required to obtain the first drop of soil pore-water as a function of (a) water content, (b) dry density, and (c) degree of saturation.

pressure required to obtain the first drop of soil pore-water is also dependent on the initial dry density and degree of saturation of specimens.

As shown in Figure 7.6., the lowest water content of specimens used were limited to 30% since there was no soil pore-water obtained from the specimen with water content less than 30% in the squeezing technique until pressure of 90 MPa (i.e., the maximum pressure that can be applied in the compression machine). This water content is higher than the estimate water content required to fulfill the hydration force on the clay surface calculated from the data presented in Table 2.1 (Chapter 2) (i.e., 15% for Ca-bentonite calculated with specific surface area of 525 m^2/g and 13-20% for Na-bentonite calculated with specific surface area of 400 m^2/g considering 2nd and 3rd of hydrate layers). It is believed that the clay particles are fully saturated. At water content higher than this, the micro-structure consists of

aggregated clays with inter-aggregate interactions consequently enclosing macro-pores which are filled with water and air. In this condition, compression under externally applied pressure occurs due to expulsion of air with water content being constant. Since there is a change in applied pressure, pores and the radius of air-water interface changes. The soil attains a new equilibrium state represented by changing in void ratio (e) and degree of saturation (S_r).

Nagaraj et al. (2006) and Nagaraj et al. (2007) suggested a generalized state parameter, $(e/e_L)\sqrt{S_r}$, obtained from the combination of unsaturated clay state (i.e., e and S_r) and type of clay parameter (i.e., void ratio at liquid limit, e_L). The state parameter was used to account for the effects of pore-water tension on the degree of saturation in the range of 40%-90% and independence of clay properties. Since in this case the pressure increased continuesly and the soil was not in equilibrium condition, the parameter was normalized by multiplying with liquid limit (w_L). The parameter was simplified to be $(e/G_S)\sqrt{S_r}$ .Figure 7.7 shows the squeezing pressure versus the generalized state parameter $(e/G_S)\sqrt{S_r}$ relationship.

As shown in Figure 7.7, the pressures required to squeeze out first drop of soil pore-water for both bentonite merge into a single curve. The data points are fitted with Equation 7.2 giving coefficient of determination (R^2) of 0.94 and standard error of estimate (SEE) of 4.3. The equation can be used to predict the pressure required to squeeze out first drop of soil pore-water in osmotic suction measurement for compacted highly plastic clay in unsaturated condition. This provides an answer to the problem on the squeezing pressure that is applied in

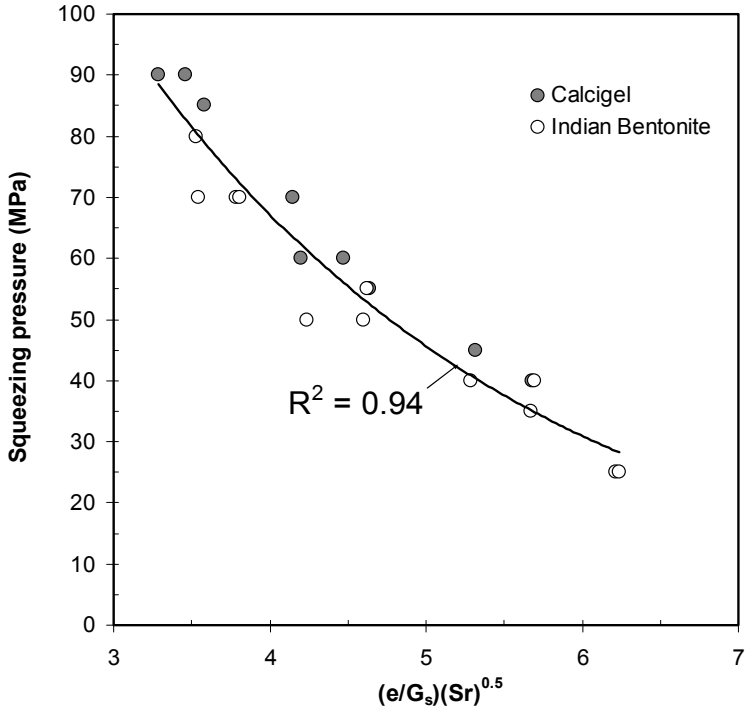

Figure 7.7 Squeezing pressure versus $(e/Gs)(Sr)^{0.5}$

the osmotic suction determination using squeezing technique particularly for compacted bentonite.

$$P_{squeeze} = 316.18 \exp\left(-0.3871 \left({}^{e}/_{G_S} \right) \sqrt{S_r} \right) \quad (7.2)$$

7.5.3 Total Suction, Matric Suction and Osmotic Suction of Compacted Bentonite

Figure 7.8 shows total, matric, and osmotic suction of compacted Calcigel. The total and matric suction (i.e., only due capillary pressure) were obtained using filter paper method presented in Chapter 6. The osmotic suction data was obtained from the squeezing technique. The figure indicates that the osmotic suction data are almost the same (i.e., 50 kPa) for the specimen compacted with different initial water contents. The data are slightly close to the osmotic suction of specimen with water content at liquid limit (i.e., 35 kPa) as shown in Figure 7.5.

Figure 7.8 shows that the osmotic suction values obtained from experimental result are lower than the values of the total suction minus matric suction curves. The result supports previous finding discussed in Chapter 6 that the total suction minus matric suction data obtained using filter paper method represent the osmotic component of total suction and

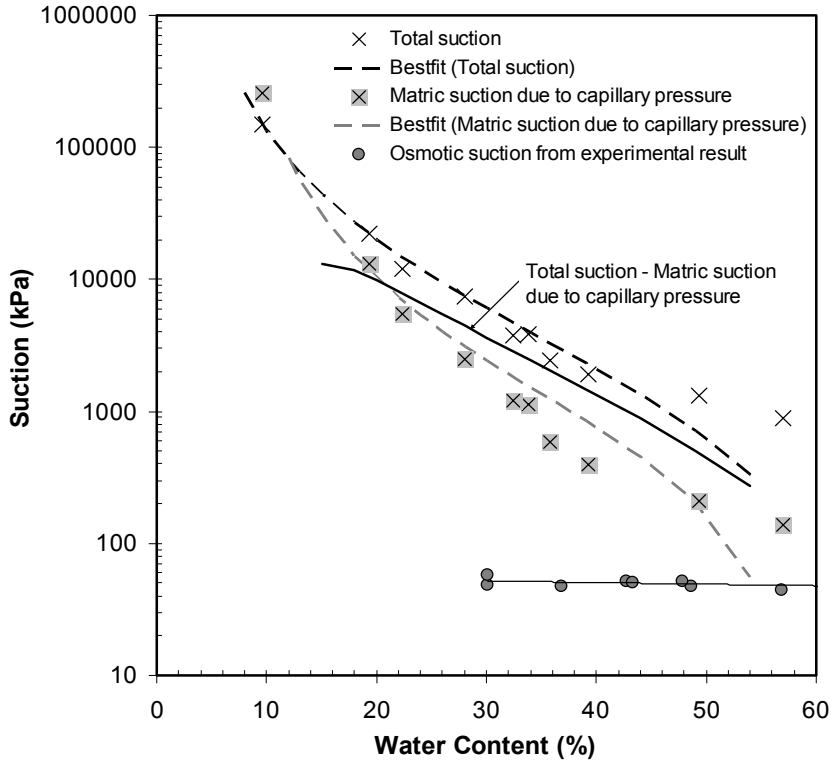

Figure 7.8 Total suction, matric suction, and osmotic suction of compacted Calcigel

hydration forces. The result also gives information that since the osmotic suction data of Calcigel are very small compared to the matric suction values; this type of bentonite is not sensitive to the change in the osmotic suction of soil pore-water.

Figure 7.9 shows the total, matric, and osmotic suction of compacted Indian bentonite. The total and matric suction (i.e., only due to capillary pressure) were measured using filter paper method and the osmotic suction data were obtained using squeezing technique.

As shown in Figure 7.9, the osmotic suction values decrease by increasing water content of specimen. The figure also shows that the magnitudes of osmotic suction of Indian bentonite are very high (i.e., almost a half of total suction values) and much higher than matric suction (i.e., capillary component) in the range of water content used in this study. Also at the liquid limit as shown in Figure 7.5, the Indian bentonite has osmotic suction of 325 kPa which is much higher than that of Calcigel. The result reveals that the osmotic suction provides significant contribution to the magnitude of total suction and influences the behavior of the Indian bentonite. Therefore, at the range of water content used in this study, the Indian bentonite is sensitive to the change in the osmotic component of soil suction. Figure 7.9 also shows that the total suction minus matric suction is higher than magnitude of

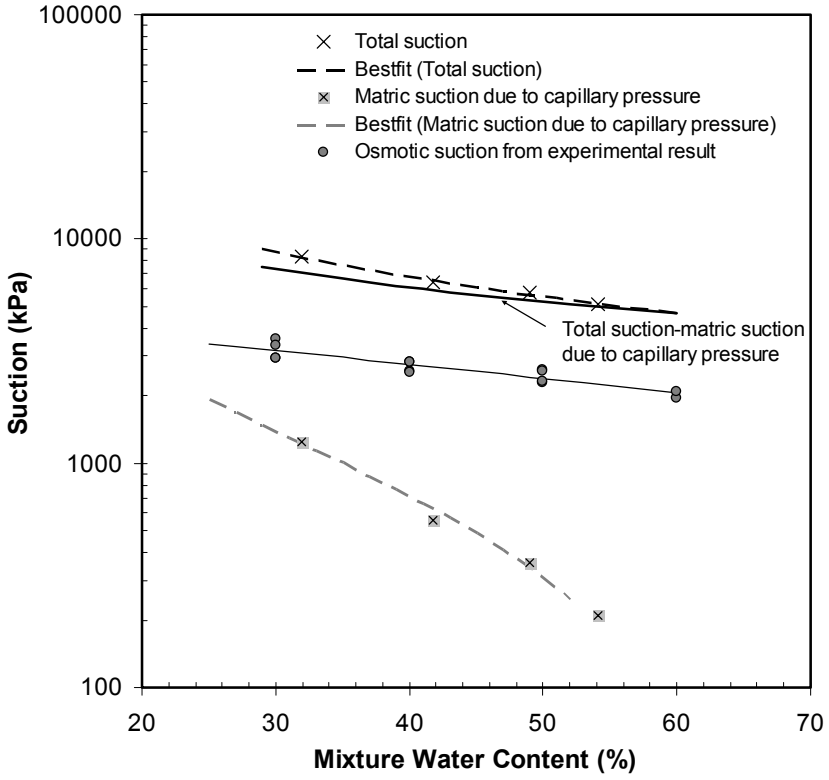

Figure 7.9 Total suction, matric suction, and osmotic suction of compacted Indian Bentonite

osmotic suction. This supports the previous finding that the total suction minus matric suction obtained from filter paper method is sum of osmotic suction and hydration forces. Figure 7.9 also shows that the matric suction increases significantly by decreasing water content, as compared to the osmotic suction.

Considering temperature effect on the suction of the salt solution as shown in Figure 3.1 that changes in temperature mainly influence the suction of the salt solution for suction higher than 1000 kPa, it can be stated that the osmotic suction of Calcigel is not influenced by temperature. This is because the osmotic suction of Calcigel obtained is constant at 50 kPa for the range of water content investigated in this study. On contrary, the osmotic suction of Indian bentonite is possibly influenced by temperature since the osmotic suction obtained is higher than 1000 kPa for the range of water content considered in this study. Therefore, the change in the total suction of compacted Calcigel due to the change in temperature as discussed in Chapter 6 is not because of the change in the suction of dissolved salt solution in the soil pore-water (or osmotic suction) of the material but the change in other components (i.e., hydration force and capillary pressure). This result is also considered for the temperature effects on the drying-wetting and swelling characteristics of compacted bentonite and bentonite-sand mixtures discussed in Chapter 8 and 9.

7.5.4 Osmotic Suction and Swelling Pressure of Compacted Bentonite

Figure 7.10 shows the osmotic suction versus swelling pressure of compacted bentonite used in this study. As shown in the figure, the magnitudes of osmotic suction are less than the swelling pressure and shows constant values by increasing swelling pressure for Calcigel bentonite. An independent measurement of osmotic suction was performed to the Calcigel specimen after swelling pressure test. The magnitude of osmotic suction obtained was 43 kPa which is almost the same as the osmotic suction of as-prepared specimens. The result reveals that the osmotic suction does not affect on the swelling pressure of compacted Calcigel. This is different from Indian bentonite. As shown in Figure 7.10, the magnitudes of osmotic suction are higher than swelling pressure values and shows tendency to increase by increasing swelling pressure. However, there was no information obtained in this study on the magnitude of pressure resulted due to the osmotic suction of the soils.

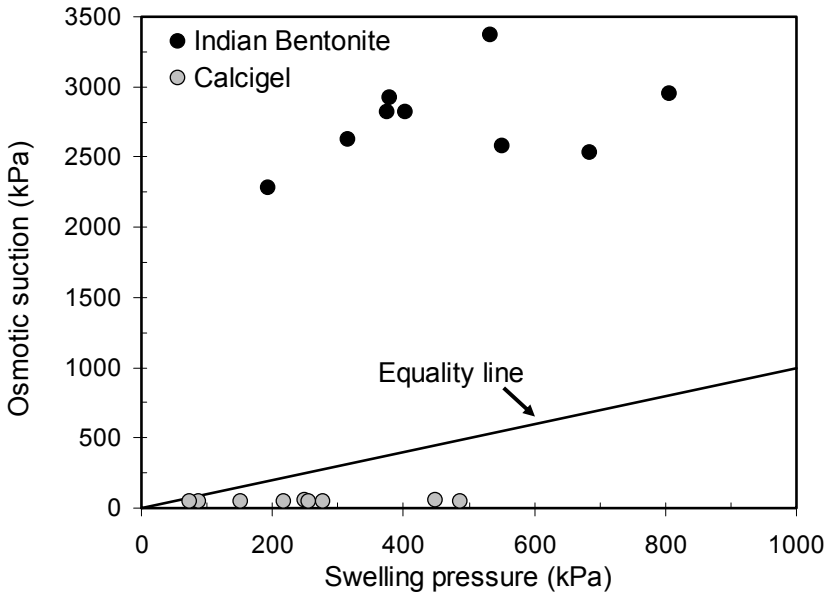

Figure 7.10 Osmotic suction versus swelling pressure of compacted bentonite

The results can be explained qualitatively by means of osmotic efficiency described by Barbour and Fredlund (1989). Considering the cation type (i.e., calcium-magnesium type) and its concentration which is very low in the free pore-water of Calcigel, the material does not behave as a semi-permeable membrane. It means that the there is no water flow from reservoir to the specimen in order to balance different concentration of cation between soil pore-water and distilled water in the reservoir. The water flows to the specimen mainly in order to fulfill the matric suction components (i.e., hydration force and capillary component). Compared to the Indian clay which contains sodium-type cation in the soil pore-water with very high concentration, it is believed that the presence of large difference in concentration of cation between soil pore-water and distilled water results in water flow from reservoir to the specimen. Therefore, the water flows not only in order to fulfill the hydration force in between elementary layers and capillary pressure but also to balance the different concentration between the soil pore-water and water in the reservoir.

As mentioned above, the high osmotic suction would delay the swelling potential (or swelling strain) development to reach maximum swelling (Rao and Shivananda, 2005) and consolidation process (Di Maio, 1996) due to migration of the cation. In this study, the effect of osmotic suction on the swelling pressure development is investigated by comparing the swelling pressure development of compacted Calcigel and Indian bentonite with almost the same initial conditions (i.e., water content of 30% and dry density of 1.27-1.3 Mg/m^3). Figure 7.11 shows the swelling pressure development of compacted Calcigel and Indian bentonite. In order to investigate the rate of swelling pressure development, the data are plotted as

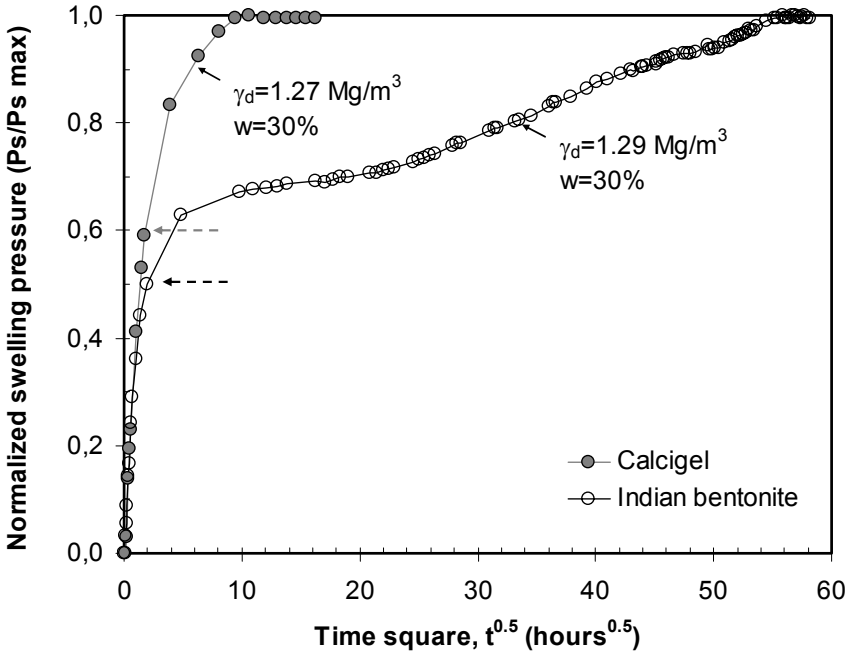

Figure 7.11 Swelling pressure development of compacted Calcigel and Indian bentonite

normalized swelling pressure (i.e., swelling pressure (P_s) divided by maximum swelling pressure ($P_{s\ max}$)) versus square root of elapsed time. The slope of $P_s/P_{s\ max}$ versus $t^{0.5}$ curve represents the rate of swelling pressure development at earlier stage (i.e., mostly up to 60% of the maximum swelling pressure) (Agus and Schanz, 2005a).

As shown in Figure 7.11, the increase in swelling pressure by time for both specimens was rapid at earlier stage of the test (i.e., up to $P_s/P_{s\ max}$ about 0.6 which also means up to 60% of the maximum swelling pressure of the specimens tested). At $P_s/P_{s\ max}$ higher than 0.6, compacted Calcigel reached a maximum swelling pressure faster than Indian bentonite. Since suction in Calcigel is mainly developed by matric suction (i.e., hydration force and capillary component), the Calcigel absorbed water mainly to dissipate the matric suction. The Indian bentonite which has high osmotic component at corresponding water content used (i.e., 30%) absorbed water to dissipate the matric suction and osmotic suction. The swelling pressure development was rapid at $P_s/P_{s\ max}$ less than 0.5 as result of matric suction dissipation. After that, overlapping of adsorbed cations on the negative clay surface behaves like a semi permeable membrane (Mitchell, 1993) resulting water flow from reservoir to the soil to response to the osmotic gradient. This gives rise to increase in swelling pressure. However, since there is no true semi permeable membrane developed in soil, very high salt concentration differences between the soil pore-water and water in reservoir cause diffusion of dissolved salts from the soil pore-water to the reservoir. As mentioned above, according to osmotic efficiency curves (Barbour and Fredlund, 1989), at the same dry density the Ca^{2+} soil

has lower osmotic efficiency compared to Na^+ soil. However, since Indian bentonite has higher salt concentration in the soil pore-water, the osmotic efficiency of this soil is small and become more permeable to the cation diffusion. This was indicated by increasing in the electric conductivity of water in the reservoir from $1x10^{-2}$ mS (i.e., electric conductivity of distilled water used in this study) to 3.5 mS after 5 months swelling pressure test. This opposite motion apparently causes slow down the rate of swelling pressure development. The small rate of migration of the cations out of the soil might be another reason why the specimen needs long time to reach maximum swelling pressure.

7.5.5 Osmotic suction of Soils

Table 7.2 summarizes the osmotic suction data obtained in this study and collected from literatures for different types of soils. Based on Unified Soil Classification System (USCS), all soils in Table 7.2 are highly plastic clays. The osmotic suction data were measured using the same technique (i.e., squeezing technique).

The data presented in Table 7.2 are divided into commercial bentonite soils (i.e., Calcigel, Indian bentonite, and FEBEX) and natural soils (i.e., Boom clay, Regina clay, Bearpaw shale, and Morden shale). Based on Table 7.2, FEBEX bentonite is calcium-

Table 7.2 Summaries of osmotic suction investigations of soils

Properties	Calcigel	Indian Bentonite	FEBEX[1]	Boom Clay[2]	Regina Clay[3]	Bearpaw Shale[4]	Morden Shale[4]
Specific gravity	2.8	2.85	2.7	2.67	2.83	2.83	2.69
Liquid limit (%)	180	400	102	67	78	103.6	67
Plastic limit (%)	56	34	53	40	30.6	29.8	29
Plasticitas Index	124	366	49	27	47.8	73.8	38
Montmorillonite content (%)	50-60‡	-	92	15	20	45	0
Clay content (%)	40	83	68	50-60	64.9	48	45
Fine content (%)	100	100	92	90-100	97.8	-	-
Total S_s (m^2/g)	500	400	725	52.5¥	53†	266	153
CEC (meq/100g)	49	62	102	34	31.7†	65.3	68
Basic cations exchange	Ca-Mg	Na	Ca-Mg	-	Ca†	Na-Ca	-
Surface charge density ($\mu eq/m^2$)	0.98	1.55	1.41	6.48	5.98	2.45	4.83
Osmotic suction (kPa)	44-57	1943-3659	319-579	443	187-202	567.97	827
Main cations in soil free pore-water	Ca	Na	Na	Na, Ca	Ca	Na	Na-K
$P_{squeeze}$ (MPa)	50-90	30-80	60	10	34.5	4.83	4.83

[1]ENRESA (2000), [2]Romero (1999), [3]Krahn and Fredlund (1972), [4]Morgenstern and Balasubramonian (1980)
‡Agus (2005), †Barbour and Fredlund (1989) †measured using ethylene glycol adsorbtion, ¥measured using BET method

magnesium bentonite. However, the dominant cation in the extracted soil-pore water is sodium (ENRESA, 2000). This supports the previous finding that the cations observed in the CEC determination are different from cations in the soil pore-water. Data in Table 7.2 also shows that soils with Na^+ dominant in the soil pore-water (i.e., Indian bentonite, FEBEX, Boom clay, Bearpaw shale, and Morden Shale) shows higher osmotic suction than the soils with Ca^+ in the soil pore-water (i.e., Calcigel and Regina clay).

In order to investigate the relationship between physico-chemical properties of soils more clearly, the data were plotted in Figure 7.12. Figure 7.12.a, 7.12.b, 7.12.c, and 7.12.d show the osmotic suction versus specific surface area (S_s), liquid limit (LL), cation exchange capacity (CEC), and surface charge density (i.e., ratio of CEC and S_s) relationships, respectively.

Figure 7.12.a shows that there is no relationship between specific surface area and osmotic suction for commercial bentonite whereas, for natural soils, the osmotic suction tends to increase by increasing specific surface area for wide range of osmotic suction. This is due to the fact that the specific surface area is a physical property. As shown in Figure 7.12.b, there is no relationship between osmotic suction and liquid limit. This is different from result reported by Sridharan et al. (1986), Di Maio (1996), and Sridharan (2002) that, for a soil type mixed with any salt solutions, the liquid limit of soil decreases by increasing salt

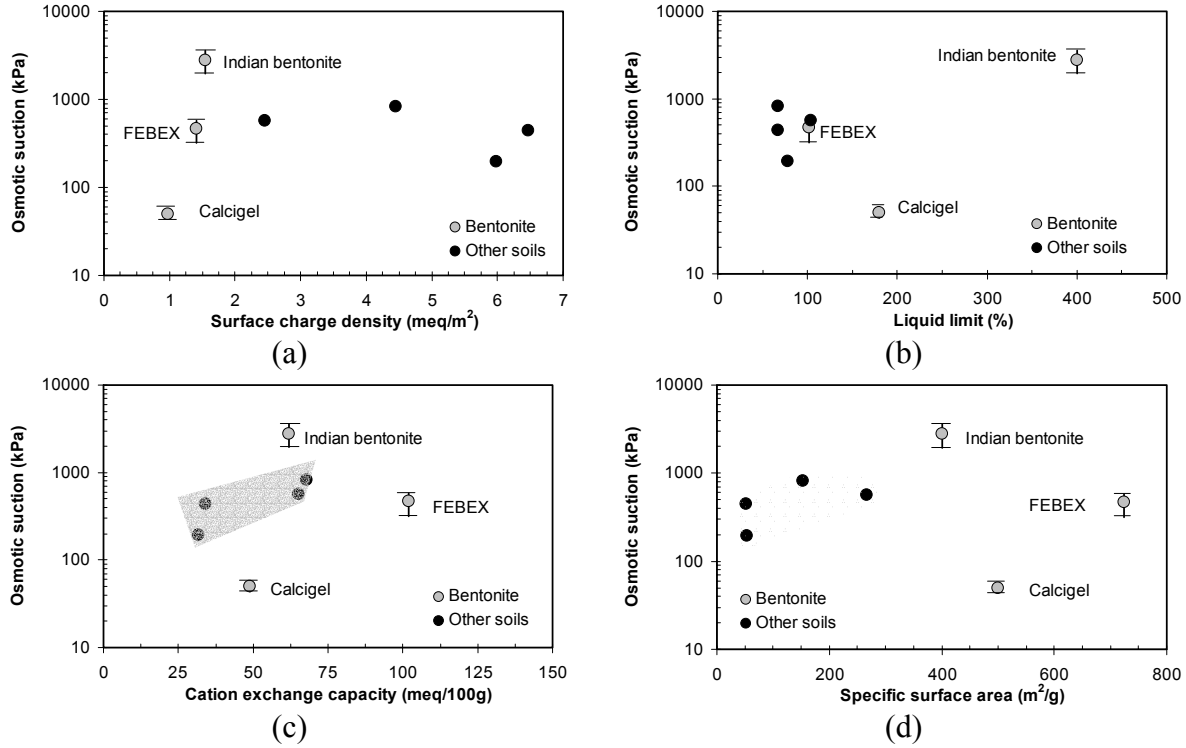

Figure 7.12 Osmotic suction of soils as a function of (a) specific surface area, (b) liquid limit, (c) cation exchange capacity, and (d) surface charge density.

concentration in the soil pore-water. This difference is possible due the variation of the physico-chemical properties and mineralogy of the soils presented in Table 7.2.

Figure 7.12.c shows that there is no relationship between osmotic suction and CEC for commercial bentonites whereas, for natural soils, the osmotic suction data tend to increase by increasing CEC. This supports previous finding that the cations obtained in the CEC determination can be different from the cations in the soil pore-water. Sridharan (2002) reported that the physical and mechanical properties of montmorillonite soils such as liquid limit and swelling potential were not influenced by the total CEC of the soils other than only by the amount of exchangeable sodium cation in the CEC. This relationship can not be observed in this study due to lack of exchangeable sodium data from literatures. Figure 7.12.d reveals that osmotic suction data of natural soils show almost constant by increasing the surface charge density of soils. For commercial bentonite soils, the osmotic suction data increase in the narrow range of surface charge density. It can be concluded that there is no unique relationship between osmotic suction and the specific surface area, the liquid limit, the cation exchange capacity, and the surface charge density of soils. For natural soils, the osmotic suction might be dependent on the origin and surrounding environment whereas, for commercial bentonite, the osmotic suction might also be influenced by the production process. Therefore, it is recommended to determine directly the osmotic suction of soils studied.

7.6 Summary

The following conclusions can be drawn based on the results of osmotic suction measurements of highly plastic clays.

1. Osmotic suction of highly plastic clay is obtained from the first drop of extracted soil pore-water.
2. Squeezing pressure applied is dependent on the initial water content of the specimens and less dependent on the initial dry density and degree of saturation.
3. The pressure required to obtain the first drop of highly plastic clays can be estimated from empirical relationship between squeezing pressure versus a generalized parameter (i.e., $(e/G_S)\sqrt{S_r}$).

4. For the two highly plastic clays used in this study, the subtraction of total and matric suction is higher than osmotic suction obtained from squeezing technique and represents the sum of osmotic suction and hydration force of soils.
5. For the soil with high osmotic suction e.g., Indian bentonite, the change in osmotic suction is important at water content range higher than the water content required to fulfill the hydration forces.
6. There is no effect of osmotic suction on the magnitude of swelling pressure of Calcigel. But, for Indian Bentonite, the magnitude of swelling pressure is apparently influenced by the osmotic suction values.
7. High osmotic suction in the Indian bentonite causes delay to reach equilibrium (or maximum swelling pressure) in the constant volume of swelling pressure measurement.
8. There is no unique relationship between the osmotic suction and the specific surface area, the liquid limit, the cation exchange capacity, and the surface charge density of soils.
9. Considering temperature effect on the suction of salt solutions discussed in Section 3.2.2 that temperature influences the suction of salt solution at suction higher than 1000 kPa, the osmotic suction of Calcigel is not influenced by temperature, whereas the osmotic suction of Indian bentonite is influenced by temperature.

This page intentionally left blank

CHAPTER 8

UNCONFINED WETTING AND DRYING BEHAVIOR

8.1 Introduction

Insitu drying-wetting processes as affected by environmental conditions are generally thought to influence the behavior of compacted clay when used; e.g., as liner and/or cover in landfills. The behavior of the clays compacted at a given compaction energy is primarily influenced by the soil fabric and stress history of the soils (Vanapalli et al., 1999).

Soils compacted dry of optimum (DOP) generally show a fabric made up of aggregates of various sizes and tend to have bimodal pore size distribution whereas soils compacted wet of optimum tend to show more homogeneous matrix-dominated fabric and pore size distribution with a single peak (Gens et al., 1995; Delage and Graham, 1996). These phenomena may be different in case of a compacted bentonite-sand mixture depending on the bentonite-sand ratio. The fabric of a compacted bentonite-sand mixture consists of arrangements of clay clusters, sand grains, and silts with macro-pores (or inter-aggregate pores) in between and shows to exhibit bimodal pore size distribution (Agus and Schanz, 2005c). The presence of sand might to a certain extent influence the drying/wetting behavior of a mixture.

Heat, gas, and leachate are primary by-products of landfill processes in the municipal solid waste landfills. Heat, which is generated as a result of biomechanical processes and decomposition of organic components in wastes, is thought to influence the hydro-mechanical behavior of the clay liner used in the landfills. Therefore, the effect of temperature on the drying-wetting behavior of bentonite-sand mixtures is one of the primary concerns in the design of landfill.

Beside low compacted materials (Proctor density), heavily compacted bentonite-sand mixture is also used as sealing and buffer material for hazardous and nuclear waste repository. In Germany, the material has been proposed to be used to seal the canister of nuclear waste which would be buried in a deep geological repository. In the real situation, it is understood that the material located close to the host rock would be in contact with water.

The temperature increase also occurs in the hazardous or nuclear waste repository as a result of decay of the waste. The material which is close to the canister would also experience increase in temperature. Therefore, study on temperature effect on the drying-wetting behavior of heavily compacted bentonite-sand mixture is being important.

Despite several research studies that have recently been performed (e.g., Vanapalli et al., 1999 and Fleureau et al., 2002), there remain very limited information concerning the drying/wetting behavior of compacted bentonite-sand mixtures with different compaction conditions exposed to high temperature. This study focused on the drying-wetting behavior of compacted bentonite-sand mixtures for Proctor density specimens and heavily compacted specimen. This study also investigated the temperature effects on the compacted bentonite-sand mixtures. The experimental program and procedures adopted are described, and the results obtained are presented and discussed.

8.2 Experimental Techniques and Procedures

The wetting and drying tests under unconfined conditions were performed on the low compacted specimens (Proctor density) and a heavily compacted specimen. For low compacted specimens, the mixtures used in this study were 30/70 and 50/50 bentonite-sand mixtures and pure bentonite. For heavily compacted specimen, the specimen used was 50/50 bentonite-sand mixture.

The tests were performed at two different temperatures (i.e., at room temperature and elevated temperature (80 °C)). In this section, procedures adopted in the determination of wetting and drying curves of the specimens at both temperatures are described. The tests performed involved tests using the axis-translation technique (ATT) in the pressure plate apparatus at 20 °C and those using the vapor equilibrium technique (VET) at 20 and 80 °C. Table 8.1 summarizes the initial conditions of specimens used in this study. Suction paths followed by each specimen in the unconfined drying and wetting tests are shown in Figures 8.1 to 8.6. Figures 8.1 to 8.6 show the drying and wetting paths for specimens of 100B DOP, 100B WOP, 50B/50S DOP, 50B/50S WOP, 30B/70S DOP, and 30B/70S WOP, respectively. For heavily compacted 50/50 bentonite-sand mixture, the drying and wetting paths is shown in Figure 8.7.

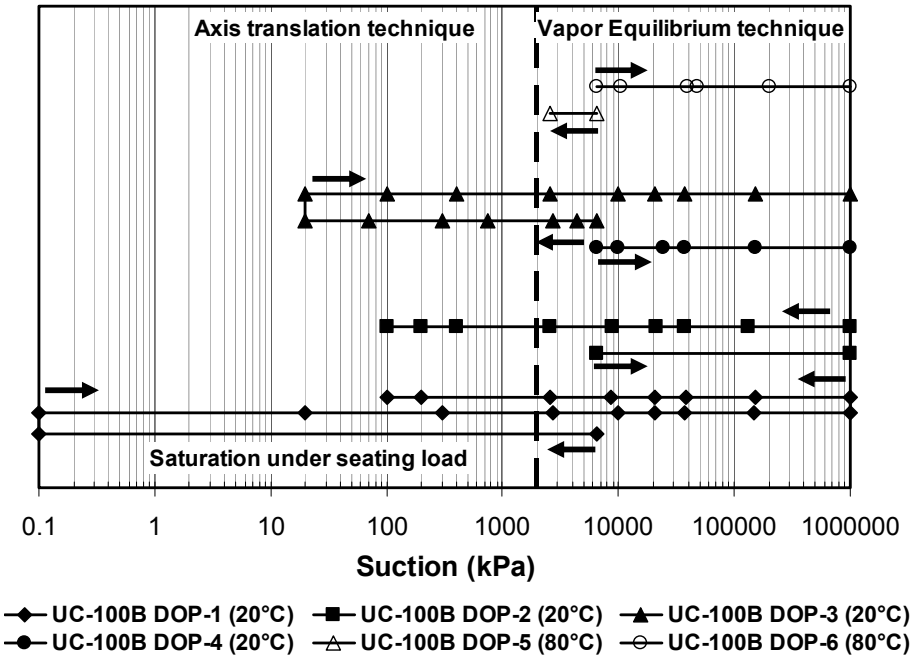

Figure 8.1 Suction paths followed in the unconfined wetting and drying tests for 100B DOP specimens

Table 8.1 Initial condition of specimens used in the unconfined drying and wetting tests

Specimen	Water content (%)	Dry density (Mg/m^3)	Initial suction* (kPa)
100B DOP	26	1.14	6524
100B WOP	45	1.15	406
50B/50S DOP	14	1.60	2186
50B/50S WOP	24	1.61	271
30B/70S DOP	14	1.75	406
30B/70S WOP	17	1.75	137
50B/50S HC ¥	9	2.00	22700
50B/50S HC §	14	1.98	3000

* measured using chilled-mirror hygrometer technique, ¥ heavily compacted specimen in as-prepared condition, § heavily compacted specimen after saturation under constant volume condition.

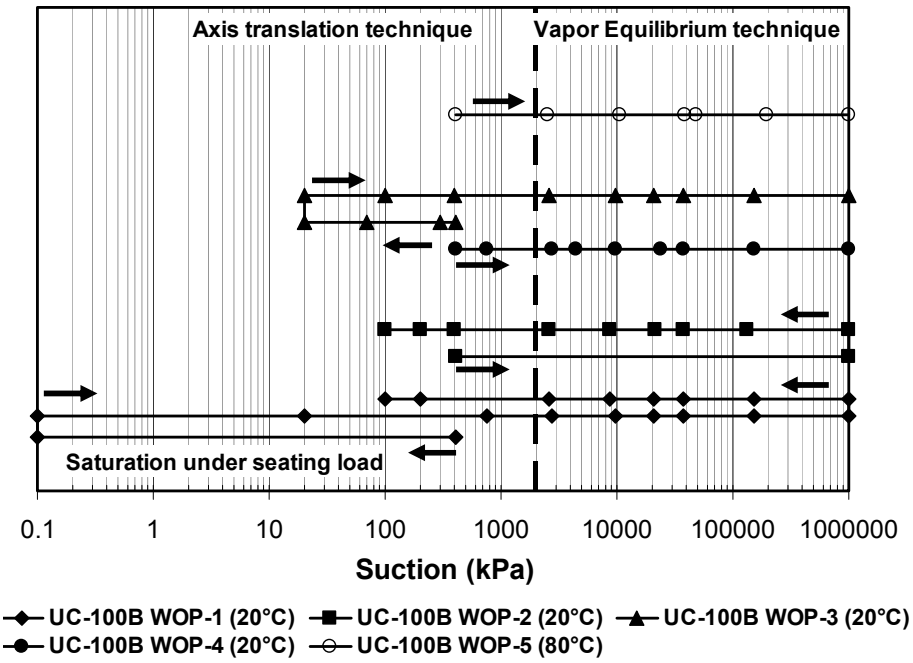

Figure 8.2 Suction paths followed in the unconfined wetting and drying tests for 100B WOP specimens

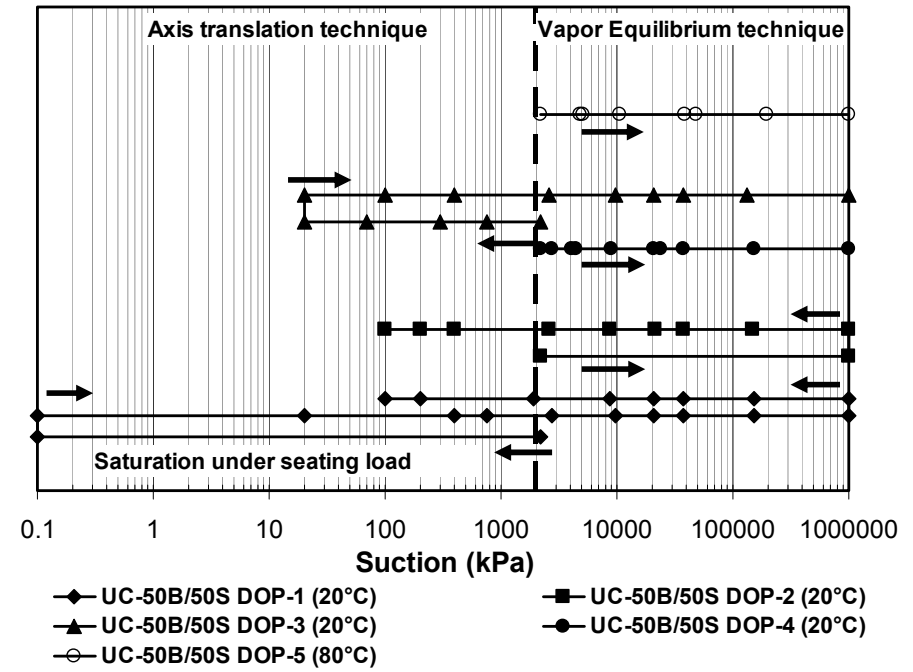

Figure 8.3 Suction paths followed in the unconfined wetting and drying tests for 50B/50S DOP specimens

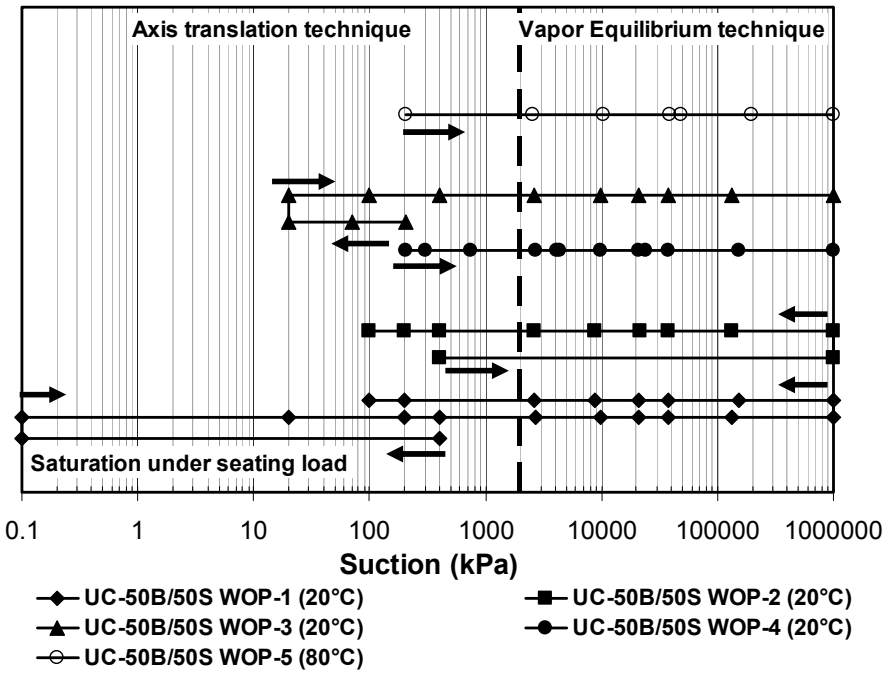

Figure 8.4 Suction paths followed in the unconfined wetting and drying tests for 50B/50S WOP specimens

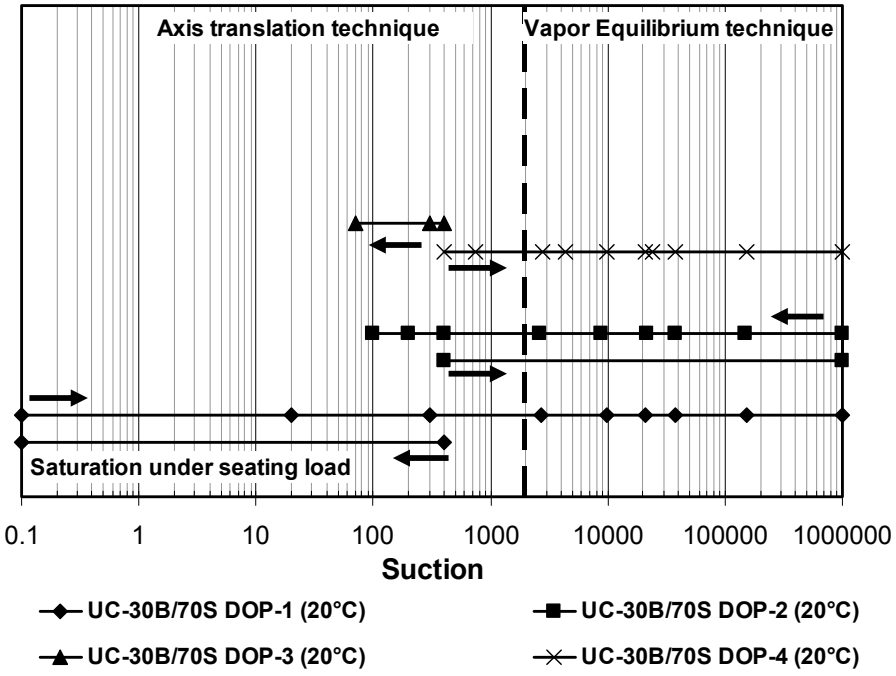

Figure 8.5 Suction paths followed in the unconfined wetting and drying tests for 70B/30S DOP specimens.

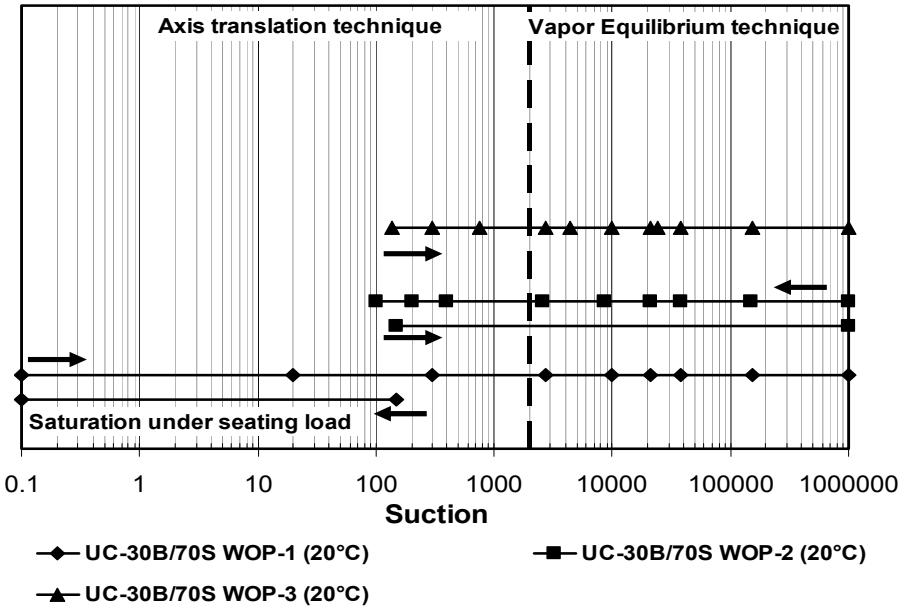

Figure 8.6 Suction paths followed in the unconfined wetting and drying tests for 70B/30S WOP specimens.

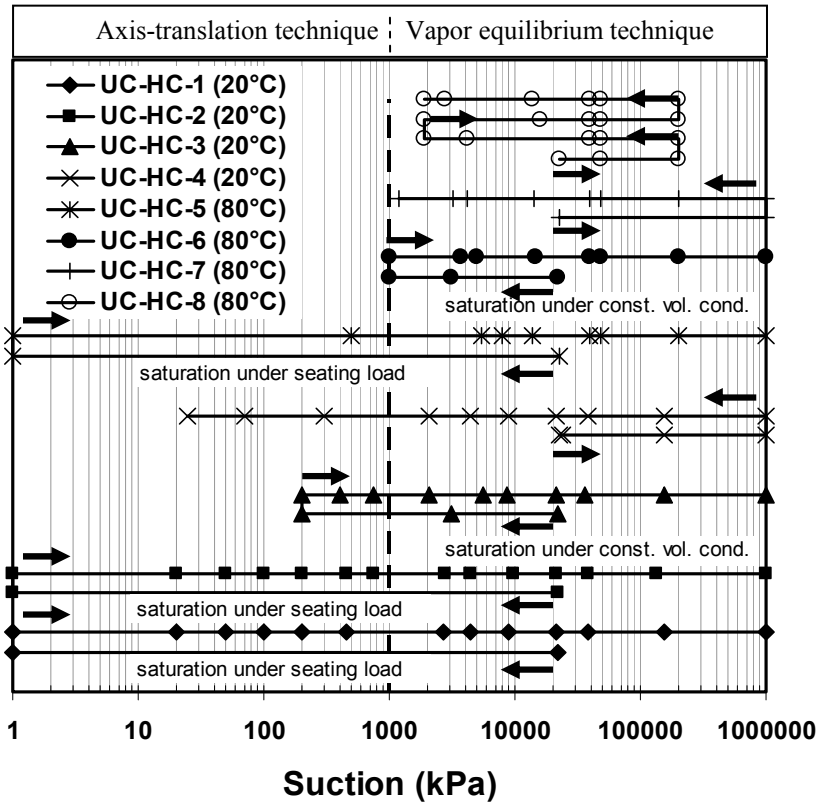

Figure 8.7 Suction paths followed in the unconfined wetting and drying tests for heavily compacted 50B/50S specimens

8.2.1 Experimental Techniques and Procedures at Room Temperature

8.2.1.1 Axis-Translation Technique Using Pressure Plate Apparatus

In this study, the axis-translation technique (ATT) was used to determine drying and wetting curves of compacted specimen for suction range less than 1500 kPa. Air pressure was applied in this technique. A pressure plate apparatus from Soil Moisture as shown in Figure 8.8 was used in this experiment. The device consists of the chamber and the high-air entry ceramic disk. Three types of ceramic disks depending on its air entry values (AEV) (i.e., 100 kPa, 500 kPa, and 1500 kPa) were used. The ceramic disks were saturated with distilled deaired water prior to use. The water outlet in the pressure plate was connected to burette for flushing purpose. The flushing of water compartment was performed regularly to remove the diffuse air bubbles collected beneath the ceramic disk.

8.2.1.2 Vapor Equilibrium Technique Using Salt Solution

The vapor equilibrium technique (VET) was used to determine drying and wetting curve of compacted specimen for suction higher than 2000 kPa. If the temperature fluctuation can be maintained as high as 0.5 °C, this technique can be used to control suction for range higher than 1000 kPa (Figure 6.10). In this study, two types of desiccator (i.e., large (standard) desiccator and small desiccator) were used. The large desiccator was used for testing up to six specimens simultaneously (Figure 8.9.a) and the small desiccator (i.e., special glass container with fastened cap) (Figure 8.9.b) was used for testing only one specimen.

Figure 8.10 shows absorbed/released water versus time for 100 DOP specimens which were placed in the large desiccator together with 100 WOP specimens. The DOP specimen has initial suction of 6524 kPa and the WOP specimen has initial total suction of 406 kPa determined using chilled-mirror hygrometer from independent specimens having the same initial condition (Table 8.1). By applying suction of 9833 kPa, the DOP specimen should release water. In fact, the specimen absorbed water due to presence of WOP specimen which has lower suction than that of DOP specimen as shown in Figure 8.10. The DOP specimen began to release water after 100 hours when the WOP specimen released more than 3 g of water. The DOP specimen appears to reach equilibrium at the same time as WOP specimen. In other desiccator where DOP specimen was equilibrated to suction of 4404 kPa, the specimen appears to absorb much water due to presence of WOP specimen in the desiccator. The specimen released water after 400 hours when the WOP specimen released more than 3 g of water. As depicted in the figure, this conditions do not only influence the water content

Figure 8.8 Pressure plate apparatus

(a) (b)

Figure 8.9 Desiccators used in VET (a) large desiccator (b) small desiccator

(i.e., by releasing/absorbing water) and the time to reach equilibrium but also the dimension of the specimens as shown in the diameter versus time. It seems that the DOP specimens underwent wetting-drying processes before the specimen reached equilibrium that is shown as constant water content. The results show that the specimens placed in the large dessicator should have the same initial suction.

The use of small desiccator can avoid the effects of the differences in initial suction of the specimens since only one specimen was placed in the desiccator. For using the small desiccator, the salt solution used was half of its volume leaving the air space of 333 cm^3. This results in proportion of 5.8 cm^3 volume of air per cm^2 of solution surface area which is smaller than the maximum value as suggested by ASTM E104-85 (i.e., 25 cm^3/cm^2) (ASTM, 1997).

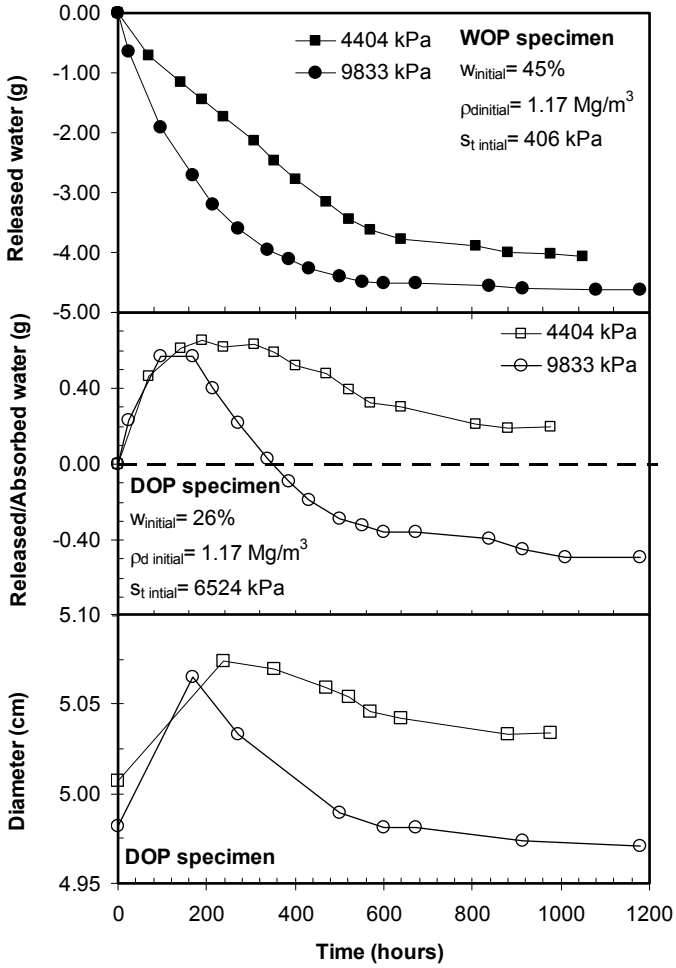

Figure 8.10 Effects of different initial suction of the specimens in large desiccator

Several saturated and molal salt solutions were used to induce total suction to the specimen by changing the relative humidity of the vapor space in the desiccator. The relative humidity of the salt solutions used was verified using the chilled-mirror hygrometer before and after the test. The experiment was conducted in a temperature-controlled room that could maintain a constant temperature of 22^{o}C ± 0.5^{o}C. The mass of the specimens was regularly measured and the dimensions of the specimen were measured using a caliper after equilibrium at each suction value was reached. The equilibrium was assumed to be reached when there was no significant change in the mass of the specimens.

8.2.2 Experimental Techniques and Procedures at 80 °C

8.2.2.1 Vapor Equilibrium Technique Using Salt Solution

In this study, the drying and wetting curves under unconfined condition at 80 °C were performed using VET. The experiment was performed using the small desiccator because it

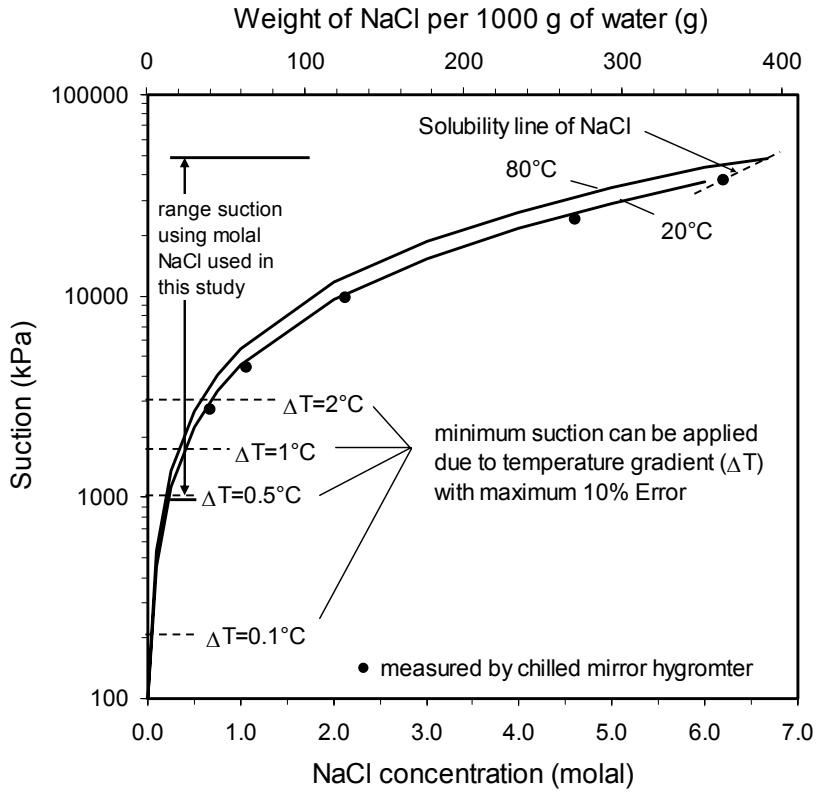

Figure 8.11 Total suction versus sodium cloride concentration

contains only one specimen, light, and equipped with fastened cap. The suction of the molal NaCl solutions used in this study was calculated according to the equations given by Lang (1967) (Equation 3.2) and the data reported by Pitzer and Pelper (1984) (Figure 8.11).

Table 8.2 summarizes the relative humidity of the vapor space above the saturated salt solutions used in this study at 20 °C and the data reported by Tang and Cui (2005) for solutions at 80 °C. The same as that of performed at 20 °C, the relative humidity (or the water activity) of vapor space above each solution was verified using the chilled-mirror hygrometer technique at 20 °C prior to use. The technique chosen in this study because of its ease to use, quick response, repeatability, and high accuracy (Leong et al., 2003, Agus and Schanz, 2005b).The total suction of molal and saturated salt solution was calculated from the measured relative humidity and temperature using Equation 3.1. The small differences between the theoretical and the measured values of *RH* of vapor space above the solution have

Table 8.2 Summary of saturated salt solutions used in this study

Temperature (°C)	Relative humidity (%)		
	KCl	NaCl	$MgCl_26H_2O$
20*	85.8	75.7	32.4
80**	78.18	73.9	28.5

* Chilled-mirror hygrometer

** Tang and Cui (2005) measured using chilled-mirror technique

Figure 8.12 Vapor equilibrium technique at 80 °C

been found to exist and is thought to be due to the NaCl powder used was not really pure and contained constituents other than sodium chloride (Tang and Cui, 2005). The concentration of molal sodium chloride corresponding to total suction obtained from chilled mirror hygrometer was corrected using Figure 8.11 and the total suction of molal salt solution at 80 °C was the total suction at the corrected concentration.

The experiment at 80^{o}C was commenced with preparation of specimen. For low compacted condition, the specimens were statically compacted to reach expected dry density as presented in Table 8.1. Specimens were placed in the small desiccator. The desiccator (with the solution and specimen) was placed in a climate chamber that can control temperature to 0.1 °C accuracy (Figure 8.12). Even the lowest suction of 200 kPa can be controlled in the chamber with temperature gradient of 0.1 °C as shown in Figure 8.11, the minimum suction applied in this study using VET was 500 kPa. In order to prevent temperature differences between air in the glass, salt solution, and the specimen, the temperature of the chamber was increase with rate increment of 1 °C per hour. The mass of the specimens was regularly measured and the dimensions of the specimen were measured using a caliper after equilibrium at each suction value was reached. The equilibrium was assumed to be reached when there was no significant change in the mass of the specimens. The same procedures were applied to the heavily compacted specimens.

8.3 Result and Discussion

8.3.1 Drying and Wetting Behavior of Low Compacted (Proctor) Specimens

Figure 8.13 shows swelling strain versus time of compacted bentonite and bentonite sand mixtures performed in oedometer under seating load of 2 kPa before the drying process is commenced. Based on the figure, the swelling strain of UC-100B DOP 1, UC-100B WOP 1, UC-50B/50S DOP 1, UC-50B/50S WOP 1, UC-30B/70S DOP 1, and UC-30B/70S WOP 1

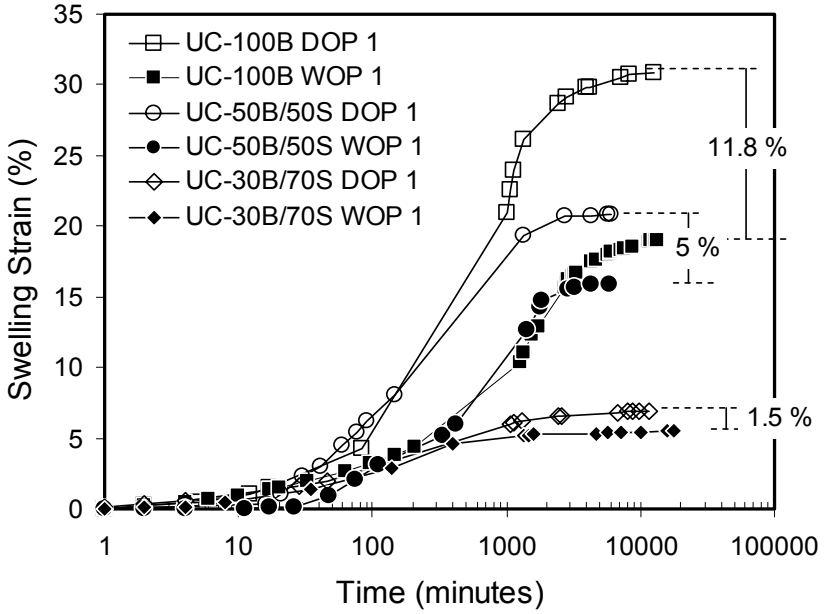

Figure 8.13 Swelling strain versus time of specimens during saturation under seating load

are 30.8, 19, 21, 16, 7, and 5.5 %, respectively. According to the swelling strain data obtained, the swelling strain of DOP specimens are higher than those of WOP specimens. These are attributed to fabric of the DOP specimen resulting more dissociated structure during hydration process. This occurs especially for 100B DOP specimen.

As shown in Figure 8.13, the differences in swelling strain between DOP and WOP specimens are 11.8, 5.0, and 1.5% for 100B, 50B/50S, and 30B/70S specimens, respectively. It seems that the differences in swelling strain between DOP and WOP specimen decreases by decreasing the bentonite content in the mixtures. It shows that the similarity of fabrics for the specimens increases by increasing sand content in the mixtures. Increase in sand content results in increasing contact between sand grains. Therefore, difference in water content does not influence significantly in the fabric of the specimen during compaction process. Differences in the initial total suction of the DOP and WOP specimens (Table 8.1) also give contribution on the differences in the swelling paths of DOP and WOP specimens. Based on Table 8.1, the differences in initial total suction of DOP and WOP decrease by increasing sand content. These features may influence the behavior of the specimens during drying and wetting processes.

Figure 8.14.a, 8.14.b, and 8.14.c show the degree of saturation versus suction relationship of low compacted bentonite and bentonite-sand mixtures. The specimens (i.e., UC-100B DOP-1 & WOP-1, UC-50B/50S DOP-1 & WOP-1, and UC-30B/70S DOP-1 &

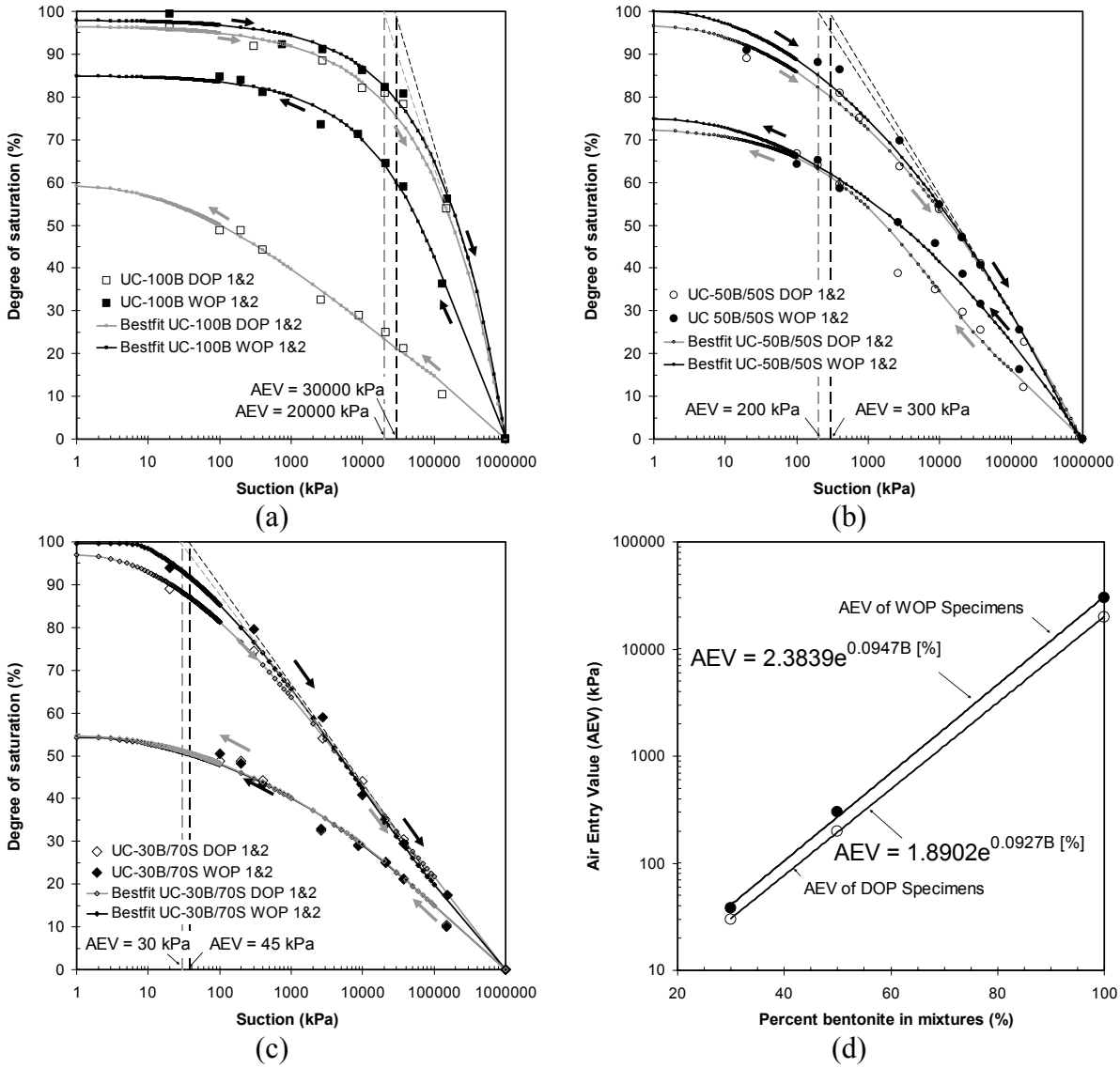

Figure 8.14 Drying-wetting curves of compacted bentonite and bentonite-sand mixtures from saturated under seating load for (a) 100B specimens, (b) 50B/50S specimens, (c) 30B/70S specimens, and (d) AEVs of specimens as a function of bentonite content.

WOP-1) with initial conditions as shown in Table 8.1 were saturated in the oedometer (Figure 8.13) and then dried by applying suction following suction paths as shown in Figures 8.1 to 8.6.

For the wetting paths, the as-prepared specimens were dried in the oven and then wetted following suction paths as shown in Figures 8.1 to 8.6. According to Figure 8.14.a, 8.14.b, and 8.14.c, the drying and wetting process show hysteresis. For the 100B specimen, the drying-wetting curve of DOP specimen shows larger hysteresis compared to that of WOP specimen. This is different from those of compacted bentonite-sand mixtures as shown in Figures 8.14.b and 8.14.c. As shown in the figures, the drying-wetting curves of DOP and WOP of bentonite-sand mixture specimens are very close.

Air entry values (AEVs) of the specimens tested in this study can also be obtained from the degree of saturation versus suction relationship (Fredlund and Rahardjo, 1993) as shown Figures 8.14.a, 8.14.b, and 8.14.c. The AEVs were plotted as a function of bentonite content in Figure 8.14.d. As shown in the figure, the AEV of the mixtures increases with increasing bentonite content of specimens. The differences of AEV of DOP and WOP specimens appear decrease by decreasing the bentonite content. The AEV data in Figure 8.14.d were fit with the exponential function of the bentonite content in the mixture. From the fitting equations, it can be obtained that, at bentonite content of zero, the AEVs are between 1.9-2.3 kPa which are close to AEV of sand.

Figure 8.15 shows the water content, void ratio, and suction relationship of compacted bentonite-sand mixtures during drying. According to the figure, small difference in the drying curve as shown in the water content versus suction curve exists between the UC-100B DOP-1 and UC-100B WOP-1 specimens at low suction (i.e., suction less than 200 kPa). The difference can also be seen in the case of UC-50B/50S DOP-1 and UC-50B/50S WOP-1 specimens even the PSD of the specimens show insignificant variation as discussed in Chapter 5. The difference in the drying curve is thought to be attributed not only to the different initial (as-compacted) fabrics of clay clusters as shown in the MIP and ESEM results but also the suction- (and stress-path) followed by the specimens during wetting before the commencement of the drying process (Figure 8.13). The differences disappear at suction higher than air entry value (AEV) which were determined from suction versus degree of saturation relationship (Figure 8.14). At suction higher than AEV, water is mainly placed in the intra-aggregate pore (or micro structure) and adsorbed by clay surface due to hydration force which is free from fabric effects.

In the void ratio versus suction relationship as shown in Figure 8.15, the specimens, except for 100B WOP-1, start to deform at yield stress of 20 kPa regardless the bantonite-sand ratio and compaction conditions of the specimens. 100B WOP-1 specimen deforms at yield stress at higher suction value (i.e., 80 kPa). The same as in the water content versus suction relationship, the differences in the drying curves are also seen in the void ratio versus suction relationship in the low suction range (i.e., less than 200 kPa) especially for 100B specimens. The differences are due to different initial (as-compacted) fabrics of clay clusters and the suction- (and stress-path) followed by the specimens during wetting. Higher than suction of 200 kPa, the void ratio versus suction curves of the 100B DOP and WOP specimens appear to merge. It seems that swell under low seating load brings the 100B

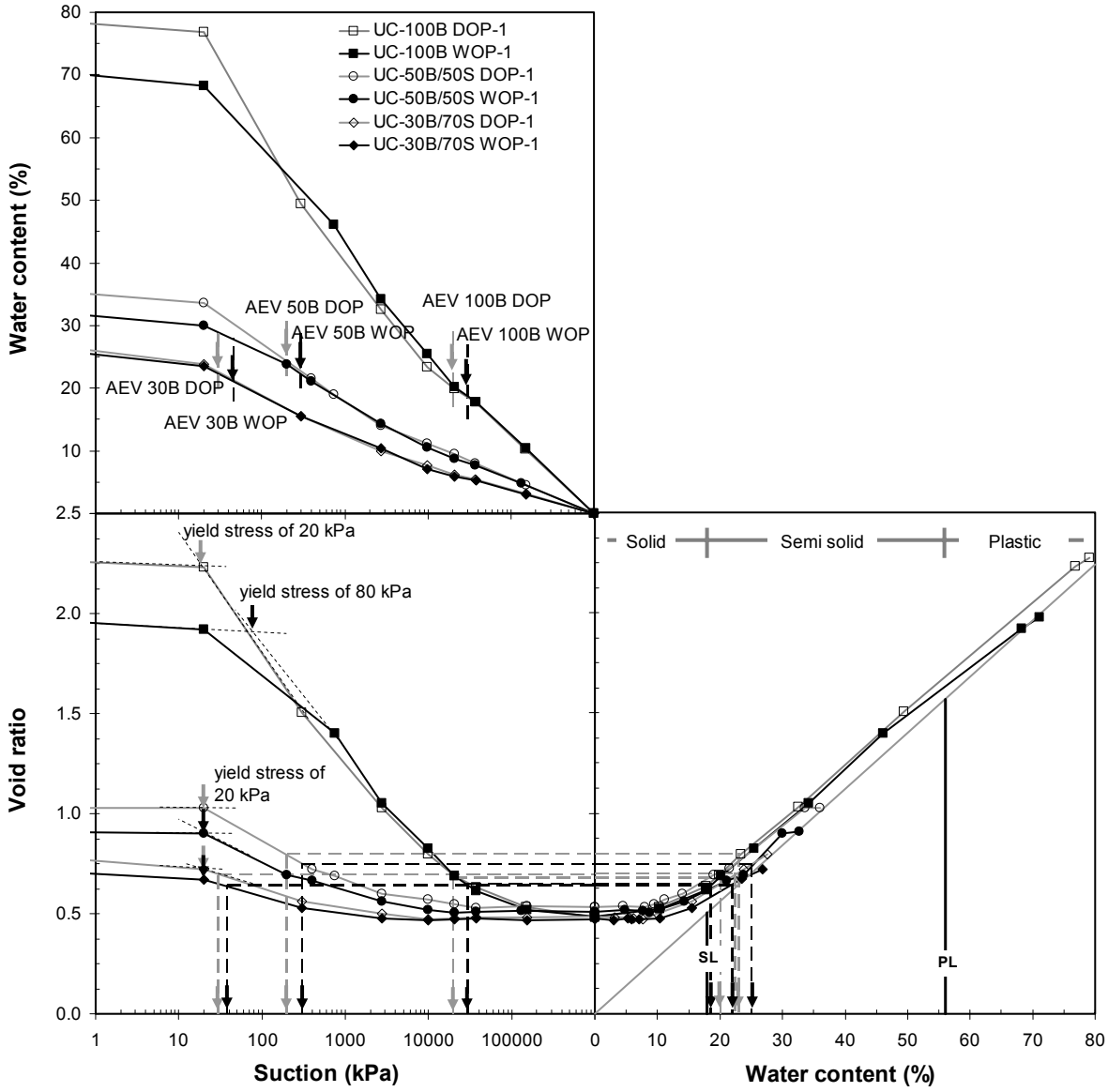

Figure 8.15 Water content, void ratio, and suction relationship of compacted bentonite-sand mixtures during drying from saturated under seating load

specimens to more dissociated structure. This condition may result in almost the same fabric and slow drying process by increasing suction results in rearrangement of the clay particles. For bentonite-sand mixtures (i.e., 50B/50S and 30B/70S), the swell under seating load results in no contact between sand grains. It is shown from the yield stresses obtained from the drying curves of the specimens which are the same as yield stress of 100B DOP-1 specimen.

Figure 8.15 also shows that there are differences in the drying curves for bentonite-sand mixtures specimens compacted at DOP and WOP conditions at low suction range. The differences decrease by decreasing bentonite-sand ratio. This agrees well with the swelling strain result as shown in Figure 8.13 that the differences in swelling strain decrease by increasing bentonite-sand ratio. Figure 8.15 also implies that the void ratio at dry conditions

depends on the amount of water release during drying process. Therefore, regardless the different compaction conditions of the specimens, the pure bentonite specimens exhibit the greater shrinkage upon drying.

Figure 8.15 also shows void ratio and water content relationship of the material tested herein. The figure reveals that the 100B specimens exhibit the greater shrinkage upon drying. As depicted in the figure, the AEVs of the specimens are placed in between the shrinkage limit and plastic limit of pure bentonite or in the semisolid range. However, the water content data shown in the figure are the mixture water content of specimen. Due to the much larger specific surface area of the bentonite compared to that of the sand in the mixture, water is mostly retained by the bentonite during drying/wetting processes. Therefore, it can be assumed that water is only bounded within the bentonite particles and based on this assumption, the bentonite water content (w_b) can be calculated according to Equation 6.9.

Bentonite void ratio can be calculated accordingly using Equation 8.1 with an assumption that the soil void in the bentonite-sand mixtures only belongs to the bentonite (Komine and Ogata, 2003).

$$e_b = \frac{G_s^{bentonite}((1+r_{bs}) - (\rho_d / G_s^{sand}))}{r_{bs}\rho_d} - 1 \tag{8.1}$$

where r_{bs} is the bentonite-sand mass ratio, ρ_d is mixture dry density in Mg/m^3, $G_s^{bentonite}$ is specific gravity of bentonite, and G_s^{sand} is the specific gravity of sand.

Figure 8.16 shows the evolution of bentonite water content, bentonite void ratio with suction for all the specimens during drying from saturated conditions. As shown in Figure 8.16, the bentonite water content versus suction curves of all mixtures are close to each other allowing small difference at low suction (i.e., less than 200 kPa). The differences completely disappear after the AEV regardless the bentonite content in the mixtures and compaction conditions.

In Figure 8.16, all mixtures show apparently the same void ratio of the specimen after drying to the oven-dried state as shown in void ratio versus suction relationship. However, the bentonite void ratio of the specimen at the end of drying process decreases with increasing bentonite content as shown in Figure 8.16 in the bentonite void ratio versus suction relationship. The results indicate that shrinkage void ratio of the mixture also decreases with decreasing bentonite content. Decrease in the shrinkage limit void ratio of the mixtures is attributed to the increase in the inter-granular contact between sand grains in the mixtures.

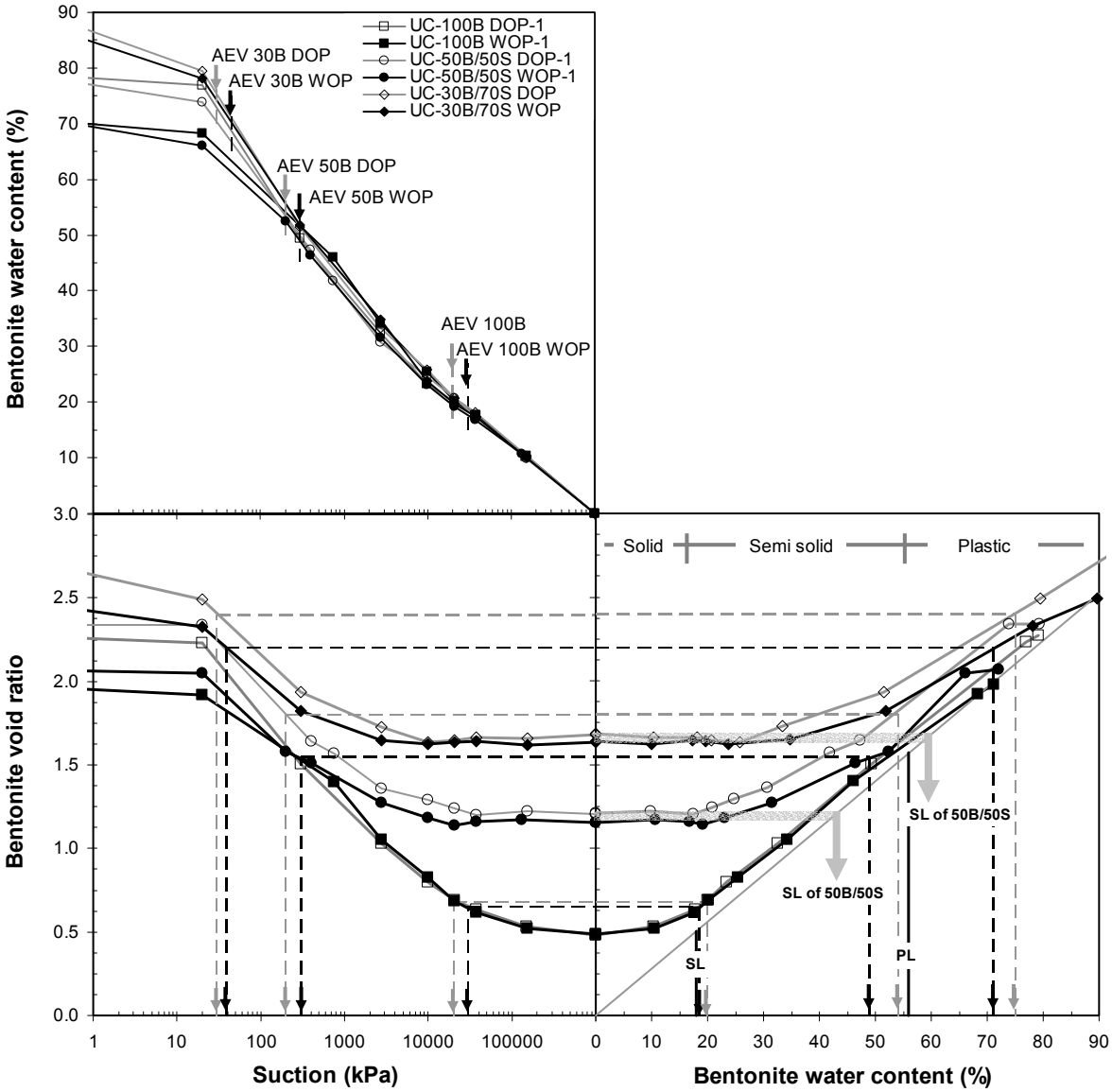

Figure 8.16 Bentonite water content, bentonite void ratio, and suction relationship of compacted bentonite-sand mixtures during drying from saturated under seating load.

The inter-granular contact between sand grains increases with increasing sand content. Hence, the specimen with higher sand content (or lower bentonite content) exhibits higher shear resistance compared to those with lower sand content (or higher bentonite content).

Considering the Atterberg limits as limits separating the clay consistency (i.e., solid, semi solid, plastic, and liquid), the inter-granular contact between sand grains also results in no decrease in bentonite void ratio even the bentonite still behaves as semi solid for 50B/50S specimens and plastic for 30B/70S specimens as shown in bentonite void ratio versus bentonite water content relationship. The figure also shows that the AEV of 30B/70S is placed in the range where the bentonite behaves as plastic condition.

A three-dimensional representation of Figures 8.15 and 8.16 is shown in Figures 8.17 and 8.18, respectively. Figure 8.17 shows the dependency of the evolution of water content and void ratio during drying from saturated state on the as-compacted conditions and bentonite content whereas Figure 8.18 shows the more significant dependency of the evolution of bentonite water content and bentonite void ratio during drying from saturated state on the bentonite content of the specimens.

In order to investigate the elasticity of drying-wetting curves of compacted bentonite and bentonite-sand mixture, the whole drying-wetting data of 100B-1 and 50B/50S-1 specimens compacted at DOP and WOP conditions are plotted in Figure 8.19 as void ratio versus suction relationship. Figures 8.19a and 8.19.b show drying-wetting curves of 100B-1 and 50B/50S-1, respectively. As shown in Figure 8.19.a and also presented in Figure 8.15, the drying curves of 100B DOP-1 and WOP-1 merge at suction higher value until the specimens reach completely dry condition (i.e., at suction of 1000000 kPa). This condition also occurs in the wetting curves of the specimens. The wetting curves of 100B DOP and WOP specimens are close each other until the end of the test (i.e., at 100 kPa). As shown in Figure 8.19.b, this also occurs to the 50B/50S specimens. The drying-wetting curves of 50B/50S DOP and WOP specimen are close at high suction. Small differences appears at low suction (i.e., less than 1000 kPa).

As depicted in Figure 8.19, the void ratio versus suction relationship generally shows a bilinear shape with a curve connecting the two linear parts. The intersection between the two linear parts of the curve indicates the limiting suction value beyond which no significant change in void ratio with suction is expected during drying. For wetting curve, the limiting suction value is suction at which significant change in void ratio with suction is commenced during wetting. The compacted pure bentonite specimens show approximately the same values of limiting suction during drying at about 30000 kPa and wetting at suction of 10000 kPa regardless the initial condition of the specimens. The compacted 50B/50S specimens indicate the limiting suctions for drying which is approximately equal to 2000-3000 kPa and for wetting 4000-5000 kPa. Since the differences in limiting suction values of drying and wetting for 50B/50S specimens are smaller than those 100B specimen, it seems that the drying-wetting curves of 50B/50S specimens are more elastic compared to the drying-wetting curves of 100B specimens.

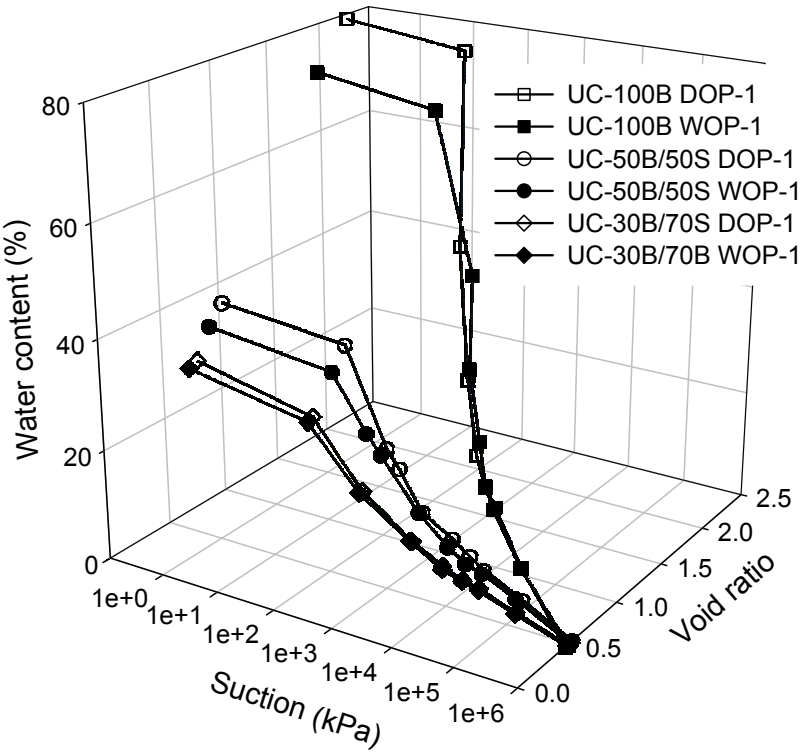

Figure 8.17 Three dimension relationship of water content, void ratio, and suction related to mixtures during drying from saturated state

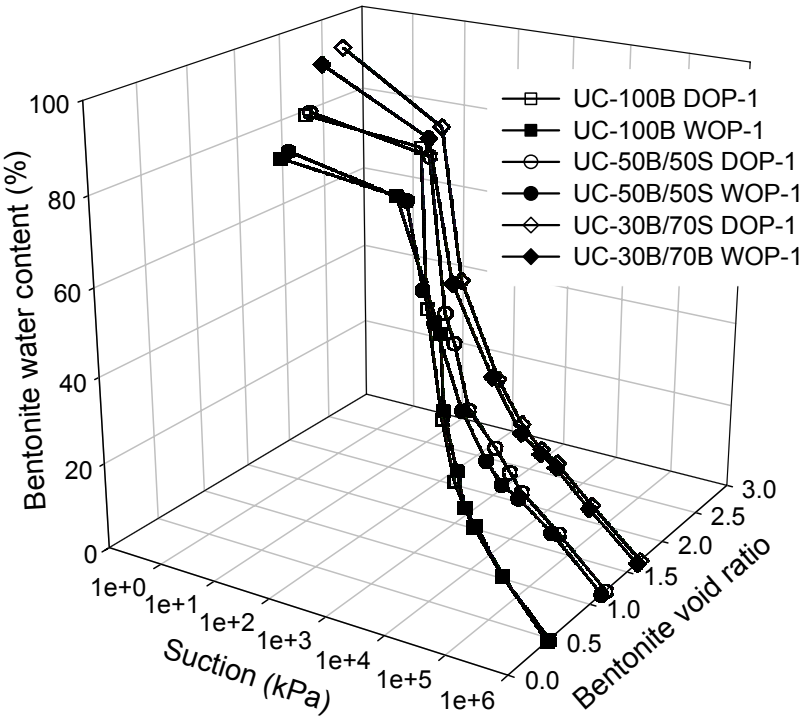

Figure 8.18 Three dimension relationship of bentonite water content, betonite void ratio, and suction related to mixtures during drying from saturated state

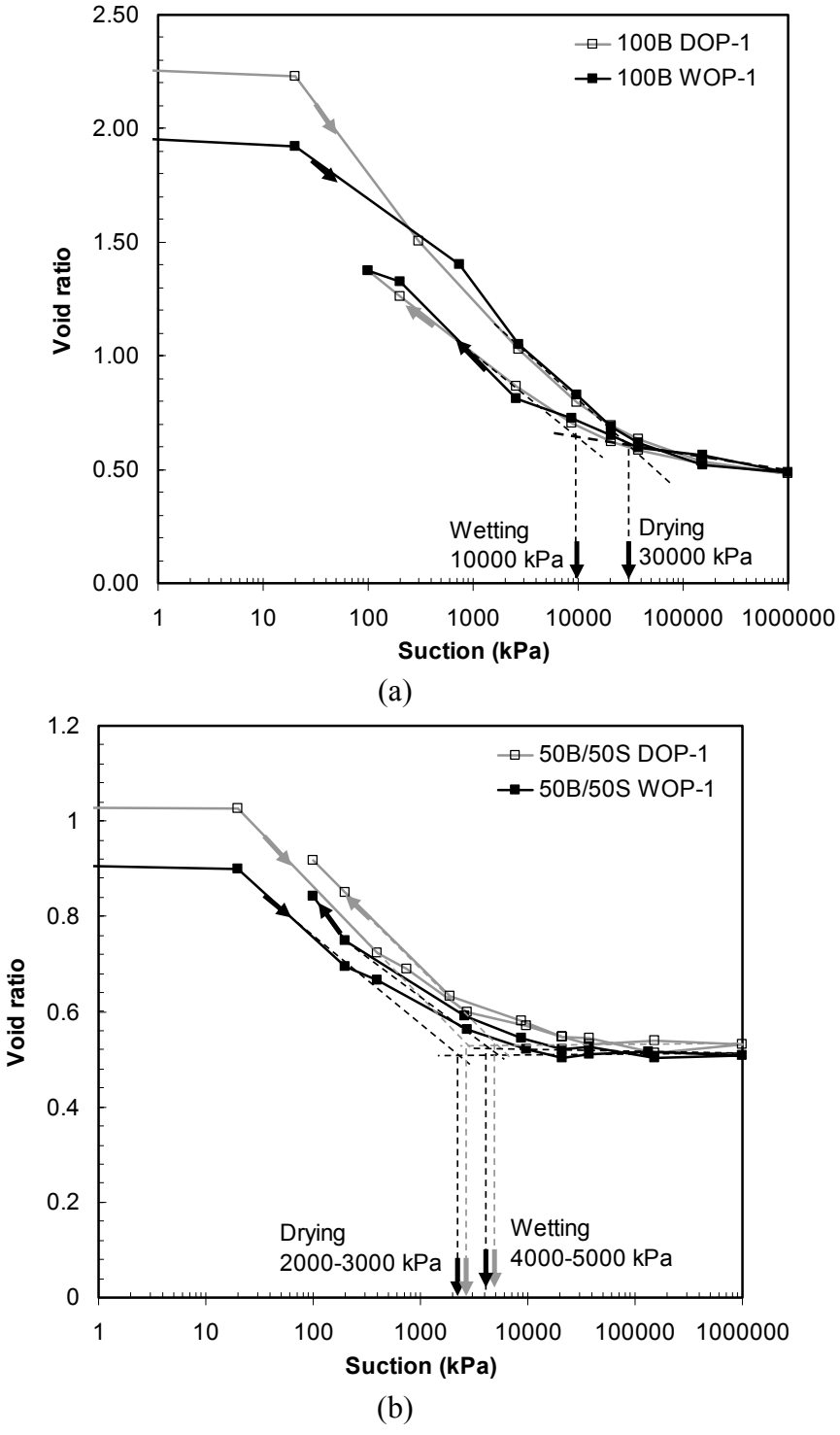

Figure 8.19 Drying-wetting curves of compacted bentonite and bentonite-sand mixture from saturated condition

Figures 8.20 to 8.22 show water content versus suction relationship of bentonite and bentonite-sand mixtures following drying-wetting processes from different conditions (i.e., from saturated and as-prepared conditions). As shown in Figure 8.20, there is small hysteresis in the drying-wetting curves of UC-100B DOP-3&4 and UC-100B WOP-3&4 specimens at low suction (i.e., less than 1000 kPa). Compared to the drying curves of specimens from

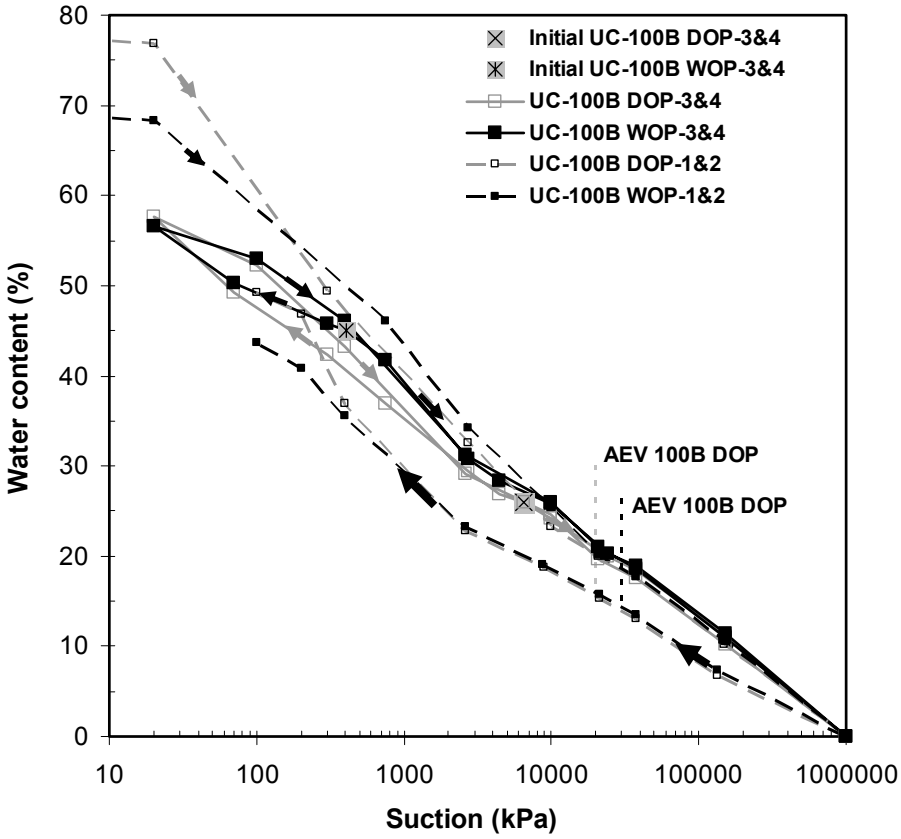

Figure 8.20 Water content versus suction relationship in the drying-wetting processes from different conditions for 100B specimens

saturated conditions (i.e., UC-100B DOP-1 and UC-100B WOP-1), the drying-wetting curves of specimens from as-prepared condition are placed below those from saturated conditions. The curves merge at suction higher than AEV of the specimen. The initial conditions of specimens appear unaffecting the ability of the specimens to retain water at suction higher than AEVs during drying process. However, when the specimen reached the very dry condition (i.e., suction of 1000000 kPa), larger hysteresis appears to the wetting curves of both conditions (i.e., DOP and WOP conditions). This condition also occurs to the bentonite-sand mixtures specimens (i.e., 50B/50S and 30B/70S specimens). As shown in Figures 8.21 and 8.22, hysteresis appears at suction less than 1000 kPa not only between the drying-wetting curves from saturated and as-prepared conditions but also between the drying-wetting curves of the DOP and WOP specimens from as-prepared condition. Larger hysteresis appears when the specimen underwent wetting from oven dry condition (i.e., at suction of 1000000 kPa).

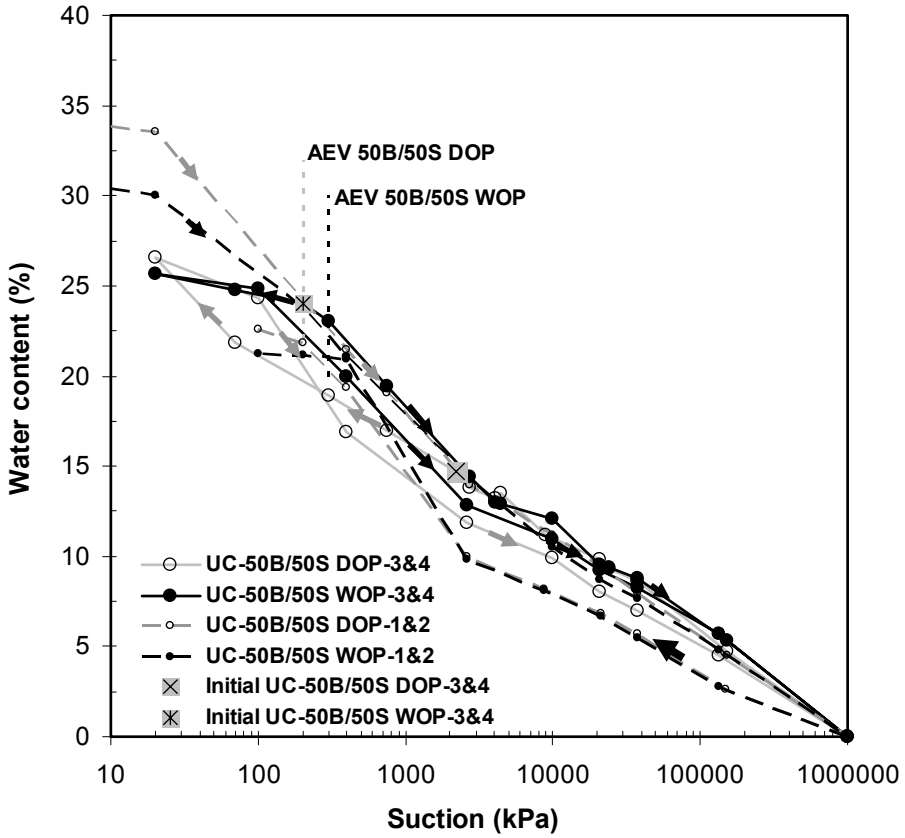

Figure 8.21 Water content versus suction relationship in the drying-wetting processes from different conditions for 50B/50S specimens

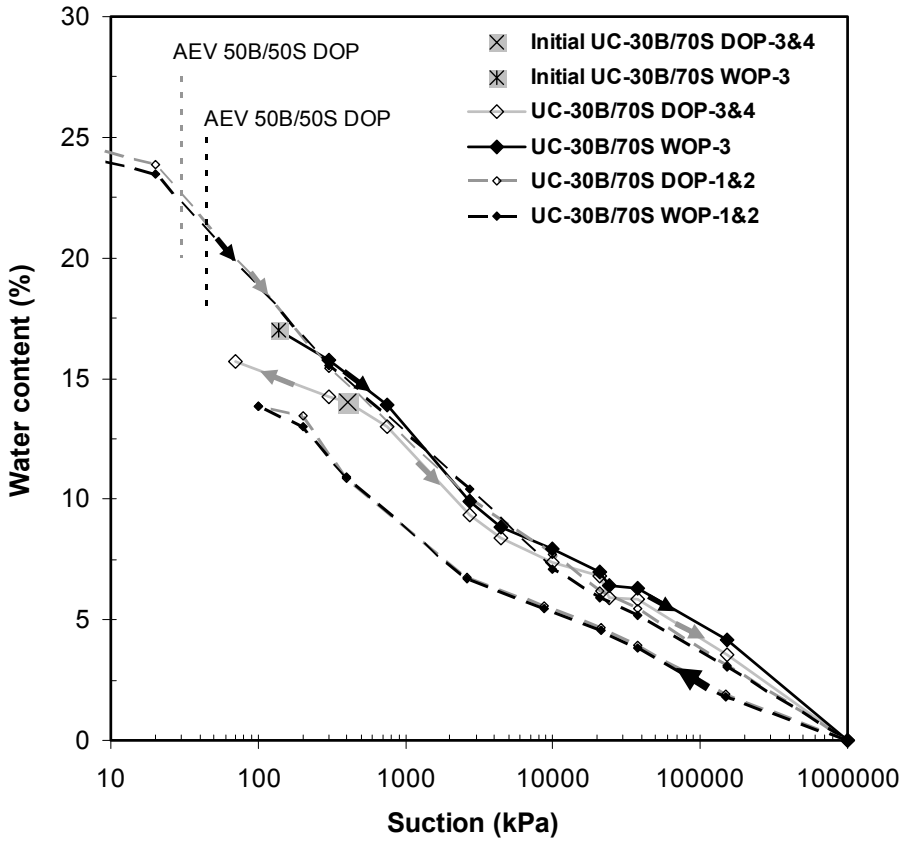

Figure 8.22 Water content versus suction relationship in the drying-wetting processes from different conditions for 30B/70S specimens.

No main drying curve appears in the result presented in Figures 8.20 to 8.22. As depicted in the figures, the drying curves of specimens which were saturated under seating load (i.e., UC-100B DOP-1 & WOP-1, UC-50B/50S DOP-1 & WOP-1, and UC-30B/70S DOP-1 & WOP-1) and wetting curves of specimens undergo wetting from oven-dried condition (i.e., UC-100B DOP-2 & WOP-2, UC-50B/50S DOP-2 & WOP-2, and UC-30B/70S DOP-2 & WOP-2) show to behave as main drying and wetting curves of the low compacted bentonite and bentonite-sand mixture investigated in this study.

Figures 8.23.a and 8.23.b show degree of saturation versus suction relationship of bentonite compacted at DOP and WOP conditions, respectively. As shown in Figures 8.23.a and 8.23.b, the drying-wetting curves of specimen from as-prepared condition appears placed inside the drying and wetting curves of specimen from saturated and oven-dried condition, respectively. Similar to the water content versus suction relationship as shown in Figure 8.20, the curves (i.e., drying and wetting curves from saturated and oven-dried conditions) behave like main drying and wetting curves. Figure 8.23 also shows that the hysteresis in the drying-wetting curves of DOP specimens (i.e., UC-100B DOP-3&4) is larger than that of WOP specimens (i.e., UC-100B WOP-3&4)

Figures 8.24.a and 8.24.b show degree of saturation versus suction relationship of 50B/50S specimens compacted at DOP and WOP conditions, respectively. Different from drying-wetting curves of 100B specimens, the drying-wetting curves from as-prepared conditions of 50B/50S are not placed in between drying-wetting curves of specimen from saturated and oven-dried conditions.

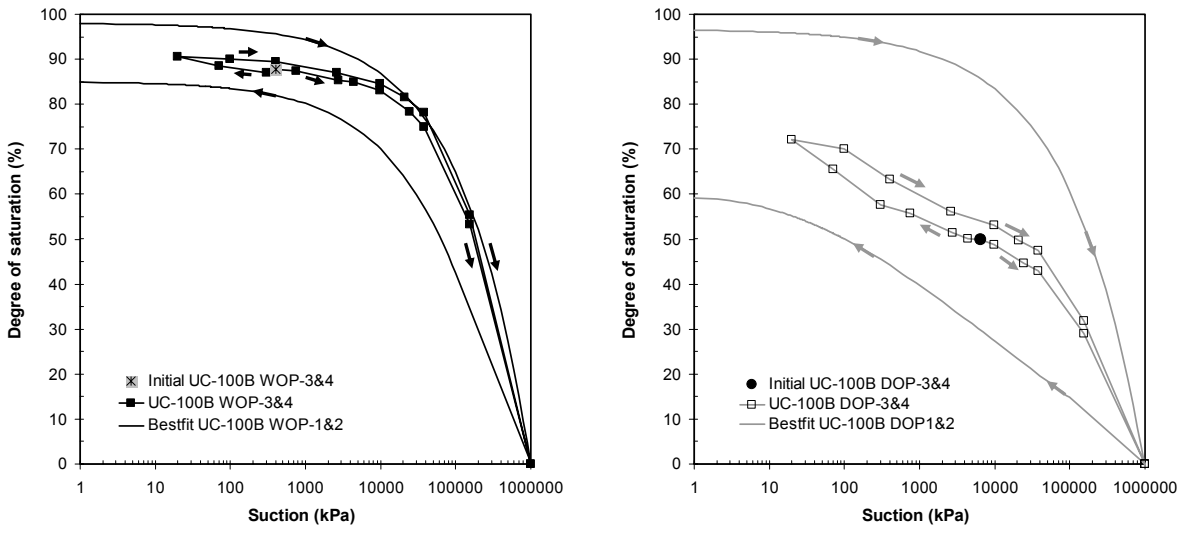

(a) (b)

Figure 8.23 Degree of saturation versus suction relationship in the drying-wetting processes from as-prepared conditions for (a) 100B WOP and (b) 100B DOP

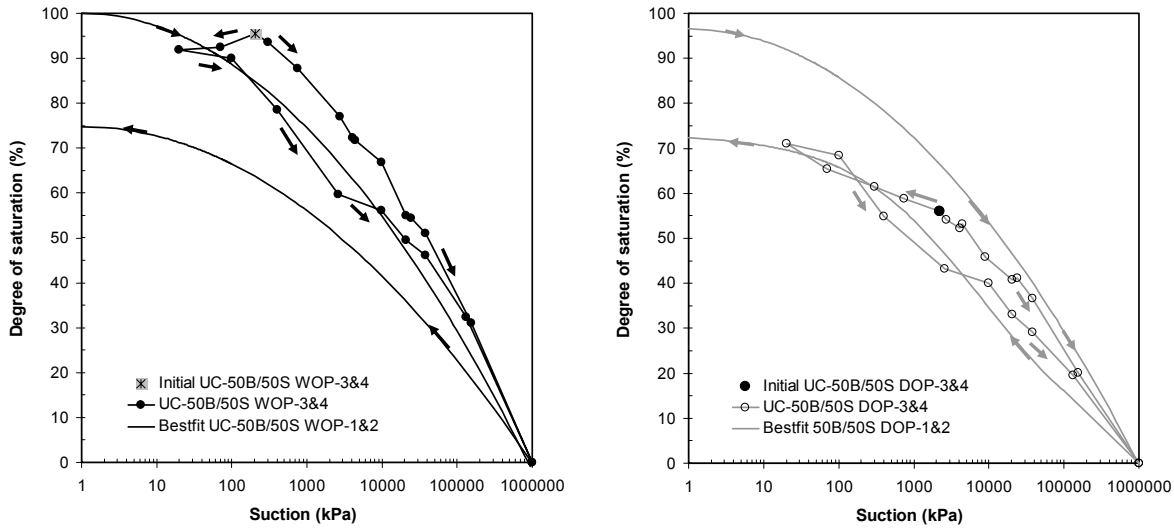

(a) (b)

Figure 8.24 Degree of saturation versus suction relationship in the drying-wetting processes from as-prepared conditions for (a) 50B/50S WOP and (b) 50B/50S DOP.

As shown in Figure 8.24.a, the as-prepared 50B/50S WOP specimen appears placed above the drying curves of 50B/50S WOP specimen from saturated condition. This results in the drying-wetting curves of 50B/50S WOP specimen from as-prepared specimen are placed slightly over the drying curves of 50B/50S WOP specimen from saturated condition. This is due to change in fabrics during swell under load in the saturation process. The more dissociated structure may result in higher void ratio and thus decrease in degree of saturation of specimen from saturated condition. For 50B/50S DOP specimen, the as-prepared condition is placed in between the drying-wetting curves of 50B/50S DOP specimen from saturated and oven-dried conditions. As a result, the drying-wetting curves of 50B/50S DOP specimen from as-prepared condition are placed in between the drying-wetting curves of specimen from saturated and oven-dried conditions. Some data that are placed under the wetting curve of 50B/50S DOP from oven-dried condition may be due to inaccuracy in the dimension measurement of the specimen. The result confirms that there are no main drying-wetting curves found in the bentonite-sand mixtures. The same phenomenon has been reported by Agus (2005) for heavily compacted bentonite-sand mixture specimen. Agus (2005) stated that this was due to the cracks that occur and were not taken into account in the computation of the degree of saturation. However, it is thought that the intact block of the specimen might be at saturation. Moreover, the inter-granular contact between sand grains during drying after wetting under seating load result in bigger void ratio compared to the drying-wetting void ratio of the as-prepared specimen.

8.3.2 Dry Density Evolution due to Drying-Wetting Processes

Figure 8.25 shows the evolution of the mixture dry density with water content during drying processes for specimens saturated under seating load condition. The standard compaction curves of bentonite and bentonite-sand mixtures reported by Agus and Schanz (2005a) were also plotted in the figure for reference. As shown in Figure 8.25, the mixture dry density of the specimens decreases with increasing water content during wetting to reach the saturation or zero air void (ZAV) line. During drying, the curves appear to move close to or along the ZAV line before starting to move away from the saturation at the AEVs. The specimens reach almost the same mixture dry density after complete drying to the oven-dried conditions.

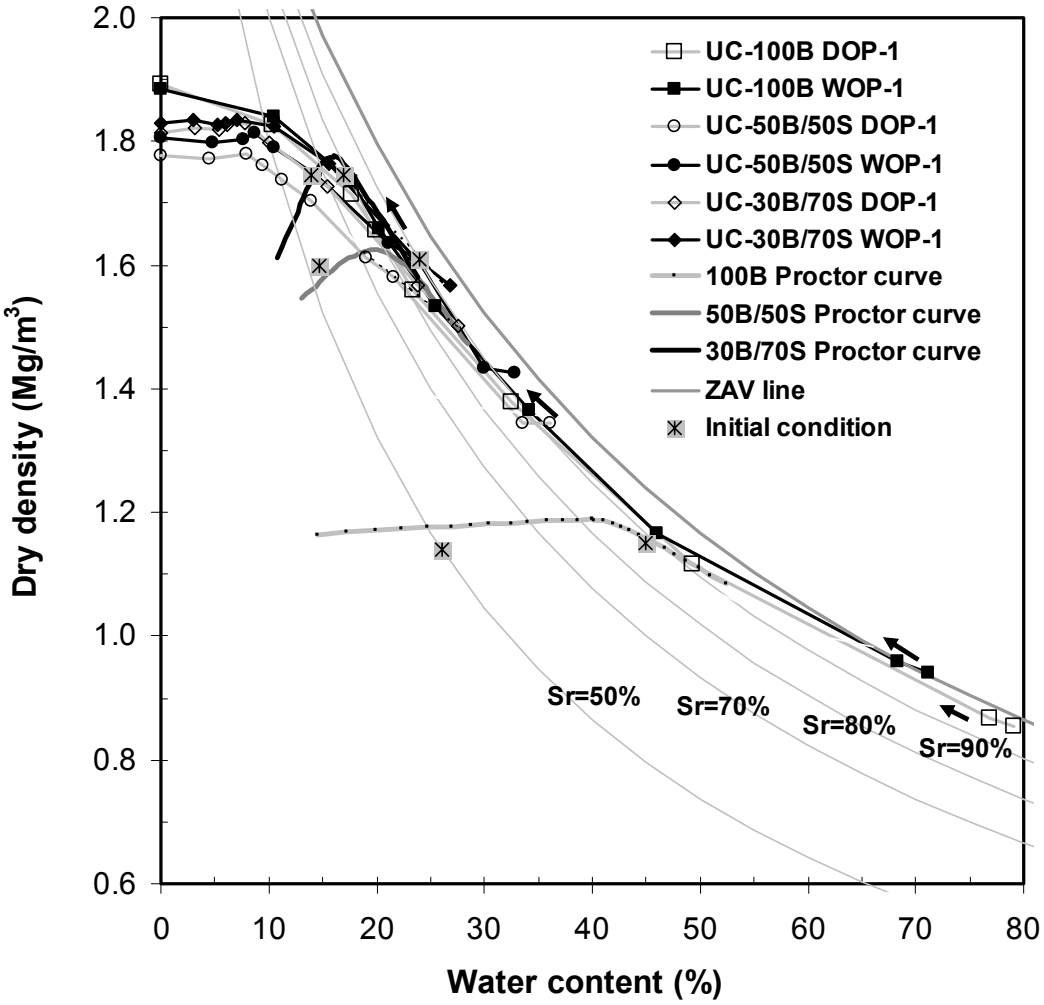

Figure 8.25 Dry density evolutions of compacted bentonite-sand mixtures during drying after saturation under seating load

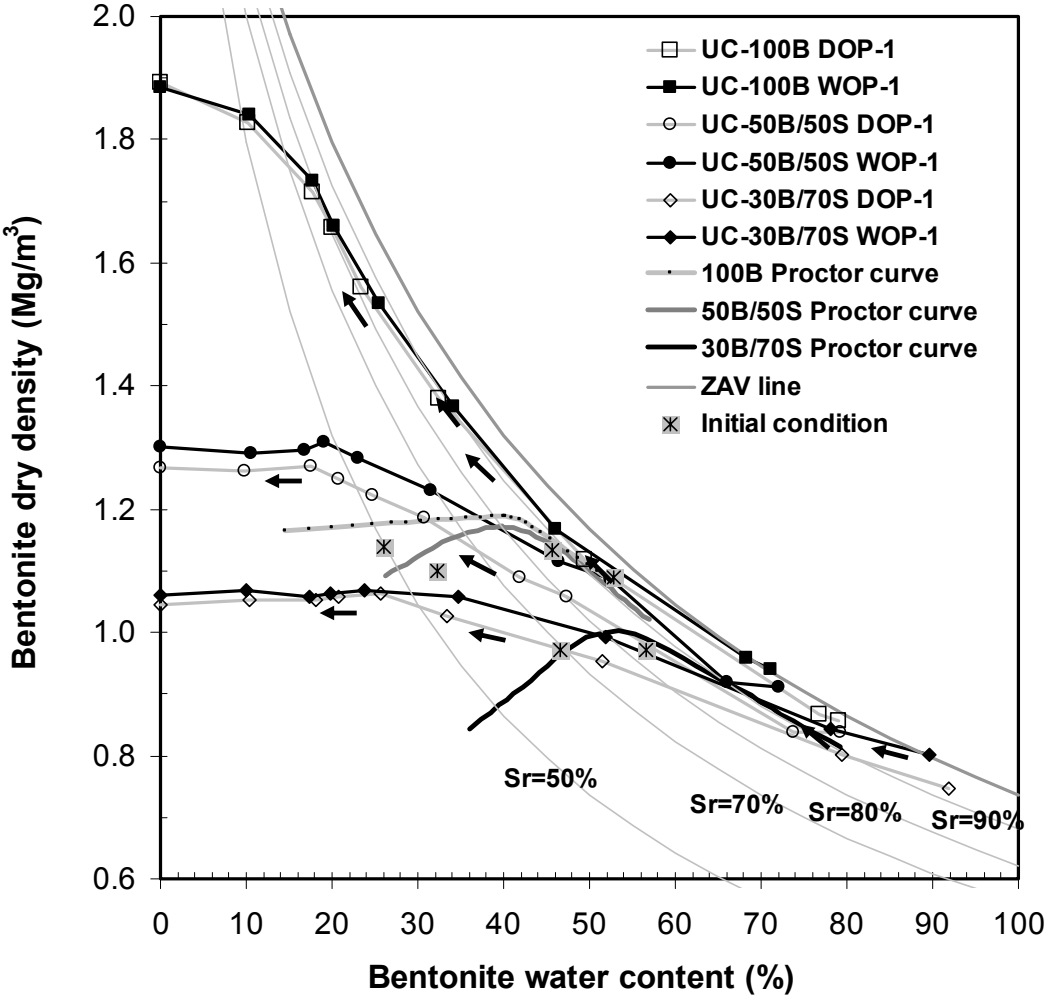

Figure 8.26 Bentonite dry density evolutions of compacted bentonite-sand mixtures during drying after saturation under seating load

The plot shown in Figure 8.25 can also be presented as bentonite dry density versus bentonite water content plot as shown in Figure 8.26. Interestingly, the standard Proctor curves of the 50B/50S mixture falls closely to that of the 100B mixture in the high bentonite water content range (i.e., greater than the optimum bentonite water content). The curves are seen to diverge at low bentonite water contents. The maximum bentonite dry densities of the two mixtures are thus similar. However, this phenomenon is not true for the 30B/70S mixture. The standard Proctor curve for this mixture is located well below the 100B and the 50B/50S curves. This fact may indicate that addition of sand beyond 50% (dry mass basis) is not effective when considering bentonite dry density as controlling factor. Since permeability of compacted bentonite-sand mixture depends on the swelling of bentonite in the mixture (Komine, 2004) and lower permeability can be achieved by decreasing the bentonite void ratio (or increasing the bentonite dry density) (Sällfors and Öberg-Högsta, 2002), 100B and 50B/50S specimens are suitable for a clay liner considering their low permeability due to their high bentonite dry density. If shrinkage behavior is also important to consider in the clay liner

behavior, 50B/50S and 30B/70S specimens are appropriate for this condition. Moreover, increasing sand content in the mixture increases the shear strength due to increase in contact between sand grains. However, increasing sand content in the mixture decreases the bentonite dry density and thus decreases the permeability. Since permeability is generally more important in the landfill applications than shear strength, the maximum performance of the compacted mixtures studied can generally be achieved at about 50% sand content.

8.3.3 Temperature Effects on Drying-Wetting Behavior of Compacted Bentonite-sand Mixtures

Figures 8.27 and 8.28 show the effects of temperature on the drying-wetting curves of the specimen compacted at DOP and WOP conditions, respectively. The figures reveals that the capability of specimens of both the 50B/50S mixtures and the pure bentonite to retain water is less at moderately high temperature (i.e., 80 °C) compared to the water retention capability at 20 °C. The figures show that the temperature effects on the water retention curves increase by decreasing suction (or at higher water content of the specimen). The result agrees well with the data reported by Romero et al. (2000), Villar and Martin (2005), and Tang and Cui (2005). However, the data plotted on the figures indicate that the difference is marginal. The result also agrees well with previous finding on temperature effects on suction characteristic curves.

Similarly, using the assumption that water in the specimens is only absorbed by the bentonite, the effect of temperature on the drying curve of the compacted bentonite-sand mixtures can be investigated by plotting the bentonite water content versus suction curve as shown in Figures 8.29 and 8.30 for the specimen compacted at DOP and WOP conditions, respectively. Insignificant difference between the two curves is also revealed in the figures with the curves for the specimens tested at 80^{o}C being below that for the specimens tested at 20^{o}C. The case is also true for the compacted pure bentonite specimens as shown in Figures 8.29 and 8.30 for the DOP and WOP specimens, respectively.

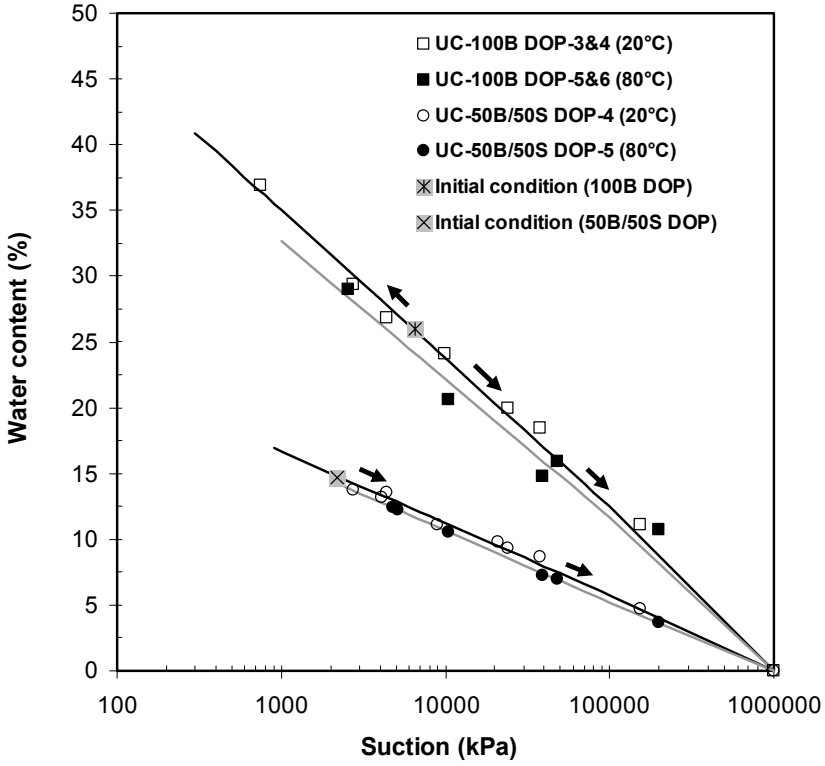

Figure 8.27 Effects of temperature on the water content versus suction curves for specimens compacted at DOP condition

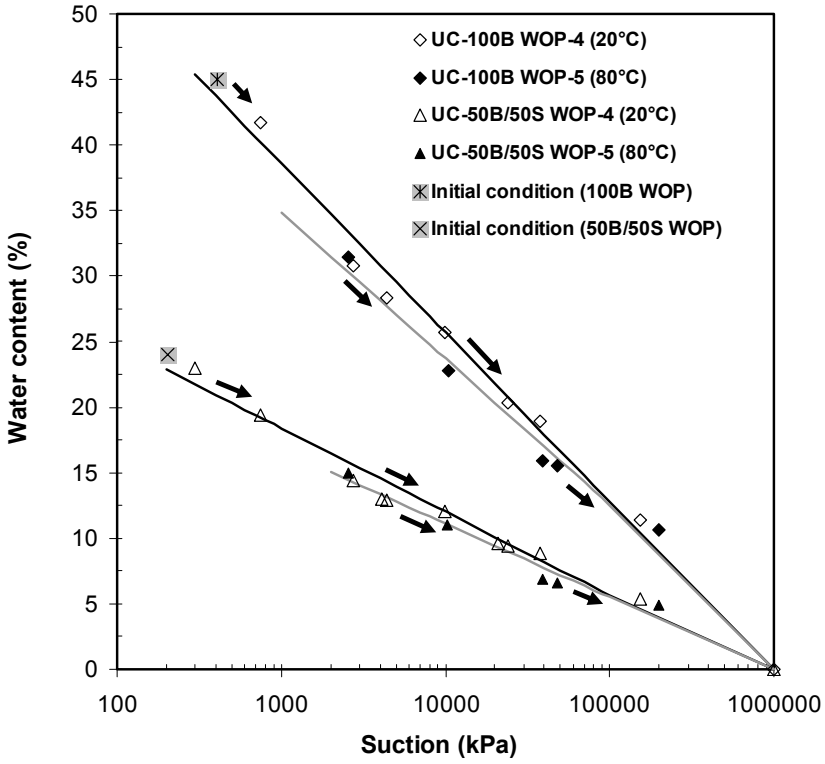

Figure 8.28 Effects of temperature on the water content versus suction curves for specimens compacted at WOP condition

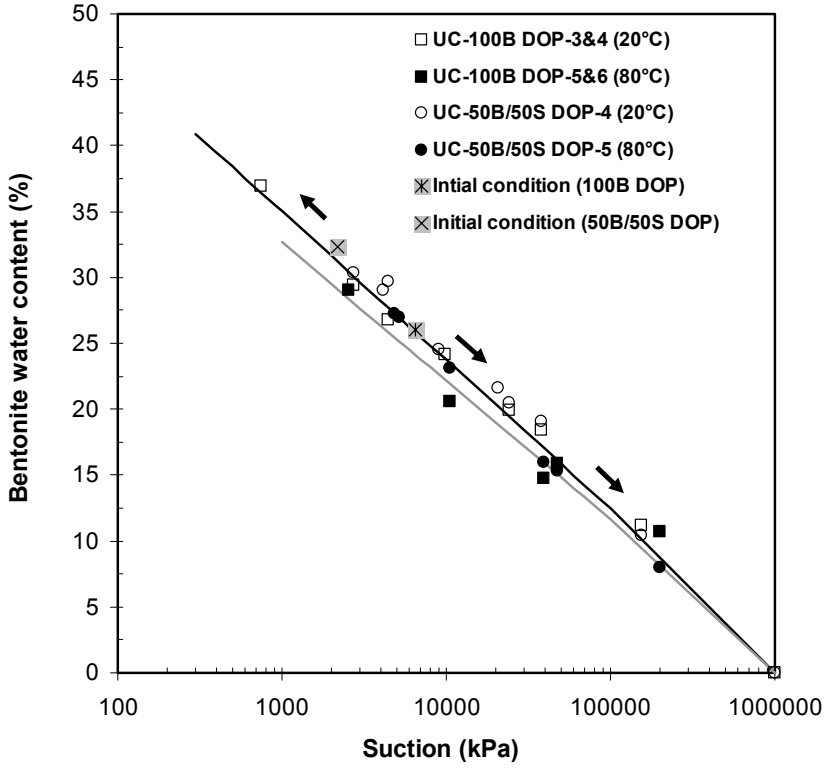

Figure 8.29 Effects of temperature on the bentonite water content versus suction curves for specimens compacted at DOP condition

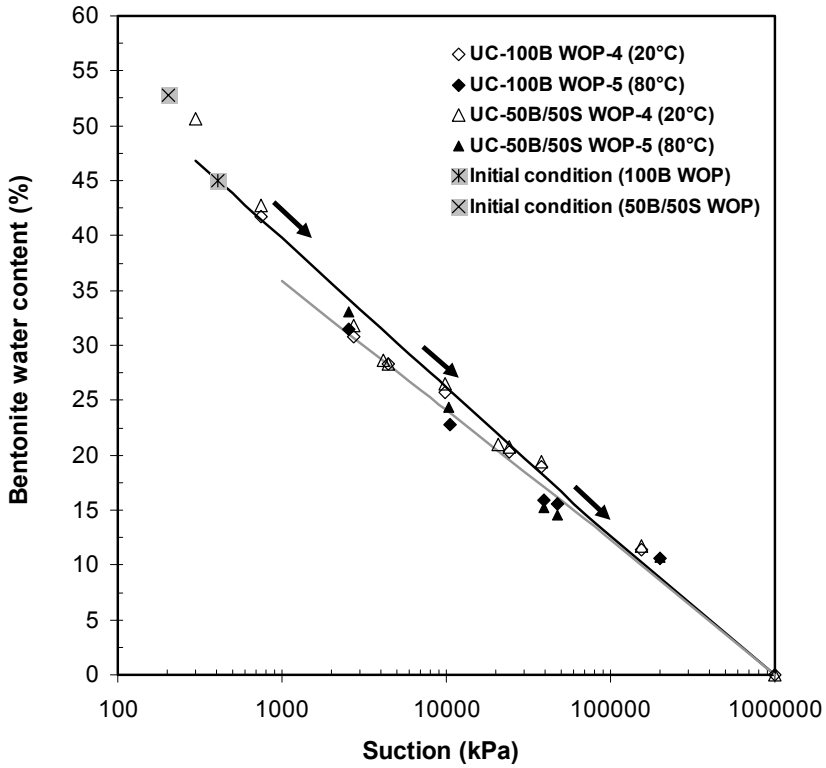

Figure 8.30 Effects of temperature on the bentonite water content versus suction curves for specimens compacted at WOP condition

The different capabilities of bentonite to retain water at different temperatures are due to the fact that the absorption process is basically exothermic in nature (Myers, 1991). The amount of vapor (or water) adsorbed by the bentonite surface reduces as the temperature increases. The effect of temperature is more significant at lower suction, as also noticed by Villar and Martin (2005), because of cumulative effects between the low capability of bentonite to absorb water at higher temperature (or decrease in hydration force) and the effect of surface tension of water which is also dependent on temperature (Grant and Salehzadeh, 1996). However, the difference between the drying and wetting curves is minor for the bentonite investigated in this study.

Figure 8.31 shows the effects of temperature on the bentonite void ratio versus suction relationship for the specimens investigated in this study. As shown in the figure, the effects of moderately high temperature on the bentonite void ratio versus suction relationship is even less pronounced than the effects on the bentonite water content versus suction relationship as shown in Figures 8.29 and 8.30.

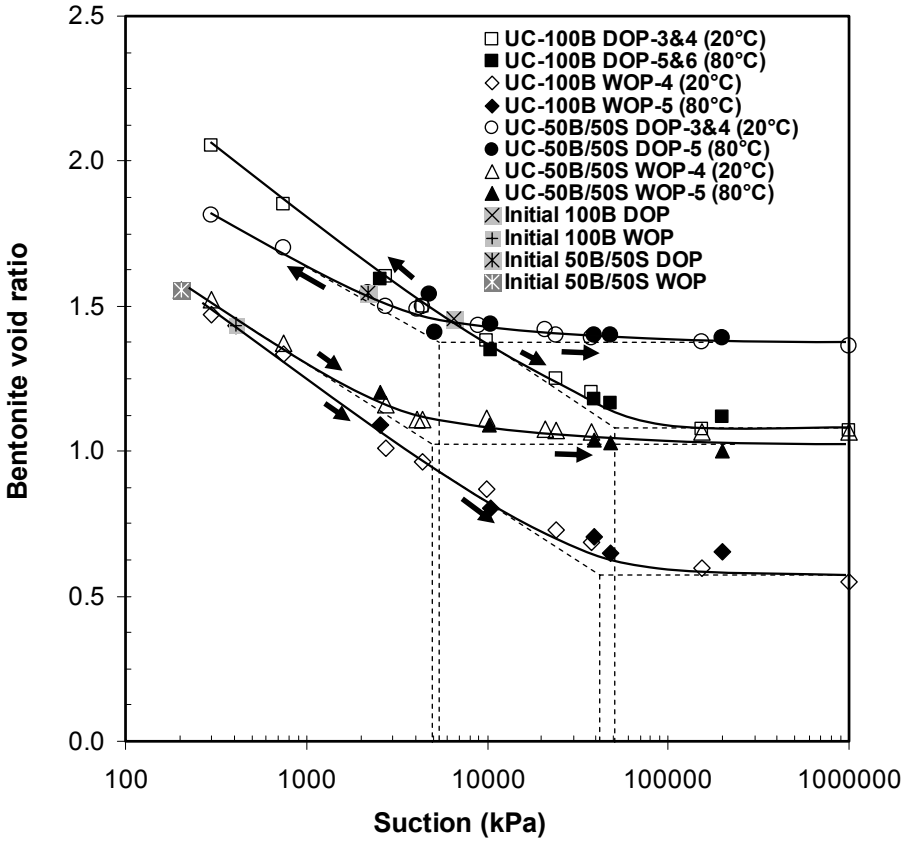

Figure 8.31 Effects of temperature on the void ratio versus suction curves for (a) 100B specimens, and (b) 50B/50S specimens

Figure 8.31 indicates a typical shape of the relationship between bentonite void ratio and suction for the specimens tested. The bentonite void ratio versus suction relationship generally shows a bilinear shape with a curve connecting the two linear parts as also found for the specimens from saturated condition as shown in Figure 8.19. The compacted pure bentonite specimens show approximately the same value of limiting suction, which is about 40000-50000 kPa, regardless the initial fabric of the specimens. Similarly, the compacted 50B/50S specimens indicate the limiting suction which is approximately equal to 5000-5500 kPa. Considering minor effects of temperature on the bentonite void ratio versus suction relationship as shown in Figure 8.31, the elasticity of the specimens may follow the elasticity of the same specimen performed at 20 °C as shown in Figure 8.19.

During drying process at suctions beyond the limiting suction value, no macroscopic shrinkage of the bentonite takes place in the specimens. Shrinkage occurs only in the cluster level. During drying, clay cluster reduces its volume which induces a drop in its water content at constant bentonite void ratio. The cluster shrinkage at constant bentonite void ratio results in cracks of the specimens which were also observed in the experiment especially in the specimens compacted wet of optimum. Cracks in the specimens create preferential flow paths for gas and affect the performance of the materials when used in landfills. Figure 8.31 also clearly shows that the presence of sand in the mixture reduces the cluster shrinkage as shown by lower limiting suction and thus risk of crack development, which is in fact beneficial to the behavior of the compacted mixtures in relation to their use as engineered barrier for landfills.

Figures 8.32 and 8.33 show temperature effects on the degree of saturation versus suction relationship for 100B and 50B/50S specimens, respectively. As shown in the figures, increase in temperature results in decreasing the degree of saturation of the specimens. This is due to decrease in water content of specimen by increasing temperature (Figures 8.27 and 8.28) without any significant effects on the void ratio of the specimens (Figure 8.31).

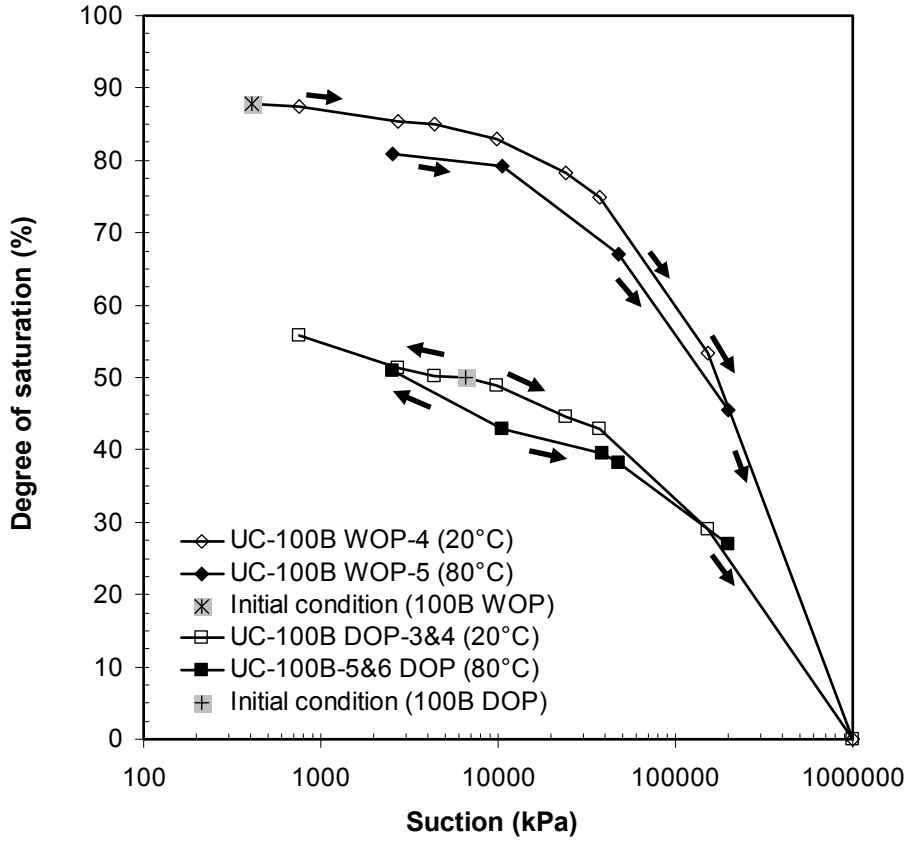

Figure 8.32 Effects of temperature on the degree of saturation versus suction curves for 100B specimens

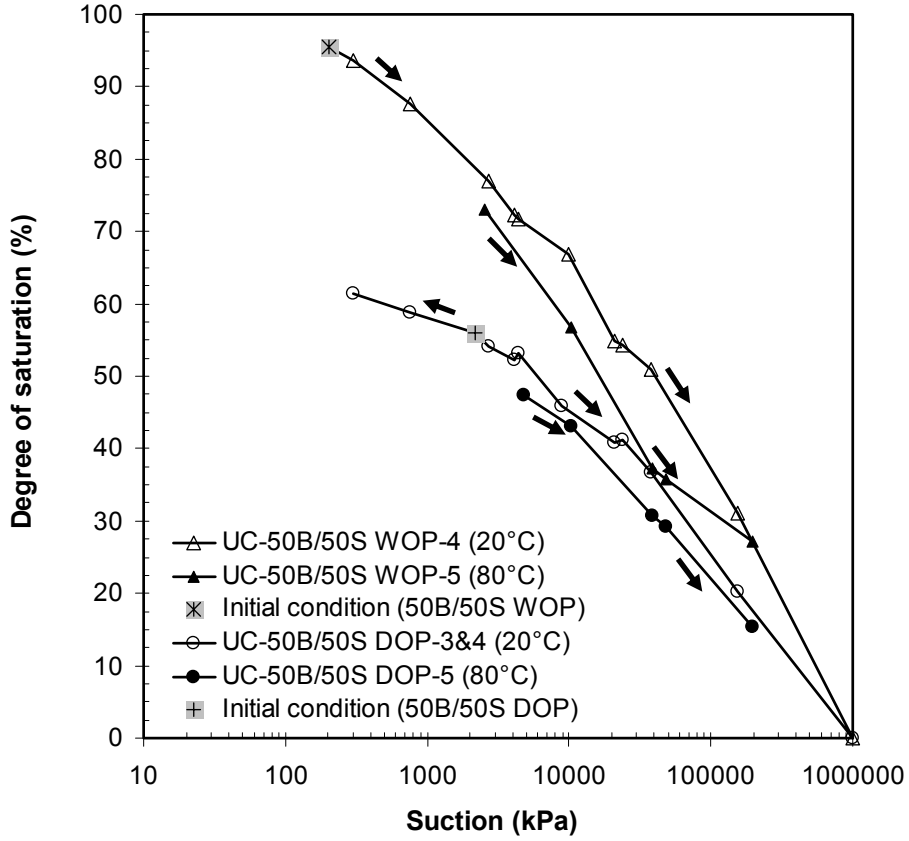

Figure 8.33 Effects of temperature on the degree of saturation versus suction curves for 50B/50S specimens

8.3.4 Drying-Wetting Behavior of Heavily Compacted Bentonite-Sand Mixture at 20 °C

Figure 8.34 shows water content versus suction relationship during drying-wetting processes for heavily compacted bentonite-sand mixture (i.e., 50B/50S specimen) from different initial conditions at 20 °C. As depicted in the figure, the drying curves of specimens (i.e., UC-HC-1 and UC-HC-2) which were saturated under seating load are placed very close showing the homogeneity of the specimens used. The UC-HC-3 specimen which was saturated under constant volume condition appears to absorb amount of water after released from the cell and placed in the pressure plate apparatus. This is due to the total suction of the specimen was not zero at saturated condition but 3028 kPa measured using chilled-mirror hygrometer (*RH* = 97.8; T = 22 °C), the value was close to the swelling pressure value (i.e., 3000 kPa). At saturated condition, the capillary component is equal to zero. The osmotic suction does not give significant contribution in the total suction of the bentonite used in this study (Chapter 7). This proves that the total suction of the specimen is not developed only by the capillary component and osmotic suction but also by the hydration force.

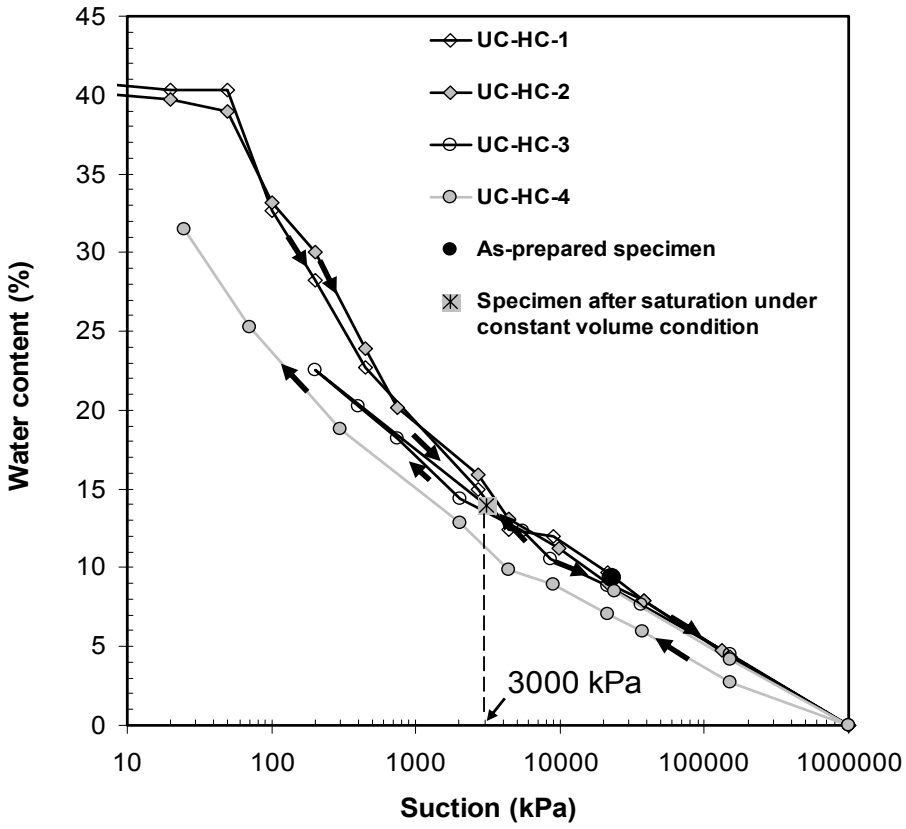

Figure 8.34 Water content versus suction of heavily compacted bentonite-sand mixture from different initial conditions at 20 °C

Figure 8.34 also shows that the initial conditions of the specimens affect the drying curves in the small suction range (i.e., less than 3000 kPa). Higher than this suction, the initial conditions do not influence the ability of the material to absorb water. The result agrees well with the result finding by Al-Mukhtar et al. (1999) that stress history does not influence the water retention behavior of bentonite at suction higher than 2700 kPa.

Figure 8.34 also exhibits that the reversibility of drying-wetting curves of heavily compacted specimen where drying curve of UC-HC-3 follows its wetting curve. However, when the specimen reached very dry condition (i.e., suction of 1000000 kPa), small hysteresis appears in the wetting curve as shown for the wetting curve of UC-HC-4. This condition also occurs to the low compacted bentonite and bentonite-sand mixtures as shown in Figure 8.20 to 8.22. This is due to the fabric effect since at loose condition applying temperature of 100°C (i.e., the way how to apply total suction of 1000000 kPa) does not influence the ability of the bentonite to hold water as shown in Figure 6.26.

Figure 8.35 shows void ratio versus suction of heavily compacted bentonite-sand mixture from different initial conditions. As shown in the figure, the drying curves of specimen which were saturated under seating load are placed over the drying curve of

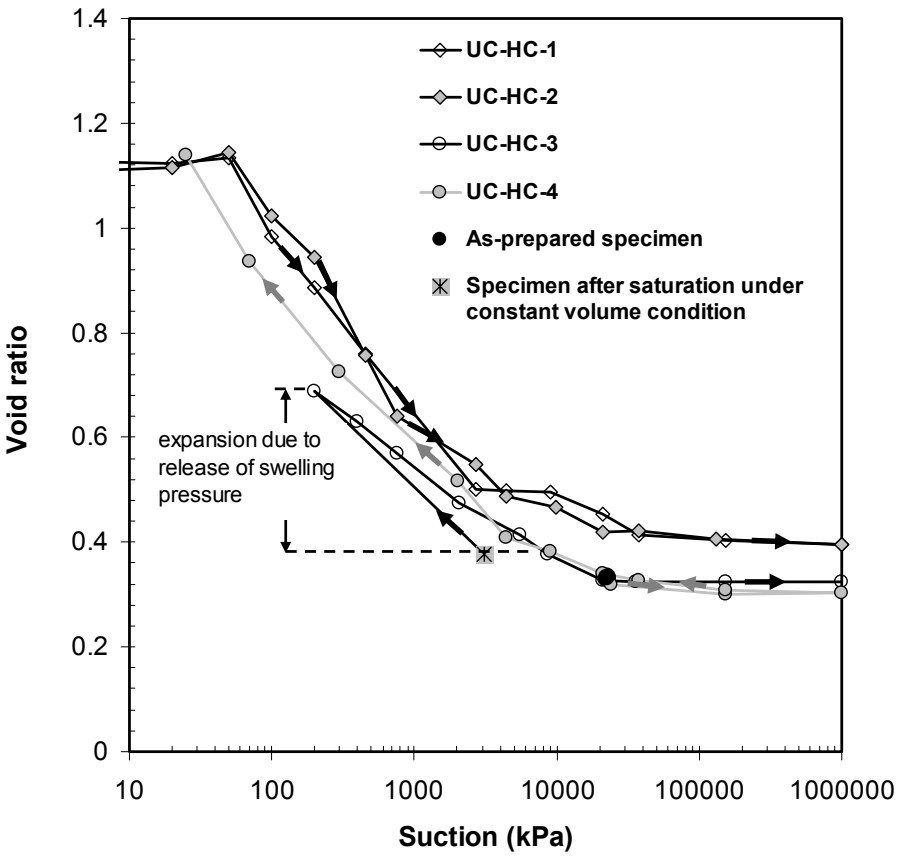

Figure 8.35 Void ratio versus suction of heavily compacted bentonite-sand mixture from different initial conditions at 20 °C

specimen which was saturated under constant volume condition. This is because the swelling pressure prevents significant change in the fabric of the specimen saturated under constant volume condition. Therefore, the curve (i.e., drying curve of UC-HC-3) is very close to the drying-wetting curve of specimen from as-prepared condition (UC-HC-4). Figure 8.35 also shows that no change in the void ratio at suction higher than the initial total suction of the as-prepared specimen (i.e., 22700 kPa).

Figure 8.36 shows degree of saturation versus suction of heavily compacted bentonite-sand mixture from different initial conditions. The result agrees well with the degree of saturation versus suction curve for low compacted specimen as shown in Figure 8.24 that no main drying curve was found in the result. In addition, the drying curves (i.e., for the specimens saturated under seating load and constant volume conditions) were placed below the as-prepared condition of the specimen.

Figure 8.36 also shows that, in the wetting process, the limiting suction of the specimen is close to the initial suction of the as-prepared specimen. Lower than the limiting suction, no significant change in the degree of saturation of the specimen can be observed. The result agrees well with previous finding reported by Agus (2005) that the limiting suction

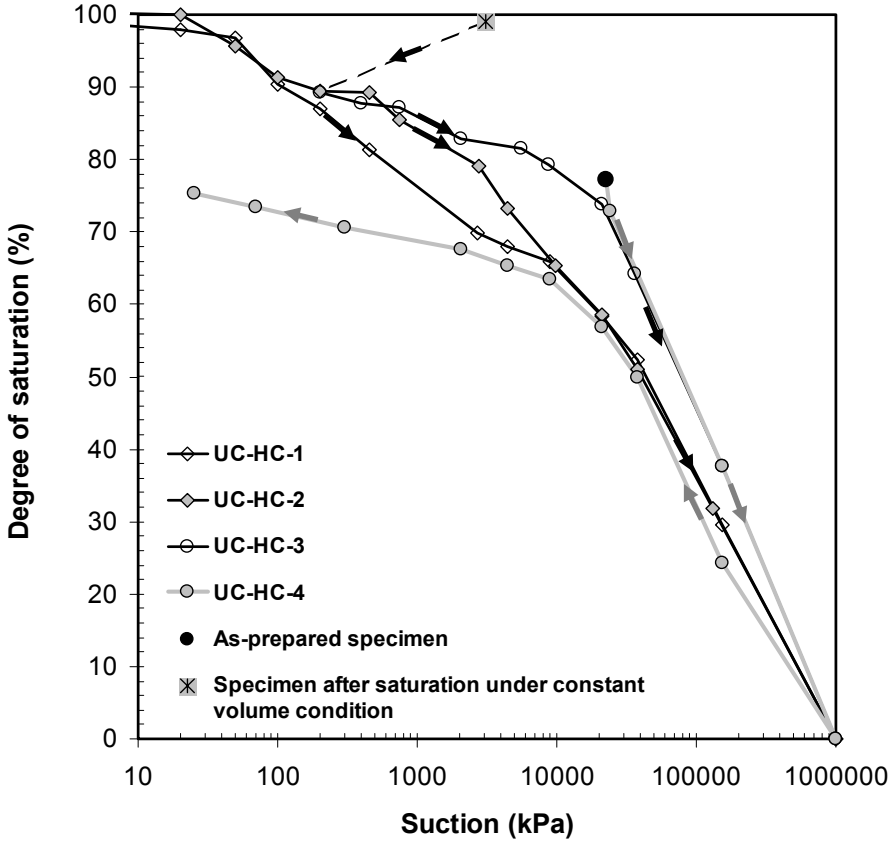

Figure 8.36 Degree of saturation versus suction of heavily compacted bentonite-sand mixture from different initial conditions at 20 °C

is a function of the highest total suction that is ever experienced by the specimen.

8.3.5 Drying-Wetting Curves of Heavily Compacted Bentonite-Sand Mixture at 80 °C

Figure 8.37 shows the temperature effects on the water content versus suction curves for the heavily compacted bentonite-sand mixture from different initial conditions. As shown in the figure, the elevated temperature (i.e., 80 °C) does not give significant effect on the ability of the specimen to absorb water. For the drying curve, the temperature effect is very small. For the wetting curve, the temperature effect appears at total suction less than 20000 kPa. As clearly shown in the wetting curve (UC-HC-4 and UC-HC-7), water content of the specimen at high temperature (i.e., 80 °C) is less than that of the specimen at room temperature.

Figure 8.38 shows temperature effect on the void ratio versus suction relationship of heavily compacted bentonte-sand mixture from different initial conditions. As depicted in the figure, elevated temperature does not show significant effect on the void ratio of the as-prepared specimen (UC-HC-7) and specimen which was saturated under constant volume condition (UC-HC-6). This is not true for the specimen, which was saturated under seating

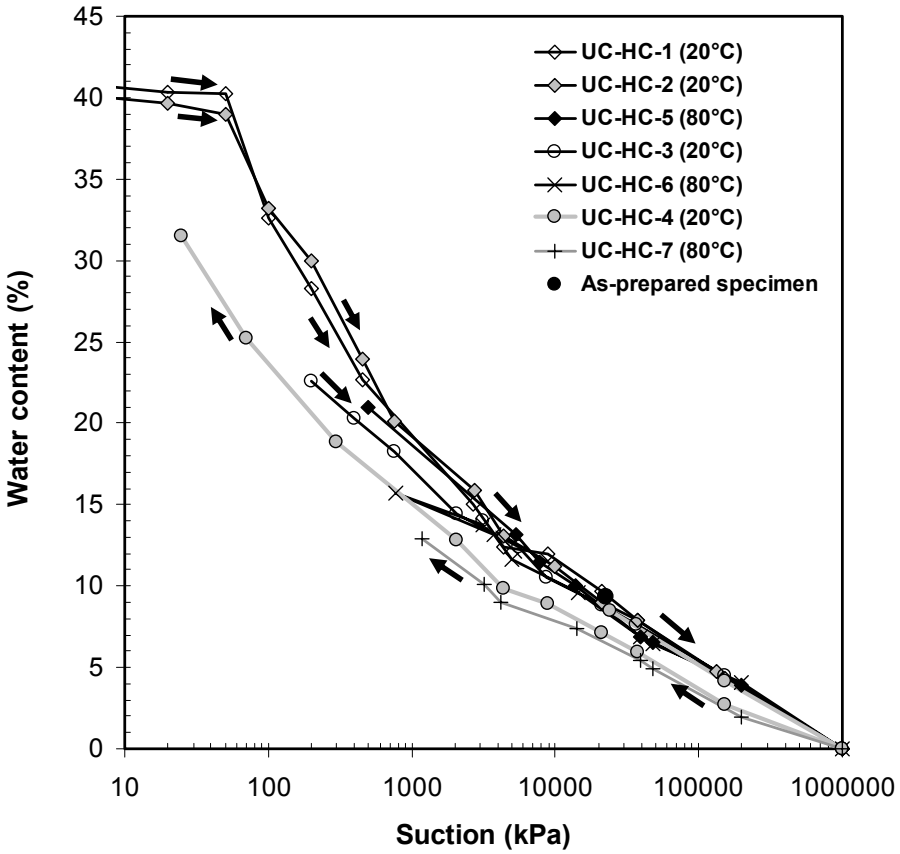

Figure 8.37 Temperature effect of the water content versus suction of heavily compacted bentonite-sand mixture from different initial conditions

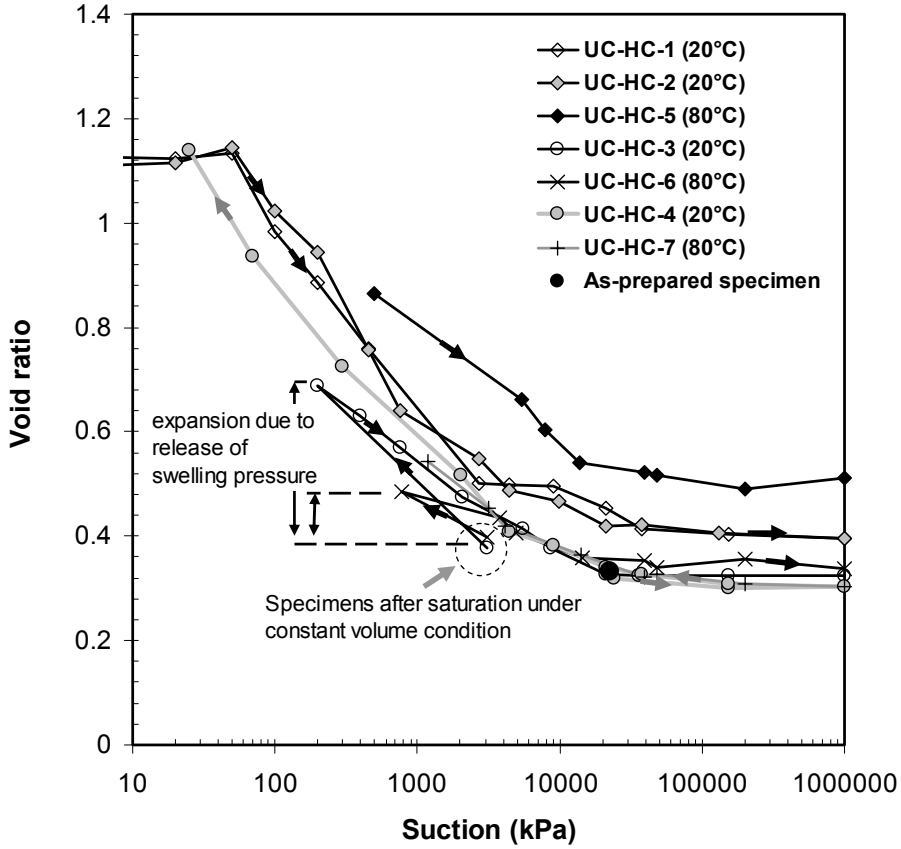

Figure 8.38 Temperature effect of the void ratio versus suction of heavily compacted bentonite-sand mixture from different initial conditions

load condition (UC-HC-5). The drying curve of UC-HC-5 obtained at 80 °C is placed over the drying curves of UC-HC-1 and UC-HC-2 which are dried at 20 °C. This difference is due to difference in wetting process of the specimens. The specimens saturated under seating load have more dissociated clay structure compared to the specimens saturated under constant volume condition. Gradual decrease in suction from saturated condition to 500 kPa results in non homogeneity of water distribution in UC-HC-5 specimen. This condition results in cracks and increases the void ratio of the specimen. Moreover, the crack was not taken into account in the dimension measurement using caliper meter.

Figure 8.39 shows the temperature effect on the degree of saturation versus suction relationship. As shown in the figure, increase in temperature result in decreasing the degree of saturation of the specimens. The changes in the degree of saturation are due to the lower water content of the specimen at elevated temperature while the void ratio is unchanged. The larger change in degree of saturation of the UC-HC-5 specimen is mainly due to high void ratio of the specimen at 80 °C (Figure 8.38) whereas decrease in the water content due to increase in temperature is very small (Figure 8.37).

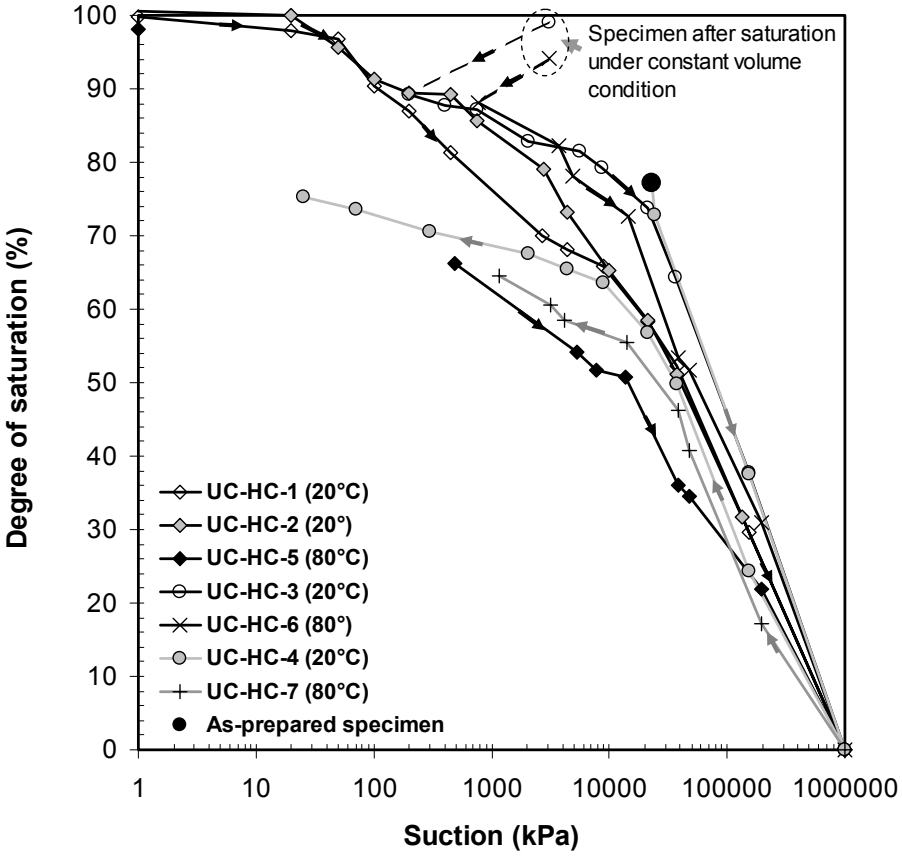

Figure 8.39 Temperature effect on the degree of saturation versus suction of heavily compacted bentonite-sand mixture from different initial conditions

Figures 8.40, 8.41, and 8.42 show water content, void ratio, and degree of saturation versus suction relationship of heavily compacted bentonite-sand mixture from as-prepared condition experienced drying-wetting cycles at 80 °C (UC-HC-8), respectively. As shown in Figure 8.40, the drying curve is placed in between the drying and wetting curves from saturated and oven-dried conditions. In the second cycle (i.e., wetting process), small hysteresis appears since the path does not follow the drying path (or path 1). In addition, the wetting path (i.e., path 2) intercepts the wetting path of specimen from oven-dried condition (UC-HC-4). In the third cycle, small hysteresis also occurs. However, as shown in Figure 8.40, the drying curve (i.e., path 3) merges to the first and second cycles at very high total suction value (i.e., about 200000 kPa) even the void ratio of the specimen is higher than the first and the second cycles as shown in Figure 8.41. A similar behavior is also seen in case of degree of saturation versus suction relationships as shown in Figure 8.42. Therefore, it can be concluded that the drying and wetting behavior of heavily compacted bentonite-sand mixture at 80 °C is irreversible except for water content versus suction relationship at very high suction. In very high suction, the fabric of specimen or crack does not influence the ability of specimen to absorb water since the water is placed in the intra-aggregate pores. The result is

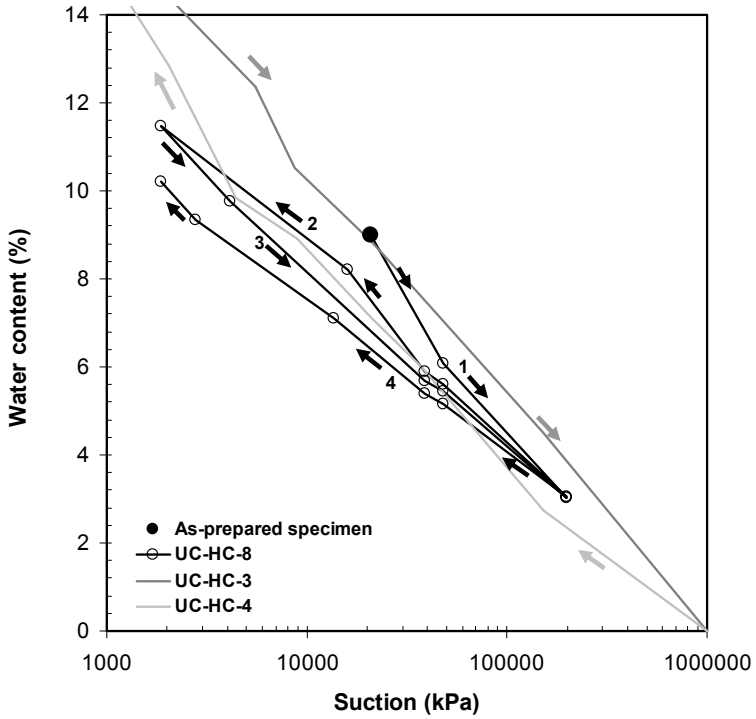

Figure 8.40 Water content versus suction for heavily compacted bentonite-sand mixture undergo drying-wetting cycles at 80 °C

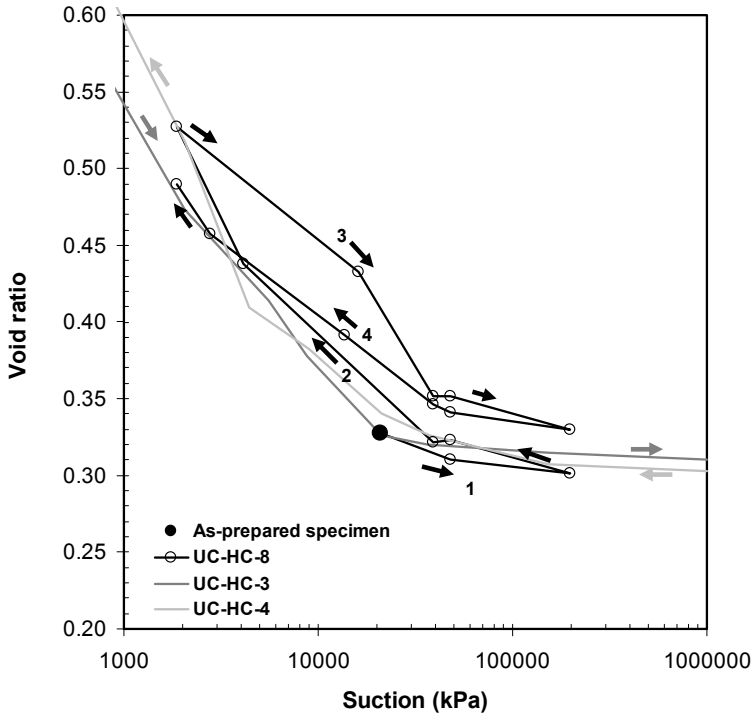

Figure 8.41 Void ratio versus suction for heavily compacted bentonite-sand mixture undergo drying-wetting cycles at 80 °C

different from the drying-wetting behavior at 20 °C that the drying-wetting behavior of compacted FoCa7 clay and Calcigel-sand mixture are reversible as reported by Cui et al. (2002b) and Agus (2005), respectively.

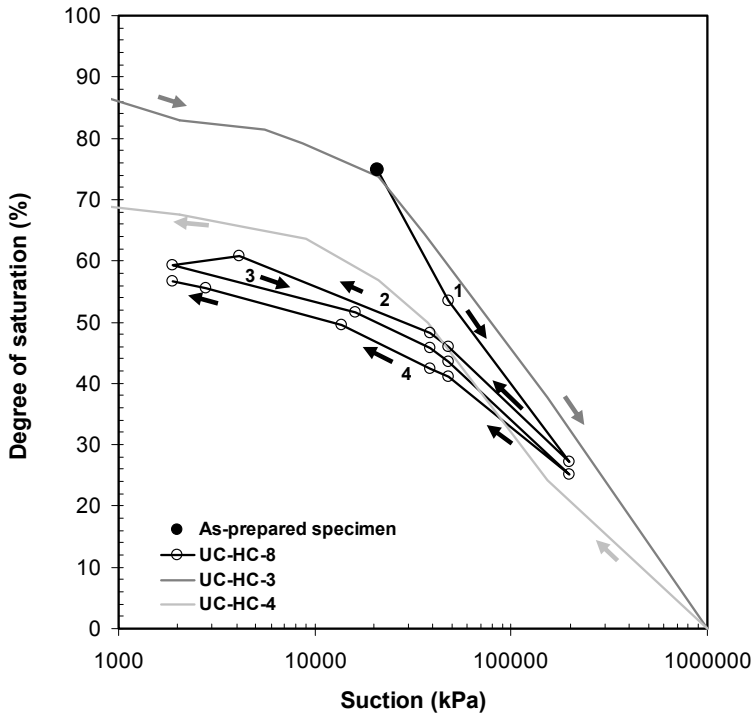

Figure 8.42 Degree of saturation versus suction for heavily compacted bentonite-sand mixture undergo drying-wetting cycles at 80 °C

Figures 8.43.a, 8.43.b, and 8.43.c show the photographs of specimen for as-prepared, oven-dried, and after drying-wetting cycles conditions, respectively. As shown in the figure, no crack appears in the oven-dried specimen. The crack is clearly shown on the surface of specimen underwent drying-wetting cycles at 80 °C (UC-HC-8). This is thought as a reason irreversible of drying-wetting curve as shown in Figures 8.40, 8.41, and 8.42.

8.4 Summary

The following conclusions can be drawn based on the results of unconfined drying-wetting investigation of compacted bentonite-sand mixture.

1. The compacted bentonite specimens exhibit the greatest shrinkage upon drying regardless the compaction conditions. The same characteristics are also shown for the 50B/50S and 30B/70S specimens. The experimental results indicate that air entry value increases with bentonite content of the specimens. Compaction conditions do not play significant roles.

2. All mixtures show apparently the same void ratio after complete drying to oven-dried state. However, the bentonite void ratio of the specimen at this state decreases with increasing bentonite content. Although no shrinkage limit test results are currently available for the material tested, the results indicate that the shrinkage void ratio of the mixtures also decreases with increasing bentonite content. If the shrinkage limit void ratio

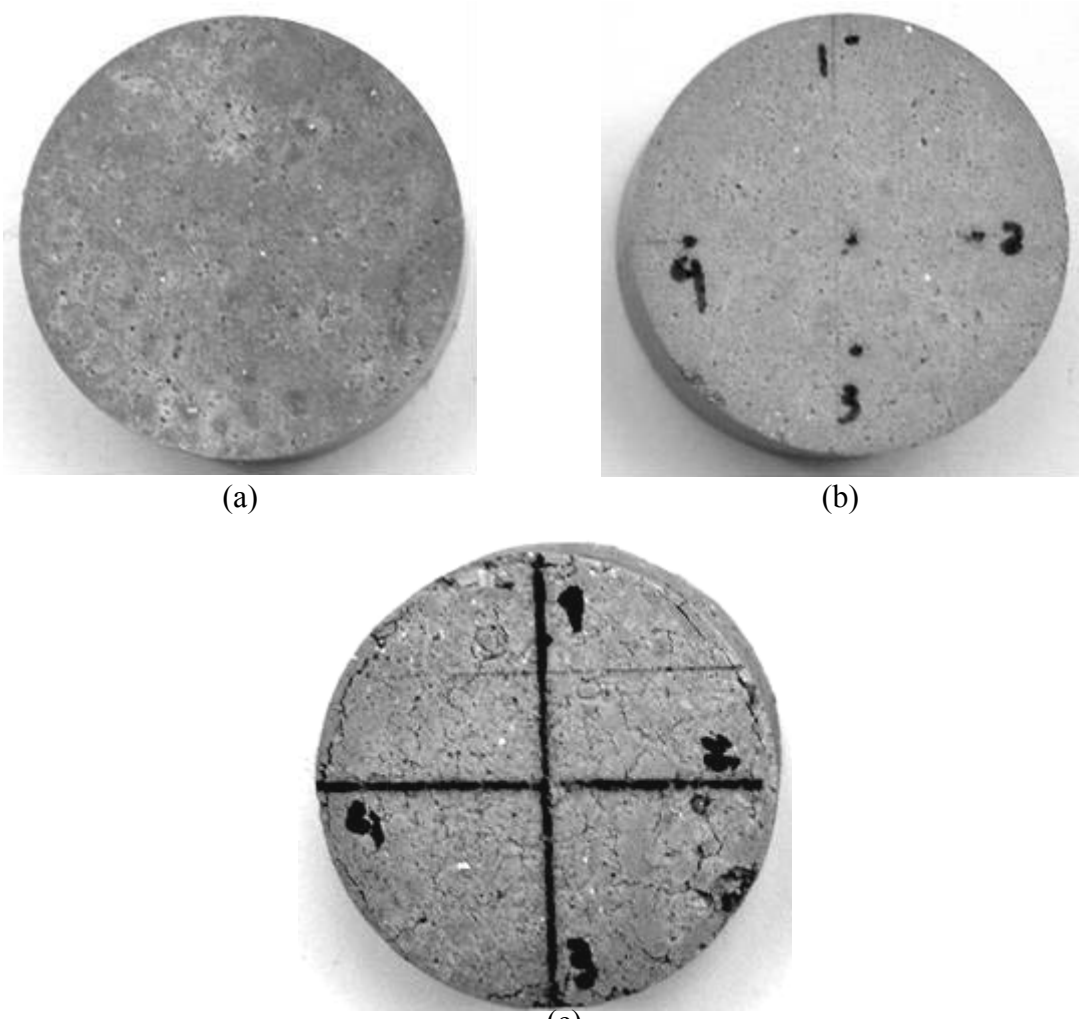

(a) (b)

(c)

Figure 8.43 Specimens Photos in different conditions: (a) as-prepared condition, (b) oven-dried condition, and (c) after drying-wetting cycles at 80 °C (UC-HC-8)

is regarded to signify the inter-granular contact between sand grains in the mixtures, the specimens with lower bentonite content exhibit higher shear strength compared to those with higher bentonite content. Further investigation is required to confirm this.

3. For the mixtures studied, generally, 50% (dry mass basis) seems to be the optimum bentonite content considering permeability, shrinkage behavior, and shear strength aspects with respect to the landfill applications. Further investigation is also required to confirm this.

4. It is observed that temperature has insignificant influence on the amount of water retained by the bentonite in the mixtures as suction decreases or increases. The presence of sand is thought to have no influence on the water retained by the bentonite in the mixtures. However, it has a beneficial impact with respect to the crack development in the

compacted mixture as it undergoes drying process since presence of sand in the mixture reduces the cluster shrinkage and thus risk of crack development.

5. For heavily compacted bentonite-sand mixture, initial conditions of the specimens affect the drying curves in the small suction range (i.e., less than 3000 kPa). Higher than this suction, the initial conditions do not influence the ability of the material to absorb water.

6. The effect of temperature on the drying-wetting curves of heavily compacted specimen is not significant compared to the effect of initial condition of the specimen.

7. Cracks occurs in the heavily compacted specimen underwent drying-wetting cycles at 80°C resulting irreversible the drying-wetting curves plotted as void ratio and degree of saturation versus suction relationships. For water content versus suction relationship, the drying-wetting curves are also irreversible at suction less than 200000 kPa.

CHAPTER 9

TEMPERATURE EFFECTS ON SWELLING CHARACTERISTICS OF BENTONITE-SAND MIXTURE AND DETERMINATION OF WETTING CURVE UNDER CONSTANT VOLUME CONDITION

9.1 Introduction

Emplaced high level wastes will emit quite significant amount of heat which is thought to change coupled hydro-mechanical behavior of the buffer element used in the waste disposal facility. Swelling pressure, which is a representation of both hydraulic and mechanical behavior of the material and indicates the performance of the sealing material, is one of important behavior that should be investigated in case when increase in temperature in the waste repository is of concern.

Earlier investigations show that the increase in temperature induced insignificant increase in the swelling pressure of bentonite (e.g., Pusch et al., 1990 for Na-bentonite, Cho et al., 2000 for Ca-bentonite). On the other hand, the reverse is also true (e.g., Pusch et al, 1990 for Ca-bentonite, Lingnau et al., 1996 for Na-bentonite, and Villar and Lloret, 2004 for FEBEX bentonite which is mainly Ca-Mg-bentonite). However, the temperature effects on the swelling pressure of bentonite remain important in the assessment of long-term performance of the whole repository construction. The investigation into the temperature effects on the behavior of bentonite provides insight into understanding the hydro-mechanical processes taking place in the bentonite in relation to its use as barrier material.

This chapter presents the effects of moderately high temperature on the swelling pressure of Calcigel. Two types of test; namely, one step swelling pressure test and multi-step swelling pressure test, were performed to study the two mechanisms of water molecules transports (i.e., in fluid phase and in vapor phase) and to obtain the wetting curves under constant volume condition. In order to understand the swelling characteristics of the bentonite used in this study particularly swell under small vertical pressure condition, the swelling strain tests at moderately high temperature were also performed. The equipment set-up, verification, and techniques adopted are described. The results obtained as well as the

comparison with the swelling pressure measured at room temperature are presented and discussed.

9.2 Literature Review on Experimental Techniques Relevant to This Study

Three different methods; namely, swell-load, swell-under-load, and constant volume test were suggested by Sridharan et al. (1986) to measure swelling pressure of expansive soils in oedometer. In swell-load, the specimen is inundated and allowed to swell under seating load. Loads are added after an equilibrium condition was reached. In swell-under load, several identic specimens are allowed to swell or to compress under different vertical loads to reach equilibrium conditions. The equilibrium points lie on a straight line which intersects the horizontal line (i.e., initial condition of the specimens). The swelling pressure is the pressure required to bring the specimen to the initial void ratio. In constant volume condition, the volume of specimen is maintained constant by applying pressure until there is neither swelling nor compression occurred during inundation. The swelling pressure determination at constant volume condition is also suggested by ASTM D 4546 (ASTM, 1997)

In constant volume method, swelling pressure of compacted bentonite can be determined by saturating the specimen with distilled water in one step; namely one step constant volume swelling pressure test, or by applying suction using axis-translation technique (ATT) and vapor equilibrium technique (VET); namely multi-step constant volume swelling pressure test.

Various techniques have been adopted for saturating the specimen in one step swelling pressure test. Bucher and Spiegel (1984), Sitz (1997), and Herbert and Moog (2002) used high water pressure to saturate the specimen in one step method. The water was supplied using liquid pump which is able to deliver high liquid pressure to specimen. Different liquid pressures were applied from the bottom of the specimen. The specimen was let to reach equilibrium of total pressure (swelling and fluid pressure) as measured by a load cell for each liquid pressure. A relationship between the measured total pressure and the applied liquid pressure is used to define the swelling pressure (i.e., the total pressure at zero liquid pressure). Sridharan et al. (1986) used water flooding method to saturate the specimen in the swelling pressure test. The test was performed on an oedometer apparatus. The specimen was allowed to swell in distilled water and the swelling is controlled to a zero value by addition of loads. The load where no further swelling is observed is swelling pressure. Agus and Schanz (2005a) used waster circulation method to saturate specimen in swelling pressure

investigation. The test was performed in an isochoric cell. The water was circulated through the top and bottom boundaries of the specimen. Water is absorbed by the specimen as a result of suction gradient between the distilled water supplied and the specimen. The method is also useful to flush entrapped air in the top and bottom boundaries that should be performed in the unsaturated soil testing.

For testing at high temperature, Bucher and Müller-Vonmoos (1989) used the apparatus as shown in Figure 9.1. In the test, the water was supplied using liquid pressure of 1000 kPa. The swelling pressure was recorded through pressure transducer. The thermal element was mounted along side of the specimen and controlled by temperature controller. The cell deformation was measured using dial gauge placed in the top of the apparatus.

Figure 9.2 shows the controlled-suction oedometer apparatus (i.e., ATT) designed for testing at moderately high temperature (i.e., 80 °C) used by Romero et al (2003). The oedometer ring was placed inside a silicone oil bath containing heater (No.1) in order to maintain thermal stability. The soil sample (No.2) is located between a high air-entry value ceramic disk at the bottom (No.3) and a coarse porous stone at the top (No.4). In order to perform constant volume test, the height of the samples was maintained constant and the variation of the vertical net stress is recorded using an external load cell. The matric suction was applied by applying air pressure through the porous stone placed on the top of the specimen and water pressure from the bottom of the specimen. The matric suction is the different between the air pressure and water pressures applied during the test.

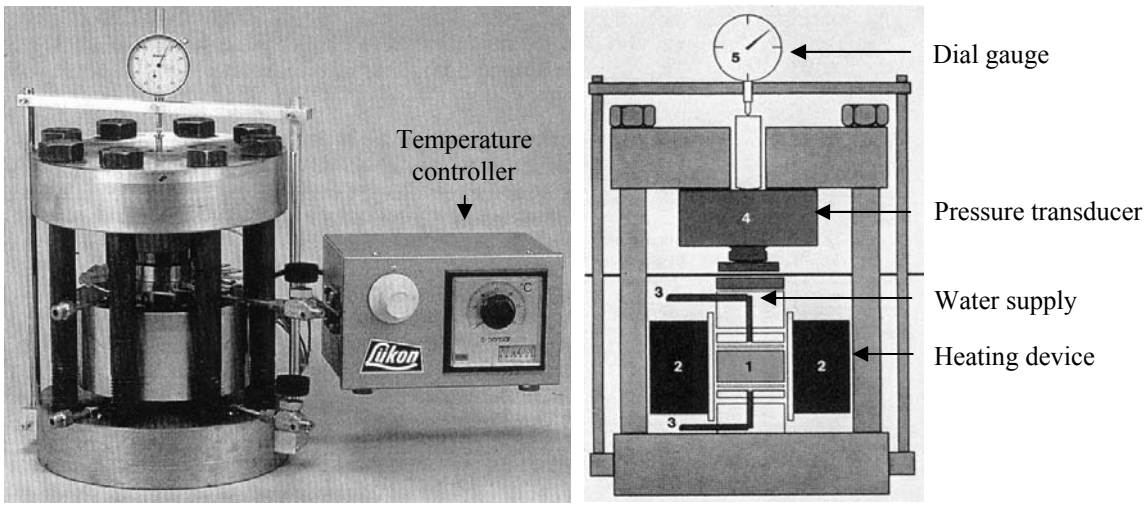

(a) (b)

Figure 9.1 Swelling pressure test apparatus for high temperature (Bucher and Müller-Vonmoos, 1989) (a) experimental setup, and (b) cross section of the apparatus.

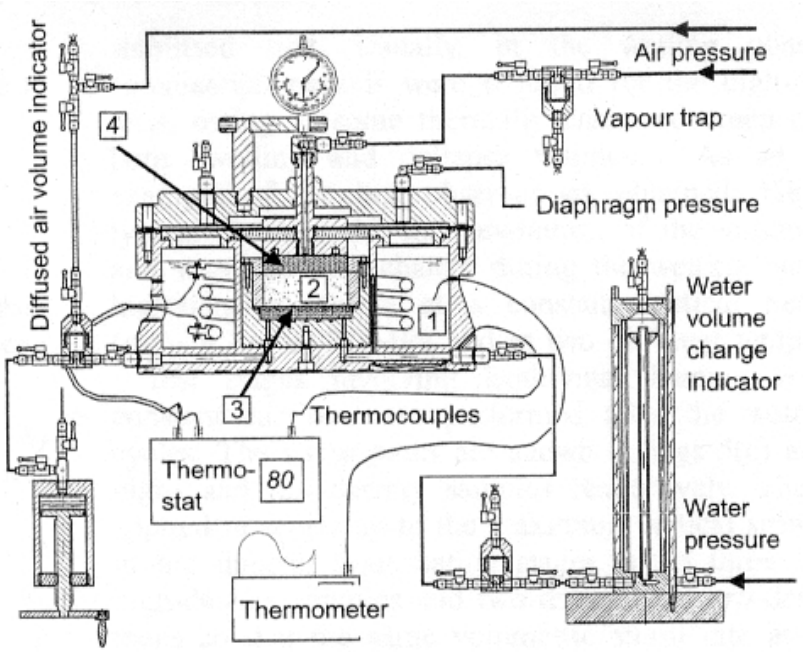

Figure 9.2 Schematic drawing of swelling pressure test using multi-step swelling pressure (Romero et al., 2003)

Two problems (i.e., evaporation fluxes in the top and dissolved air beneath the ceramic disk) occur when using ATT at high temperature. The evaporation flux is solved by installing a vapor trap in the air pressure line to maintain a relative humidity higher than 98.5%. The dissolved air beneath the ceramic disk is solve by installing diffuse air volume indicator incorporated in the water pressure system in order to periodically flush the dissolved air passing through the high air entry value ceramic disk.

In order to apply VET using the same equipment, Romero and Li (2005) change the ceramic disk with the porous stone. The vapor is transferred from the bottom and the top of the specimen through porous stones. The vapor comes from the vessel containing saline aqueous solution that is installed in a heating chamber that maintained the same temperature of the soil. However, the temperature of connection between the chamber and the equipment is not controlled. Consequently, vapor condensate in the certain parts of the vapor transfer lines and should be drained periodically.

9.3 Experimental Techniques and Procedures

9.3.1 Description and Verification of the Equipment Used

The constant volume test performed in this study was conducted using isochoric cell developed at the Universitat Politècnica de Catalunya (UPC), Barcelona, Spain. The cell was used to measure swelling pressure of compacted bentonite and bentonite-sand mixture from

low to high density at room temperature by Villar et al. (2001) and Agus and Schanz (2005a). The cell was modified by installing a flexible wire heater attached to the outer wall of the cell. The heater was controlled using a proportional integral differential (PID) temperature with programmable ramp and soak temperature features. Two small thermocouples were installed in a hole drilled through the top cap of the cell for measuring the temperature of the specimen during experiment. The swelling pressure was measured using a load cell connected to a handled voltmeter.

Prior to use, the deformation of the cell ring and the load cell due to the non-isothermal test conditions were studied and verified so that the effects can be taken into account. Figure 9.3.a and 9.3.b show the zero offset and calibration curve of the load cell as affected by temperature and pressure, respectively. Increasing temperature results in decreasing zero offset of the calibration curve as shown in Figure 9.3.a. However, the intercept of the calibration curves, which was also used for calculating the swelling pressure, does not show significant change.

The coefficient of thermal expansion of the cell used in this study was found about $1.58\text{x}10^{-5}$ /°C, which is close to the coefficient of linear thermal expansion of stainless steel (American Iron and Steel Institute, AISI), $\alpha_r = 1.60\text{x}10^{-5}$ /°C). Small deviation from the value is expected since the non-steel components of the cell also affect the thermal behavior of the cell as a whole. The change in void ratio, Δe, due to the change in radial ring deformation can be calculated using Equation 9.1 (Romero, 1999).

$$\Delta e \approx (1+e_o)\left(\frac{(2\alpha_r - \alpha_s)\Delta T}{1+\alpha_s \Delta T}\right) \tag{9.1}$$

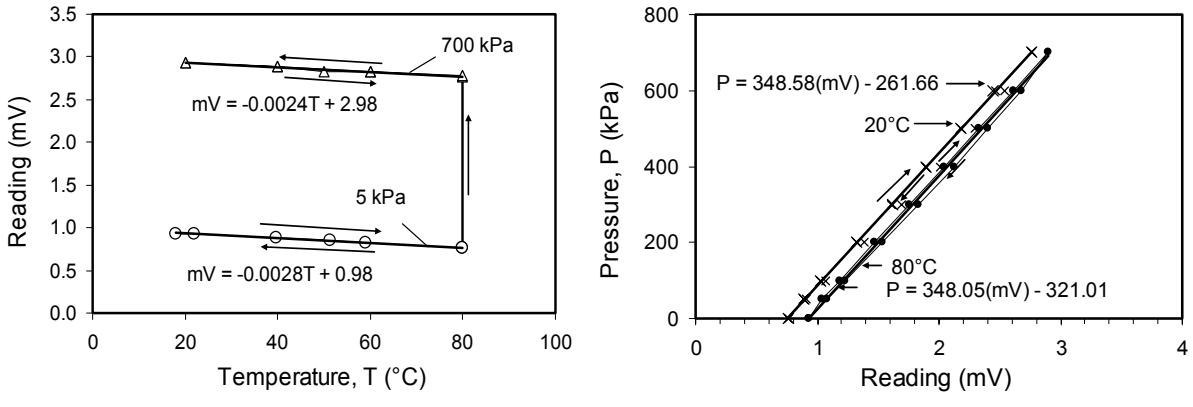

(a) (b)

Figure 9.3 Temperature effects on (a) zero offset the load cell and (b) the calibration curve of the load cell.

where e_o is initial void ratio, α_r is the coefficient of thermal expansion of the ring, α_s is volumetric thermal dilatation of the clay particle ($\alpha_s \approx 2.9 \times 10^{-5}$/°C, Horseman and McEwen, 1996), and ΔT is temperature change (in this study ΔT=60 °C). By inserting all known parameters, Equation 9.1 can be simplified to be the following equation:

$$\Delta e \approx 0.0002\,(1 + e_o) \tag{9.2}$$

The change in the dry density of the specimen tested due to the change in void ratio can be computed using Equation 9.3, which is derived from substituting Equation 2 to the first derivative of the relationship between dry density and void ratio.

$$\Delta \rho_d \approx -0.0002 \rho_d \tag{9.3}$$

where $\Delta\rho_d$ is dry density change in Mg/m^3, and ρ_d is initial dry density of specimen. Although the swelling pressure result is an exponential function of dry density of specimen (Villar and Lloret, 2004; Agus and Schanz, 2005a), it is clear that the swelling pressure change due to thermal deformation of the ring and thermal dilatation of the clay particles is not significant provided that corrections are applied to the specimen's dry density.

9.3.2 One Step Constant Volume Swelling Pressure Test

Figure 9.4 shows the schematic diagram of the one-step swelling pressure test. In this test, the cell was connected to a water column filled with distilled water. A flexible wire temperature-controlled heater was also installed in the water column to monitor the temperature of the water used in the permeation.

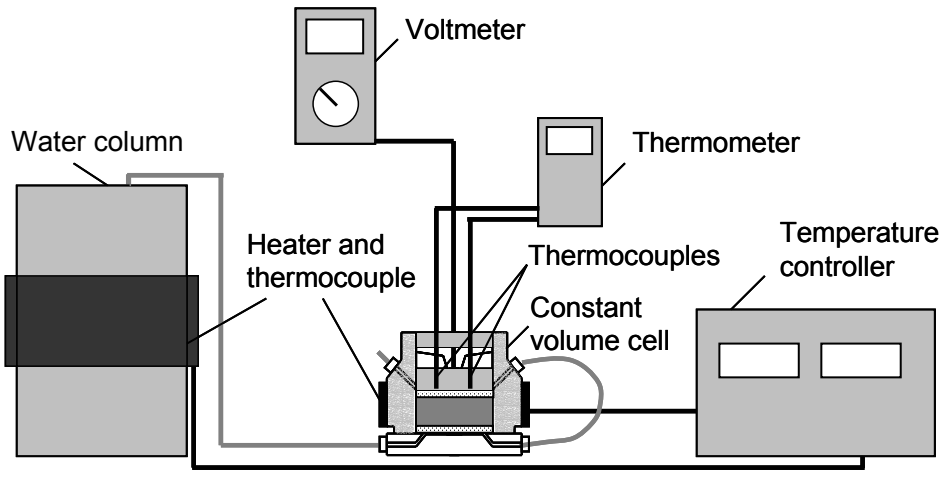

Figure 9.4 Schematic drawing of the one-step swelling pressure test

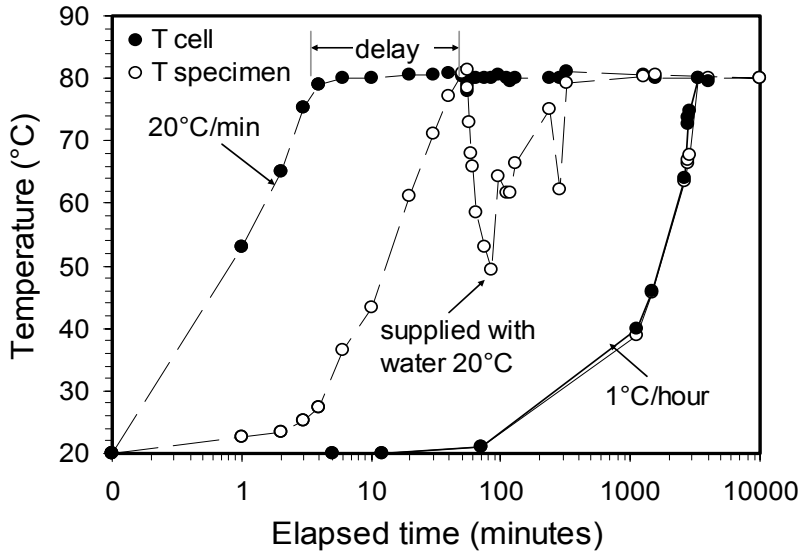

Figure 9.5 Investigation of the rate of temperature and supplied water to the specimen temperature

The test was commenced by placing the specimen (i.e., compacted bentonite (Calcigel) and bentonite-sand mixture) in the cell. The initial conditions of the specimens summarizes in Table 9.1. The temperature of specimen was elevated by heating the cell using the temperature-controlled heater. The temperature increment should be slow enough to avoid temperature difference between the cell and the specimen. Rapid temperature increment results in decreasing the relative humidity of the air space which is existed in the cell (e.g. porous disks) due to increase its saturation water vapor (Agus and Schanz, 2006a). Some amount of water from the specimen will evaporate to balance this condition. Trial tests had been done to determine the appropriate rate of temperature increase. Figure 9.5 shows the temperature difference between the cell and the specimen at different rate of temperature increase. For rapid temperature increase (i.e., 20 °C/min) as shown in dashed line, the specimen temperature reached 80 °C several minutes after the cell temperature had reached 80 °C. From the trial tests performed, it is found that the appropriate rate of temperature increase is 0.016 °C/min (or 1 °C/hour) where the temperature of the cell and the specimen reached 80 °C at the same time.

Table 9.1 Specimen conditions of one-step swelling pressure test

Specimen	Water content (%)	Dry density (Mg/m^3)	Specimen	Water content (%)	Dry density (Mg/m^3)
100B-1	9	1.43	50B/50S HC	9	2.00
100B-2	9	1.26	50B/50B-2	17	1.77
100B-3	9	1.05	50B/50B-3	20	1.66
			50B/50B-4	25	1.49

After the temperature of both the cell and the specimen had reached 80 °C, warmed distilled-deaired water was circulated through the bottom and the top boundaries of specimen. Warmed water was used in this study with a reason that the use of fresh water decreases the temperature of the specimen as also shown in Figure 9.5. The decrease in the water temperature due to heat release in the water circulation line was anticipated by increasing the water temperature in the water supply column up to 86 °C. During test, the swelling pressure of the specimen was measured using the handled voltmeter. The equilibrium was reached after the swelling pressure readings stabilized for a significant period of time.

9.3.3 Multi-Step Swelling Pressure Test Using Axis-Translation Technique

The axis-translation technique (ATT) was used to investigate the change in swelling pressure with decreasing matric suction. For this purpose, the pedestal with a high air-entry ceramic disk (i.e., AEV of 1500 kPa) and coefficient of permeability of 1.12×10^{-10} m/s was used. Figure 9.6 shows schematic drawing of the multi-step swelling pressure test using ATT. The bottom water inlet of the isochoric cell was connected to burette at a constant height of 50 cm to the bottom water outlet. Therefore, a constant water pressure of 5 kPa was maintained throughout the experiment. The bottom water outlet is connected to a two-way valve for flushing purpose. In this test, the water supply had temperature of 20 °C because the water was not in contact directly to the specimen. The 5 kPa constant water pressure was used to flush the water compartment. Air pressure was applied using an air pressure controller (i.e., a stepper motor) that could deliver a constant air pressure with 1 kPa accuracy. To prevent high evaporation occured in the top surface of the specimen, the air pressure was connected to a vapor column to reduce the relative humidity of the main air pressure supply. The vapor

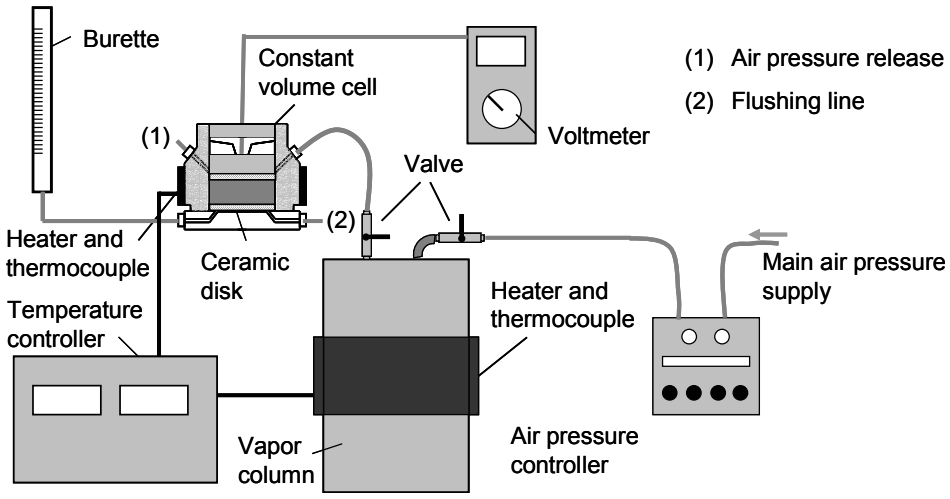

Figure 9.6 Schematic drawing of the multi-step swelling pressure test using ATT

column has the same temperature applied to the isochoric cell. The temperature of the isochoric cell and the column was controlled by temperature controller.

The heavily compacted 50B/50S specimens were tested using ATT. The test was started by placing the specimen in the isochoric cell. After the cell was assembled completely, the temperature of the cell was directly increased with temperature increment of 20 °C/menit. The temperature increment applied was higher than that used in the one step swelling pressure test because the specimen swells immediately after in contact with saturated ceramic disk. Air pressure was applied to the specimen through the air pressure inlet. Flushing was performed regularly to remove air bubbles that were collected in the water compartment as a result of air diffusion through the soil specimen and the saturated ceramic disk. Condensed vapor which was raised in the air pressure tube close to the cell was flushed by closing the valve in the vapor column and opening the air pressure release. The measurement of swelling pressure was performed according to the procedures similar to those adopted in the one-step swelling pressure test. The test reached equilibrium when the swelling pressure reading shows constant value. Water content of each specimen after the test was measured by weighing the cell after the test and the amount of absorbed water was back-calculated.

9.3.4 Multi-Step Swelling Pressure Test Using Vapor Equilibrium Technique

Figure 9.7 shows the schematic drawing of the multi-step swelling pressure test. Vapor equilibrium technique (VET) was used in this test whereby the total suction of the specimen was reduced by increasing the relative humidity of the vapor in the specimen's pore space.

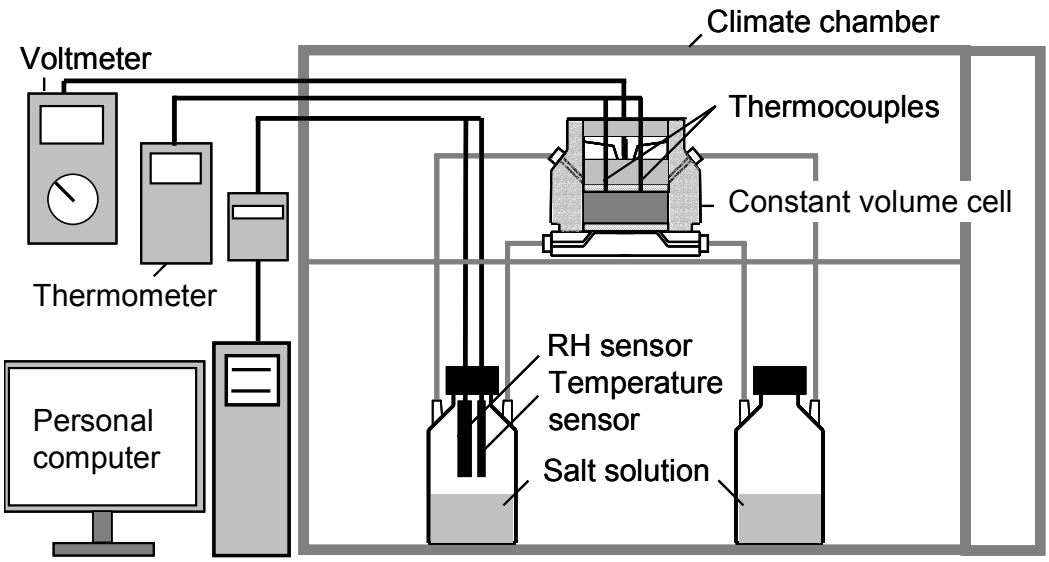

Figure 9.7 Schematic drawing of the multi-step swelling pressure test using VET

In this test, the heavily compacted 50B/50S specimens were tested following the multi-step swelling pressure test method. After the specimen had been placed in the cell and the arrangement shown in Figure 9.7 had been set up, the temperature of the chamber was gradually increased at a rate of 0.01 °C/min which was much lower than the rate used in the one-step swelling pressure test for anticipating temperature gradient between the specimen, the cell and the salt solution. The molal and saturated sodium chloride solutions were used to induce relative humidity to the specimen. The use of molal and saturated sodium chloride solutions for controlling suction (or relative humidity) at room temperature and moderately high temperature (i.e., 80 °C) was verified and discussed in Chapter 8. It was found that the technique is applicable provided that the temperature gradient in the system is minimized. The swelling pressure development, specimen temperature, and relative humidity and temperature of salt solution were periodically recorded.

The multi-step swelling pressure test in this study was performed in a climate chamber that could control temperature to ±0.1 °C. The cell was connected to two Erlenmeyer flasks filled with salt solution. A relative humidity and temperature sensor were installed to one of the Erlenmeyer flasks to monitor the relative humidity of the water vapor above the salt solution in the flask that was used to induce relative humidity to the specimen. The sensor (together with a temperature sensor) was connected to a digital data display connectable to a personal computer. The sensor used has an excellent performance not only at room temperature but also at moderately high temperature (Agus and Schanz, 2005b).

9.3.5 Swelling Potential Test at Moderately High Temperature

The swelling potential test was performed using UPC oedometer device that was developed by the Universitat Politècnica de Catalunya (UPC), Barcelona, Spain. In this study, the equipment was modified by installing the flexible heater and thermocouple which were connected to a temperature controller. To avoid the heat release from the heater to atmosphere, the surface of the oedometer was covered with insulator made from fiberglass and aluminium foil. Figure 9.8 shows photograph of the experimental setup used to measure the swelling potential of heavily compacted specimen.

The test was commenced by placing the heavily compacted specimen in the oedometer. Air pressure of 50 kPa was applied to the specimen in order to apply vertical pressure after the equipment and heating system were assembled. After applying seating load was performed, the temperature of oedometer was increased from room temperature to 80 °C

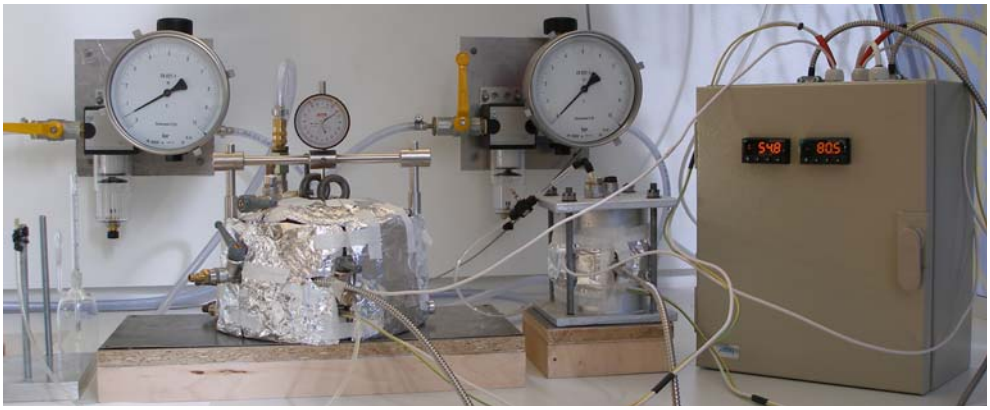

Figure 9.8 Experimental setup used to measure the swelling potential for the heavily compacted specimen.

with slow rate (i.e., 1 °C/hour). The hot water (i.e., 86 °C) was supplied to the specimen through the porous stones in the top and bottom boundaries. After reaching equilibrium at 80°C, the temperature of the equipment was reduced back to the room temperature. The swelling was recorded from the dial gauge. Considering existing data obtained using the same equipment at room temperature reported by Agus (2005) (i.e., swell under vertical loads of 50 and 100 kPa), the two vertical pressures were also applied in this study.

9.4 Results and Discussions

9.4.1 One Step Swelling Pressure Test

Figure 9.9.a and 9.9.b show swelling pressure development versus elapsed time plotted in semi-logarithmic scale performed with one-step swelling pressure test for 100B and 50B/50S specimens, respectively. The swelling pressure recorded after distilled water supply show increase rapidly at earlier stage of the test for both specimens. Generally, after the swelling pressure maximum was reached (i.e., after about 100 hours duration), the swelling pressure of the 100B specimen slightly decreased possibly due to meta-stable structure of the compacted pure bentonite at low water content, whereas the swelling pressure of the 50B/50S specimen remained constant.

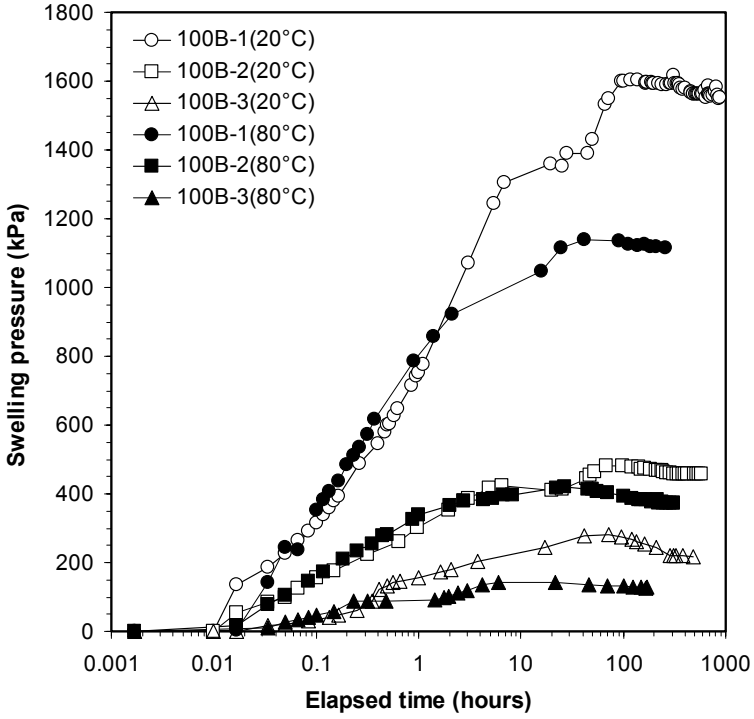

(a)

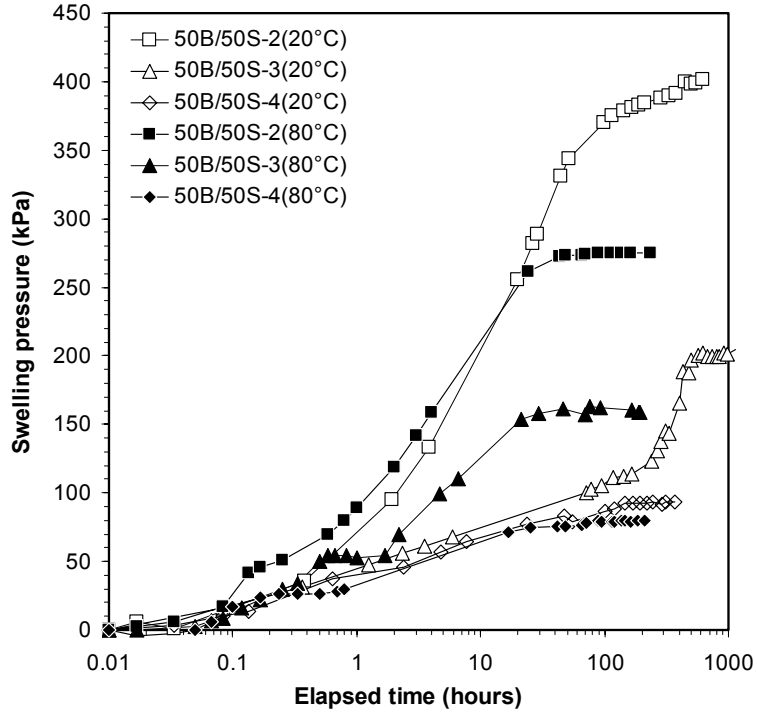

(b)

Figure 9.9 Development of swelling pressure as a function of time for (a) 100B specimens and (b) 50B/50S specimens performed using one-step swelling pressure method (the initial conditions of the specimens shown in Table 9.1)

As shown in Figure 9.9, the swelling pressure development of the specimens tested at 80 °C was more rapid than that of the specimens tested at 20 °C. Agus and Schanz (2005a) found that the rate of swelling pressure development is a function of the initial total suction of the compacted specimen tested. However, the increase in temperature causes decrease in total

suction in compacted bentonite (Villar and Loret, 2004, Romero et al., 2000). The faster of swelling pressure development rate of specimen tested at 80 °C is due to decrease in water viscosity. Decrease in water viscosity speeds up the hydration rate at higher temperature (Pusch and Yong, 2003).

Figure 9.9 also shows that the magnitude of swelling pressure of the specimens tested at 80°C was smaller than that of the specimens tested at 20 °C. The result agrees well with the results reported by Pusch et al. (1990), Villar and Lloret (2004), and Lingnau et al. (1996). According to Pusch et al. (1990), the effects of temperature on the swelling pressure depend on the net of two opposite effects (i.e., the increase in osmotic pressure and the decrease in hydration force). Considering the main cation in the soil pore-water which is responsible in the osmotic suction development is Ca^{2+} (Chapter 7), increase in temperature results in slightly decreasing in the osmotic suction of the specimen due to decrease in suction of $CaCl_2$ solution (Figure 3.1.b). However, since the osmotic suction of Calcigel is found very small (i.e., 50 kPa) (Chapter 7) and less than 1000 kPa, the change in temperature does not influence the osmotic suction of the specimen. The osmotic suction component does not influence the swelling pressure value of the compacted Calcigel as discussed in Section 7.5.3. In addition, since the final conditions of the specimens were in saturated or close to satured conditions, diffuse double layer might be developed to give contribution to the swelling pressure. Temperature increase results in increasing swelling pressure of compacted bentonite as discussed in Section 3.2.4. Therefore, decrease in swelling pressure is considerably due to the net of two opposite effects (i.e., the decrease in hydration force of the soil and the increase in diffuse double layer effects). The reduction in capillary component due to decrease in surface tension of the specimen is considerably very small or neglected because in one-step swelling pressure test the final condition of the specimens are in saturated or close to saturated condition.

Figure 9.10 shows the development of swelling pressure at 80 °C followed by cooling to the room temperature (i.e., ±20 °C) for the test at 80 °C. As shown in the figure, the decrease in swelling pressure due to increase in temperature is reversible. The swelling pressure of the specimen tested increased and reached an equilibrium value which is very close to the swelling pressure performed at 20 °C. Therefore, transformation of smectite to non-expandable illite layers due to temperature increase is not evident in the range of temperature and time duration considered in this study.

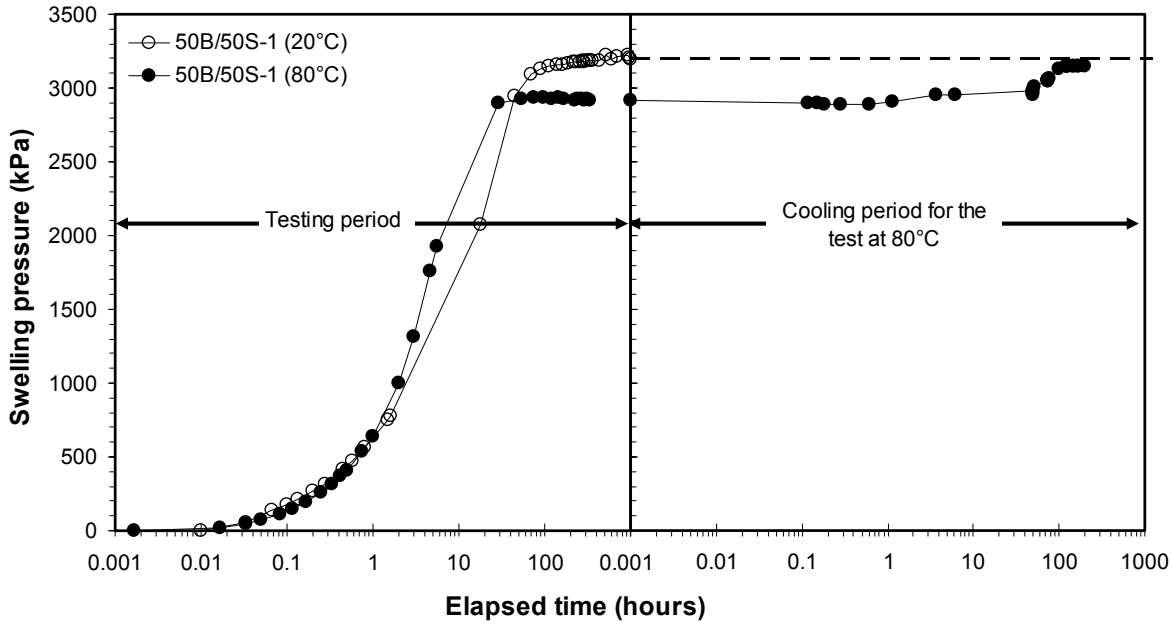

Figure 9.10 Development of swelling pressure of heavily compacted bentonite-sand mixture after tested at 80 °C

Figure 9.11.a shows the swelling pressure of the 100B and 50B/50S specimens plotted against the mixture dry density. As expected and supported by other's findings such as Komine and Ogata (2003), Villar and Lloret (2004), and Agus and Schanz (2005a), the swelling pressure of the specimens shows exponential function against mixture dry density. As depicted in the figure, the curve of swelling pressures obtained for the specimens tested at 80 °C is located below the curve of swelling pressure obtained for the specimens tested at 20°C. The reduction of swelling pressure due to increase in temperature of pure bentonite specimens appears to be higher than that of the 50B/50S specimens. Agus and Schanz (2005a) reported that the swelling pressure of compacted bentonite-sand mixtures with different bentonite contents is a function of bentonite dry density. The bentonite dry density ($\rho_d^{bentonite}$) is computed using Equation 9.4 by assuming that the soil void in the compacted bentonite-sand mixtures only belongs to the bentonite (Komine and Ogata, 2003).

$$\rho_d^{bentonite} = \frac{r_{bs}\rho_d}{(1+r_{bs}) - (\rho_d / G_s^{sand})} \tag{9.4}$$

where r_{bs} is the bentonite-sand mass ratio, ρ_d is mixture dry density in Mg/m^3, and G_s^{sand} is the specific gravity of sand.

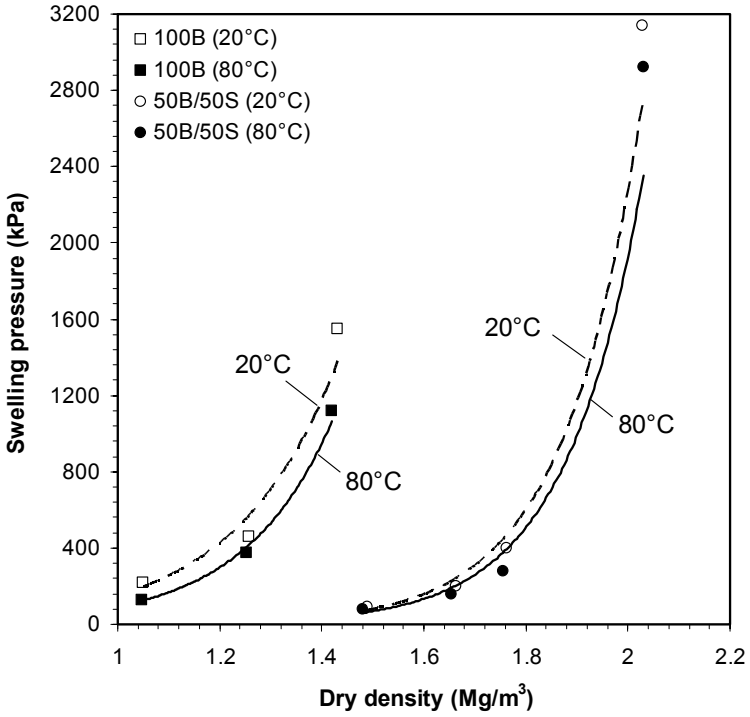

(a)

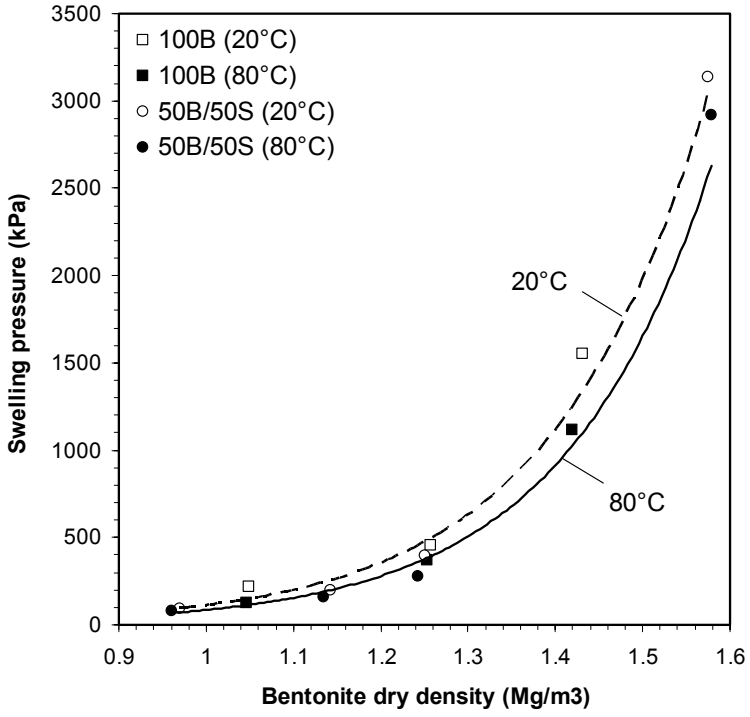

(b)

Figure 9.11 (a) Swelling pressure as a function of dry density, and (b) swelling pressure as a function of bentonite dry density.

Figure 9.11.b shows the relationship between swelling pressure and bentonite dry density for the compacted bentonite and compacted bentonite-sand mixtures. Allowing slight scatters in the data, the curve of swelling pressure for the 50B/50S specimens tested at 80 °C coincides with that for the pure bentonite specimens. It indicates that at 80 °C the swelling

pressure of bentonite-sand mixtures also shows similar trend as the swelling pressure curve obtained at 20 °C. The increase in temperature only affects the magnitude of the swelling pressure which represents the effects of temperature on the bentonite mineral in the mixture. Therefore, the presence of sand in the mixture is expected to give benefit in increasing the dry density of the specimen but the change in swelling pressure due to elevated temperature is considerably the same as compacted pure bentonite at the same bentonite dry density. Or, at the same dry density, the change in swelling pressure due to the change in temperature of compacted pure bentonite is higher than that of bentonite-sand mixture since bentonite-sand mixture has lower bentonite dry density.

9.4.2 Multi-step Swelling Pressure Tests

Figure 9.12 shows the swelling pressure developments of as-prepared heavily compacted bentonite-sand mixture performed using VET at 80 °C under total suction of 2484 and 11300 kPa. The figure also shows the evolution of the total suction applied calculated from the measured relative humidity. The good performance of the testing system is indicated by the constant relative humidity or total suction throughout the test as shown in the figure.

As depicted in Figure 9.12, the swelling pressure tested using VET shows slow development at earlier stage of test. The swelling pressure increased rapidly after 50 hours and reached equilibrium after 200 hours. Ignoring the magnitude of the swelling pressure, the results indicate a delay when compared with the development of swelling pressure when the

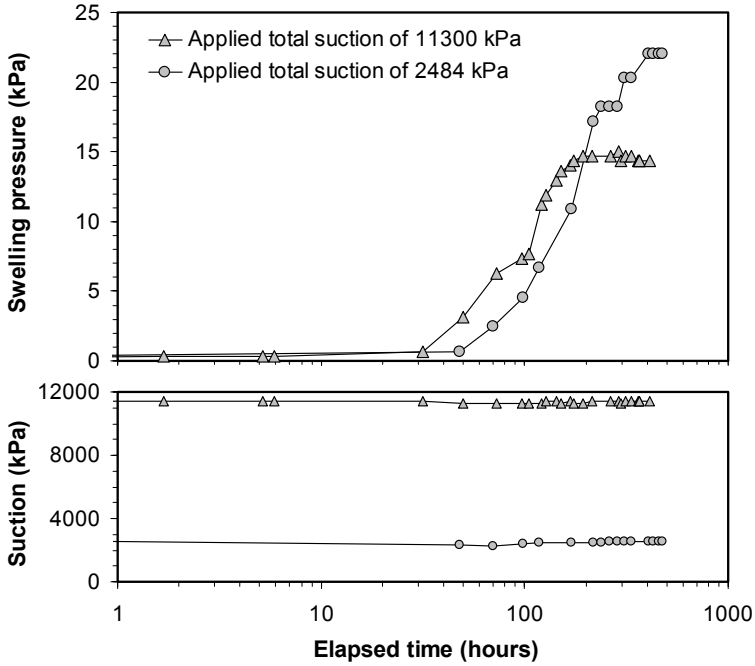

Figure 9.12 Swelling pressure development from the multi-step swelling pressure test using vapor equilibrium technique for heavily compacted 50B/50S specimens

specimens were tested using water in its liquid phase (i.e., in the one-step swelling pressure test). The delay was probably caused by the retarding transport mechanism of water molecules in the vapor form which occurs when using VET in the test. The water molecules first migrate into the open voids in the specimen and are subsequently adsorbed when in contact with the exposed surfaces of clay clusters (Pusch, 2001; Pusch and Yong, 2003). A water potential gradient (suction) that exists between the inter-aggregate and intra-aggregate pore-water and the mixture permeability at micro and macro scales control the mechanism of water movement from the exposed surface of the clay clusters to the intra-particle pores (Agus and Schanz, 2006b). These postulations also seem to be true at an elevated temperature of 80 °C as indicated by the results presented herein.

Figure 9.13 shows the swelling pressure development of heavily compacted bentonite-sand mixture tested using axis-translation technique (ATT) at 80 °C under matric suction of 50 and 100 kPa. As shown in Figure 9.13, the swelling pressure of specimens tested using ATT are developed in the first hour of the test. The specimens reached equilibrium after 800 hours. Compared to the development of swelling pressure performed using VET (Figure 9.12), the swelling pressure development using ATT is faster. This is due to the fact that the specimen tested using ATT is directly in contact with water. The water flows in liquid phase from the burette to the specimen through the ceramic disk placed in the bottom of the specimen. However, the development of swelling pressure using ATT is slower than that of

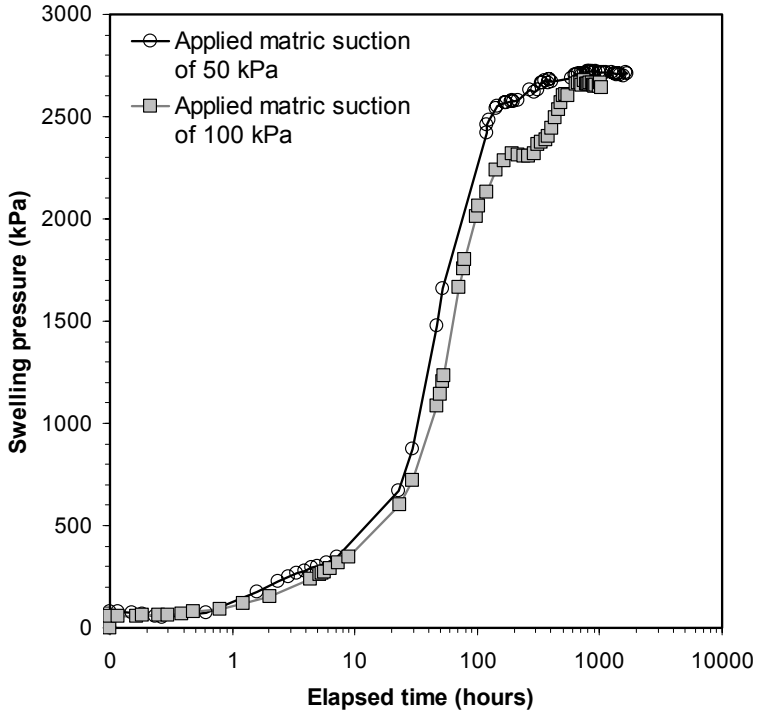

Figure 9.13 Swelling pressure development from the multi-step swelling pressure test using axis-translation technique for heavily compacted 50B/50S specimens

specimen tested using one-step swelling pressure test as shown in Figure 9.10. In the one-step swelling pressure test, the water flows from the water compartment to the specimen through porous stone placed in the top and in the bottom of the specimen whereas, in the ATT, the water flows only from the bottom of the specimen. Moreover, the permeability of the ceramic disk that is placed in the bottom pedestal of the isochoric cell in ATT is very small (i.e., 1.12×10^{-10} m/s). This influences the swelling pressure development of the specimen as shown in Figure 9.13 that the swelling pressure development seems to reach constant swelling pressure after 150 hours, increases again after 300 hours, and reachs equilibrium after 600 hours. Since after 150 hour the specimen reached more than 80% maximum swelling pressure, the decrease in suction gradient between the specimen and water was possible to cause the rate of swelling pressure development decrease. As shown in Figure 9.13, these phenomena happen for both specimens.

Figure 9.14 shows the development of swelling pressure with decreasing suction for the heavily compacted 50B/50S specimens performed in this study. The data of the swelling pressure development obtained for the same material tested at room temperature (i.e., ±20 °C) and reported by Agus (2005) using the two different methods (i.e., ATT and VET) are also plotted for comparison. As shown in Figure 9.14, the difference between the swelling pressure performed at room temperature and the swelling pressure performed at 80 °C using VET

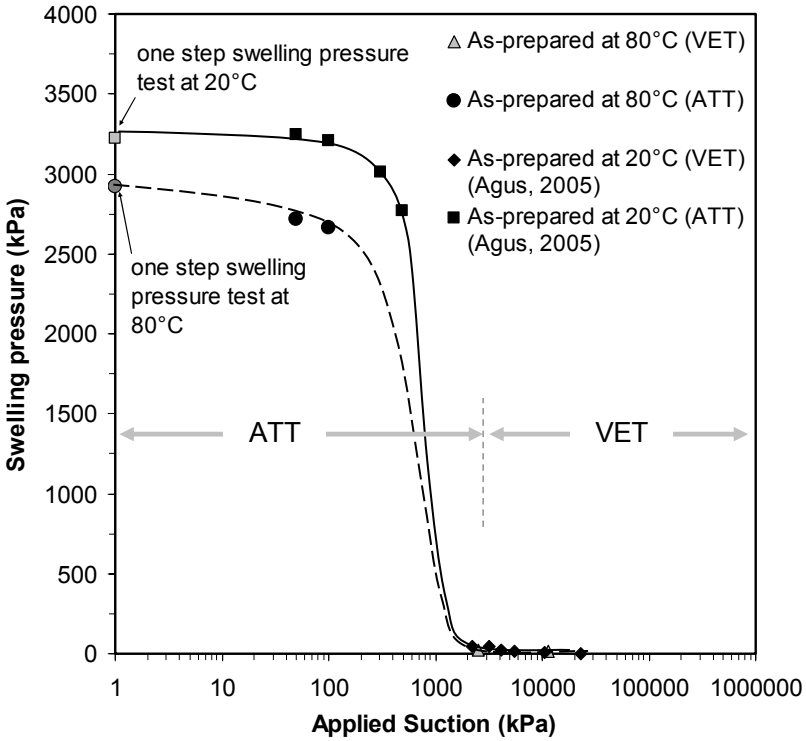

Figure 9.14 Swelling pressure versus suction following wetting obtained using the multi-step swelling pressure test for heavily compacted 50B/50S specimens

appears unclear since the development of swelling pressure is insignificant up to a suction of about 2000 kPa. Agus (2005) states that the insignificant swelling pressure development might be due to a delayed 'true' equilibrium in the specimen by considering the water movement mechanism. But this might also happen because the corresponding water content of the specimens at the suction range applicable in this method is close to the shrinkage limit of the specimen as reported by Agus and Schanz (2006c) (i.e., 9.8% correspond to total suction of 3000 kPa). This condition also appears in the void ratio versus suction relationship for the same material following wetting-drying in unconfined condition as shown in Figure 8.35 (i.e., specimen of UC-HC-4). As shown in Figure 8.35, the increase in water content with decreasing suction at the range of suction used in VET (i.e., from 22700-2000 kPa) does not result in significant change in the void ratio of the specimen. As a result, when the specimen is hydrated, the pressure required to keep the void ratio constant (or swelling pressure) is also low.

The difference between swelling pressure performed at 20 °C and swelling pressure performed at 80 °C using ATT appears obvious that the swelling pressure of specimen at 80°C is less than the swelling pressure at 20 °C. This agrees well with previous finding using one-step swelling pressure test as shown in Figure 9.11.

Figures 9.15 and 9.16 show the relationship between water content versus suction and

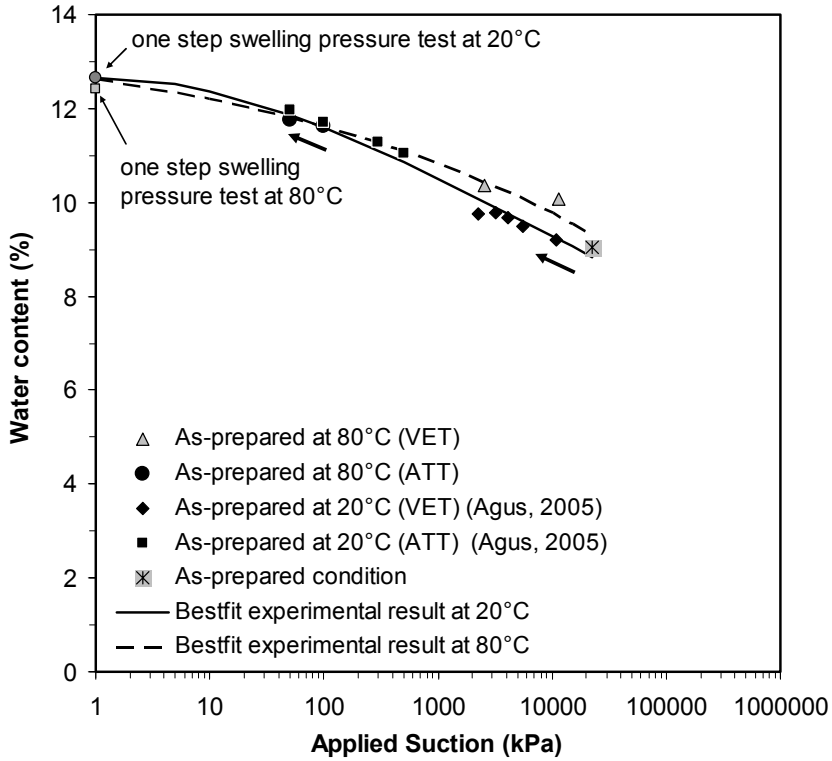

Figure 9.15 Temperature effects on water content versus suction of heavily compacted 50B/50S specimens following wetting under constant volume condition

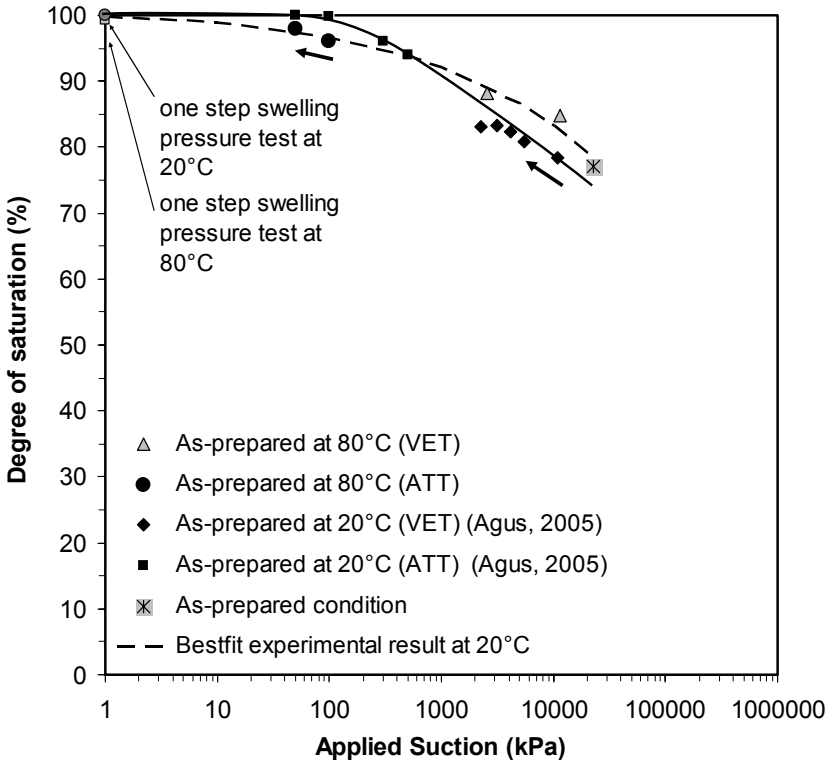

Figure 9.16 Temperature effects on degree of saturation versus suction of heavily compacted 50B/50S specimen following wetting under constant volume condition

degree of saturation versus suction of the specimen at two different temperatures, respectively. The data at 80 °C were obtained in this study whereas the data at 20 °C were obtained by Agus (2005). As shown in Figure 9.15, the water content of specimen at suction higher than 2000 kPa (i.e., performed using VET) at 80 °C is higher than that of specimen at 20 °C. This is not consistent with previous finding discussed in Chapter 6 and 8 that the ability of specimen to absorb water at elevated temperature (i.e., 80 °C) is lower than that of specimen at room temperature (i.e., 20 °C). This might be influenced by the temperature fluctuation in the climate chamber where the VET at 80 °C performed is 0.1 °C which is smaller than room temperature fluctuation (i.e., 0.5 °C (Agus, 2005)). The temperature fluctuation influences the accuracy of the suction which is applied to the specimen. However, at suction less than 2000 kPa where the suction was applied using ATT, the water content of specimen at 80 °C is less than that of specimen at 20 °C. This agrees well with previous finding obtained in this study.

Similar to the water content versus suction as shown in Figure 9.15, the degree of saturation of specimen at 80 °C for suction higher than 2000 kPa is higher than that of specimen at 20 °C as shown in Figure 9.16. For suction less than 2000 kPa, the degree of saturation of the specimen at 80 °C is lower than that of specimen at 20 °C. These is related to the relationship between water content versus suction relationship. Since the test was

performed at constant volume condition or constant void ratio and the water content of specimens tested at 80 °C for suction higher than 2000 kPa is higher than that of specimens tested at 20 °C, the degree of saturation for specimens tested at 80 °C is also higher than that of specimens tested at 20 °C. Conversely, for suction less than 2000 kPa, the degree of saturation of specimens tested at 80 °C is less than that of specimens tested at 20 °C since the water content of specimens tested at 80 °C is less than that of specimens tested at 20 °C.

Figure 9.17 shows the swelling pressure of heavily compacted 50/50 bentonite-sand mixture as a function of suction performed using one step swelling pressure test. Figure 9.17.a shows the initial conditions of specimens used in this study for swelling pressure test at 80 °C and specimens used by Agus (2005) for swelling pressure testing at 20 °C. In the wetting process, the as-prepared specimens were equilibrated to different suction values (i.e., 700, 300, and 70 kPa). In the drying process, the as-prepared specimen was placed in the oven at

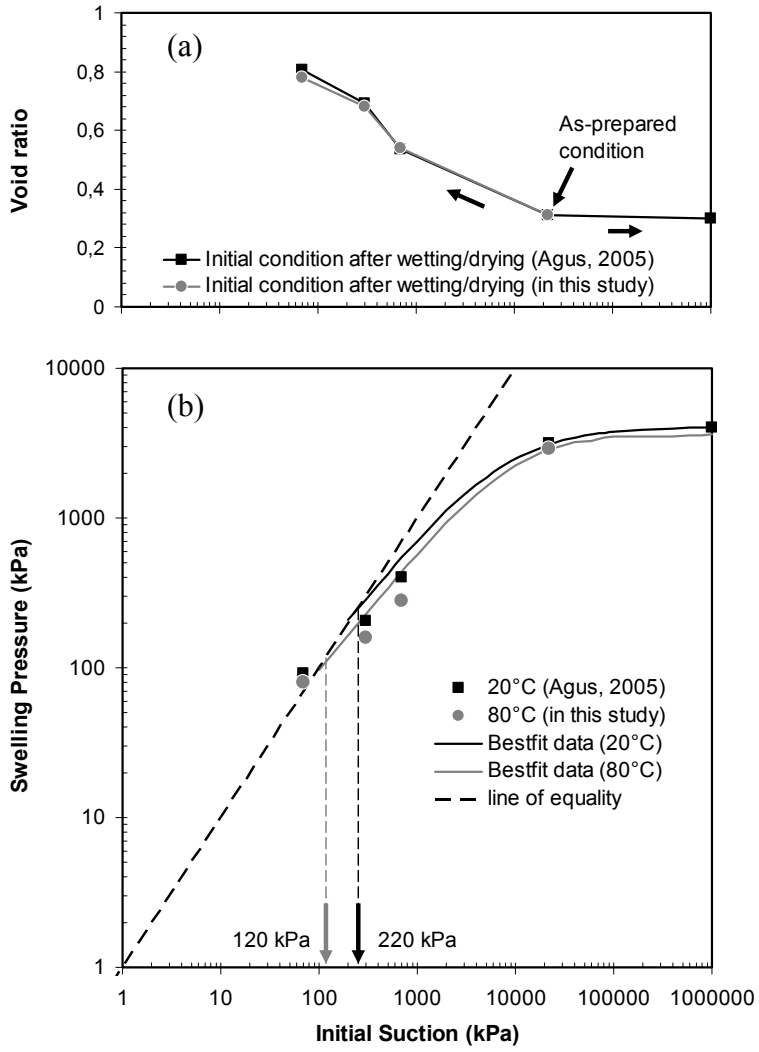

Figure 9.17 Effects of initial suction on the swelling pressure of heavily compacted 50B/50S specimen at room and elevated temperature

temperature of 100 °C for 24 hours to obtain the initial total suction of 1000000 kPa. As shown in Figure 9.17.a, the initial conditions of specimens tested at 20 and at 80 °C are comparable.

Figure 9.17 shows that the initial suction of the specimen does not influence significantly the swelling pressure of the specimen for the specimen having suction higher than as-prepared specimen (or drying process). This is due to the fact that the swelling pressure is influenced by the initial void ratio (or dry density) of the specimen (e.g., Komine and Ogata, 2003; Agus and Schanz, 2005a) and the initial void ratio of the specimen is not changed significantly at suction of 1000000 kPa. This is different from specimen experienced wetting process that the void ratio of the specimens increases resulting decrease in swelling pressure of the specimens obtained. As shown in Figure 9.17, the swelling pressure of the specimens at 80 °C is smaller than that of the specimens at 20 °C. This supports the previous finding in this study. Figure 9.17 also shows that the suction value at which the swelling pressure is the same as its initial suction at 80 °C (i.e., 120 kPa) is less than that of the specimen at 20 °C (i.e., 220 kPa).

Figure 9.18 shows a three-dimensional plot of swelling pressure test performed at 80°C in present study which are presented in Figures 9.14 and 9.17 and at 20 °C reported by Agus (2005) and. In this study, the plot is used to show the effect of temperature to the swelling pressure of the specimen which is measured using constant volume condition for both one-step and multi-step swelling pressure methods. As shown in Figure 9.18, the paths of constant volume swelling pressure at 80 °C lie under the paths of constant volume swelling pressure at 20 °C.

9.4.3 Swelling Potential of Heavily Compacted Bentonite-Sand Mixture

Figure 9.19 shows swelling potential of heavily compacted 50/50 bentonite-sand mixture shown as swelling strain versus time performed at 20 °C by Agus (2005) and in this study at 80 °C under seating load of 50 kPa (Figure 9.19.a) and 100 kPa (Figure 9.19.b). As shown in Figure 9.19.a and 9.19.b, the swelling strain of specimens at 80 °C is less than that of specimens at 20 °C. The figures also show that the rate of swelling strain development by time at 80 °C is faster than that of at 20 °C. This results are similar to the previous results (i.e., swelling pressure) that increase in temperature results in decreasing the hydration force and, thus, decrease in the swelling strain of the specimen. the rate of swelling development at 80°C is more rapid than that at 20 °C due to decrease in water viscosity at 80 °C.

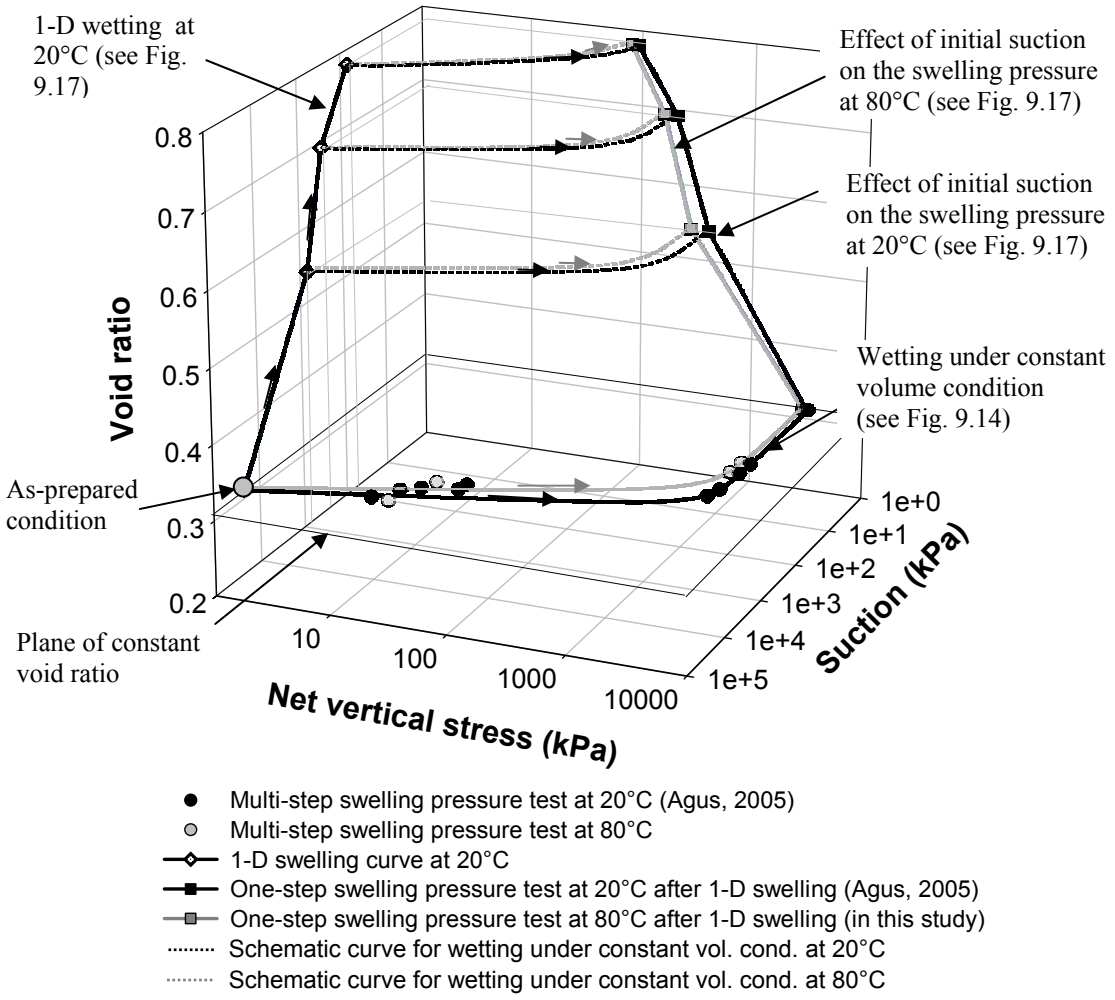

Figure 9.18 Three-dimensional visualization of temperature effects on the swelling pressure of heavily compacted 50B/50S bentonite-sand mixture

Figure 9.19 also shows that the swelling strain of the specimens after cooling to 20 °C is less than the swelling potential of the specimen performed at 20 °C. This is different from swelling under constant volume condition that swelling pressure of the specimen performed at 80 °C increased due to decrease in temperature and reached an equilibrium value which is very close to the swelling pressure performed at 20 °C. The swelling under constant volume condition results in swelling pressure of 3200 kPa. It means that the specimen is hydrated under load of 3200 kPa which is more than the loads applied in the swelling potential test (i.e., 50 and 100 kPa). The result shows that the effect of heating on swelling capacity increases by decreasing the confining stress. This is due to the process (i.e., water transfer phenomena from elementary layer to external water) that reduces the swelling capacity at high temperature is hindered when the volume change is obstructed. The result agrees with previous finding by Pusch et al. (1990) and Villar and Lloret (2004).

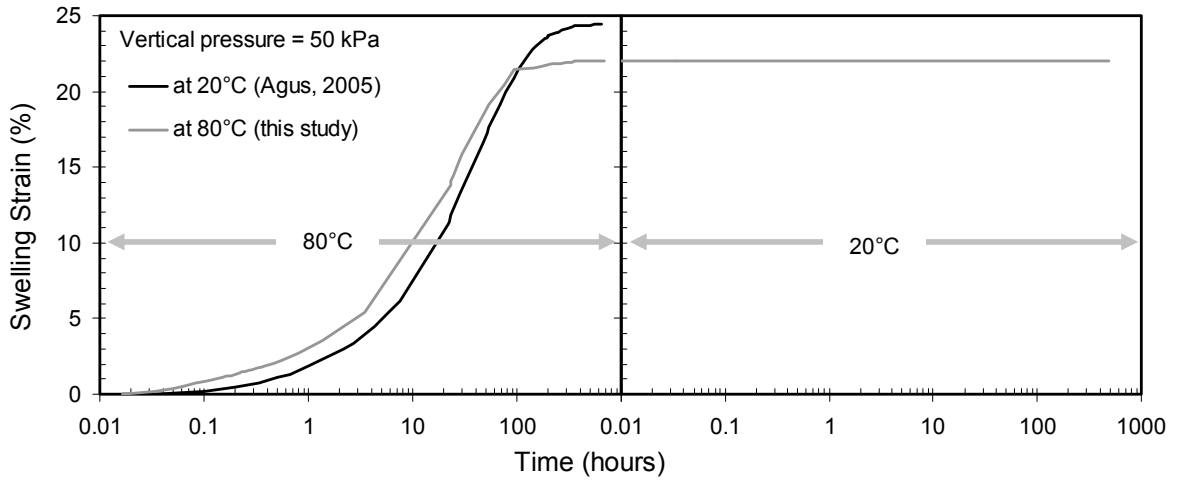

(a)

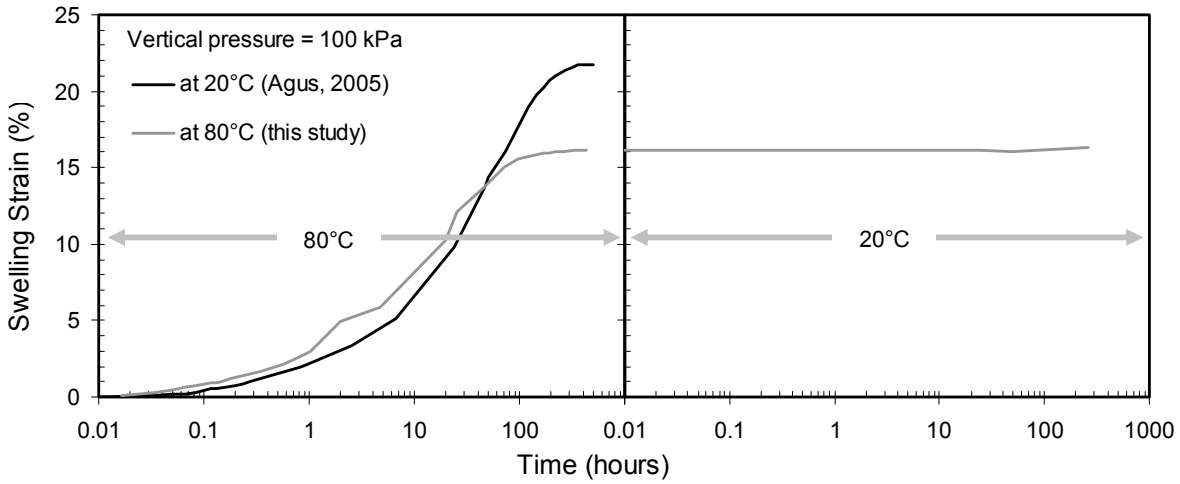

(b)

Figure 9.19 Swelling under load of heavily compacted 50/50 bentonite-sand mixture at 20 °C and 80 °C (a) vertical pressure of 50 kPa and (b) vertical pressure of 100 kPa.

9.5 Summary

The following conclusions can be drawn based on the results of the temperature and suction controlled swelling pressure test of compacted bentonite and bentonite-sand mixture.

1. The increase in temperature results in reduction in swelling pressure. The reduction of swelling pressure found in this study is reversible.
2. The swelling pressure of compacted bentonite-sand mixture is a function of bentonite dry density not only at room temperature but also at elevated temperature.
3. The transport mechanism of water molecules controlled the development of swelling pressure and wetting characteristics (i.e., water content and degree of saturation versus

suction relationships) of the heavily compacted bentonite-sand mixture specimens not only at 20 °C but also at 80 °C.

4. Three-dimensional view of temperature effect on the swelling pressure shows that the paths of swelling pressure at 80 °C is placed under the paths of swelling pressure at 20 °C.
5. Temperature increase results in decreasing the swelling strain of heavily compacted bentonite-sand mixture.

This page intentionally left blank

CHAPTER 10

CONCLUSIONS AND RECOMMENDATIONS

10.1 Conclusions

An experimental study on the temperature effects on the hydro-mechanical behavior of compacted bentonite and bentonite-sand mixtures has been presented. Based on the analysis of the experimental data presented in Chapter 5 to Chapter 9, the following conclusions can be drawn.

10.1.1 Micro-structure and Fabric Studies

1. The Pore size distribution (PSD) of specimens tested in this study show bimodal characteristics in spite of their different compaction conditions. For 100B mixture, at the same void ratio, the specimen compacted DOP has a greater volume of macro-pores compared to the specimen compacted WOP. The 50B/50S mixture specimens do not show the same phenomenon. The volumes of macro-pores are the same for both the DOP and WOP specimens.
2. New pore population (i.e., pores between clay aggregate and sand surface) is developed in the PSD of compacted bentonite-sand mixture.
3. The non-intruded pores exist in all specimen tested in this study and mainly affected by water content.
4. The limits of macro- and micro-pores are almost the same for specimens tested in this study and those of compacted bentonite and bentonite-sand mixtures obtained from literature.
5. The aggregation is clearly shown in the fabric of specimen compacted at 100B DOP condition.
6. Wavy flake-like structure is shown not only in the specimen compacted at WOP condition but also in the specimen compacted at DOP condition.

10.1.2 Temperature effects on suction characteristic curves

1. No influence of compaction condition (or dry density) on the total suction is observed. Total suction of the bentonite-sand mixtures is a function of mixture water content and mixture bentonite content or collectively a function of bentonite water content. These are valid not only at room temperature but also at elevated temperature.
2. At a constant temperature, different techniques for measuring suction results in different values of suction depending on accuracy of the sensor and calibration technique used.
3. At a given water content, increase in temperature results in decreasing total suction. The reduction of the total suction is due to reduction in the capillary component of total suction for total suction less than 20000 kPa. For total suction higher than 2000 kPa, the reduction in total suction is due to reduction of capillary component and/or hydration force.
4. The change in total suction due to change in temperature is reversible and no evidence of mineralogical change is found to the bentonite exposed to temperature less than 100 °C.

10.1.3 Osmotic suction of Calcigel and other soils

1. Osmotic suction of highly plastic clay is obtained from the first drop of extracted soil pore-water. The pressure required to obtain the first drop of highly plastic clays can be estimated from empirical relationship between squeezing pressure versus a generalized parameter (i.e., $(e/e_L)\sqrt{S_r}$).
2. For the two highly plastic clays used in this study, the subtraction of total and matric suction is higher than osmotic suction obtained from squeezing technique and represents the sum of osmotic suction and hydration force of soils.
3. The osmotic suction of Calcigel does not influence the magnitude of its swelling pressure.
4. There is no unique relationship between the osmotic suction and the specific surface area, the liquid limit, the cation exchange capacity, and the surface charge density of soils.
5. The osmotic suction of the material used in this study is very small compared to the matric suction components. Therefore, the change in total suction due to increase in temperature is mainly due to change in matric suction components (i.e., hydration forces and capillary component).

10.1.4 Drying-wetting behavior of compacted bentonite and bentonite-sand mixtures

1. The compacted bentonite specimens (100B) exhibit the greatest shrinkage upon drying regardless the compaction conditions. The same characteristics are also shown for the 50B/50S and 30B/70S specimens. The experimental results also indicate that air entry value increases with bentonite content of the specimens. Compaction conditions do not play significant roles.

2. It is observed that temperature has insignificant influence on the amount of water retained by the bentonite in the mixtures as suction decreases or increases. The presence of sand is thought to have no influence on the water retained by the bentonite in the mixtures. However, it has a beneficial impact with respect to the crack development in the compacted mixture as it undergoes drying process.

3. For heavily compacted bentonite-sand mixture, initial conditions of the specimens affect the drying curves in the low suction range (i.e., less than 3000 kPa). Higher than this suction, the initial conditions do not influence the ability of the material to absorb water.

4. The effect of temperature on the drying-wetting curves of heavily compacted specimen is not significant compared to the effect of initial conditions of the specimens.

5. Cracks occurred in the heavily compacted specimen undergo drying-wetting cycles resulting irreversible the drying-wetting curves especially in the void ratio and degree of saturation versus suction relationship and water content versus suction relationships at suction less than 200000 kPa.

10.1.5 Temperature effects on swelling characteristics of bentonite-sand mixture

1. The increase in temperature results in reduction in swelling pressure. The reduction of swelling pressure found in this study is reversible.
2. The increase in temperature affects only the bentonite. Therefore, the swelling pressure of compacted bentonite-sand mixture is a function of bentonite dry density not only at room temperature but also at elevated temperature

3. The transport mechanism of water molecules controlled the development of swelling pressure and wetting characteristics (i.e., water content and degree of saturation versus suction relationships) of the heavily compacted bentonite-sand mixture specimens not only at 20 °C but also at 80 °C.

4. Temperature increase results in decreasing the swelling strain of heavily compacted bentonite-sand mixture.

10.2 Recommendations

1. All bentonite-sand mixtures compacted at Proctor density show apparently the same void ratio after complete drying to oven-dried state. However, the bentonite void ratio of the specimen at this state decreases with increasing bentonite content. If the shrinkage limit void ratio is regarded to signify the inter-granular contact between sand grains in the mixtures, the specimens with lower bentonite content exhibit higher shear strength compared to those with higher bentonite content. Further investigation is required to confirm this.
2. The real situation occurs in the field that there is temperature gradient in the barrier of nuclear waste repository. The material located close to the host rock would be in contact with water at temperature of 20 °C and the material located close to the canister would experience increase in temperature (i.e., 80 °C). This condition is not found in this study since the test was conducted in isothermal conditions (i.e., at 20 °C and at 80 °C). The temperature gradient may cause water flow from higher temperature to lower temperature due to suction gradients. Test conducted using thermal column is suitable for this condition.
3. Suction and water content measurement directly in the column is necessary to provide contour of suction and water content during experiment. Together with suction and water content sensors, thermocouples are used in order to study the temperature distribution along the column.
4. Applying high temperature from one side and water in the other side is possible to perform in thermal column test to give condition close to the real condition in the field.
5. Good calibration in experiment using thermal column should be performed prior the test to distinguish the responses of sensors used due to temperature and due to the soil behavior.

REFERENCES

Agus S.S. (2005) An experimental study on hydro-mechanical characteristics of compacted bentonite-sand mixtures. PhD dissertation. Bauhaus-Universität Weimar, Germany.

Agus S.S. and Schanz T. (2005a) Swelling pressure and total suction of compacted Bentonite-sand mixtures. Proceeding of International Conference on Problematic Soils (Eds. Bilsel, H and Nalbantoglu, Z). North Cyprus. Vol.**1**, pp. 61-70.

Agus S.S. and Schanz T. (2005b) Comparison of four methods for measuring total suction. Vadose Zone Journal. Special section: Soil Water Sensing. Soil Science Society of America, **4**(4), 1087-1095.

Agus S.S. and Schanz T. (2005c) Effect of shrinking and swelling on microstructures and fabric of a compacted bentonite-sand mixture. Proceeding of International Conference on Problematic Soils (Eds. Bilsel, H and Nalbantoglu, Z). North Cyprus Vol.**2**, pp. 543-550.

Agus S.S. and Schanz T. (2006a) Discussion of paper "Free energy of water-suction-in filter papers" by R. Bulut and W.K. Wray, Geotechnical Testing Journal, ASTM **29** (6).

Agus S.S. and Schanz T. (2006b) Discussion of paper "Parameters affecting soil-water characteristic curves of fine-grained soils" by Vikas K.S. Thakur, S. Sreedeep, and Devendra N. Singh, Journal of Geotechnical and Geoenvironmental Engineering, ASCE **132** (11).

Agus S.S. and Schanz T. (2006c) Drying, wetting, and suction characteristic curves of a bentonite-sand mixture. Proceeding of the Fourth International Conference on Unsaturated Soils (Eds. Miller G.A, Zapata C.E., Houston S.L., and Fredlund D.G), Arizona, USA. ASCE Vol. **2**, pp 1405-1414.

Agus S.S., Schanz T. (2007) Error in total suction measurement. Proc. 2nd International Conference: Mechanics of Unsaturated Soils (Ed. Tom Schanz), Weimar, Germany. Springer proceedings in physics. Vol. **1**, pp. 59-70.

Agus S.S., Leong, E.C., and Schanz, T. (2003) Assessment of statistical models for indirect determination of permeability functions from soil-water characteristic curves. Géotechnique, **53** (2): 279-282.

Albrecht B.A., Benson, C.H., and Beuermann, S. (2003) Polymer capacitance sensors for measuring soil gas humidity in drier soils. Geotechnical Testing Journal, ASTM, **26**(1), 1-9.

Al-mukhtar M., Qi Y., Alcover J.F., and Bergaya F. (1999) Oedometric and water-retention behavior of highly compacted unsaturated smectites. Canadian Geotechnical Journal, **36**: 675-684.

Al-Mukhtar M. (1995) Macroscopic behavior and microstructural properties of a kaolinite clay under controlled mechanical and hydraulic state. In Proceedings of the 1st International Conference on Unsaturated Soils (UNSAT 95), Paris, France (Eds. E.E. Alonso and P. Delage), Balkema, Rotterdam: 3-9.

Archer D.G. (1999) Thermodynamic properties of the KCl + H20 system, Journal Phys. Chem. Reference data, **28**(1), pp. 1-16

ASTM (1997) Annual Book of Standards. Volumes 04.08 and 04.09, Soil and rock, ASTM International. West Conshohocken. PA.

Barbour S.L. and Fredlund D.G. (1989) Mechanisms of osmotic flow and volume change in clay soils. Canadian Geotechnical Journal, **26**: 551-562.

BC Components (1999) Humidity Sensor Brochure

Bolt G.H. (1956) Physico-chemical analysis of the compressibility of pure clays. Géotechnique, **6**(2): 82-93.

Bradbury M.H. and Baeyens B. (2003) Porewater chemistry in compacted re-saturated MX-80 bentonite, Journal of Contaminant Hydrology, Elsevier. **61**: 329-338.

British Standards Institution (1990) BS 1377-2:1990 Method of tests for soils for civil engineering purposes. Classification test.

Bucher F. and Müller-Vonmoos, M. (1989) Bentonite as a containment barrier for the disposal of highly radioactive wastes. Applied Clay Science, Elsevier. **4**: 157-177.

Bucher F. and Spiegel U. (1984) Quelldruck von hochverdichteten Bentoniten. Technischer Bericht 84-18, The Swiss National Cooperative for the Storage of Radioactive Waste (NAGRA), Wettingen, Switzerland.

Bulut R. and Wray W.K. (2005) Free Energy of Water-Suction-in Filter Papers. Geotechnical Testing Journal, ASTM **28**(4):1-10.

Carlsson T. (1986) Interaction in MX-80 bentonite/water/electrolyte systems, PhD Thesis, University of Luleá, Sweden.

Campbell J.R. (2003) Limitations in the laser particle sizing of soils. Advances in Regolith. CRC LEME, pp. 38-42.

Cerato A.B. and Lutenegger A.J. (2002) Determination of surface area of fine-grained soils by the ethylene glycol monoethyl ether (EGME) method. Geotechnical Testing Journal, ASTM **25**(3): 315-321.

Chiou C., Rutherford D., and Manes M. (1993) Sorption of N2 and EGME vapors on some soils, clays and mineral oxides and determination of sample surface areas by use of sorption data. Environmental Science Technology, **27**: 1587–1594.

Cho W.J., Lee J.O., and Kang C.H. (2000) Influence of temperature elevation on the sealing performance of the potential buffer material for a high-level radioactive waste repository. Annals of Nuclear Energy, **27**: 1271-1284.

CRC Handbook of Chemistry and Physics (1995) 75th edition (Ed. D.R. Lide), CRC Press, New York.

Croney D. and Coleman J.D. (1961) Pore pressure and suction in soil. In Proceedings of Conference on Pore Pressure and Suction in Soils, London, Butterworths: 31-37.

Cui Y.J., Loiseau C., and Delage P. (2002a) Microstructure changes of a confined swelling soil due to suction controlled hydration, In Proceeding of the 3rd International Conference on Unsaturated Soils (UNSAT 2002), Recife, Brazil (Eds. J.F.T. Juca, T.M.P. de Campos, and F.A.M. Marinho), Swet&Zeitlinger, Lisse:593-598.

Cui Y.J., Yahia-Aissa, M., and Delage P. (2002b) A model for the volume change behavior of heavily compacted swelling clays. Engineering Geology, Elsevier, **64**: 233-250.

de la Fuente S., Cuadros J., Fiore S., and Linares J. (2000) Electron microscopy study of volcanic tuff alteration to illite-smectite under hydrothermal conditions. Clays and Clay Minerals, **48**(3): 339-350.

Decagon Device Inc (2002) Dewpoint PotentiaMeter: overators manual version 2.1

Deka R.N., Wairiu M., Mtakwa P.W., Mullins C.E., Veenendaal E.M., and Townend J. (1995) Use and accuracy of the filter-paper technique for measurement of soil matric potential. European Journal of Science, **46**: 233-238.

Delage P. (2007) Microstructure features in the behaviour of engineered barriers for nuclear waste disposal, Proc. 2nd International Conference: Mechanics of Unsaturated Soils (Ed. Tom Schanz), Weimar, Germany. Springer proceedings in physics. Vol.1, pp. 11-32.

Delage P and Cui Y.J. (2008) An evaluation of the osmotic method of controlling suction. Geomechanics and Geoengineering: An International Journal, **3**(1): 1-11.

Delage P. and Graham J. (1996) Mechanical behaviour of unsaturated soils: Understanding the behaviour of unsaturated soils requires reliable conceptual models. In Proceedings of the 1st International Conference on Unsaturated Soils (UNSAT 95), Paris, France (Eds. E.E. Alonso and P. Delage), Balkema, Rotterdam: 1223-1256.

Delage P., Audiguier M., Cui Y.J., and Howat M. (1996) The microstructure of a compacted silt. Canadian Geotechnical Journal, **33**: 150-158.

Delage P., Howat M., and Cui Y.J. (1998) The relationship between suction and swelling properties in a heavily compacted unsaturated clay. Engineering Geology, **50** (1-2): 31-48.

Delage P., Marcial D., Cui Y.J., and Ruiz, X. (2006) Ageing effects in the compacted bentonite: a microstructure approach. Géotechnique, **56** (4): 291-304.

Diamond S. (1970) Pore size distribution in clays. Clays and clay minerals, **18**: 7-23.

Di Maio C. (1996) Exposure of bentonite to salt solution: osmotic and mechanical effects. Géotechnique, **46**(4): 695-707.

DIN (1987) Baugrund und Grundwasser. Benenen und Beschreiben von Boden und Fels. Deustche Institut für Normung e.V., Beuth Verlag GmbH, Berlin.

Dixon D.A. (2000) Porewater salinity and the development of swelling pressure in bentonite-based buffer and backfill materials. POSIVA Report 2000-04. Posiva Oy, Helsinki, Finland.

Dohrmann R. (1997) Kationenaustauschkapazität von Tonen. Bewertung bisheriger Analysenverfahren und Vorstellung einer neuen und exakten Silber-Thioharnstoff-Methode. Doctoral thesis, RWTH Aachen, Germany.

DOW (2003) Calcium chloride handbook: A guide to properties, forms, storage, and handling, DOW chemical company, USA.

Drief A., Martinez- Ruiz F., Nieto F., and Sanchez N.V. (2002) Transmission electron microscopy evidence for experimental illitization of smectite in K-enriched seawater solution at 50°C and basic pH. Clays and Clay Minerals, **50**(6): 746-756.

Drief A., and Nieto F. (2000) Chemical composition of smectites formed in clastic sediments. Implications for the smectite-illite transformation. Clay minerals, **35**(4): 665-678.

Dueck A., and Börgesson L. (2001). Constant volume tests with suction control performed on a swelling clay. 6th International Workshop on Key Issues in Waste Isolation Research, Paris, 83-101.

EN-ISO 11885 (1985) Water Quality-Ditermination of 33 Elements by Inductively Coupled Plasma (ICP) emission spectroscopy.

ENRESA (2000) FEBEX project—full-scale engineered barriers experiment for a deep geological repository for high level radioactive waste in crystalline host rock. Final Report, Publicatión Técnica 1/2000, Empresa Nacional de Residuos Radiactivos SA (ENRESA), Madrid, Spain.

Fleureau J.M., Verbrugge J.C., Huergo P.J., Correia A.G., and Kheirbek-Saoud, S. (2002) Aspects of the behaviour of compacted clayey soils on drying and wetting paths. Canadian Geotechnical Journal, **39**: 1341-1357.

Fredlund D.G. and Rahardjo H. (1993) Soil mechanics for unsaturated soils, John Willey & Son, Canada.

Fredlund D.G. and Xing A. (1994). Equation for the soil-water characteristic curve. Canadian Geotechnical Journal, **31**: 521-532.

Gens A., Alonso E.E., Suriol J., and Lloret A. (1995) Effect of the structure and volumetric behaviour of a compacted soil. Proceedings of the first International Conference on unsaturated soils (Eds. Alonso and Delage), Paris, France, Vol. 1. pp. 83-88.

Gens, A. and Alonso E.E. (1992) A framework for the behaviour of unsaturated expansive clays. Canadian Geotechnical Journal, **29**: 1013-1032.

Grant, S. and Salehzadeh A. (1996) Calculation of temperature effects on wetting coefficients of porous solids and their capillary pressure function. Water Resources Research, **32**(2), 261-270.

Griffiths F.J. and Joshi R.C. (1989) Change in pore-size distribution due to consolidation of clays. Géotechnique, **39**(1): 159-167.

Herbert H.J. and Moog H.C. (2002) Untersuchungen zur Quellung von Bentoniten in hochsalinaren Lösungen. Abschlussbericht GRS-179, Förderkennzeichen 02 E 8986 5 (BMBF). Gesellschaft für Anlagen und Reaktorsicherheit (GRS)mbH, Germany.

Horseman S.T. and McEwen T.J. (1996) Thermal constraints on disposal of heat-emitting waste in argillaceous rocks. Engineering Geology, Elsevier. **41**: 5-16.

Houston S.L., Houston W.R., and Wagner A.M. (1994) Laboratory filter paper measurements. Geotechnical Testing Journal, ASTM **17**(2): 185-194.

Huang S., Barbour S.L., and Fredlund D.G. (1998) Development and verification of a coefficient of permeability function for a deformable unsaturated soil. Canadian Geotechnical Journal, **35**: 411-425.

Iyer B. (1990) Pore water extraction-comparison of saturation extract and high-pressure squeezing. Physico-chemical aspects of soil and related materials. ASTM STP 1095 (Eds. K.B. Hoddinott and R.O. Lamb), Philadelphia, pp. 159-170.

JNC (2000) H12: Project to establish the scientific and technical basis for HWL disposal in Japan. Supporting Report 2. Repository design and engineering technology, JNC TN1410 2000-003. Japan Nuclear Cycle Development Institute, Tokai, Japan.

Jurin J. (1718) An account of some experiments shown before the Royal Society; with the enquiry into the cause of ascent and suspension of water in capillary tubes. Philosophical Transactions of the Royal Society **30**: 739-747.

Kahr G., Kraehenbuehl F., Müller-Vonmoos M., and Stöckli H.F. (1986) Wasseraufnahme und Wasserbewegung in hochverdictetem Bentonit. Technischer Bericht 86-14, The Swiss National Cooperative for the Storage of Radioactive Waste (NAGRA), Wettingen, Switzerland.

Kelleners T.J., Robinson D. A., Shouse P. J., Ayars J. E., and Skaggs T. H. (2005) Frequency Dependence of the Complex Permittivity and Its Impact on Dielectric Sensor Calibration in Soils, Soil Science Society of America Journal. **69**: 67–76.

Komine H (2004) Simplified evolution on hydraulic conductivities of sand-bentonite mixture backfill. Applied Clay Science, Elsevier. **26**:13-16.

Komine H. and Ogata N (2003) New equations for swelling characteristics of bentonite-based buffer materials. Canadian Geotechnical Journal. **40**: 460-475.

Komine H. and Ogata N. (1998) Thermal influence on compacted bentonite for nuclear waste disposal. Proceedings of the 3rd International Congress on Environmental Geotechnics, pp. 39-44.

Komine H. and Ogata N. (2003) New equations for swelling characteristics of bentonite-based buffer materials. Canadian Geotechnical Journal, **40**: 460-475.

Krahn J. and Fredlund D.G. (1972) On total, matric and osmotic suction. Soil Science, **115**(5): 339-348.

Laird D.A. (2006) Influence of layer charge on swelling of smectites, Applied Clay Science, Elsevier. **34**: 74-87.

Lambe T.W. (1960) Structure of compacted clay. Transaction Am. Soc. Civ. Eng. **125**: 682-705.

Lang A.R.G. (1967) Osmotic coefficients and water potentials of sodium chloride solution from 0 to 40°C, Australian Journal of Chemistry, **20**: 2017-2023.

Leong E.C., Widiastuti S., Lee C.C., Rahardjo H. (2007) Accuracy of suction measurement. Géotechnique, **57** (6): 547-556.

Leong, E. C., He, L. and Rahardjo, H. (2002) Factors affecting the filter paper method for total and matric suction measurements. Geotechnical Testing Journal, ASTM **25** (3): 321-332.

Leong E.C. and Rahardjo H. (1997) Permeability functions for unsaturated soils. Journal of Geotechnical and Geoenvironmental Engineeing, ASCE. **123**(12): 1118-1826.

Leong E.C., Tripathy S., and Rahardjo R. (2003) Total suction measurement of unsaturated soils with a device using the chilled-mirror dew-point technique. Géotechnique, **53**(2): 173-182.

Likos W.J. and Lu N. (2001) Automated measurement of total suction characteristics in high-suction range: application to assessment of swelling pressure. Journal of Transportation Research Board No.1755, pp. 119-128.

Likos W.J.and Lu N. (2003a) Filter paper column for measuring transient suction profiles in expansive clay. Journal of the transportation research board No. 1821, pp. 83-89.

Likos W.J. and Lu N. (2003b) Automated humidity system for measuring total suction characteristics of clay. Geotechnical Testing Journal, ASTM **26**(2): 1-12.

Lingnau BE, Graham J, Yarechewski D., Tanaka N., and Gray M.N. (1996) Effects of temperature on strength and compressibility of sand-bentonite buffer. Engineering Geology, Elsevier. **41**: 103-115.

Lloret, A., Villar M.V., Sánchez M., Gens A., Pintado X., and Alonso E.E. (2003) Mechanical behaviour of heavily compacted bentonite under high suction changes. Géotechnique, **53** (1): 27-40.

Madsen F.T. (1998) Clay mineralogical investigations related to nuclear waste disposal. Clay minerals, **33**: 109-129.

Madsen F.T., and Müller-Vonmoos M. (1989) The swelling behaviour of clays. Applied Clay Science, Elsevier. **4**: 143-156.

Manheim F.T. (1966) A hydraulic squeezer for obtaining interstitial water from consolidated and unconsolidated sediments. U.S. Geological Survey, Prof. Paper 550C, pp. 256-261.

Manheim F.T. and Giekes J.M. (1983) Interstitial water methods. Sedimentology, Physical Properties and Geochemistry in the Intial Reports of the Deep Sea Drilling Project: An Overview (Ed. G. Ross Heath) Boulder, Colorado, pp. 163-176.

Marinho F.A.M. (2005) Nature of soil-water characteristic curve for plastic soils. Journal of Geotechnical and Geoenvironmental Engineering, ASCE. **131** (5): 654-661.

Mata C. Romero E. and Ledesmana A. (2002) Hydro-chemical effects on water retention in bentonite-sand mixtures. Proc. 3rd Int. Conf. on Unsaturated Soils, UNSAT 2002 (Eds. Jucá, J.F.T., de Campos, T.M.P. and Marinho, F.A.M.), Recife, Brazil. Swets& Zeitlinger Vol. **1**, pp. 283-288

McKeen R.G. (1980) Field studies of airport pavements on expansive soils. In Proceedings of the 4th International Conference on Expansive Soils: 242-261.

Mesri G., Pakbaz M.C. and Cepeda-Diaz A.F. (1994) Meaning, measurement and field application of swelling pressure of clay shales. Geotechnique, **44** (1): 129-145.

Miller D.J. and Nelson J.D. (1992) Osmotic suction as a valid stress state variable in unsaturated soil mechanics. Proceeding of the 7th international conference on expansive soils, Dallas 1992. pp. 179-184.

Mitchell J.K. (1993) Fundamentals of Soil Behavior. 2nd Edition. John Wiley & Sons Inc., NY.

Mokrejš P., Zikánová A., Hradil D., Štulik K., Pacáková V., Kočiřík M., Eič M. (2005) The influence of heat pre-treatment on the sorption of water vapour on bentonite. Adsoption, **11**: 57-63.

Morgenstern N. and Balasubramonian B.I. (1980) Effect of pure fluid on the swelling of clay-shale. Proceeding 4th International Conference on Expansive Soil, Denver, CO, 190-205.

Morris P.H., Graham J., and Williams D.J. (1992) Cracking in drying soils. Canadian Geotechnical Journal, **29**: 263-277.

Mualem Y. (1976). A new model for predicting the hydraulic conductivity of unsaturated porous media. Water Resources Research, **12**: 513-522.

Müller-Vonmoos K. and Kahr G. (1983) Mineralogische Untersuchungen von Wyoming Bentonit MX80 und Montigel. NTB 83-12, NAGRA, Wettingen, Switzerland, 1983. In German with English Abstract.

Myers D. (1991) Surfaces, Interfaces, and Colloids. Principles and Applications, VCH Publisher Inc., USA.

Nagaraj T.S., Schanz T., and Nagendra P.K. (2006) Generalized state parameter for constitutive relations in unsaturated clays. IGC 2006, Chennai. India.

Nagaraj T.S., Schanz T., and Nagendra P.K. (2007) Discussion of "Suction stress characteristics curve for unsaturated soil" by Ning Lu and W. J. Likos. Journal of Geotechnical and Geoenvironmental Engineering. ASCE. **133** (5).

Peroni N. and Tarantino A. (2005) Measurement of osmotic suction using the squeezing technique. Proceeding of the International Conference "From Expermental Evidence towards Numerical Modelling of Unsaturated Soil", Weimar, Germany ,2002. Springer proceedings in physics. (Ed.Tom Schanz). pp 159-168.

Pitzer K.S. and Pelper J.C. (1984) Thermodynamic properties of aqueous sodium cloride solutions, Journal Phys. Chem. Reference data, **13**(1), pp. 1-102.

Pusch R. (2000) On the effect of hot water vapor on MX-80 clay. SKB TR-00-16, Swedish Nuclear Fuel and Waste Management Co.

Pusch R., Karlnland O., and Hokmark H. (1990) GMM-a general microstructural model for qualitative and quantitative studies of smectite clays. SKB Technical Report 90-43, Stockholm, Sweden.

Pusch R., and Yong R. (2003) Water saturation and retention of hydrophilic clay buffer-microstuctural aspects, Applied Clay Science, Elsevier. **23**: 61-68.

Pusch R. (2001) The microstructure of MX-80 clay with respect to its bulk physical properties under different environmental conditions. SKB Technical Report, TR-01-08. The Swedish Nuclear Fuel and Waste Management Company (SKB), Stockholm, Sweden.

Puthela R.C. and Pitzer K. (1983) Thermodynamics of aqueous calcium chloride, Journal of Solution Chemistry. Springer. **12**(3), pp. 201-207.

Rao K.S. and Tripathy S. (2003) Effect of aging on swelling and swell-shrink behaviour of a compacted expansive soil, Geotechnical Testing Journal, ASTM **26** (1): 36-46.

Rao S.M. and Shivananda P. (2005) Role of osmotic suction in swelling of salt amended clays, Canadian Geotechnical Journal, **42**: 307-315.

Richards B.G. (1965) Measurement of the free energy of soil moisture by the psychrometric technique using thermistors. In moisture equilibria and moisture changes in soils beneath covered area (Eds. G.D. Aitchison). Butterworth & Co. Ltd. Sydney. Australia. pp. 39-46.

Ridley A.M. and Burland J.B. (1993) A new instrument for the measurement of soil moisture suction. Géotechnique, **43**(2): 321-324.

Ridley A.M. and Wray W.K. (1996) Suction measurement: a review of current theory and practices. In Proceedings of the 1st International Conference on Unsaturated Soils (UNSAT 95) Paris, France. (Eds. E.E. Alonso and P. Delage). Balkema, Rotterdam: 1293-1322.

Robinson D.A., Jones S.B., Wraith J.M., Or D., and Friedman S.P. (2003) A review of advances in dielectric and electrical conductivity measurement in soils using time domain reflectometry. Vadose Zone Journal. **2** :444–475.

Romero E. (1999) Characterization and thermo-hydro-mechanical behavior of unsaturated Boom clay: an experimental study. Ph.D. Thesis. Universidad Politécnica de Cataluňa; Barcelona, Spain.

Romero E. Gens, A. and Lloret, A. (2000) Temperature effects on water retention and water permeability of an unsaturated clay, Proceeding of Unsaturated Soils for Asia (Eds. Rahardjo, Toll and Leong), Balkema, Rotterdam, pp. 433-438.

Romero E., Li X.L. (2005) Thermo-hydro-mechanical tests using vapour and liquid transfer on a clay-based mixture. Advance Experimental Unsaturated Soil Mechanics (Eds. Tarantino A., Romero E., and Cui Y.J.), Taylor and Francis Group, London. pp. 483-488.

Romero E., Villar M.V., Lloret A. (2005) Thermo-hydro-mechanical behaviour of two heavily overconsolidated clays. Engineering Geology, Elsevier. **81**(3): 255-268.

Romero E., Gens A., and Lloret A. (2003) Suction effects on a compacted clay under non-isothermal conditions. Géotechnique, **53**(1): 65-81.

Sacchi E., Michelot J.L., Pitsch H., Lalieux P., Aranyossy J.F. (2001) Extraction of water and solutes from argillaceous rocks for geochemical characterisation: Methods, processes, and current understanding. Hydrology Journal, Spinger. **9**: 17-33.

Saiyouri N, Tessier D, Hicher P.Y. (2004) Experimental study of swelling in unsaturated compacted clays, Clay Minerals, **39**: 469-479.

Sällfors G. and Öberg-Högsta (2002) Ditermination of hydraulic conductivity of sand-bentonite mixtures for engineering purposes. Geotechnical and Geological Engineering. **20**:65-80.

Schanz T., and Tripathy S. (2005) Soil water characteristic curves of clays from physico-chemical concepts. Proceeding of International Conference on Problematic Soils. (Eds. Bilsel, H and Nalbantoglu, Z). North Cyprus. Vol. **1**, pp. 219-228.

Sitz P. (1997) Materialuntersuchungen für Mehrkomponentensysteme auf Ton/Bentonit Basis für Dichtung und Lastabtrag, mit hohem Ruckhaltvermögen, für den langzeitsicheren Verschluß von UTD und Endlagern im Salinar. Abschlußbericht 02 C 0193 (BMBF), TU Bergakademie Freiberg, Germany.

SKB (1999) SR-97: Waste, repository design and site. SKB Technical Report TR-99-08, Stockholm, Sweden.

Sposito G. (1981) The thermodynamic of soil solution. Oxford Clarendon Press. London.

Sreedep S. and Singh D.N. (2006) Methodology for determination of osmotic suction of soils. Geotechnical and Geological Engineering, **24**: 1469-1479.

Sridharan A. (2002) Engineering behaviour of clays: Influence of mineralogy. Chemo-Mechanical Coupling in Clays; from Nano-Scale to Engineering Applications (Eds. Di Miao, Hueckel and Lloret). Swets & Zeitlinger. Lisse. pp. 3-27.

Sridharan A. and Choudhury D. (2002) Swelling pressure of sodium montmorillonites. Géotechnique, **52**(6): 459-462.

Sridharan A., Rao S.M., and Murthy N.S. (1986a) Liquid limit of montmorillonite soils. Geotechnical testing journal, ASTM **9**(3):156-159.

Sridharan A., Sreepada Rao A. and Sivapullaiah P.V. (1986b) Swelling pressure of clays. Geotechnical Testing Journal, ASTM **9**(1): 24-33.

Sridharan A., and Jayadeva M.S. (1982) Double layer theory and compressibility of clays. Geotechnique, **32**(2): 133-144.

Sridharan A., Altschaeffl A. G., and Diamond S. (1971) Pore size distribution studies. Journal of Soil Mechanics and Foundation Engineering, **97** (SM 5): 771–787.

Tang A.M. and Cui Y.J. (2005): Controlling suction by the vapor equilibrium technique at different temperatures and its application in determining the water retention properties of MX80 clay, Canadian Geotechnical Journal, **42**: 287-296.

Tessier D., Dardaine M., Beaumont A., and Jaunet A.M. (1998) Swelling pressure and microstructure of an activated swelling clay with temperature, Clay Minerals, **33**: 255-267.

Thom R., Sivakumar R., Sivakumar V., Murray E.J., and Mackinnon P (2007) Pore size distribution of unsaturated compacted kaolin: the initial states and final states following saturation. Géotechnique **57**(5): 469–474.

Thomson W.T. (1871) Philosophical Magazine. **42**: 448.

Topp G.C., Davis J.L., and Annan A.P. (1980) Electromagnetic determination of soil water content: Measurements in coaxial transmission lines. Water Resources Research, **6**(3): 574-582.

Tripathy S., Kessler W., Schanz T. (2006) Determination of interparticle repulsive pressure in clays. Proceeding of the Fourth International Conference on Unsaturated Soils (Eds. Miller G.A, Zapata C.E., Houston S.L., and Fredlund D.G), Arizona, USA. ASCE Vol.**2**, pp 2198-2209.

Tripathy S., Schanz T., and Sridharan A. (2004) Swelling pressures of compacted bentonites from diffuse double layer theory. Canadian Geotechnical Journal, **41**: 437-450.

USDA (1950) USDA Agricurtural Handbook 60. Diagnosis and improvement of saline and alkali soils.

Vaisala (2002) HMP240 series transmitters. User's guide. Vaisala Oyj., Helsinki, Finland

van Olpen, H. (1963) An introduction to clay colloid chemistry. New York and London: Interscience.

Vanapalli S.K., Fredlund, D.G., and Pufahl, D.E. (1999) Influence of soil structure and stress history on the soil-water characteristics of a compacted till. Geotechnique. **49**: 2. pp. 143-159.

Villar M.V., Lloret A. (2004) Influence of temperature on the hydro-mechanical behaviour of a compacted bentonite, Applied Clay Science, Elsevier. **26**: 337-350.

Villar MV, Rivas P, Campos R, Lloret A, Romero E, and Mariano A (2001) First report on thermo-hydro-mechanical laboratory tests. Report 70-IMA-L-0-86

Villar M.V. and Martin P.L (2005): Determination of water retention curves of two bentonites at high temperature, Advanced Experimental Unsaturated Soil Mechanics (Tarantino A., Romero E., and Cui Y.J.). Taylor and Francis Group, London. pp. 77-82.

von Engelhardt W. and Gaida K.H. (1963) Concentration changes of pore solutions during the compaction of clay sediments. Journal Sediment Petrology **33**: 919-930.

Wan A.W.L, Gray M.N., and Graham J. 1995. On relations of suction, moisture content, and soil structure in compacted clays. In Proceedings of the 1st International Conference on Unsaturated Soils (UNSAT 95), Paris, France (Eds. E.E. Alonso and P. Delage), Balkema, Rotterdam. pp. 215-222.

Wang P., Pitzer K.S., Simonson J.M. (1998) Journal Phys. Chem. Reference data, **27**(5), pp. 971-991.

Washburn E.W. (1921) A method of determining the distribution of pore sizes in a porous material. Proceedings of the National Academy of Sciences, **7**: 115.

Wersin P., Johnson L.H., and McKinley I.G. (2006) Performance of the bentonite barrier at temperatures beyond 100°C: A critical review. Physics and Chemistry of the Earth, **32**(8): 780-788.

Woessner D.E. (1980) An NMR investigation onto the ranges of the surface effect on the rotation of water molecules, Journal of Magnetic Resonance., **39**: 297-308.

Yahia-Aissa M., Delage P., and Cui Y.J. (2000) Volume change behavior of a densce compacted swelling clay under stress and suction change. Experimental evidence and teoritical approachs in unsaturated soil. Trento 10-12 April. 65-74.

Yong R.N. (1999) Soil suction and soil-water potentials in swelling clays in engineered clay barriers. Engineering Geology, Elsevier. **54**: 3-13.

Yong R.N. and Warkentin B.P. (1975) Introduction to soil behaviour. The Macmillan Company, New York.